SISSA
Scuola
Internazionale
Superiore di
Studi Avanzati

Physics Area - Ph.D. course in
Astroparticle Physics

# Aspects of Leptogenesis Scenarios at Grand Unification and Sub-TeV Scales and Their Possible Low-Energy Tests

Candidate:
Alessandro Granelli

Advisor:
Prof. Serguey T. Petcov
Co-advisor:
Prof. Piero Ullio

Academic Year 2021-22

**Abstract**

In the present Thesis, we investigate various aspects of leptogenesis scenarios based on the type-I seesaw extension of the Standard Model (SM) with 2, 3 heavy Majorana neutrinos $N_j$ with masses $M_j$, $j = 1, ..., 3$, as well as the possibilities to test the scenarios considered by us in currently running and/or future planned low-energy experiments. We focus first on the high-scale leptogenesis framework with strongly hierarchical mass spectrum of the heavy Majorana neutrinos, namely $M_1 \ll M_2 \ll M_3$, with $M_1$ in the range $(10^8 - 10^{14})\,\text{GeV}$, concentrating on the possibility that the requisite CP-violation for the generation of the baryon asymmetry of the Universe $\eta_B$ is provided solely by the low-energy Dirac and/or Majorana phases of the light neutrino mixing (PMNS) matrix. A detailed numerical analysis of the solution to the quantum density matrix equations in this scenario, performed with the powerful `ULYSSES` code we have developed, reveals a number of novel features: i) $\eta_B$ going through zero and changing sign at the transitions between different flavour regimes (1-to-2 and 2-to-3) in the case of vanishing initial abundance of $N_1$ and strong wash-out effects; ii) inadequate description of the transitions between different flavour regimes by the corresponding Boltzmann equations; iii) flavour effects persisting beyond $10^{12}$ GeV and making it possible to reproduce the observed value of $\eta_B$ at these high-scales even though the CP-violation is provided only by the Dirac and/or Majorana phases of the PMNS matrix. Considering the somewhat simpler case of just two heavy Majorana neutrinos $N_{1,2}$ (with the heaviest $N_3$ decoupled) we show that relatively large part of the viable leptogenesis parameter space can be probed in low-energy neutrino experiments. We find, in particular, that, when the CP-violation is provided exclusively by the Dirac phase $\delta$ of the PMNS matrix, there is a correlation between the sign of $\sin\delta$ and the sign of $\eta_B$. This opens up the possibility to test part of the parameter space of this scenario in low-energy experiments on CP-violation in neutrino oscillations. A measurement of the Dirac and/or Majorana phases would also constrain the range of scales for which one can have viable leptogenesis in the considered scenario. Next, we show that in the low-scale resonant leptogenesis scenario with two heavy Majorana neutrinos $N_{1,2}$ forming a pseudo-Dirac pair, with $M \simeq M_{1,2}$ and a small mass splitting $|M_2 - M_1| \ll M$, the observed $\eta_B$ can be reproduced for $M$ in the range $(0.1 \sim 100)\,\text{GeV}$ by relying only on the decay mechanism, either during the production ("freeze-in") or departure from equilibrium ("freeze-out") of $N_{1,2}$. In this context, the inclusion of flavour and thermal effects in the formalism of Boltzmann equations is crucial for predicting the observed value of $\eta_B$. Also, we find that the viable parameter space of this resonant scenario is compatible with values of the heavy Majorana neutrino couplings to the SM that could be probed at future colliders, like at the discussed FCC-ee facility. When low-scale leptogenesis with three quasi-degenerate in mass heavy Majorana neutrinos $N_{1,2,3}$ with $M \simeq M_{1,2,3}$ is considered in the formalism of density matrix equations and, in particular, with both the heavy Majorana neutrino oscillation and decay mechanisms taken into account, the viable parameter space for $M$ in the range $(0.05 - 7 \times 10^4)\,\text{GeV}$ enlarges considerably and becomes accessible to direct searches at the LHC, as well as in fixed target experiments and future colliders. We demonstrate that planned and upcoming experiments on charged lepton flavour violating processes with muons $\mu^\pm$, specifically MEG II on $\mu \to e\gamma$ decay, Mu3e on $\mu \to eee$ decay, Mu2e and COMET on $\mu - e$ conversion in aluminium and PRISM/PRIME on $\mu - e$ conversion in titanium, can test significant region of the viable leptogenesis parameter space and may potentially establish the first hint of such low-scale leptogenesis scenario.

# List of Publications and Abbreviations

What is presented in this Thesis is largely based on the following publications (Pubs.):

[I] A. Granelli, K. Moffat and S. T. Petcov, *Aspects of High Scale Leptogenesis with Low-Energy Leptonic CP Violation*, *Journal of High Energy Physics* **11** (2021) 149, [2107.02079].

[II] A. Granelli, K. Moffat and S. T. Petcov, *Flavoured Resonant Leptogenesis at sub-TeV scales*, *Nuclear Physics B* **973** (2021) 115597, [2009.03166].

[III] A. Granelli, J. Klarić and S. T. Petcov, *Tests of Low-Scale Leptogenesis in Charged Lepton Flavour Violation Experiments*, Submitted for Publication in Physics Letters B, [2206.04342].

[IV] A. Granelli, K. Moffat, Y. F. Perez-Gonzalez, H. Schulz and J. Turner, *ULYSSES: Universal LeptogeneSiS Equation Solver*, *Computer Physics Communications* **262** (2021) 107813, [2007.09150].

The publications above are listed in order of appearances in the main text and, when cited, will be differentiated by capital Roman numbering from the other references (Refs.), for which we will use instead the Arabic numerals. In particular, Chapter 3 will focus on the results of Pub. [I], Chapter 4 on Pubs. [II, III] and Appendix A on Pub. [IV].

**Other Works**

During my Ph.D. activity I have also worked on topics related to the dark matter problem under the guidance of Professor Piero Ullio. The results of these studies were collected in the following two publications, which, however, will not be included in the present Thesis:

[A] J.-W. Wang, A. Granelli and P. Ullio, *Direct Detection Constraints on Blazar-Boosted Dark Matter*, *Physical Review Letters* **128** (2022) 221104, [2111.13644].

[B] A. Granelli, P. Ullio, and J.-W. Wang, *Blazar-Boosted Dark Matter at Super-Kamiokande*, *Journal of Cosmology and Astroparticle Physics* **07** (2021) 013, [2202.07598].

**Abbreviations**

We also define here some abbreviations that will be widely adopted in the Thesis: e.g. = exempli gratia; i.e. = id est; Eq(s). = equation(s); Fig(s). = figure(s), Sec(s). = section(s), Subsec(s). = subsection(s). Other abbreviations that will appear will be defined on the run. We will also adopt the Einstein's notation for which summations over equal indices, if not specified, are implicit. We finally point out that, most of the times in the text of this Thesis, we will express the relevant physical quantities in units of speed of light $c$, reduced Planck constant $\hbar$ and Boltzmann constant $k_B$, i.e. $c = \hbar = k_B = 1$.

# Contents

# CHAPTER 1

# The Matter-Antimatter Asymmetry of the Universe

## 1.1 The Search for Antimatter

In 1928, Paul A. M. Dirac proposed a unification of special relativity with quantum mechanics to explain the nature of electron [1]. His theory admitted also the presence of electrons with negative energy, or, equivalently, with positive electric charge. Soon after, evidence of "positive electrons" was observed by Carl D. Anderson, who, in 1932, during his experiments on cosmic rays (CRs), detected tracks of positively-charged particles as massive as electrons, called *positrons* by the editor of the journal in which the discovery was published [2] (also named *antielectrons* afterwards). With their pioneering works, the two Nobel Prize winner physicists were establishing, both theoretically and experimentally, the existence of *antiparticles*. Further confirmation came later from the Bevatron particle accelerator after the first observations of the *antiproton* in 1955 [3], giving a Nobel Prize to Owen Chamberlain and Emilio Segrè, and the *antineutron* in 1956 [4] by Bruce Cork, Glen Lambertson, Oreste Piccioni and William Wenzel.

Since then, antiparticles have been repeatedly created at laboratories and used to unveil the microscopic realm of particle physics. Among the greatest successes, it is worth mentioning the discovery of $W^{\pm}$ and $Z^0$ bosons at the Super Proton-Antiproton Synchrotron (Sp$\overline{\text{p}}$S), for which Simon van der Meer and Carlo Rubbia received the Nobel Prize in 1984 [5]. Of great importance was also the Low Energy Antiproton Ring (LEAR) at CERN, that permitted to accumulate antiprotons and create, for the first time, atoms of *antihydrogen* [6]. Moreover, apart from artificial production, antiparticles are emitted naturally by radioactive isotopes (e.g. our own body emits positrons due to the $\beta^+$ decay of $^{40}$K). Besides, positrons have also applications such as, e.g., in medicine for the Positron Emission Tomography (PET) technique [7]. Recent studies have also suggested that positrons can originate via pair-production in the vicinity of a thunderstorm [8]. Nevertheless, CRs remain the primary source of positrons and antiprotons at Earth (see further).

From the theoretical perspective, a classification of all the known elementary particles is furnished by the Standard Model (SM) of particle physics (e.g., Ref. [9] contains extensive reviews on the SM and related topics). The SM is a four-dimensional renormalisable quantum field theory that admirably well describes the electromagnetic, the weak and the strong interactions under the action of the $\mathrm{SU(3)_C \times SU(2)_L \times U(1)_Y}$ gauge group and explain the generation of the masses of all the elementary particles, apart from neutrinos, via the Higgs mechanism. In the SM picture, to each particle corresponds an antiparticle with equal mass and opposite charges (neutral particles, such as photons, are antiparticles of themselves). Particles and antiparticles can annihilate with each other and produce other particles, like electron and

positrons annihilating into a pair of photons (depending on the total energy, other final states are also possible).

In principle, there is nothing that prohibits antiparticles from forming the same complex structures that in our planet are composed only of particles, such as atoms, molecules and crystals, i.e. *matter*. Substance made solely of antiparticles is dubbed *antimatter*. However, there is evidence for an overabundance of matter with respect to antimatter in our Universe. For instance, it is pretty obvious that everything we interact with during our everyday experience on Earth is made of matter and not antimatter. The only fact that we exist without annihilating with what we touch is irrefutable proof. Yet, the matter domination extends to much larger scales. We have direct proofs that matter dominates over antimatter in the whole Solar System: Neil Armstrong (and other astronauts after him) survived his "one small step" on the Moon [10], proving that our natural satellite is indeed made of matter; artificial probes and spacecrafts have "safely" (some with crashes, but still without annihilations) reached the surfaces of celestial objects, like, most recently, the latest NASA's Perseverance rover on Mars [11] and the Philae landler of the ESA's Rosetta mission [12] on the comet 67P/Churyumov-Gerasimenko. Moreover, the particles composing the solar wind (mostly protons, electrons and nuclei of helium) with a flux of $\sim 2 \times 10^8\,\mathrm{cm}^{-2}\,\mathrm{s}^{-1}$, do not annihilate with the material and objects in our stellar system, which otherwise would be shining $\gamma$-rays. For example, from a hypothetical *antiplanet* with radius $r$ at a distance $d$ we would receive a $\gamma$-ray flux of $\sim 10^8\,(r/d)^2\,\mathrm{cm}^{-2}\,\mathrm{s}^{-1}$ [13], definitely larger than, e.g., the experimental limits for Jupiter [14]. Limited is also the existence of *antiasteroids*, that could in principle lead to powerful $\gamma$-ray flashes after impacting on the surfaces of the Sun or, more rarely, Jupiter and Earth [15].

At the galactic level, CRs provide the most direct evidence of matter overabundance. CRs are particles from outer space bombarding the Earth's atmosphere from every direction, at a rate of $\sim 10^3\,\mathrm{cm}^{-2}\,\mathrm{s}^{-1}$ and with energies that extend to $\sim 10^{20}$ eV. The composition of CRs is about 90% of protons, 9% of light nuclei, and only 1% of heavier nuclei and electrons (see, e.g., Refs. [16–18] for monographs on the topic). In the standard paradigm, the bulk of CRs is believed to be generated within our galaxy [19, 20] after supernovae explosions [21, 22], that can accelerate protons up to $\sim 1$ PeV, and heavier nuclei like iron to $\sim 0.1$ EeV. Above $0.1 \sim 1\,\mathrm{EeV}$ the origin of CRs is believed to be extragalactic [23] (see, e.g., Ref. [24] for a recent review on the standard paradigm of CRs origin and its critical points). The flux of CRs is also composed by a small percentage of positrons (roughly 10% of the total leptonic component) and antiprotons (roughly one every $10^4$ protons), as detected, for example, most recently by the Alpha Magnetic Spectrometer (AMS) [25]. The exact production mechanism of antiprotons and positrons, despite being most likely secondary, is currently subject of debate and can even be related to dark matter [1] (see, e.g., Ref. [24] and references therein), but their appearance in the CR flux does not prove the existence of, in any case few, antimatter objects in our galaxy or nearby. Instead, what could hint towards the presence of some kind of galactic antimatter-made objects is the detection of nuclei of *antihelium* – anyway estimated to be less than one for every million helium nuclei [28] – or heavier *antinuclei* [29]. Following recent announcements on some antihelium signals detected by AMS, the idea that such nuclei can originate from confined *anticlouds* and *antistars* in our galaxy has been investigated [30]. However, these tentative signals require further verification and other explanations for their origin are not ruled out (see, e.g., Ref. [31] and references quoted there). To sum up, CRs suggest that, in the Milky Way, objects made of antimatter are very few, if not absent, and

[1] The search for *antideuterons* in CRs is also active in connection to dark matter models [26, 27].

matter reigns [2].

Indirect methods looking at particle-antiparticle annihilation products allow to extrapolate information on the existence (absence) of antimatter regions even at extragalactic scales. Observations of $\gamma$-rays impose the most stringent limits [13, 32] (see also [33]). The fraction of antimatter in the intergalactic medium is constrained by $\gamma$-ray observations and it cannot exceed $10^{-6}$ up to scale of galaxy clusters, i.e. around the Mpc [32]. Considering the Bullet Cluster [34] as representative, the limits can be extended to scales of tens of Mpc [32, 33]. The possibility that purely antimatter patches of the Universe exist and are well separated from us is also excluded, as argued in Ref. [35], unless the separation is of the order of or larger than the size of the observable Universe. Indeed, the homogeneity of the Cosmic Microwave Background (CMB) [36, 37] rule out any void that could eventually separate matter and antimatter patches between the time of recombination and the onset of large-scale structure formations. During this temporal gap, the annihilations at the boundaries would have contributed to the diffuse $\gamma$-ray background and oversaturated its observed value [35]. Overall, combining together the above reasonings and observations, we end up with the conclusion that the observable Universe has a net cosmological matter-antimatter asymmetry.

## 1.2 The Baryon Asymmetry of the Universe

In cosmology, the matter-antimatter asymmetry is translated in terms of the Baryon Asymmetry of the Universe (BAU) and parametrised by the baryon-to-photon ratio

$$\eta_B \equiv \frac{n_b - n_{\bar{b}}}{n_\gamma}, \tag{1.1}$$

where $n_b$, $n_{\bar{b}}$ and $n_\gamma$ are the number densities of baryons, *antibaryons* and photons, respectively, with baryons being at present mainly protons and $^4$He. We note that, as discussed in the previous section, since no reasonable amount of antimatter appears to be present in the observable Universe, today $n_b \gg n_{\bar{b}}$, so $\eta_B \approx n_b/n_\gamma$. Alternatively, the BAU can be expressed in terms of the baryonic density parameter

$$\Omega_B h^2 = \frac{m_N(n_b - n_{\bar{b}})}{\rho_c h^{-2}} = \eta_B \frac{m_N n_\gamma}{\rho_c h^{-2}} \simeq \frac{\eta_B}{2.73 \times 10^{-8}}\,, \tag{1.2}$$

or the baryon-to-entropy density ratio

$$Y_B = \frac{n_b - n_{\bar{b}}}{s} = \eta_B \frac{45\zeta(3)}{\pi^4 g_{*,\,s}(t_{\rm rec})} \simeq \frac{\eta_B}{7.04} \tag{1.3}$$

where $m_N$ is the nucleon mass approximately equal to that of the protons, i.e. $m_N \simeq m_p \simeq 0.938\,\text{GeV}$, $\rho_c \simeq 1.88 \times 10^{-29} h^2\,\text{g}\,\text{cm}^{-3}$ is the critical density of the Universe, $h$ is the Hubble expansion rate of the Universe ($H$) per unit of 100 (km/s)/Mpc, the photon number density at present reads $n_\gamma \simeq 411\,\text{cm}^{-3}$, $\zeta$ is the Riemann zeta function with $\zeta(3) \simeq 1.2$, $g_{*,\,s}(t_{\rm rec}) = 43/11$ are the entropic effective degrees of freedom at the time of recombination and $s$ is the entropy of

[2] Moreover, due to annihlitations with matter, antinuclei in the matter-dominated interstellar medium (ISM) have a lifetime of about $\sim 300\,\text{yr}$ and therefore the antimatter fraction at present in the ISM cannot exceed $\sim 10^{-15}$ [13, 32, 33].

the Universe (an extensive compendium of all the relevant physical constants and corresponding numerical values can be found in Ref. [38]).

The present BAU has been determined with high precision from the measurements of the CMB anisotropies made by the PLANCK observatory. The (acoustic) oscillations of baryons and photons in the primordial plasma caused inhomogeneities in the dark matter distribution and thus in the gravitational potential, with the baryon-to-photon ratio $\eta_B$ affecting the height of odd and even peaks of the CMB power spectrum. The global fit presented in Ref. [39] of the CMB observations by PLANCK gave the following value for the amount of baryon in the Universe (at 68% C.L.):

$$\Omega_B h^2 = 0.02242 \pm 0.00014\,(\text{CMB}). \tag{1.4}$$

Another accurate estimate of the present baryon-to-photon ratio comes from the Big Bang Nucleosynthesis (BBN) predictions on the abundances of light elements in the Universe (see Ref. [40] for a recent review). The BBN predictions rely on just one parameter, precisely the baryon-to-photon ratio $\eta_B$. The present abundances of light elements (D,$^3$He, $^4$He, and$^7$Li) are all given in terms of $\eta_B$ at present. Fitting the observational data for the present abundances of light elements, the BBN gives the following value for the BAU (at 68% C.L.) [41]:

$$\Omega_B h^2 = 0.02235 \pm 0.00049\,(\text{BBN}), \tag{1.5}$$

which indeed is in perfect agreement with the result from PLANCK [3]. The "cosmic" concordance of the two independent observations is a striking proof of the validity of the standard model of cosmology up to the time scale of BBN (when the Universe was at a temperature of the order of 1 MeV or, equivalently, 1 s after the beginning of the expansion). From both the CMB and BBN estimates we obtain the best-fit value of

$$\eta_B \simeq 6.1 \times 10^{-10}\,, \tag{1.6}$$

that is going to be our reference value throughout this Thesis.

The smallness of the baryon-to-photon ratio as given in Eq. (1.6) can be interpreted in terms of the difference in numbers between baryons and antibaryons at early times, when $n_b \approx n_{\bar{b}} \approx n_\gamma$. From the definition of $\eta_B$ in Eq. (1.1) we get

$$n_b \approx (1 + 6.1 \times 10^{-10}) n_{\bar{b}}\,, \tag{1.7}$$

which means that for every two billion antibaryons, there were roughly two billion and one baryons. Nevertheless, the present value of $\eta_B$ is just seemingly small: a Universe that was locally symmetric at early times could not have produced so many baryons. When in equilibrium with the plasma at temperatures greater than their masses, baryons and antibaryons annihilate into photons and vice versa equally, keeping their number density constant. As the Universe cools down to temperatures smaller than the masses of baryons, photons are not energetic enough to produce pairs with the inverted process. At this point, the number of baryons and antibaryons starts to decrease exponentially due to annihilations: this event is sometimes referred to as "annihilation catastrophe" [42]. When the temperature of the Universe drops below $\sim 22$ MeV, the baryon-antibaryon annihilation rate becomes slower than the Universe's expansion rate and the number of baryons and antibaryons freezes, leading to $n_b = n_{\bar{b}}$ and

[3] More precisely, the CMB estimate corresponds to the one reported in the last column of Table 2 in Ref. [39], while that from BBN is extrapolated from Eq. (14) of Ref. [41].

$n_b/n_\gamma \approx n_{\bar{b}}/n_\gamma \approx 10^{-20}$, that is ten orders of magnitude smaller compared to the number of baryons observed today. This suggests that the excess of baryons must have been present in the primordial plasma before the "catastrophe".

In principle, an excess of baryons over antibaryons could have been imprinted in the Universe as an initial condition, but this is probably not the case. Apart from being rather "unnatural" to initiate the Universe with a small dimensionless number ($\eta_B$), given that the Universe most likely has experienced an early period of inflation [43] (see, e.g., Ref. [44] for recent lectures on the topic), any initial asymmetry would have been washed out by the accelerated expansion. In this view, a dynamical generation of the baryon asymmetry after inflation and before the "annihilation catastrophe" at $\mathcal{O}(10)$ MeV is necessary. In the literature, an early mechanism for the generation of the BAU is referred to as *Baryogenesis* (see, e.g., Refs. [45,46] for reviews).

## 1.3 The Lepton Asymmetry of the Universe

Strictly speaking, $\eta_B$ does not quantify completely the matter-antimatter asymmetry of the Universe as the definition of matter includes also leptons, namely electrons ($e$), muons ($\mu$), tauons ($\tau$) and relative neutrinos ($\nu_{e,\,\mu,\,\tau}$). We can define, as for baryons, the parameters $\eta_{\nu_\ell}$ and $\eta_\ell$ as

$$\eta_{\nu_\ell} \equiv \frac{n_{\nu_\ell} - n_{\overline{\nu}_\ell}}{n_\gamma} \tag{1.8}$$

and

$$\eta_\ell \equiv \frac{n_\ell - n_{\overline{\ell}}}{n_\gamma}\,, \tag{1.9}$$

where $n_{\nu_\ell}$ ($n_{\overline{\nu}_\ell}$), $n_e$, $n_\mu$ and $n_\tau$ ($n_{\overline{e}}$, $n_{\overline{\mu}}$ and $n_{\overline{\tau}}$) are the number densities of (anti)neutrinos of lepton flavour $\ell = e,\,\mu,\,\tau$, (anti)electrons, (anti)muons and (anti)tauons, respectively. The Lepton Asymmetry of the Universe (LAU) can therefore be quantified by

$$\eta_L \equiv \sum_{\ell=e,\,\mu,\,\tau} \left(\eta_{\nu_\ell} + \eta_\ell\right)\,. \tag{1.10}$$

While electrons are absolutely stable, with a lower bound on the lifetime that reads $\tau_e \gtrsim 6.6 \times 10^{28}\,\mathrm{s}$ [47], muons and tauons have a very short lifetime of about $\tau_\mu \simeq 2.2 \times 10^{-6}\,\mathrm{s}$ and $\tau_\tau \simeq 2.9 \times 10^{-13}\,\mathrm{s}$ [47], respectively. Therefore, muons and tauons, as well as antimuons and antitauons, cannot exist in an appreciable amount in the present Universe and $\eta_e + \eta_\mu + \eta_\tau \simeq \eta_e$. In addition, the electric charge neutrality of the Universe ensures that the electron-positron asymmetry is of the order of the BAU with $\eta_e \approx \eta_B$ (see, e.g., Ref. [48] for some tight constraints on the electric neutrality of the Universe).

Little is known instead about the asymmetry in the neutrino sector. A non-zero $\eta_{\nu_\ell}$ would alter the neutron-to-proton ratio at BBN, as well as the Universe's expansion by changing the effective number of degrees of freedom $N_{\mathrm{eff}}$, with impacts also on the CMB. The requirement that a lepton asymmetry does not spoil BBN and CMB features imposes the rather weak constraint $|\eta_\nu| \equiv |\eta_{\nu_e} + \eta_{\nu_\mu} + \eta_{\nu_\tau}| \lesssim \mathcal{O}(0.1)$ [49–52]. Apart from this, we currently lack direct evidence for $\eta_{\nu_\ell}$ and, consequently, $\eta_L$. This could come in the future from, e.g., the observation of the cosmic neutrino background [53]. For models of physics above the electroweak scale, measuring that $\eta_L \approx \eta_B$ would be a strong evidence in favour of the $(B-L)$-conserving SM sphaleron processes (we will later discuss about those in relation to the scenarios of baryogenesis subject of this

Thesis). Besides, a direct measurement of $\eta_L$ would either support our current understanding of the Universe or open up an exciting window of new physics.

## 1.4 The Sakharov's Conditions

Explaining the matter-antimatter asymmetry in the Universe is one of the most intriguing problems of modern physics [4] and the scientific effort during the past half-century in understanding its generation mechanism has been enormous, but probing the physics behind it remains rather challenging. In turns, there are some very general considerations that one can make. Andrei D. Sakharov was the first who studied the conditions necessary to generate dynamically a baryon asymmetry in the Universe [54]. The three conditions that today go under his name are the following:

1. baryon number $B$ violation;
2. charge conjugation C and charge conjugation combined with parity CP violation;
3. out-of-equilibrium dynamics.

The first condition is evident: any $B \neq 0$ initial condition is diluted away by the accelerated expansion during inflation, but then, a state with equal number of baryons and antibaryons can evolve into a state with more baryons only if processes producing more baryons than antibaryons are allowed. The other two conditions perhaps deserve a closer look and we will describe them in more details in the following subsections. Of course, the same considerations apply to the case of a generation of an asymmetry in each individual flavour lepton number $L_e$, $L_\mu$ and $L_\tau$, or in the total lepton number $L \equiv L_e + L_\mu + L_\tau$.

### 1.4.1 C- and CP-violation

The necessity of C- and CP-violations in the generation of a baryon (lepton) asymmetry can be proven formally with some basic quantum field theory considerations (see, e.g., Ref. [33] for a similar discussion). Consider the baryon number operator defined as

$$\hat{B}_{\rm tot}(t) \equiv \frac{1}{3}\sum_q \int_V d^3x \; q^\dagger(x) q(x), \tag{1.11}$$

where $q(x)$ are the quark fields (spinors) at $x = (t, \vec{x})$, $t$ being the time and $\vec{x}$ the position in space. The operator $\hat{B}_{\rm tot}(t)$ applied to a quantum physical state counts the number of baryons (baryons is made of three quarks) in a volume $V$ at time $t$. It can be shown, using the properties of spinors and discrete symmetries, that the following relations hold:

$$\begin{cases} \hat{P}\hat{B}_{\rm tot}(t)\hat{P}^{-1} = \hat{B}_{\rm tot}(t)\,, \\ \hat{C}\hat{B}_{\rm tot}(t)\hat{C}^{-1} = -\hat{B}_{\rm tot}(t)\,. \end{cases} \tag{1.12}$$

where $\hat{P}$ and $\hat{C}$ are the operators associated with parity (P) and charge conjugation, respectively. Therefore,

$$(\hat{C}\hat{P})\hat{B}_{\rm tot}(t)(\hat{C}\hat{P})^{-1} = -\hat{B}_{\rm tot}(t). \tag{1.13}$$

[4] The problem is interesting at least from the point of view of explaining our own existence.

| **Decays of $X$** | | |
|---|---|---|
| Decay | Branching Ratios | $\Delta B$ |
| $X \to qq$ | $r$ | 2/3 |
| $X \to \overline{q}\overline{\phi}$ | $1-r$ | -1/3 |
| $X \to \overline{qq}$ | $\overline{r}$ | -2/3 |
| $X \to q\phi$ | $1-\overline{r}$ | 1/3 |

**Table 1.1.** All the possible $B$ violating decays of the particle $X$ and its antiparticle $\bar{X}$ of the example discussed in the text, together with the relative branching ratios and variations of baryon number.

The expectation value of $\hat{B}_{\rm tot}(t)$ at time $t$ can be computed as

$$\left\langle \hat{B}_{\rm tot}(t) \right\rangle \equiv {\rm Tr}\left[\rho(t)\hat{B}_{\rm tot}(t)\right], \tag{1.14}$$

where $\rho(t) = \exp(i\hat{H}t)\rho(0)\exp(-i\hat{H}t)$ is the density matrix of the system at time $t$, $\hat{H}$ is the Hamiltonian operator of the system and "Tr" denotes the trace operation. If C was conserved, then the associated operator would commute with the Hamiltonian, i.e. $[\hat{C},\hat{H}] \equiv \hat{C}\hat{H} - \hat{H}\hat{C} = 0$. Consequently, a symmetric state at $t = 0$, for which $\hat{C}\rho(0)\hat{C}^{-1} = \rho(0)$, would remain so at time $t$, namely $\hat{C}\rho(t)\hat{C}^{-1} = \rho(t)$. Hence, we have the following relation:

$$\left\langle \hat{B}_{\rm tot}(t) \right\rangle = {\rm Tr}\left[\rho(t)\hat{B}_{\rm tot}(t)\right] = {\rm Tr}\left[\hat{C}\rho(t)\hat{C}^{-1}\hat{C}\hat{B}_{\rm tot}(t)\hat{C}^{-1}\right] = -\left\langle \hat{B}_{\rm tot}(t) \right\rangle = 0, \tag{1.15}$$

and the same goes for $\hat{C}\hat{P}$, meaning that there would not be any asymmetry at time $t$ if neither C or CP were conserved. The analogous demonstration is valid for the total and flavour lepton numbers. If C and CP were conserved, processes generating baryons and antibaryons (leptons and *antileptons*) would happen at equal rate, thus producing no asymmetry.

The fact that both C and CP needs to be violated for a baryon number non-conservation can be clarified by an example, following Ref. [42]. Suppose to have a non-baryon particle $X$ (and its antiparticle $\overline{X}$), that can decay into a pair of quarks $qq$ (antiquarks $\overline{qq}$) with branching ratio $r$ ($\overline{r}$), or into one antiquark $\overline{q}$ (quark $q$) and some other non-baryon antiparticle $\overline{\phi}$ (particle $\phi$) with branching ratio $1-r$ ($1-\overline{r}$), violating the baryon number by $\Delta B$ units. We assume for simplicity the quarks to be massless (we are interested in temperatures $T \gg T_{\rm EW}$, with $T_{\rm EW} \simeq 160\,{\rm GeV}$ being the temperature of electroweak phase transition [62]). The decay channels, branching ratios and variations of baryon number for the processes of the considered example are summarised in Table 1.1.

Each process can be divided into the one going into left-handed (LH) quarks (antiquarks) with branching ratio $r_L$ ($\overline{r}_L$) and that into right-handed (RH) quarks (antiquarks) with branching ratio $r_R$ ($\overline{r}_R$). The net variation of baryon number is given by

$$B \propto \frac{2}{3}r - \frac{1}{3}(1-r) - \frac{2}{3}\bar{r} + \frac{1}{3}(1-\bar{r}) = r - \bar{r} = r_L + r_R - \bar{r}_L - \bar{r}_R\,. \tag{1.16}$$

If C was conserved, then $r_L = \bar{r}_L$ and $r_R = \bar{r}_R$ and $B$ would be zero. Therefore C violation is needed. If CP is conserved, then we would have $r_L = \bar{r}_R$ and $r_R = \bar{r}_L$, corresponding to a violation of parity, but still $B = 0$. In order to have $B \neq 0$, both C and CP must be violated.

For later purposes, it is useful to illustrate the following other example regarding flavour lepton number violation. Suppose to add to the SM $n \geq 2$ singlet Majorana neutrinos $N_j$ with non-zero masses $M_j > 0$, $j = 1, 2, ..., n$, that couple to a lepton $\ell$ and the Higgs $\Phi$ via Yukawa interaction, namely:

$$-\mathcal{L}_{Y,N}(x) = \sum_{\ell,\, j} Y_{\ell j} \overline{\psi_{\ell L}}(x) i\sigma_2 \Phi^*(x) N_{jR}(x) + \text{h.c.}\,, \tag{1.17}$$

where $Y_{\ell j}$ are the entries of the matrix of the Yukawa couplings, $\psi_{\ell L}(x)$ is the left-handed (LH) lepton doublet field describing the lepton $\ell = e,\, \mu,\, \tau$, $\Phi(x)$ is the Higgs doublet field, $N_{jR}(x)$ is the RH field for the singlet Majorana neutrino $N_j$ and $\sigma_2 = \left(\begin{smallmatrix} 0 & -i \\ i & 0 \end{smallmatrix}\right)$. The Majorana neutrino $N_j$ can either decay into a LH lepton $\ell$ and a Higgs doublet $\Phi$ [5], with the branching ratio $\alpha_\ell^{(j)}$, or into a RH antilepton $\overline{\ell}$ and a conjugate Higgs doublet $\Phi^*$, with branching ratio $\overline{\alpha}_\ell^{(j)} = 1 - \alpha_\ell^{(j)}$. In this case, the net variation of lepton number of flavour $\ell$ is given by:

$$L_\ell \propto \sum_{j=1}^{n} \left(\alpha_\ell^{(j)} - \overline{\alpha}_\ell^{(j)}\right)\,. \tag{1.18}$$

Within this example, since the decays into LH antileptons or RH leptons are not permitted, C is maximally violated. Then, conservation of CP would imply $\alpha_\ell^{(j)} = \overline{\alpha}_\ell^{(j)}$ for any flavor $\ell$ and neutrino index $j$, and thus zero lepton asymmetry. From the explicit expression of Eq. (1.18) in terms of the decay rates into leptons and antileptons, respectively $\Gamma\left(N_j \to \ell\,\Phi\right)$ and $\Gamma\left(N_j \to \overline{\ell}\,\Phi^*\right)$, we can define the *CP-asymmetry parameter*, or simply the *CP-asymmetry*:

$$\epsilon_{\ell\ell}^{(j)} \equiv \frac{\Gamma\left(N_j \to \overline{\ell}\,\Phi^*\right) - \Gamma\left(N_j \to \ell\,\Phi\right)}{\Gamma_{N_j}}\,, \tag{1.19}$$

where $\Gamma_{N_j} \equiv \sum_{\ell=e,\,\mu,\,\tau}\left[\Gamma\left(N_j \to \ell\,\Phi\right) + \Gamma\left(N_j \to \overline{\ell}\,\Phi^*\right)\right]$ is the total decay rate of $N_j$. The CP-asymmetry parameter $\epsilon_{\ell\ell}^{(j)}$ can be non-vanishing for some flavour $\ell$ and Majorana neutrino index $j$ only if CP is violated, implying violation of individual flavour lepton number when $\Sigma_j\, \epsilon_{\ell\ell}^{(j)} \neq 0$ [6]. Since the tree level contribution to $N_j \to \ell\,\Phi$ and $N_j \to \overline{\ell}\,\Phi^*$ decay rates are equal and read (at zero temperature)

$$\sum_{\ell=e,\,\mu,\,\tau} \Gamma^{(0)}\left(N_j \to \ell\,\Phi\right) = \sum_{\ell=e,\,\mu,\,\tau} \Gamma^{(0)}\left(N_j \to \overline{\ell}\,\Phi^*\right) = \frac{(Y^\dagger Y)_{jj}}{16\pi} M_j\,, \tag{1.20}$$

the CP-asymmetry vanishes at tree level. A non-zero CP-asymmetry arises due to the interference of the tree level and one-loop vertex and self-energy diagram contributions depicted in Fig. 1.1. Considering in particular the case of a hierarchical RH Majorana neutrinos mass spectrum, i.e. $M_1 \ll M_2 \ll ... \ll M_n$, the CP-asymmetry related to the decays of $N_1$ takes the following form [55]:

$$\epsilon_{\ell\ell}^{(1)} \simeq \frac{3M_1}{16\pi} \sum_{j\neq 1} \frac{\Im\left[Y_{\ell 1}^* Y_{\ell j} (Y^\dagger Y)_{1j}\right]}{M_j\,(Y^\dagger Y)_{11}}\,, \tag{1.21}$$

with the condition $\epsilon_{\ell\ell}^{(1)} \neq 0$ implying, in general, a non-trivial relation between the entries of the Yukawa matrix and masses of the RH neutrinos.

[5] In the temperature regime we are interested in, i.e. $T \gg T_{\rm EW} \simeq 160\,\text{GeV}$, and neglecting any kind of thermal masses in this discussion, we consider the leptons and the Higgs boson to be massless.

[6] We note also that, within the considered example and CP still violated, the total lepton number $L = L_e + L_\mu + L_\tau$ remains conserved if $\Sigma_\ell\, \Sigma_j\, \epsilon_{\ell\ell}^{(j)} = 0$.

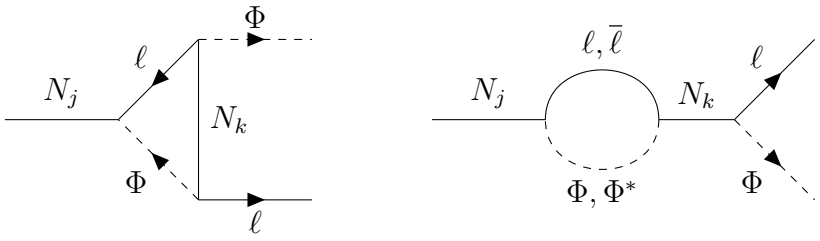


**Figure 1.1.** The Feynman diagrams for the vertex (left) and self-energy (right) contributions to the CP-asymmetry in the example under consideration ($j$, $k = 1, 2, ..., n$). See the text for further details.

### 1.4.2 Out-of-equilibrium dynamics

Similarly to the condition regarding C- and CP-violation, the necessity of out-of-equilibrium dynamics can be proven formally as follows. At equilibrium, the density matrix of the system is, by definition, time translation invariant with $\rho(t) = \rho(0)$ and thus $\rho(t)$ commutes with the Hamiltonian operator. This means that the expectation value of $\hat{B}_{\rm tot}$ is time independent:

$$\left\langle \hat{B}_{\rm tot}(t) \right\rangle = {\rm Tr}\left[\rho(t) e^{i\hat{H}t} \hat{B}_{\rm tot}(0) e^{-i\hat{H}t}\right] = {\rm Tr}\left[e^{i\hat{H}t} \rho(0) \hat{B}_{\rm tot}(0) e^{-i\hat{H}t}\right] = \left\langle \hat{B}_{\rm tot}(0) \right\rangle . \quad (1.22)$$

Denoting by $\hat{\theta}$ the operator of the CPT symmetry transformation, where T is the time reversal operation, we have that $\hat{\theta}\hat{B}_{\rm tot}\hat{\theta}^{-1} = -\hat{B}_{\rm tot}$. According to the CPT theorem [56], CPT is a symmetry of a system in thermal equilibrium, in particular $\left[\hat{\theta}, \rho(0)\right] = 0$, and thus we get that

$$\left\langle \hat{B}_{\rm tot}(0) \right\rangle = {\rm Tr}\left[\rho(0)\hat{B}_{\rm tot}(0)\right] = {\rm Tr}\left[\hat{\theta}\rho(0)\hat{\theta}^{-1}\hat{\theta}\hat{B}_{\rm tot}(0)\hat{\theta}^{-1}\right] = -{\rm Tr}\left[\rho(0)\hat{B}_{\rm tot}(0)\right] = 0 . \quad (1.23)$$

This means that there cannot be any baryon asymmetry at any time $t$ in thermal equilibrium. Again, the same demonstration holds for the total lepton number, as well as for the individual lepton number of any flavour.

The out-of-equilibrium condition can further be understood with the following argument. In thermodynamic equilibrium, inverse processes happen at the same rate as the direct ones, so that the chemical potentials of baryons and antibaryons are equal to zero. Also, CPT theorem ensures that the masses of a particle and its antiparticle are equal. Therefore, the distribution at equilibrium for baryons and antibaryons are the same, implying that $n_b = n_{\bar{b}}$, and, of course, the same goes for leptons.

In the early Universe, a way out-of-equilibrium is ensured by the expansion. As the Universe expands and cools down to smaller temperatures, the primordial plasma experiences various regimes for which different processes become faster or slower than the Universe's expansion, contributing or not to the maintenance of thermal equilibrium. A mathematical tool to study the departure from equilibrium of the system are the Boltzmann Equations (BEs), or generalisations of those obtained from first principles in non-thermal equilibrium quantum field theory, which allow to study the temporal evolution of particle distributions in an expanding environment. Considering the example in the previous section regarding lepton number violation due to the decays of RH neutrinos with hierarchical mass spectrum and assuming, for simplicity, that each lepton flavour asymmetry evolves equally (this is equivalent to consider just one lepton family), we can write the following set of BEs (see, e.g., Ref. [42] for a straightforward

derivation of the BEs in the context of baryogenesis, or Refs. [46,57] for a derivation related to our example):

$$\frac{dN_{N_1}}{dt} = -\langle\Gamma_{N_1}\rangle\left(N_{N_1} - N_{N_1}^{\rm eq}\right) , \tag{1.24}$$

$$\frac{dN_L}{dt} = -\sum_{\ell=e,\,\mu,\,\tau}\epsilon_{\ell\ell}^{(1)}\langle\Gamma_{N_1}\rangle\left(N_{N_1} - N_{N_1}^{\rm eq}\right) - \frac{N_\ell^{\rm eq}}{2N_{N_1}^{\rm eq}}\langle\Gamma_{N_1}\rangle N_L , \tag{1.25}$$

where the quantities $N_{N_1}$ and $N_L$ are respectively the number of RH neutrinos $N_1$ and $L$ asymmetry in a comoving volume, $N_{N_1}^{\rm eq}$ and $N_\ell^{\rm eq}$ are the number of neutrinos and leptons in a comoving volume when in thermal equilibrium and $\langle\Gamma_{N_1}\rangle$ is the thermally-averaged total decay rate of $N_1$. We give below a brief description of each term entering the above equations. The terms proportional to $\langle\Gamma_{N_1}\rangle N_{N_1}$ and $\langle\Gamma_{N_1}\rangle N_{N_1}^{\rm eq}$ describe the destruction and creation of RH neutrinos and, correspondingly, of a lepton asymmetry, due to decays and the relative inverse processes, respectively. The term proportional to $N_L$ in Eq. (1.25) describe the so-called *wash-out* processes, namely the effects due to inverse decays that, in thermal equilibrium, tend to damp exponentially any pre-existing or initially generated asymmetry.

The time scale for variations of the number densities is given by the inverse of the Hubble parameter $1/H$, i.e. $d/dt \propto H$. We can then distinguish two relevant regimes. At temperatures for which $\langle\Gamma_{N_1}\rangle \gg H$, decays and inverse decays are fast enough to maintain thermal equilibrium and $N_{N_1} = N_{N_1}^{\rm eq}$. In this situation, there is no generation of a lepton asymmetry as the source term in Eq. (1.25) proportional to $(N_{N_1} - N_{N_1}^{\rm eq})$ vanishes and the wash-out effects erase any relic asymmetry. Conversely, at temperatures for which $\langle\Gamma_{N_1}\rangle \ll H$, decays and inverse decays are too slow to keep thermal equilibrium (wash-outs are also not effective) and the time evolution stops, with the number of neutrinos and lepton asymmetry freezing at some constant values. Such departure from equilibrium permits to accumulate an asymmetry in the early Universe. Within this mathematical framework and only from dimensional considerations, the necessity of an out-of-equilibrium dynamics appears evident, but, of course, to make quantitative estimations, a more accurate description must be provided. Moreover, one should take into account other processes eventually contributing to the asymmetry generation, such as, e.g., scatterings, and consider additional terms in the BEs. The overall picture, however, remains qualitatively similar to the one we have outlined above.

## 1.5 Baryogenesis Within the Standard Model

As we are going to discuss in this section, the SM contains all the ingredients for an early mechanism of baryon asymmetry generation, in the sense that the three Sakharov's conditions are fulfilled without assuming any new physics. The baryon and lepton number violation proceeds as follows. In the SM there are four global $U(1)$ symmetries that are accidental, meaning that they are present only because of the particle content and the renormalisability condition of the theory. The conserved charges associated with these symmetries are indeed the baryon number $B$ and the three lepton numbers of different flavour $L_e$, $L_\mu$ and $L_\tau$ (clearly also $L = L_e + L_\mu + L_\tau$ is conserved). However, these symmetries taken separately are anomalous, namely they are broken at the quantum level. It can be shown that the baryonic and leptonic currents, respectively $J_B^\mu$ and $J_L^\mu$, at the non-perturbative level do not satisfy the continuity

equation, but rather the following condition [58]:

$$\partial_\mu J^\mu_B = \partial_\mu J^\mu_L = \frac{n_f}{32\pi^2}\left(-g^2 \mathrm{Tr}\left[G_{\mu\nu}\tilde{G}^{\mu\nu}\right] + g'^2 G'_{\mu\nu}\tilde{G}'^{\mu\nu}\right) , \tag{1.26}$$

where $g$, $G_{\mu\nu}$ and $g'$, $G'_{\mu\nu}$ are the gauge coupling and field strength tensor of the $\mathrm{SU(2)_L}$ and $\mathrm{U(1)_Y}$ gauge interaction, respectively; $\tilde{G}^{(\prime)}_{\mu\nu} \equiv (1/2)\varepsilon_{\mu\nu\rho\sigma}G^{(\prime)\rho\sigma}$, $\varepsilon$ being the antisymmetric tensor and $\mu$, $\nu$, $\rho$, $\sigma = 0$, 1, 2, 3 Lorentz indices; $n_f$ is the number of fermionic families, that is $n_f = 3$ in the SM. Evidently, $B - L$ remains conserved as $\partial_\mu(J^\mu_B - J^\mu_L) = 0$, and the same goes for $B/3 - L_\ell$ for any $\ell = e$, $\mu$, $\tau$, while $B + L$ is violated. Assuming that currents vanish at the boundaries, the variation of either baryonic or leptonic charges at time $t$ in a volume $V$ are given by:

$$\Delta B(t) = \Delta L(t) = n_f Q(t) , \tag{1.27}$$

with

$$Q(t) \equiv \frac{1}{n_f}\int_0^t dt' \int_V d^3x' \partial_\mu J^\mu_B \tag{1.28}$$

The configuration of the gauge fields in the vacua of the theory are such that the quantity $\int_V d^3x' J^0_B/n_f$ is an integer number, called the *Chern-Simons number* $N_{\mathrm{CS}}$, so that $Q(t) = N_{\mathrm{CS}}(t) - N_{\mathrm{CS}}(0)$. There are infinite vacuum configurations, distinguished by different values of $N_{\mathrm{CS}}$ and separated by energy barriers, and there can be non-perturbative processes that change fields configurations from one vacuum to another, violating the baryon and lepton number by multiples of $n_f$. Tunnelling processes, also called *instantons*, are possible at vanishing temperatures, but their rate is strongly suppressed by $\sim \exp(-16\pi^2/g^2) \approx 10^{-170}$ [58–60]. At high temperatures, thermal fluctuations make the transitions possible through the so-called *sphalerons* [61], which are the field configurations at the maxima of the energy barriers and are characterised by half-integer Chern-Simons numbers. Compared to the Universe's expansion, the rate of sphaleron processes is larger than the Hubble parameter $H$ for temperatures in the range $T_{\mathrm{sph}} \lesssim T \lesssim 10^{12}\,\mathrm{GeV}$, with $T_{\mathrm{sph}} = 131.7\,\mathrm{GeV}$ [62]. In this regime of temperatures, $B + L$ is violated effectively, while $B - L$ remains conserved.

Taking under consideration the processes that are in thermal equilibrium at temperature above $T_{\mathrm{sph}}$, namely the gauge and the non-perturbative sphaleron processes, as well as the quark and lepton Yukawa interactions (that are in equilibrium for every flavour at $T \lesssim 85\,\mathrm{TeV}$ [63]), together with the conservation of the hypercharge, it is possible to write relations between the chemical potential of the various particles composing the plasma and, correspondingly, between the numbers $B$, $L$ and $B - L$ (see, e.g., Ref. [64]):

$$B = c_s(B - L) , \quad L = (c_s - 1)(B - L) . \tag{1.29}$$

with the sphaleron coefficient $c_s$ given by [64, 65]

$$c_s = \begin{cases} (8n_f + 4n_H)/(22n_f + 13n_H) & T \gtrsim T_{\mathrm{EW}} , \\ [8n_f + 4(n_H + 2)]/[24n_f + 13(n_H + 2)] & T \lesssim T_{\mathrm{EW}} , \end{cases} \tag{1.30}$$

where $T_{\mathrm{EW}} \simeq 160\,\mathrm{GeV}$ [62] is the temperature of the electroweak phase transition (EWPT) and $n_H$ is the number of Higgs doublets in the theory [7]. In the SM we have $n_f = 3$ and $n_H = 1$, so

[7] A more precise calculation depending on the Higgs expectation value and temperature can be found in Ref. [66].

that

$$c_s = \begin{cases} 28/79 & T \gtrsim T_{\rm EW}\,, \\ 12/37 & T \lesssim T_{\rm EW}\,. \end{cases} \tag{1.31}$$

The relations in Eq. (1.29) mean that the $(B+L)$-violating sphaleron processes, as long as they are in thermal equilibrium, convert any $B-L$ asymmetry into a baryon and a lepton asymmetry. However, it also follows that, if $B-L$ is preserved, any baryon and lepton asymmetry is cancelled by sphaleron processes at equilibrium [67].

As regards the other two Sakharov's conditions, C is maximally violated in the SM, the condition of CP-violation is satisfied in the quark sector due to the complexity of the Cabibbo-Kobayashi-Maskawa quark-mixing matrix $V_{\rm CKM}$ [68–71] and the out-of-equilibrium dynamics can be achieved around the EWPT and sphaleron decoupling [72]. More specifically, in this context an asymmetry in the baryon number can be achieved during/after the departure from equilibrium of the sphaleron processes. However, such mechanism of matter-antimatter asymmetry generation generation cannot predict a BAU as large as the one observed today assuming just SM physics. First of all, the CP-asymmetry due to $V_{\rm CKM}$ computed at the relevant electroweak scale is tremendously small $\approx 10^{-20}$ [73, 74]. Secondly, given the mass of the Higgs $m_H \simeq 125\,\text{GeV}$ [75, 76], the EWPT is not enough of the first-order kind (it is more like a smooth crossover rather than a phase transition) to prevent the sphaleron erasure of the baryon asymmetry [67, 72, 77–79]. It is therefore rather challenging, if not impossible, to think of a mechanism of baryogenesis within the SM physics.

## 1.6 Baryogenesis Beyond the Standard Model

The need for an early generation of baryon asymmetry and the impossibility for the SM to predict a mechanism that does the job force us to consider new physics Beyond the SM (BSM). Besides, there is further motivation to look for BSM physics since the SM faces many other issues (like, to list a few, it lacks an explanation for the neutrino masses and mixing [80]; it does not contain a viable dark matter candidate [81]; it fails to describe dark energy [82]), which is why it is typically a good approach to search for SM extensions that solve more than one problem at the same time. Following the first work by Sakharov [54], a plethora of BSM models for baryogenesis has been proposed, but with the caveat of being, in general, rather complicated to be probed at laboratories. The first efforts were done in the context of Grand Unified Theories (GUTs) [83–87].

The principal scope of GUTs is to unify the electroweak and strong forces by grouping together the known particles into few fundamental representations of a large gauge group, e.g. SU(5) or SO(10) (see, e.g., Ref [88] for a recent review). As a consequence, massive scalar bosons and spin-1 mediators appear together with C-, CP- and $B$-violating interactions, providing a framework of baryogenesis in the expanding Universe. However, apart from suffering from constraints on the proton decay that sets the mass of the GUT bosons (i.e. the GUT scale) to $\sim 10^{15}\,\text{GeV}$, the simplest scenarios based on SU(5) violate $B+L$ but conserve $B-L$ and thus, as pointed out already in the previous section, any asymmetry would be destroyed by sphaleron processes in thermal equilibrium. On the other hand, GUTs based on the SO(10) gauge group implement $(B-L)$-violation with RH Majorana neutrinos with masses below the GUT scale, and thus are safe from the sphaleron erasure.

A natural way to introduce RH Majorana neutrinos, not necessarily related to GUTs, is by means of the type-I seesaw extension of the SM [89–93] that, as we will review in details in the next chapter, provides an explanation of the smallness of neutrino masses and the existence of the baryon asymmetry. More precisely, a lepton asymmetry generated in the early Universe by the $L$-, C- and CP-violating processes involving RH neutrinos (e.g. decays, as in the second example of Sec. 1.4.1) is translated into the present BAU by sphalerons. This mechanism, that was first proposed by Masataka Fukugita and Tsutomu Yanagida [94] and later investigated in many different variants, is referred to as (thermal) *leptogenesis* (LG), or, perhaps more rigorously, as baryogenesis via leptogenesis [95] (see, e.g., Refs. [57, 96] for reviews on the topic and Ref. [97] for a useful analytical description). An intriguing feature of LG is its connection to neutrino properties. In particular, the requirement of reproducing the present BAU, i.e. successful/viable LG, can impose conditions on the parameters of the neutrino sector, like the CP-violating phases of the matrix regulating the neutrino mixing and the couplings of the RH neutrinos to the SM (we will introduce all the relevant parameters in the next chapter). Moreover, the low-energy scenarios of *resonant leptogenesis* [98–100], in which the small mass splitting of (at least) two RH neutrinos enhances the CP-asymmetry, and *leptogenesis via oscillations* [101, 102], where the CP-asymmetry is provided by the oscillations of RH neutrinos, are viable for RH Majorana neutrino masses at or below the electroweak scale, corresponding to energies that are accessible at laboratories. Excitingly, during the past decades there have been many important findings in the neutrino sector explainable only with BSM physics and there are current and planned experiments on neutrino physics with potential for discoveries in the near future. Therefore, establishing a solid connection between experiments on neutrino physics and LG scenarios has acquired a vital importance. Moreover, advances in technologies and computational tools made it possible in the past recent years to develop fast and efficient codes for handling the tough numerical computations necessary to make precise LG predictions. The combination of these last points justifies the fact that, despite the LG idea has more than 35 years, the related field of research is still very active. As a matter of fact, this Thesis is about LG and its testability at low-energy experiments on neutrino physics. After reviewing the neutrino physics and the type-I seesaw extension in Chapter 2, in Chapters 3 and 4 we will discuss novel aspects of various thermal LG scenarios at different scales, from the MeV to the GUT scale, as we have studied in Pubs. [II, I, III], and concentrate on their connection to low-energy observables, highlighting the possibility to either test or falsify the considered scenarios at currently running or planned experiments on neutrino and flavour physics. We will describe the powerful `ULYSSES` Python package we have developed in Pub. [IV] and used for our numerical analyses in Appendix A.

A remarkable result which has recently drawn much attention is the possibility to test the scale of LG in the type-I seesaw extension with gravitational waves (GWs). Even if we are not going to discuss this point further, as it lies beyond the scope of the present Thesis, we think it is worth mentioning such very attractive possibility that could provide complementary probe of LG, establishing a link between particle physics, gravitation and cosmology. The seesaw extension and RH neutrino masses can be the result of the spontaneous breaking of a $\mathrm{U}(1)_{B-L}$ gauge symmetry that protects the $B-L$ number at high-energy scales [103–105]. The breaking of $\mathrm{U}(1)_{B-L}$ is accompanied by a stochastic background of GWs generated by one-dimensional cosmological defects, i.e. cosmic strings [106–108], the detection of which at ongoing and future GWs detectors could probe the entire mass range that is relevant for successful LG [109, 110].

In the next chapters of the present Thesis, we are going to focus only on thermal LG within

the type-I seesaw extension and we are not going to discuss about any other mechanism of generation of the BAU. However, we end this section by listing, for completeness, some alternative and most popular models of baryogenesis. For instance, there is the idea of *electrowaeak baryogenesis* [67, 111, 112], for which the baryon asymmetry generation happens around the EWPT, properly modified with respect to the SM version. This scenario relies on: a first-order phase transition with efficient nucleation and propagation of bubbles of broken and unbroken phases; CP-violating processes at the boundaries of such bubbles; variations in the rate of $(B + L)$-violating sphaleron processes across the boundaries. An attractive property of electroweak baryogenesis is the possibility to impose conditions on masses and couplings of Higgs bosons. Moreover, GW signals can originate from early first-order phase transitions, making electroweak baryogenesis in principle testable at, e.g., the proposed Laser Interferometer Space Antenna (LISA) [113]. In turns, models of electroweak baryogenesis are constrained by Large Hadron Collider (LHC) observations [114]. Actually, most of the known models are ruled out by stringent bounds on the electric dipole moment [115, 116], making the construction of viable models very challenging (see Ref. [46] and references quoted therein). Another possibility is the *Affleck-Dine mechanism* [117, 118], in which baryogenesis is induced by a scalar field with a large expectation value, that, while "rolling" towards the origin of its potential, decays into SM particles satisfying the three Sakhraov's conditions. A reason why this mechanism is attractive is that, in principle, it can lead to an asymmetry in any combination of $B$ and $L$. However, it typically deals with supersymmetric models (few alternatives of the Affleck-Dine mechanism without involving supersymmetry has been recently proposed in Refs. [119, 120]), for which there is thus far no evidence at colliders. To conclude, it is worth mentioning that there are multiple variants of LG differing from the thermal scenarios of interest for this Thesis. For example, there are many non-thermal models related to inflation, such as those proposed in Refs. [121, 122] where the RH neutrinos are produced via the decay of an inflaton. Such non-thermal inflation-related models are of particular interest because the measurements of primordial GWs could set the scale of the reheating temperature [123] and thus the scale of LG. Those listed in this paragraph are only some popular possibilities for mechanisms of baryon and lepton asymmetry generations, but many other proposals exist in the literature and we refer to, e.g., Ref. [46], and references quoted therein, for a comprehensive recent review on the topic.

# CHAPTER 2

# Neutrino Physics, the Seesaw Extension and Leptogenesis

## 2.1 Neutrino Masses and Mixing

Solar, atmospheric, reactor and accelerator neutrino experiments have proven that neutrinos oscillate between different flavours (see, e.g., Ref. [124] and references therein): a phenomenon that can only happen if neutrinos have masses [125–127] and mix. The neutrino flavour oscillations can be explained by assuming that the flavour neutrinos, that is, the neutrinos that take part in the electroweak interactions, are a mixture of mass eigenstates. It follows that there is a non-zero probability for a travelling neutrino (or antineutrino) of initial flavour $\ell$ to be detected with a different flavour $\ell' \neq \ell = e,\, \mu,\, \tau$, after a certain distance. In the 3-neutrino mixing scheme, which is the one we have employed in Pubs. [I, II, III], the mixing relation reads [124]:

$$\nu_{\ell L}(x) = \sum_{a=1}^{3} (U_{\rm PMNS})_{\ell a} \nu_{aL}(x), \tag{2.1}$$

where $\nu_{\ell L}(x)$, $\ell = e, \mu, \tau$, is the LH flavour neutrino field (which enters into the expression of the weak interaction Lagrangian), $\nu_{aL}(x)$, $a = 1, 2, 3$, is the LH component of the field of a light neutrino $\nu_a$ with mass $m_a$, and $U_{\rm PMNS}$ is the $3 \times 3$ unitary Pontecorvo-Maki-Nakagawa-Sakata (PMNS) neutrino (lepton) mixing matrix. In the standard parametrisation [124], which we have adopted in Pubs. [I, II, III], the PMNS matrix takes to following form:

$$U_{\rm PMNS} = \begin{pmatrix} c_{12}c_{13} & s_{12}c_{13} & s_{13}e^{-i\delta} \\ -s_{12}c_{23} - c_{12}s_{23}s_{13}e^{i\delta} & c_{12}c_{23} - s_{12}s_{23}s_{13}e^{i\delta} & s_{23}c_{13} \\ s_{12}s_{23} - c_{12}c_{23}s_{13}e^{i\delta} & -c_{12}s_{23} - s_{12}c_{23}s_{13}e^{i\delta} & c_{23}c_{13} \end{pmatrix} \times \begin{pmatrix} 1 & 0 & 0 \\ 0 & e^{\frac{i\alpha_{21}}{2}} & 0 \\ 0 & 0 & e^{\frac{i\alpha_{31}}{2}} \end{pmatrix}. \tag{2.2}$$

Here, $c_{ab} \equiv \cos\theta_{ab}$, $s_{ab} \equiv \sin\theta_{ab}$, the angles $\theta_{ab} = [0, \pi/2]$, with $a,\, b = 1,\, 2,\, 3$; $\delta = [0, 2\pi)$ is the Dirac CP-violating (CPV) phase; $\alpha_{21}$ and $\alpha_{31}$ are the two Majorana CPV phases [128], $\alpha_{21(31)} = [0, 4\pi]$ [1]. The Majorana phases cannot be removed by a redefinition of the fields in case the neutrinos are Majorana particles, which is what we have assumed in Pubs. [I, II, III]. The Dirac and Majorana phases can be sources of low-energy leptonic CP-violation. In the case of CP-invariance, we have $\delta = 0,\ \pi$ and $\alpha_{21(31)} = k_{2(3)1}\pi$, with $k_{2(3)1} = 0, 1, 2, 3, 4$.

[1] Within the type-I seesaw mechanism of neutrino mass generation we will consider the mass-eigenstate neutrinos to be Majorana fermions and it proves convenient to work with this extended range of possible values of the two Majorana phases $\alpha_{21,31}$ [129] (see the end of Sec. 2.2).

| Neutrino Masses and Mixing Parameters | | | | | | |
|---|---|---|---|---|---|---|
| **Ordering** | $\theta_{12}$ (°) | $\theta_{13}$ (°) | $\theta_{23}$ (°) | $\delta$ (°) | $\Delta m^2_{\odot}$ ($10^{-5}$ eV$^2$) | $\Delta m^2_{\rm atm}$ ($10^{-3}$ eV$^2$) |
| **NO** | $33.44^{+0.77}_{-0.74}$ | $8.57^{+0.12}_{-0.12}$ | $49.2^{+0.9}_{-1.2}$ | $197^{+27}_{-24}$ | $7.42^{+0.21}_{-0.20}$ | $2.517^{+0.026}_{-0.028}$ |
| **IO** | $33.45^{+0.78}_{-0.75}$ | $8.60^{+0.12}_{-0.12}$ | $49.3^{+0.9}_{-1.1}$ | $282^{+26}_{-30}$ | $7.42^{+0.21}_{-0.20}$ | $-2.498^{+0.028}_{-0.028}$ |

**Table 2.1.** Best-fit values and $1\sigma$ allowed ranges of the neutrino mixing angles $\theta_{12}$, $\theta_{13}$, $\theta_{23}$, and of the $\Delta m^2_{\odot} \equiv \Delta m^2_{21}$ and $\Delta m^2_{\rm atm} \equiv \Delta m^2_{31}$ ($\Delta m^2_{\rm atm} \equiv \Delta m^2_{32}$) in the case of NO (IO) light neutrino mass spectrum, obtained in Ref. [131]. We quote also, for completeness, the best-fit value and $1\sigma$ allowed range of the Dirac CPV phase $\delta$ from [131], even though in the analyses of Pubs. [I, II, III] we have treated it as a free parameter.

In what concerns the light neutrinos masses $m_{1,2,3}$, the "standard" convention of numbering the neutrino mass eigenstates, the one we have adopted in Pubs. [I, II, III], means that $\Delta m^2_{21} \equiv m^2_2 - m^2_1 > 0$ and $\Delta m^2_{31(32)} \equiv m^2_3 - m^2_{1(2)}$ are associated, together respectively with the angles $\theta_{12}$ and $\theta_{23}$, with the observed flavour conversion of solar (electron) neutrinos $\nu_e$ and the dominant oscillations of atmospheric muon neutrinos and antineutrinos, $\nu_\mu$ and $\bar{\nu}_\mu$, while the angle $\theta_{13}$, together with $\Delta m^2_{31(32)}$, is associated with the reactor $\bar{\nu}_e$ oscillations observed in the Daya Bay, RENO and Double Chooz experiments [124]. The enormous amount of neutrino oscillation data accumulated over many years of research (see, e.g., Ref. [9]) made it possible to determine $\Delta m^2_{21}$, $\sin^2\theta_{12}$, $|\Delta m^2_{31}|$ ($|\Delta m^2_{32}|$), $\sin^2\theta_{23}$ and $\sin^2\theta_{13}$ with remarkably high precision (see, e.g., Refs. [130, 131]). We report in Table 2.1 the best-fit values and $1\sigma$ ranges of the three neutrino mixing (or PMNS) angles and the two neutrino mass squared differences obtained from the global neutrino oscillation data analysis in Ref. [131]. The values quoted in Table 2.1 correspond to those used in the numerical analyses we have performed in Pubs. [I, II, III]. It follows from Ref. [131], in particular, that the $3\sigma$ allowed interval of values of the Dirac CPV phase $\delta$ is rather large. Furthermore, the Majorana phases $\alpha_{21}$ and $\alpha_{31}$ cannot be constrained by the neutrino oscillation experiments [132]. Thus, as in the analyses of Pubs. [I, II, III], in the remaining part of this Thesis the Dirac and Majorana CPV phases will be treated as free parameters.

The existing neutrino data, as is well known, do not allow to determine the sign of $\Delta m^2_{31(32)}$, and the two values of $\mathrm{sgn}(\Delta m^2_{31(32)})$ correspond to two possible types of light neutrino mass spectrum, with normal ordering (NO) and inverted ordering (IO), also reflected in Table 2.1. In the widely employed convention, also adopted in Pubs. [I, II, III], the two spectra read:

- **Normal Ordering (NO):** $m_1 < m_2 < m_3$, $\Delta m^2_{31} \equiv \Delta m^2_{\rm atm} > 0$;
- **Inverted Ordering (IO):** $m_3 < m_1 < m_2$, $\Delta m^2_{32} \equiv \Delta m^2_{\rm atm} < 0$.

Depending on the value of the lightest neutrino mass, the light neutrino mass spectrum can also be:

- **Normal Hierarchical (NH):** $0 \simeq m_1 \ll m_2 < m_3$, with $m_2 \simeq \sqrt{\Delta m^2_{21}}$ and $m_3 \simeq \sqrt{\Delta m^2_{31}}$;
- **Inverted Hierarchical (IH):** $0 \simeq m_3 \ll m_1 < m_2$, with $m_1 \simeq \sqrt{|\Delta m^2_{32}| - \Delta m^2_{21}}$ and $m_2 \simeq \sqrt{|\Delta m^2_{32}|}$;

- **Quasi Degenerate (QD):** $m_1 \simeq m_2 \simeq m_3$, with $m^2_{1,2,3} \gg |\Delta m^2_{31(32)}|$.

All the considered spectra are compatible with the existing data on the light neutrino masses [124]. The IO spectrum is disfavoured at approximately $2.7\sigma$ C.L. with respect to the NO spectrum by the global neutrino oscillation data [131].

As it follows from Table 2.1, we have $\Delta m^2_{21} \ll |\Delta m^2_{31(32)}|$, $\Delta m^2_{21}/|\Delta m^2_{31(32)}| \simeq 1/30$. Apart from some hints from the data of the T2K and NO$\nu$A experiments [133, 134] for the possible value of the Dirac phase $\delta$, no other experimental information on the Dirac and Majorana CPV phases in the PMNS matrix is available at present. We recall that, with $\theta_{13} \simeq 0.15$, the Dirac phase $\delta$ can generate CPV effects in neutrino oscillations [128, 135, 136], i.e., a difference between the probabilities of the $\nu_\ell \to \nu_{\ell'}$ and $\bar{\nu}_\ell \to \bar{\nu}_{\ell'}$ oscillations, $\ell \neq \ell' = e, \mu, \tau$. The magnitude of CP-violation in $\nu_\ell \to \nu_{\ell'}$ and $\bar{\nu}_\ell \to \bar{\nu}_{\ell'}$ oscillations ($\ell \neq \ell'$) is determined by the rephasing invariant $J_{\rm CP}$ [137] which [2], in the standard parametrisation of the PMNS matrix, has the form:

$$J_{CP} = \frac{1}{8} \cos\theta_{13} \sin 2\theta_{12} \sin 2\theta_{23} \sin 2\theta_{13} \sin\delta \,. \tag{2.3}$$

If the hints that $\delta$ has a value close to $3\pi/2$ are confirmed by future more precise data, then one would have $J_{CP} \simeq -0.03$, implying that the CP-violating effects in neutrino oscillations would be relatively large and observable in currently running and/or future neutrino oscillation experiments (T2K, NO$\nu$A, T2HK, DUNE, see, e.g., Refs. [9, 124]).

In what concerns the Majorana CPV phases in the PMNS matrix, the flavour neutrino oscillation probabilities $P(\nu_\ell \to \nu_{\ell'})$ and $P(\bar{\nu}_\ell \to \bar{\nu}_{\ell'})$, $\ell, \ell' = e, \mu, \tau$, do not depend on $\alpha_{21}$ nor $\alpha_{31}$ [128, 132]. The Majorana phases can play important roles, e.g., in $|\Delta L| = 2$ processes like the neutrinoless double beta ($(\beta\beta)_{0\nu}$-) decay $(A, Z) \to (A, Z+2) + e^- + e^-$ in which the Majorana nature of massive neutrinos manifests itself (see, e.g., Refs. [138–140]).

Our interest in the Dirac and Majorana CPV phases present in the neutrino mixing matrix is stimulated also by the intriguing possibility that the Dirac phase and/or the Majorana phases in the PMNS matrix can provide the CP-violation necessary for the generation of the observed BAU [129, 141–143], as we have also demonstrated and analysed in detail in Pub. [I] (see Chapter 3).

Finally, we comment briefly on the current limits on the absolute scale of light neutrino masses (or equivalently on the lightest neutrino mass). Using the existing best lower bounds on the $(\beta\beta)_{0\nu}$-decay half-lives of $^{136}_{54}$Xe [144] and $^{76}_{32}$Ge [145], one can obtain the following "conservative" upper limit on the light Majorana neutrino masses, which is in the range of the QD spectrum [146]: $m_{1,2,3} \lesssim 0.58$ eV. The most stringent upper limit on the light neutrino masses, which does not depend on the nature of massive neutrinos, was obtained in the KATRIN experiment by measuring the spectrum of electrons near the end point in tritium $\beta$-decay [147, 148]: $m_{1,2,3} < 0.8$ eV (90% C.L.). The CMB data of the WMAP and PLANCK experiments, combined with supernovae and other cosmological and astrophysical data, can be used to obtain information in the form of an upper limit on the sum of neutrino masses. Depending on the model complexity and the input data used, one typically finds [149] (see also Ref. [130]): $\sum_j m_j < (0.11 - 0.54)$ eV (95% CL).

[2] The $J_{\rm CP}$ factor is analogous to the rephasing invariant associated with the Dirac CPV phase in the quark mixing matrix [70, 71].

## 2.2 The Type-I Seesaw Extension of the Standard Model

The results on LG we are going to discuss in this Thesis, related to our works in Pubs. [I,II,III], are based on the type-I seesaw extension of the SM, which provides a natural explanation of the smallness of neutrino masses and via LG establishes a link between the existence and smallness of neutrino masses and the existence of the baryon asymmetry [89–93]. This rather simple mechanism is realised, as is well known, by extending the SM with $n \geq 2$ RH neutrinos $\nu_{\kappa R}$ (RH neutrino fields $\nu_{\kappa R}(x)$), with $\kappa = 1, 2, ..., n$ [3], that are singlets (sterile) under $\mathrm{SU(3)_C} \times \mathrm{SU(2)_L} \times \mathrm{U(1)_Y}$, possess a Majorana mass term and couple through a Yukawa-type interaction to the SM lepton and Higgs doublets, $(\psi_{\ell L}(x))^T = (\nu^T_{\ell L}(x) \;\; \ell^T_L(x))$, with $\ell = e, \mu, \tau$, and $(\Phi(x))^T = (\Phi^{(+)}(x) \; \Phi^{(0)}(x))$, $(\Phi^*(x))^T = (\Phi^{(-)}(x) \; \Phi^{(0)}(x))$. The minimal type-I seesaw scheme in which LG can be realised is with $n = 2$ RH neutrinos. In this scenario, the lightest neutrino – $\nu_1$ ($\nu_3$) for NO (IO) neutrino mass spectrum – is massless at tree and one-loop level. To this Thesis, both the cases with $n = 3$ and $n = 2$ RH neutrinos are relevant. To keep the discussion more general as possible, we fix $n = 3$ for the following discussion.

In the basis in which the charged lepton Yukawa couplings and mass matrix are diagonal but the Majorana mass term of the RH neutrinos $\nu_{\kappa R}$ is not, the Lagrangian $\mathcal{L}_{\mathrm{Y,M}}(x)$ has the form:

$$\mathcal{L}_{\mathrm{Y,M}}(x) = -\,\widetilde{Y}_{\ell\kappa}\overline{\psi_{\ell L}}(x)\, i\sigma_2\, \Phi^*(x)\, \nu_{\kappa R}(x) - \frac{1}{2}\,\overline{\nu^c_{\kappa L}}(x)\, (M_N)_{\kappa\rho}\, \nu_{\rho R}(x) + \mathrm{h.c.}\,, \tag{2.4}$$

where $\widetilde{Y}$ is the matrix of neutrino Yukawa couplings in the chosen basis, $\nu^c_{\kappa L}(x) \equiv C\,(\overline{\nu_{\kappa R}}(x))^T$, with $C$ being the charge conjugation matrix, and $M_N$ is the Majorana mass matrix of $\nu_{\kappa R}(x)$, $(M_N)_{\kappa\rho} = (M_N)_{\rho\kappa}$ and $\kappa, \rho = 1, 2, 3$. Without loss of generality, one can also work in the basis in which the Majorana mass matrix of RH neutrinos is diagonal and positive, $\hat{M} \equiv \mathrm{diag}(M_1, M_2, M_3)$ with $M_{1,2,3} > 0$. In this case, the neutrino Yukawa and the RH neutrino Majorana mass terms are given by:

$$\mathcal{L}_{\mathrm{Y,M}}(x) = -\,\left(Y_{\ell j}\overline{\psi_{\ell L}}(x)\, i\sigma_2\, \Phi^*(x)\, N_{jR}(x) + \mathrm{h.c.}\right) - \frac{1}{2}\, M_j\, \overline{N_j}(x)\, N_j(x)\,, \tag{2.5}$$

where $Y_{\ell j}$ are the entries of neutrino Yukawa matrix in the considered basis, with $j = 1, 2, 3$ and $\ell = e, \mu, \tau$, while $N_j(x) = N_{jR}(x) + N^c_{jL}(x) = C(\overline{N_j}(x))^T$, with $N^c_{jL}(x) \equiv C(\overline{N_{jR}}(x))^T$. The matrix Y is related to $\tilde{Y}$ via $Y = \widetilde{Y}\widetilde{V}^*$, with $\widetilde{V}$ being a unitary matrix which diagonalises $M_N$ (see, e.g., Ref. [150] and further). Correspondingly, the fields $N_{jR}(x)$ are given in terms of $\nu_{\kappa R}(x)$ by $N_{jR}(x) = \widetilde{V}_{\kappa j}\nu_{\kappa R}(x)$. The fields $N_{1,2,3}(x)$ correspond to Majorana neutrinos $N_{1,2,3}$ with masses $M_{1,2,3} > 0$ which, in the LG scenarios we are going to consider, can have values $M_{1,2,3} \sim (0.1 - 10^{14})$ GeV, much larger than the eV scale of the light neutrino masses, and so we will refer to $N_{1,2,3}$ further on as "heavy Majorana neutrinos" or just "heavy neutrinos".

When the electroweak symmetry is broken spontaneously, the neutrino Yukawa coupling in Eq. (2.4) generates a Dirac mass term, $(M_D)_{\ell\kappa}\,\overline{\nu_{\ell L}}(x)\,\nu_{\kappa R}(x) + \mathrm{h.c.}$, with $M_D = (v/\sqrt{2})\tilde{Y}$, $v = 246$ GeV being the Higgs doublet vacuum expectation value (VEV), and the neutrino mass

[3] The labelling of the RH neutrinos is arbitrary; we could also choose the index $\kappa$ to take, e.g., the values $\kappa = \tilde{e}, \tilde{\mu}, \tilde{\tau}, ..., \tilde{\sigma}$.

Lagrangian takes the form:

$$\begin{aligned}\mathcal{L}^m_\nu(x) &= -\,\overline{\nu_{\ell L}}(x)(M_D)_{\ell\kappa}\nu_{\kappa R}(x) - \frac{1}{2}\overline{\nu^c_{\kappa L}}(x)(M_N)_{\kappa\rho}\,\nu_{\rho R}(x) + \text{h.c.} = \\ &= -\,\frac{1}{2}\begin{pmatrix}\overline{\nu_{\ell L}}(x) & \overline{\nu^c_{\kappa L}}(x)\end{pmatrix}\begin{pmatrix}\mathbb{O}_{\ell\ell'} & (M_D)_{\ell\rho} \\ (M_D^T)_{\kappa\ell'} & (M_N)_{\kappa\rho}\end{pmatrix}\begin{pmatrix}\nu^c_{\ell' R}(x) \\ \nu_{\rho R}(x)\end{pmatrix} + \text{h.c.}\,,\end{aligned} \tag{2.6}$$

where $\nu^c_{\ell' R}(x) \equiv C(\overline{\nu_{\ell' L}}(x))^T$, with $\ell' = e,\,\mu,\,\tau$, and $\mathbb{O}$ is a matrix with all entries null. The two matrices $M_D$ and $M_N$ are complex, in general. Equivalently, in the basis in which the RH Majorana mass matrix is diagonal, one has:

$$\mathcal{L}^m_\nu(x) = -\,\frac{1}{2}\begin{pmatrix}\overline{\nu_{\ell L}}(x) & \overline{N^c_{jL}}(x)\end{pmatrix}\begin{pmatrix}\mathbb{O}_{\ell\ell'} & \frac{v}{\sqrt{2}}Y_{\ell k} \\ \frac{v}{\sqrt{2}}(Y^T)_{j\ell'} & M_j\delta_{jk}\end{pmatrix}\begin{pmatrix}\nu^c_{\ell' R}(x) \\ N_{kR}(x)\end{pmatrix} + \text{h.c.}\,, \tag{2.7}$$

where the index $k$, as for $j$, runs from 1 to 3.

The mass matrix in the second line of Eq. (2.6) can be diagonalised by means of the Takagi transformation, which gives

$$\begin{pmatrix}\mathbb{O} & M_D \\ M_D^T & M_N\end{pmatrix} = \exp\begin{pmatrix}\mathbb{O} & -R \\ R^\dagger & \mathbb{O}\end{pmatrix}\begin{pmatrix}m_\nu^{\rm tree} & \mathbb{O} \\ \mathbb{O} & V\hat{M}_N V^T\end{pmatrix}\exp\begin{pmatrix}\mathbb{O} & R^* \\ -R^T & \mathbb{O}\end{pmatrix}\,, \tag{2.8}$$

where $V$ is a unitary matrix, $\hat{M}_N$ is diagonal and positive, $m_\nu^{\rm tree}$ is the mass matrix of the light neutrinos at tree level and $R$ a complex matrix with "small" entries (see further). Expanding Eq. (2.8) around $R$, gives [150]:

$$R \;\simeq\; M_D M_N^{-1}\,, \tag{2.9}$$

$$m_\nu^{\rm tree} \;\simeq\; -M_D M_N^{-1} M_D^T\,, \tag{2.10}$$

$$V\hat{M}_N V^T \;\simeq\; M_N + \frac{1}{2}(M_N^{-1})^* M_D^\dagger M_D + \frac{1}{2}M_D^T M_D^*(M_N^{-1})^*\,, \tag{2.11}$$

up to corrections of the second order in $M_D M_N^{-1}$. At leading order in $M_D M_N^{-1}$, we have $V \simeq \widetilde{V}$ and $\hat{M}_N \simeq \hat{M}$, as well as

$$RV \simeq M_D M_N^{-1} V = \frac{v}{\sqrt{2}} Y V^T M_N^{-1} V \simeq \frac{v}{\sqrt{2}} Y \hat{M}^{-1}\,, \tag{2.12}$$

the entries of which are typically much smaller than unity, i.e. $|(RV)_{\ell j}| = |(v/\sqrt{2})Y_{\ell j}|/M_j \ll 1$. The relation in Eq. (2.10) is the well known expression for the tree level light neutrino mass matrix $m_\nu^{\rm tree}$, the entries of which, in terms of the Yukawa couplings, read:

$$\left(m_\nu^{\rm tree}\right)_{\ell\ell'} \simeq -\,\frac{v^2}{2} Y_{\ell j}\; M_j^{-1}\left(Y^T\right)_{j\ell'}\,,, \tag{2.13}$$

with $\ell,\,\ell' = e,\,\mu,\,\tau$. The above equation is the essence of the seesaw mechanism and is also referred to as the "seesaw formula" for the light neutrino masses. It is clear from the seesaw formula that the smallness of the light neutrino masses arises naturally if the heavy neutrino masses are larger than the electroweak scale $v$, so that $vM_j^{-1} \ll 1$. However, tiny Yukawa couplings, as well as cancellations between the various terms in the a summation over $j$, could

fairly well be responsible for the smallness of the light neutrino masses. Consequently, for any heavy neutrino masses, one can, in principle, always accommodate the seesaw parameters to generate the light neutrino mass spectrum.

In some situations, like, e.g., when heavy Majorana neutrino masses are not hierarchical and have relatively low values, $M_1 \sim 10^6$ GeV, $M_2 \simeq 3M_1$, $M_3 \simeq 3M_2$, the one-loop radiative correction to the light neutrino mass matrix can be non-negligible [143, 151] [4]. Moreover, the one-loop correction to light neutrino mass matrix has an opposite sign with respect to the tree level contribution. This, in principle, allows for a partial cancellation between the two contributions. In certain cases the cancellation has to be fine-tuned in order to obtain neutrino masses compatible with the existing data. A rather detailed study of this fine-tuning problem was performed in Ref. [143] and we refer to this article for further details. The one-loop contribution to the light neutrino mass matrix is given by [153–155] (see also, e.g., Ref. [156]):

$$(m_\nu^{\text{1-loop}})_{\ell\ell'} = Y_{\ell j}\, \frac{M_j}{32\pi^2} \left( \frac{\log\left(M_j^2/m_H^2\right)}{M_j^2/m_H^2 - 1} + 3\frac{\log\left(M_j^2/m_Z^2\right)}{M_j^2/m_Z^2 - 1} \right) \left(Y^T\right)_{j\ell'} , \tag{2.14}$$

where $m_H = 125$ GeV and $m_Z = 91.2$ GeV are the Higgs and $Z^0$ boson masses, respectively.

The light neutrino mass matrix including the one-loop correction reads [152]:

$$(m_\nu)_{\ell\ell'} \equiv \left(m_\nu^{\text{tree}} + m_\nu^{\text{1-loop}}\right)_{\ell\ell'} = -\frac{v^2}{2}\, Y_{\ell j}\; f(M_j)\, \left(Y^T\right)_{j\ell'} , \tag{2.15}$$

with $\ell,\, \ell' = e,\, \mu,\, \tau$ and

$$f(M_j) \equiv M_j^{-1} - \frac{M_j}{16\pi^2 v^2} \left( \frac{\log\left(M_j^2/m_H^2\right)}{M_j^2/m_H^2 - 1} + 3\frac{\log\left(M_j^2/m_Z^2\right)}{M_j^2/m_Z^2 - 1} \right) , \tag{2.16}$$

with $j = 1,\, 2,\, 3$. The light neutrino mass matrix $m_\nu$ can be diagonalised as

$$\hat{m}_\nu = U^\dagger m_\nu U^* , \tag{2.17}$$

where $\hat{m}_\nu \equiv \text{diag}(m_1,\, m_2,\, m_3)$ and $U$ is a unitary $3 \times 3$ matrix.

The flavour neutrino fields $\nu_{\ell L}(x)$, $\ell = e, \mu, \tau$, which enter into the expressions of the charged and neutral currents in the weak interaction Lagrangian of the SM, are related to the fields of light and heavy neutrinos $\nu_a(x)$ and $N_j(x)$ with definite mass $m_a$ and $M_j$, i.e. the mass eigenstates, via

$$\nu_{\ell L}(x) = (1+\eta) U_{\ell a} \nu_{aL}(x) + (RV)_{\ell j} N_{jL}(x) , \tag{2.18}$$

where $N_{jL}(x)$, $j = 1,\, 2,\, 3$, are the LH components of the fields of the heavy neutrinos $N_j$, $\nu_{aL}(x)$, $a = 1, 2, 3$, are the LH components of the fields of three light Majorana neutrinos $\nu_a$ having masses $m_a \lesssim 0.5\,\text{eV} \ll M_j$ and $\eta = -(1/2)(RV)(RV)^\dagger$. It follows from Eq. (2.18) that, in the seesaw scenario we are considering, the PMNS matrix has the form:

$$U_{\text{PMNS}} = (1+\eta)\, U . \tag{2.19}$$

The matrix $\eta$ describes the deviations from unitarity of the PMNS matrix. The elements of $\eta$ are constrained by electroweak data and data on flavour observables [157, 158]. For $M_j \gtrsim 500$

[4] The higher-order corrections to the light neutrino mass matrix were shown to be suppressed with respect to the tree level and one-loop contributions [151, 152].

MeV and depending on the element of $\eta$, these constraints are in the range $(10^{-4} - 10^{-3})$ at $2\sigma$ C.L. For $M_j$ larger than the electroweak scale, the constraint on $\eta_{e\mu} = \eta_{\mu e}$ is even stronger: $|\eta_{e\mu}| < 1.2 \times 10^{-5}$. Given the stringent upper bounds on the elements of $\eta$, to a very good approximation one has: $U_{\rm PMNS} \simeq U$, which is given in the standard parametrisation by Eq. (2.2).

The quantity $(RV)_{\ell j}$ in Eq. (2.18), with $\ell = e$, $\mu$, $\tau$ and $j = 1$, 2, 3, determines the strength of the charged current (CC) and neutral current (NC) weak interaction couplings of the heavy Majorana neutrino $N_j$ (field $N_j(x)$) to the $W^{\pm}$ bosons ($W^{\mu}(x)$ vector field) and the charged LH lepton $\ell$ (field $\psi_{\ell L}(x)$), and to the $Z^0$ boson ($Z^{\mu}(x)$ vector field) and the LH flavour neutrino $\nu_{\ell L}$ (field $\nu_{\ell L}(x)$) in the weak interaction Lagrangian:

$$\mathcal{L}^{N}_{\rm CC}(x) \;=\; -\frac{g}{2\sqrt{2}}\,\overline{\psi_{\ell L}}(x)\,\gamma_{\mu}\,(RV)_{\ell j}(1-\gamma_5)\,N_j(x)\,W^{\mu}(x) \;+\; \text{h.c.}\,, \tag{2.20}$$

$$\mathcal{L}^{N}_{\rm NC}(x) \;=\; -\frac{g}{4c_w}\,\overline{\nu_{\ell L}}(x)\,\gamma_{\mu}\,(RV)_{\ell j}\,(1-\gamma_5)\,N_j(x)\,Z^{\mu}(x) \;+\; \text{h.c.}\,, \tag{2.21}$$

where $c_w \equiv \cos\theta_w$, $\theta_w$ is the weak mixing angle and $\gamma_{\mu}$, $\mu = 0$, 1, 2, 3, are the gamma matrices. The magnitude of the couplings $(RV)_{\ell j}$ in the region of the parameter space of successful LG is crucial for the possibility to test the low-scale LG scenarios studied in Pubs. [II, III].

With $m_{\nu}$ given by Eq. (2.15), the Casas-Ibarra parametrisation [159] of the neutrino Yukawa couplings takes the form [152]:

$$Y_{\ell j} = \pm i\frac{\sqrt{2}}{v}U_{\ell a}\sqrt{m_a}O_{ja}\sqrt{f^{-1}(M_j)}\,, \tag{2.22}$$

where $O$ is a complex orthogonal matrix, $O^T\,O = O\,O^T = \mathbb{1}$. The infinite possibilities to explain the mass spectrum and mixing of light neutrinos given any heavy neutrino masses $M_j$ are encoded in the Casas-Ibarra matrix $O$ (also simply called, in what follows, the "matrix $O$" or the "$O$-matrix"). The usual parametrisation for the matrix $O$, e.g., adopted in Pubs. [II, I], is that given in terms of three Euler complex angles and reads:

$$O = \mathcal{R}^{(23)}(\theta_1)\,\mathcal{R}^{(13)}(\theta_2)\,\mathcal{R}^{(12)}(\theta_3)\,, \tag{2.23}$$

where $\mathcal{R}$ are $3 \times 3$ rotation matrices (complex, in general) with $\mathcal{R}\mathcal{R}^T = \mathbb{1}$ and their entries defined as:

$$\left[\mathcal{R}^{(ab)}(\theta_c)\right]_{jk} = \left\{\delta_{jk}\left[\delta_{jc} + (\delta_{ja} + \delta_{jb})\cos\theta_c\right] + (\delta_{ja}\delta_{kb} - \delta_{jb}\delta_{ka})\sin\theta_c\right\}_{a\neq b\neq c}\,, \tag{2.24}$$

where $j$, $k$, $a$, $b$, $c = 1$, 2, 3, $\theta_c \equiv x_c + i\,y_c$ and $x_c$, $y_c \in \mathbb{R}$, for any $c$.

The parametrisation has six parameters. An equivalent alternative parametrisation was utilised in Ref. [160] and Pub. [III], with the following form:

$$O^T = \mathcal{R}^{(13)}(\omega_2^{(\nu)})\,\mathcal{R}^{(23)}(\omega_1^{(\nu)})\,\mathcal{R}^{(12)}(\theta_C)\,\mathcal{R}^{(23)}(\omega_1^{(N)})\,\mathcal{R}^{(13)}(\omega_2^{(N)}), \tag{2.25}$$

where $\theta_C \equiv \omega_C + i\xi_C$ and $\omega_1^{(\nu)}$, $\omega_2^{(\nu)}$, $\omega_1^{(N)}$, $\omega_2^{(N)}$, $\omega_C$, $\xi_C \in \mathbb{R}$. This parametrisation proves convenient in the three heavy Majorana neutrino case since it involves just one complex angle $\theta_C$.

In discussing our works of Pubs. [I, II], we will be interested also in the case of decoupled heavy Majorana neutrino $N_3$, for which the lightest neutrino, as is well known, is massless at

tree and one loop level, i.e., $m_1 \simeq 0$ ($m_3 \simeq 0$), and the light neutrino mass spectrum is either NH or IH. In such framework, the six parameters of the $O$-matrix reduce to two and, for the NH and IH light neutrino mass spectra of interest, the matrix $O$ takes the following forms:

$$O^{(\mathrm{NH})} = \begin{pmatrix} 0 & O_{12} & O_{13} \\ 0 & O_{22} & O_{23} \\ 1 & 0 & 0 \end{pmatrix} = \begin{pmatrix} 0 & \cos\theta & \sin\theta \\ 0 & -\sin\theta & \cos\theta \\ 1 & 0 & 0 \end{pmatrix}, \tag{2.26}$$

$$O^{(\mathrm{IH})} = \begin{pmatrix} O_{11} & O_{12} & 0 \\ O_{21} & O_{22} & 0 \\ 0 & 0 & 1 \end{pmatrix} = \begin{pmatrix} \cos\theta & \sin\theta & 0 \\ -\sin\theta & \cos\theta & 0 \\ 0 & 0 & 1 \end{pmatrix}, \tag{2.27}$$

with $\theta \equiv \omega + i\xi$. In Pub. [I] a different notation was used for which $\theta \equiv x + iy$. In this Thesis we will interchange between the two different notations, namely $\omega \equiv x$ and $\xi \equiv y$. The parameters $\omega$ and $\xi$ play important roles in the LG scenario considered, e.g., in our work of Pub. [II]. For large values of $\xi$, such that $e^{\xi} \gg e^{-\xi}$, the couplings $(RV)_{\ell j}$ are enhanced and, e.g., for NH (IH) spectrum we have:

$$\sum_{\ell,j} |(RV)_{\ell j}|^2 = \frac{1}{M}(m_{2(1)} + m_{3(2)})\cosh(2\xi) \simeq \frac{1}{2M}(m_{2(1)} + m_{3(2)})e^{2\xi}. \tag{2.28}$$

The $O$-matrix given in Eqs. (2.23) to (2.27) for different parametrisations have $\det(O) = 1$. Often, in the literature on the subject, a factor $\varphi = \pm 1$ is included in the definition of certain elements of $O$ to allow for the both cases $\det(O) = \pm 1$. In discussing our works of Pubs. [I,II,III], we will alternate between the different parametrisations in Eqs. (2.23) to (2.27) without the factor $\varphi$, but extend the range of the Majorana phases $\alpha_{21(31)}$ from $[0, 2\pi]$ to $[0, 4\pi]$, which effectively accounts for both cases of $\det(O) = \pm 1$ [129]. In this way, the same full set of $O$ and Yukawa matrices is considered.

## 2.3 Leptogenesis Within the Type-I Seesaw Extension

The generation of a matter-antimatter asymmetry in the expanding Universe can naturally be accomplished within the type-I seesaw framework through thermal LG [94]. Provided the Yukawa couplings and/or Majorana mass terms in Eqs. (2.4) or (2.5) are CPV, the out-of-equilibrium processes involving the heavy Majorana neutrinos, the leptons and the Higgs doublets in the early expanding Universe generate CP-asymmetries in the individual lepton flavour charges $L_e$, $L_\mu$ and $L_\tau$, as well as in the total lepton charge $L$ (therefore violating the $B/3 - L_{e,\mu,\tau}$ charges and total $B - L$ number). The so generated lepton asymmetry is then translated into an asymmetry in the baryon charge $B$ by the SM $(B+L)$-violating, but $(B-L)$-conserving, sphaleron processes, which are effective at temperatures between $T \simeq T_{\mathrm{sph}} - 10^{12}$ GeV, $T_{\mathrm{sph}} \simeq 131.7\,\mathrm{GeV}$ being the sphaleron decoupling temperature [62].

Naively, the LG idea may appear rather simple, but the formalism with which it is usually described can become quite complicated. In fact, depending on the spectrum and the values of the masses of the heavy Majorana neutrinos, thus also the LG scale, various effects and processes other than the heavy neutrino decays can play a determinant role in the generation of the BAU. Additional contributions can arise, e.g., from resonances, flavour and thermal effects,

oscillations, scattering and spectator processes (see, e.g., Ref. [57] were many of the relevant effects are extensively reviewed). Correspondingly, the sets of differential equations that, in the various regimes of LG, are relevant to describe the time evolution of the asymmetries and the number densities of heavy Majorana neutrinos can become numerically demanding [IV].

Another challenging task is to connect the minimal scenarios of LG to quantities that can be measured (or fitted) at currently running or future experiments. If the heavy neutrinos are way too massive compared to the energy reach of experimental facilities, say with masses at roughly the TeV to the GUT scale, it is hard, if not impossible, to produce them at colliders. Moreover, for such large masses, the couplings of the heavy neutrinos with the SM that are also compatible with successful LG are usually too small for any detectable signal. Nevertheless, in the case of *low-energy CP-violation*, for which only the CPV phases of the PMNS matrix could provide the necessary amount of CP-asymmetry to generate the BAU [129, 141–143], the requirement of having successful LG can impose conditions on the PMNS phases or, conversely, LG can receive constraints from measurements that are sensitive to the CPV phases [I, 143]. If instead the masses of the heavy neutrinos are at or below the $\sim$ TeV scale, and, in addition, the couplings are sufficiently large, there are chances to probe the parameter space of low-energy scenarios of LG [II, III, 160–163].

In the subsections that follow, we are going to describe the various scenarios of LG that were considered in our works of Pubs. [I, II, III] and thus are of interest for this Thesis. We will illustrate the relevant effects that were taken into account in the mass ranges of interest, together with the sets of equations that were solved in order to predict the generation of the present BAU. The specific results obtained in the works in Pub. [I] and Pubs. [II, III] will be expanded in Chapters 3 and 4, respectively, where we will also focus the attention on how to eventually probe or falsify the various scenarios at low-energy experiments. We devote Appendix A to the description of the `ULYSSES` Python package that was developed and published in our work of Pub. [IV] and that was used in the numerical analyses of Pubs. [I, II] to solve the relevant equations [5].

### 2.3.1 High-Scale Thermal Leptogenesis

In the classical high-scale thermal LG scenario, the generation of the BAU happens due to the out-of-equilibrium $L$-, C- and CP-violating decays (and inverse decays) of $N_{1,2,3}$ [6]. In the widely studied scenario with the heavy neutrinos having (strongly) hierarchical mass spectrum, i.e. $M_1 \ll M_2 \ll M_3$, for which the decays of the lightest heavy neutrino $N_1$ dominate the BAU generation, LG takes place at *high-scales* which are typically by a few to several orders of magnitude smaller than the scale of unification of the electroweak and strong interactions, say for $M_1 \sim 10^9 - 10^{14}\,\text{GeV}$ [165] (see also further in Sec. 2.3.2 and Chapter 3). Testing experimentally this high-scale LG scenario seems impossible at present. Nevertheless, an important connection to low-energy observables that one can make in such scenarios is provided by the request of low-energy CP-violation, with the Dirac CPV phase $\delta$ and/or the Majorana CPV phases $\alpha_{21}$ and/or $\alpha_{31}$, as well as any combination of those, being the only source of CP-violation. However, in such minimal LG scenario, it is well-known that the unitarity of the

[5] The equations considered in Pub. [III] were solved numerically with a different code, which is currently under development and thus not available yet.

[6] In such scenario, the contributions from scattering processes and thermal effects are typically sub-leading (if not negligible) compared to the contributions from the $N_{1,2,3}$ decays [57, 97, 143, 164].

PMNS matrix leads to zero CP-asymmetry in the total lepton number when CP-violation is only at low-energy. Successful LG with low-energy CP violation is only possible if the asymmetry in each individual lepton flavour evolves differently. The effects of flavour separations in the context of LG are called *flavour effects* [166–169] (see also Refs. [170–172]), to which we give a description in what follows.

**Flavour effects in leptogenesis**

The charged lepton final states in the decays of the heavy neutrino $N_j$, $N_j \to \Phi^+ \psi_j$ and $N_j \to \Phi^- \overline{\psi_j}$, are a superposition of the charged lepton flavour states, namely,

$$|\psi_j\rangle = \sum_{\ell=e,\,\mu,\,\tau} C_{j\ell} |\psi_\ell\rangle \,, \tag{2.29}$$

$$|\overline{\psi_j}\rangle = \sum_{\ell=e,\,\mu,\,\tau} \overline{C}^*_{j\ell} |\overline{\psi_\ell}\rangle \,, \tag{2.30}$$

with the coefficients $C_{j\ell}$ and $\overline{C}_{j\ell}$ at tree level [7] given by

$$C_{j\ell} = \overline{C}_{j\ell} = \frac{Y_{\ell j}}{\sqrt{(Y^\dagger Y)_{jj}}} \,. \tag{2.31}$$

We will be interested in the decays of $N_1$, $N_1 \to \Phi^+ \psi_1$ and $N_1 \to \Phi^- \overline{\psi_1}$, so further on we replace index $j$ with 1.

If it were not for the SM charged lepton Yukawa interactions, the quantum states $|\psi_1\rangle$ and $|\overline{\psi_1}\rangle$ would be coherent superpositions of the charged lepton flavour states. However, when these interactions are in thermal equilibrium, i.e., their rates are larger than the expansion rate of the Universe, given the difference between the charged lepton Yukawa couplings, $h_e$, $h_\mu$, $h_\tau$, the flavour states become distinguishable and each flavour state experiences a different time-evolution – actually, it is enough for the SM $\tau$- and $\mu$-Yukawa interactions to be in equilibrium for the three lepton flavours to be distinguishable. If the SM charged lepton Yukawa interactions are faster than the process of the heavy neutrino decay into (anti)leptons, then the coherence in $|\psi_1\rangle$ ($|\overline{\psi_1}\rangle$) is efficiently destroyed [174] (see, e.g., also [169]) – in this sense these are *decoherence effects*. The relevant processes are the interchanges between the LH leptons with their respective RH components and vice-versa through scattering processes involving the Higgs doublet. By means of the optical theorem, the rates of these processes involving the tauon and the muon, $\Gamma_\tau$ and $\Gamma_\mu$, are given by the imaginary part of the $\tau$, $\mu$ thermal self-energy and read [151, 173] (see also, e.g., Ref. [57] and references therein): $\Gamma_{\tau,\,\mu} \simeq 8 \times 10^{-3} h^2_{\tau,\,\mu}\, T$. The comparison of $\Gamma_\tau$

[7] The one-loop contributions to the $N_j$ decay would lead to corrections to $C_{j\ell}$ and $\overline{C}_{j\ell}$ (see, e.g., Eqs. (24) and (25) of [173]). However, as these corrections would lead to sub-leading $\mathcal{O}(\epsilon^2)$ effects, we do not consider them here.

and $\Gamma_\mu$ with the Hubble expansion rate $H$ gives [8]:

$$\frac{\Gamma_\tau}{H} \simeq \frac{M_P}{T}\, 4.85\times 10^{-8} \simeq \left(\frac{1\ \text{GeV}}{T}\right)\, 5.92\times 10^{11}\,, \tag{2.32}$$

$$\frac{\Gamma_\mu}{H} \simeq \frac{M_P}{T}\, 1.72\times 10^{-10} \simeq \left(\frac{1\ \text{GeV}}{T}\right)\, 2.10\times 10^{9}\,, \tag{2.33}$$

where $M_P \simeq 1.22\times 10^{19}$ GeV is the Planck mass.

**Single-flavour regime**

At $T \gg 10^{12}$ GeV, the rates of the $\tau$- and $\mu$-Yukawa interactions are much smaller than the expansion rate of the Universe, i.e. $\Gamma_{\tau,\mu}/H \ll 1$. As a consequence, the flavour states are indistinguishable and the (anti)leptons produced via the $N_1$'s decay are always found in the coherent superposition defined in Eq. (2.29) ((2.30)). This is the *unflavoured* or *single-flavour regime*. For $M_1 \gg 10^{12}$ GeV, LG proceeds in the unflavoured regime for its entire duration and is usually studied within the *single-flavour approximation*, under which the $\mu$- and $\tau$-decoherence effects are neglected. Correspondingly, this scenario is typically dubbed *unflavoured* or *single-flavoured leptogenesis*. In the single-flavour approximation, the time-evolution of the number densities of $N_1$ and $B-L$ charge can be described by the set of semi-classical *single-flavoured Boltzmann equations* (1BE1F):

$$\frac{dN_{N_1}}{dz} = -D_1\left(N_{N_1} - N_{N_1}^{\text{eq}}\right)\,, \tag{2.34}$$

$$\frac{dN_{B-L}}{dz} = \epsilon^{(1)} D_1\left(N_{N_1} - N_{N_1}^{\text{eq}}\right) - W_1 N_{B-L}\,, \tag{2.35}$$

where $z \equiv M_1/T$. The quantities $N_{N_1}$ and $N_{B-L}$ are respectively the number of heavy neutrinos $N_1$ and $B-L$ asymmetry in a comoving volume. In the present work and in Pubs. [I, II, III, IV] the comoving volume is normalised as in Refs. [143, 151, 175] so that it contains one photon at z = 0, i.e., $N_{N_1}^{\text{eq}}(0) = 3/4$. This normalisation within the Boltzmann statistics is equivalent to using $N_{N_1}^{\text{eq}}(z) = (3/8) z^2 K_2(z)$, where $K_n(z)$, $n = 1\,, 2\,,$ ..., is the modified $n^{\text{th}}$ Bessel function of the second kind.

The decay parameter $D_1$ is given by:

$$D_1(z) = \kappa_1 z \frac{K_1(z)}{K_2(z)}, \tag{2.36}$$

where $\kappa_1$ is defined as the ratio between the total decay rate of $N_1$ at zero temperature, $\Gamma_{N_1}^{(0)} = (Y^\dagger Y)_{11} M_1/8\pi$, and the Hubble expansion rate $H$ at $z = 1$. It proves convenient to write $\kappa_1$ in the following form:

$$\kappa_1 = \frac{\tilde{m}_1}{m_*}, \tag{2.37}$$

[8] The $\tau$- and $\mu$-Yukawa couplings are given by $h_\tau = \sqrt{2} m_\tau/v \simeq 1.02\times 10^{-2}$ and $h_\mu = \sqrt{2} m_\mu/v \simeq 6.08\times 10^{-4}$, where $m_\tau$ and $m_\mu$ are the $\tau^\pm$ and $\mu^\pm$ masses, respectively, and $v = 246$ GeV. Given the smallness of the $e$-Yukawa coupling $h_e = \sqrt{2} m_e/v \simeq 2.94\times 10^{-6}$, $m_e$ being the $e^\mp$ mass, the $e$-Yukawa interactions come into thermal equilibrium only at $T \lesssim 10^5$ GeV, being therefore ineffective at the temperatures of interest to the analysis under discussion.

where

$$\tilde{m}_1 \equiv (Y^\dagger Y)_{11} v^2/2M_1\,, \quad m_* \equiv (8\pi^2 v^2/3M_P)\sqrt{g_*\pi/5} \approx 10^{-3}\ \text{eV}\,, \tag{2.38}$$

$g_* = 106.75$ being the number of relativistic degrees of freedom at $z = 1$. The wash-out parameter $W_1$ reads:

$$W_1(z) = \frac{1}{2N_\ell^{\rm eq}}\, D_1(z)\, N_{N_1}^{\rm eq}(z)\,, \tag{2.39}$$

where $N_\ell^{\rm eq}$ is the equilibrium number density of leptons at $z = 0$, which, within the adopted normalisation, is given by $N_\ell^{\rm eq} = N_{N_1}^{\rm eq}(0) = 3/4$ [9].

Finally, the CPV-asymmetry parameter $\epsilon^{(1)}$ is given by [55, 176, 177] [10]:

$$\epsilon^{(1)} = \frac{3}{16\pi (Y^\dagger Y)_{11}} \sum_{j\neq 1} \Im\left[(Y^\dagger Y)^2_{1j}\right] \frac{\xi(x_j)}{\sqrt{x_j}}\,, \tag{2.40}$$

with $x_j \equiv M_j^2/M_1^2$ and

$$\xi(x) \equiv \frac{2}{3} x \left[(1+x)\log\left(1+\frac{1}{x}\right) - \frac{2-x}{1-x}\right]\,. \tag{2.41}$$

We note that for large $x$, $\xi(x) = 1 + \mathcal{O}(1/x)$, so that, in the hierarchical limit $M_1 \ll M_2 \ll M_3$, $\epsilon^{(1)} \propto M_1$ since $1/\sqrt{x_j} = M_1/M_j$ and in this limit $(Y^\dagger Y)_{11} \propto M_1$ and $\Im\left[(Y^\dagger Y)^2_{1j}\right] \propto M_1 M_j$ [11].

Since the Yukawas enter in $\epsilon^{(1)}$ only through the product $Y^\dagger Y$, there is no dependence on the PMNS matrix. There is therefore no contribution to $\epsilon^{(1)}$ from the CPV Dirac and Majorana phases in the PMNS matrix and, in particular, $\epsilon^{(1)} = 0$ when the CP-violation is only of the low-energy type.

### 1-to-2 flavour transition

As the mass scale of LG is lowered to $M_1 \sim 10^{12}$ GeV, the single-flavour approximation becomes inaccurate since the SM $\tau$-Yukawa interactions enter in equilibrium during the generation of the lepton asymmetry, i.e. $\Gamma_\tau/(Hz) \sim 1$. This is a transition regime, which we will refer to as *1-to-2 flavour transition*, where the $\tau$-decoherence effects cannot be neglected. Moreover, as was noticed in Ref. [143], when the requisite CP violation in LG is provided exclusively by the Dirac and/or Majorana CPV phases of the PMNS matrix, the 1-to-2 flavour transition proceeds with an unusual behaviour of the baryon asymmetry $\eta_B$, which extends into the region of the unflavoured regime at $M_1 > 10^{12}$ GeV. We have investigated this unusual behaviour in Pub. [I] and we will discuss it in details in Chapter 3. Here it suffices to mention that due to CPV quantum decoherence effects caused by the SM $\tau$-Yukawa interactions, in which CP-violation is provided by the low-energy leptonic CPV phases, the generation of the BAU in the single-flavour approximation as described by Eqs. (2.34) and (2.35) fails and that the observed BAU

[9] A detailed derivation of Eqs. (2.36) - (2.39) is given, e.g., in Ref. [97].

[10] We work with the same sign convention used in Ref. [143], so the CP-asymmetry has an opposite sign with respect to that defined in [55]. As we also noted in Pub. [I], there is a wrong sign typo in the last expression in Eq. (2.44) in Ref. [143] – this can be checked by summing Eq. (2.53) of the same article over the flavour indices.

[11] To be more precise, in $\epsilon^{(1)}$ also factors of the form $f^{-1}(M_{2,3})/M_{2,3}$, given in Eq. (2.16), appear inside the summation. However, the mass dependence of these factors is logarithmic and, in the mass range $10^9 \lesssim M_1/\text{GeV} \lesssim 10^{14}$ of interest to us, $f^{-1}(M_1)/M_1$ changes only by a factor of 1.1 taking values in the interval $1.1 - 1.3$.

can still be generated at $M_1 > 10^{12}$ GeV even if $\epsilon^{(1)} = 0$ and the $\tau$-Yukawa interactions are not in full thermal equilibrium. The basic reason is that the flavour asymmetries evolve differently due to wash-out differences caused by the $\tau$-Yukawa wash-out interactions.

### Two-flavour regime

For $10^9 \ll T/\text{GeV} \ll 10^{12}$, the $\tau$-Yukawa interactions are in thermal equilibrium while that of muons are not, namely $\Gamma_\tau/H \gg 1$ while $\Gamma_\mu/H \ll 1$ . Correspondingly, the $\tau$-(anti)lepton state becomes distinguishable from the other flavour states and the coherence in $|\psi_1\rangle$ ($|\overline{\psi_1}\rangle$) gets eventually destroyed. As a consequence, the CP-asymmetry in $L_\tau$ evolves differently with respect to the asymmetry in the sum of $L_e$ and $L_\mu$ charges, $L_{\tau^\perp} \equiv L_{e+\mu} \equiv L_e + L_\mu$. This corresponds to the *two-flavour regime* of LG.

For $10^9 \ll M_1/\text{GeV} \ll 10^{12}$, the $\tau$-Yukawa ($\mu$-Yukawa) interactions enter in thermal equilibrium at $z \ll 1$ ($z \gg 1$) and LG can be studied within the *two-flavour approximation* under which only the $\mu$-decoherence effects are neglected. If in addition the $\tau$-Yukawa interactions are assumed to be infinitely (="sufficiently") fast during the whole period of LG, the *two-flavoured Boltzmann equations* (1BE2F) can be used to describe the time-evolution of the CPV asymmetries in the $L_\tau$ and $L_{\tau^\perp}$ charges and of BAU. This scenario of LG with two flavours is typically called *two-flavoured leptogenesis*. The set of 1BE2F equations in the two-flavour approximation reads:

$$\frac{dN_{N_1}}{dz} = -D_1 \left(N_{N_1} - N_{N_1}^{\text{eq}}\right) , \tag{2.42}$$

$$\frac{dN_{\tau\tau}}{dz} = \epsilon^{(1)}_{\tau\tau} D_1 \left(N_{N_1} - N_{N_1}^{\text{eq}}\right) - W_1 p_{1\tau} N_{\tau\tau} , \tag{2.43}$$

$$\frac{dN_{\tau^\perp\tau^\perp}}{dz} = \epsilon^{(1)}_{\tau^\perp\tau^\perp} D_1 \left(N_{N_1} - N_{N_1}^{\text{eq}}\right) - W_1 p_{1\tau^\perp} N_{\tau^\perp\tau^\perp} , \tag{2.44}$$

where $p_{1\tau} = |C_{1\tau}|^2$ and $p_{1\tau^\perp} = |C_{1e}|^2 + |C_{1\mu}|^2 = 1 - p_{1\tau}$, while $N_{\tau\tau}$ and $N_{\tau^\perp\tau^\perp}$ are respectively the values of the asymmetries in the charges $B/3 - L_\tau$ and $2B/3 - L_{\tau^\perp}$ in a comoving volume, so that $N_{B-L} = N_{\tau\tau} + N_{\tau^\perp\tau^\perp}$. The expressions for the relevant CPV lepton asymmetries $\epsilon^{(1)}_{\tau\tau}$ and $\epsilon^{(1)}_{\tau^\perp\tau^\perp} = \epsilon^{(1)}_{ee} + \epsilon^{(1)}_{\mu\mu}$ will be given below.

### 2-to-3 flavour transition

As the mass scale is lowered to $M_1 \sim 10^9$ GeV, LG approaches the *2-to-3 flavour transition*, where the $\mu$-decoherence effects cannot be neglected since the $\mu$-Yukawa interactions enter in equilibrium during LG, i.e. $\Gamma_\mu/(Hz) \sim 1$. Therefore, the two-flavour approximation ceases to be accurate. Actually, as we have shown in Pub. [I] and will review in details in Chapter 3, there are choices of the parameters for which the 1BE2F equations are never accurate and cannot be used for the description of LG in the whole range $10^9 \lesssim M_1/\text{GeV} \lesssim 10^{12}$. In addition, in certain regions of the parameter space, the scale below which the 1BE2F set of equations starts to be valid can be significantly lower than $\sim 10^{12}$ GeV.

### Three-flavour regime

At $T \ll 10^9$ GeV, also the $\mu$-Yukawa interactions are in thermal equilibrium, i.e. $\Gamma_\mu/H \gg 1$. This is the *three-flavour regime*: all the flavours are distinguishable, the coherent superposition

in $|\psi_1\rangle$ ($|\overline{\psi_1}\rangle$) is fully destroyed and each flavoured asymmetry in $L_\ell$ ($\ell = e,\, \mu,\, \tau$) evolve separately. At $M_1 \ll 10^9$ GeV, both the $\mu$- and $\tau$-Yukawa interactions enter in equilibrium at $z \ll 1$ corresponding to the *three-flavoured leptogenesis* scenario. If the $\mu$- and $\tau$-Yukawa interactions are assumed to be infinitely (≡"sufficiently") fast, then LG can be described by the *three-flavoured Boltzmann equations* (1BE3F), namely:

$$\frac{dN_{N_1}}{dz} = -D_1 \left(N_{N_1} - N_{N_1}^{\rm eq}\right) , \tag{2.45}$$

$$\frac{dN_{ee}}{dz} = \epsilon_{ee}^{(1)} D_1 \left(N_{N_1} - N_{N_1}^{\rm eq}\right) - W_1 p_{1e} N_{ee} , \tag{2.46}$$

$$\frac{dN_{\mu\mu}}{dz} = \epsilon_{\mu\mu}^{(1)} D_1 \left(N_{N_1} - N_{N_1}^{\rm eq}\right) - W_1 p_{1\mu} N_{\mu\mu} , \tag{2.47}$$

$$\frac{dN_{\tau\tau}}{dz} = \epsilon_{\tau\tau}^{(1)} D_1 \left(N_{N_1} - N_{N_1}^{\rm eq}\right) - W_1 p_{1\tau} N_{\tau\tau} , \tag{2.48}$$

where $p_{1\ell} = |C_{1\ell}|^2$, while $N_{\ell\ell}$ is the value of the asymmetry in the charge $B/3 - L_\ell$ in a comoving volume, so that $N_{B-L} = \sum_{\ell=e,\,\mu,\,\tau} N_{\ell\ell}$.

The CP-asymmetries $\epsilon_{\ell\ell}^{(1)}$ in the both set of equations 1BE2F and 1BE3F are given by [55, 176, 177] [12]:

$$\epsilon_{\ell\ell}^{(1)} = \frac{3}{16\pi \left(Y^\dagger Y\right)_{11}} \sum_{j\neq 1} \left\{ \Im \left[Y_{\ell 1}^* Y_{\ell j} (Y^\dagger Y)_{1j}\right] f_1 \left(x_j\right) + \Im \left[Y_{\ell 1}^* Y_{\ell j} (Y^\dagger Y)_{j1}\right] f_2 \left(x_j\right) \right\} , \tag{2.49}$$

where

$$f_1 \left(x\right) \equiv \frac{\xi \left(x\right)}{\sqrt{x}} , \quad f_2 \left(x\right) \equiv \frac{2}{3 \left(x-1\right)} . \tag{2.50}$$

In Eq. (2.49), $\ell = \tau^\perp, \tau$ and $\ell = e, \mu, \tau$ for the 1BE2F and 1BE3F equations (2.43) - (2.44) and (2.46) - (2.48), respectively, and $\epsilon_{\tau^\perp\tau^\perp}^{(1)} = \epsilon_{ee}^{(1)} + \epsilon_{\mu\mu}^{(1)}$. We have: $\sum_\alpha \epsilon_{\alpha\alpha}^{(1)} = \epsilon^{(1)}$, with $\epsilon^{(1)}$ as given in Eq. (2.40). We note that the expression in Eq. (2.49) corresponds to that of Eq. (1.21) in the limit of $x_{2,3} \simeq 0$.

**Density matrix equations – a unifying formalism**

To obtain a better description of the physics of LG, the decoherence effects should always be included in the calculations. As already shown in, e.g., Refs. [173, 174, 178], the *density matrix equations* (DMEs) provide an accurate tool to study thermal LG accounting for quantum decoherence processes, especially when these are neither infinitely fast nor their effects negligible. The DMEs describe the time evolution of the entries of the charged lepton flavour density matrix, which, in the three-flavour basis, is given by

$$N = \sum_{\alpha,\beta} N_{\alpha\beta} |\psi_\alpha\rangle\langle\psi_\beta| \tag{2.51}$$

with $\alpha,\, \beta = e,\, \mu,\, \tau$. The diagonal entries $N_{\alpha\alpha}$ are the already defined number densities for the $B/3 - L_\alpha$ asymmetry, so that $N_{B-L} = {\rm Tr}(N) = \sum_\alpha N_{\alpha\alpha}$. The off-diagonal elements $N_{\alpha\beta}$

[12] As will later be clarified, the double indices are necessary in the quantum treatment since the off-diagonal terms become relevant.

describe the degree of coherence between the flavour states. The DMEs in the three-flavour basis explicitly read [173, 174, 178]:

$$\frac{dN_{N_1}}{dz} = -D_1(N_{N_1} - N_{N_1}^{\rm eq}) \tag{2.52}$$

$$\frac{dN_{\alpha\beta}}{dz} = \epsilon_{\alpha\beta}^{(1)} D_1(N_{N_1} - N_{N_1}^{\rm eq}) - \frac{1}{2} W_1 \left\{P^{0(1)}, N\right\}_{\alpha\beta} - \frac{\Gamma_\tau}{Hz}\left[I_\tau, [I_\tau, N]\right]_{\alpha\beta} - \frac{\Gamma_\mu}{Hz}\left[I_\mu, [I_\mu, N]\right]_{\alpha\beta} , \tag{2.53}$$

where $I_\tau$ and $I_\mu$ are $3\times 3$ matrices such that $(I_\tau)_{\alpha\beta} = \delta_{\alpha\tau}\delta_{\beta\tau}$ and $(I_\mu)_{\alpha\beta} = \delta_{\alpha\mu}\delta_{\beta\mu}$, and

$$P_{\alpha\beta}^{0(1)} \equiv C_{1\alpha} C_{1\beta}^* , \tag{2.54}$$

are projection matrices which generalise the notion of the projection probability. They appear in the anti-commutator structure, which explicitly reads:

$$\left\{P^{0(1)}, N\right\}_{\alpha\beta} = \sum_{\gamma=e,\,\mu,\,\tau} \left(C_{1\alpha} C_{1\gamma}^* N_{\gamma\beta} + C_{1\gamma} C_{1\beta}^* N_{\alpha\gamma}\right) . \tag{2.55}$$

The double-commutator structures in Eq. (2.53) give rise to an exponentially damping term proportional to $\Gamma_{\tau,\,\mu}/(Hz)$ for the equations describing the off-diagonal elements of $N$. If these terms are infinitely large, i.e., $\Gamma_{\tau,\,\mu}/(Hz) \to +\infty$, the density matrix is driven towards a diagonal form and the DMEs reduce to the three-flavoured set of Boltzmann equations 1BE3F. The CPV-asymmetry parameters are [55, 167, 173, 176–179]:

$$\epsilon_{\alpha\beta}^{(1)} = \frac{3}{32\pi\,(Y^\dagger Y)_{11}} \sum_{j\neq 1} \Bigg\{ i\left[Y_{\alpha 1} Y_{\beta j}^* (Y^\dagger Y)_{j1} - Y_{\beta 1}^* Y_{\alpha j} (Y^\dagger Y)_{1j}\right] f_1\left(x_j\right) + i\left[Y_{\alpha 1} Y_{\beta j}^* (Y^\dagger Y)_{1j} - Y_{\beta 1}^* Y_{\alpha j} (Y^\dagger Y)_{j1}\right] f_2\left(x_j\right) \Bigg\} . \tag{2.56}$$

Setting $\alpha = \beta = \ell$ in the above expression reproduces the asymmetry $\epsilon_{\ell\ell}^{(1)}$ defined in Eq. (2.49), while the trace coincides with the expression for $\epsilon^{(1)}$ given in Eq. (2.40).

In Pub. [IV], we have introduced the `ULYSSES` Python package, that is a numerical solver for BEs and DMEs in the context of LG. Specifically, given a certain set of equations like those introduced in the present section, the code computes $N_{B-L} = N_{ee} + N_{\mu\mu} + N_{\tau\tau}$, which is then converted into the baryon asymmetry of the Universe $\eta_B$ expressed in terms of the baryon-to-photon ratio using the following relation:

$$\eta_B = \frac{c_s}{27} N_{B-L}(z_{\rm sph}) , \tag{2.57}$$

where $z_{\rm sph} \equiv M_1/T_{\rm sph} \ll 1$, $c_s \approx 0.3$ is the SM sphaleron conversion coefficient given in Eq. (1.30) and the 1/27 factor comes from the dilution of the baryon asymmetry due to the change of the photon density between LG and recombination [97]. We give a detailed description of the code in Appendix A and postpone to Chapter 3 the discussion of the results we have obtained in Pub. [I] by solving with `ULYSSES` the sets of equations described in this section.

### 2.3.2 Flavoured Resonant Leptogenesis

The simplest "unflavoured" scenario of high-scale thermal LG with hierarchical heavy Majorana neutrinos suffers from the Davidson-Ibarra bound [165], which imposes a lower limit on the mass of the lightest $N_j$ for successful LG. The Davidson-Ibarra bound arises from the following argument. The CP-asymmetry for the total lepton number related to $N_1$ (see Eqs. (1.21) and (2.49)), after adopting the Casas-Ibarra parametrisation in Eq. (2.22) (neglecting the one-loop contribution, i.e. $f^{-1}(M_j) \simeq M_j$), results in [57, 165]:

$$\left|\epsilon^{(1)}\right| \simeq \left|\frac{3M_1}{8\pi v^2}\frac{\sum_a m_a^2 \Im\left(O_{1a}^2\right)}{\sum_a m_a |O_{1a}|^2}\right| \lesssim \frac{3M_1}{8\pi v^2}\sqrt{|\Delta m^2_{\rm atm}|} \simeq 10^{-7}\left(\frac{M_1}{10^9\,{\rm GeV}}\right) . \tag{2.58}$$

The form of the solution to the 1BE1F sets of equations given in Eqs. (2.34) to (2.35) is $N_{B-L}^{\rm 1BE1F} = \epsilon^{(1)}\kappa_{\rm eff}$, and, from Eq. (2.57), $\eta_B \simeq 10^{-2}\epsilon^{(1)}\kappa_{\rm eff}$, where $\kappa_{\rm eff} \lesssim 1$ is an efficiency factor arising from the out-of-equilibrium dynamics [97]. It then follows from Eq. (2.58) that it is possible to have $\eta_B \approx 10^{-9}$ in the unflavoured scenario only for $M_1 \gtrsim 10^9\,{\rm GeV}$. This is the Davidson-Ibarra bound on the LG scale first discussed in Ref. [165]. More precise numerical calculation would of course result in an improved constraint [13]. Actually, a rather detailed analysis of the high-scale thermal (non-resonant) LG scenario with three RH neutrinos performed in Refs. [143, 151] showed that, with flavour effects taken into account and mildly hierarchical heavy Majorana neutrino masses, $M_2 \sim 3M_1$, $M_3 \sim 3M_2$, the Davidson-Ibarra bound can be relaxed and the LG scale can be as low as $M_1 \sim 10^6$ GeV. Nevertheless, the scale remains too high to be tested at present (if ever) at laboratories.

A unique possibility to have a significantly lower mass scale of LG is provided by the scenario of resonant leptogenesis (RLG) [98–100, 176, 177, 182–185]. In this scenario, the generation of the BAU is compatible with masses of the heavy Majorana neutrinos at the sub-TeV scales, i.e. *low-scales*, making RLG testable, in principle, at colliders (LHC and/or future planned) and/or at low-energy experiments (see, e.g., our works in Pubs. [II, III]). In the simplest case with two heavy Majorana neutrinos $N_{1,2}$, the resonant regime is realised if $N_{1,2}$ form a pseudo-Dirac pair [14] [187, 188] such that the splitting between their masses, $\Delta M \equiv M_2 - M_1 > 0$, is of the order of the $N_{1,2}$ decay widths $\Gamma_{N_{1,2}}$: $\Delta M/\Gamma_{N_{1,2}} \sim 0.5$, which typically implies also that $\Delta M \ll M_{1,2}$. Under such condition, the CP-asymmetry receives an enhanced contribution from the self-energy part (the diagram on the right in Fig. 1.1) with the exact form (see further) depending on the ratio $\Delta M/\Gamma_{N_{1,2}}$ rather than the mass scale, thus being free from the Davidson-Ibarra bound.

In RLG the baryon asymmetry is produced exclusively by the CP-violating $N_j$ and Higgs decays mediated by the neutrino Yukawa couplings. We have re-visited this scenario using the formalism of BEs most recently in Pub. [II], concentrating on the case of $M_{1,2} \lesssim 100$ GeV, $\Delta M \ll M_{1,2}$ (for earlier discussions see, e.g., Refs. [189, 190]). For such small mass scales, the sphaleron decoupling happens when $z_{\rm sph} \equiv M/T_{\rm sph} \lesssim 1$, $M \equiv M_1 \simeq M_2$, regime for which thermal effects are important [57, 97, 164] and relevant, e.g., in activating kinematically the Higgs decay into leptons and heavy neutrinos. Both the relevant $1 \leftrightarrow 2$ heavy neutrinos and Higgs direct and inverse decays, as well as $2 \leftrightarrow 2$ scattering processes (involving quarks and

[13] Also, it has been demonstrated in Refs. [180, 181] that one can use the Davidson-Ibarra bound to obtain an upper limit on the scale of the light neutrino masses in the case of a QD spectrum.

[14] It was shown in Ref. [186] that, in this case, the radiative corrections to the light neutrino masses are negligible.

gauge fields), including flavour effects and thermal effects (thermal masses and soft collinear processes involving gauge fields in the thermal plasma), were taken into account in Pub. [II]. The relevant systems of equations in this framework are the three-flavoured BEs with two heavy neutrinos (2BE3F) and are given by (see, e.g., Refs. [57, 166, 191]) [15]:

$$\frac{dN_{N_j}}{dz} = -\left(D_j + S_j^t + S_j^s\right)\left(N_{N_j} - N_{N_j}^{\rm eq}\right), \tag{2.59}$$

$$\frac{dN_{\ell\ell}}{dz} = \sum_j \left[\epsilon_{\ell\ell}^{(j)} D_j (N_{N_j} - N_{N_j}^{\rm eq}) - \left(W_j^D + W_j^t + \frac{N_{N_j}}{N_{N_j}^{\rm eq}} W_j^s\right) p_{j\ell} N_{\ell\ell}\right] . \tag{2.60}$$

Here, $z \equiv M/T$ and the quantities $N_{N_j}$, $N_{N_j}^{\rm eq}$, $N_{\ell\ell}$ and $p_{j\ell}$, $j = 1, 2$, are defined as in the previous Sec. 2.3.1 (it is straightforward to adapt the definitions in the case of a single heavy neutrino $N_1$ to the case of a pair $N_{1,2}$). The other quantities $D_j$, $S_j^t$, $S_j^s$, $W_j^D$, $W_j^t$, $W_j^t$ and the CP-asymmetry $\epsilon_{\ell\ell}^{(j)}$ in the resonant case are functions of $z$ and defined in what follows.

### The decay and scattering terms

The terms $D_j$ and $W_j^D$ are due to the $1 \leftrightarrow 2$ decays and inverse decays, while

$$S_j^t = 4\left[S_{A_t j}^{(\rm gauge)} + S_{H_t j}^{(\rm quark)}\right] , \tag{2.61}$$

$$S_j^s = 2\left[S_{A_s j}^{(\rm gauge)} + S_{H_s j}^{(\rm quark)}\right] , \tag{2.62}$$

$$W_j^t = 4\left[W_{A_t j}^{(\rm gauge)} + W_{H_t j}^{(\rm quark)}\right] , \tag{2.63}$$

$$W_j^s = 2\left[W_{A_s j}^{(\rm gauge)} + W_{H_s j}^{(\rm quark)}\right] , \tag{2.64}$$

account for scattering processes. The terms $S_{A_t j}^{(\rm gauge)}$ ($W_{A_t j}^{(\rm gauge)}$) and $S_{A_s j}^{(\rm gauge)}$ ($W_{A_s j}^{(\rm gauge)}$) are contributions respectively from $t$- and $s$-channel $2 \leftrightarrow 2$ scattering processes ($\Delta L = 1$) involving the SM gauge fields [164]. Similarly, $S_{H_t j}^{(\rm quark)}$ ($W_{H_t j}^{(\rm quark)}$) and $S_{H_s j}^{(\rm quark)}$ ($W_{H_s j}^{(\rm quark)}$) are contributions from $t$- and $s$-channel $2 \leftrightarrow 2$ scattering processes ($\Delta L = 1$) involving the top quark.

For the total contributions of the $2 \leftrightarrow 2$ processes involving the SM gauge fields and the top quark to the production of $N_j$ and to the wash-out terms we get from Eqs. (2.61) - (2.64):

$$S_i^{(\rm gauge)} = 4\, S_{A_t j}^{(\rm gauge)} + 2\, S_{A_s j}^{(\rm gauge)} , \tag{2.65}$$

$$S_i^{(\rm quark)} = 4\, S_{H_t j}^{(\rm quark)} + 2\, D_{H_s j}^{(\rm quark)} , \tag{2.66}$$

$$W_j^{(\rm gauge)} = 4\, W_{A_t j}^{(\rm gauge)} + 2\, W_{A_s j}^{(\rm gauge)} , \tag{2.67}$$

$$W_j^{(\rm quark)} = 4\, W_{H_t j}^{(\rm quark)} + 2\, W_{H_s j}^{(\rm quark)} . \tag{2.68}$$

In Pub. [II] we took into account the thermal effects in the production of $N_{1,2}$ in Eqs. (2.59) and (2.60) using the results derived in Ref. [196] for $D_j$, $S_j^{(\rm gauge)}$ and $S_j^{(\rm quark)}$ in the relevant case

[15] These equations approximate the results of Refs. [192, 193] for RLG. The latter results should agree with those of Ref. [194] to within a factor $\sim 2$ [195] in the nearly degenerate mass regime considered in this analysis. Also, in the mass range of interest to RLG at sub-TeV scales, the three lepton flavours are fully decoupled and thus evolve independently from each other, so that a density matrix treatment for the flavour asymmetries is not necessary.

of relativistic $N_{1,2}$. As was shown in Ref. [196], the indicated three contributions vary little in the interval of temperatures of interest, $T \sim (100 - 1000)$ GeV, and we have approximated them as constants equal to their respective average values in this interval. Adapting the results obtained in Ref. [196] to the set-up utilised by us in Pub. [II] we get:

$$D_j = 0.232 \frac{\kappa_j}{z^2 K_2(z)}\,, \tag{2.69}$$

$$S_j^{(\text{quark})} = 0.102 \frac{\kappa_j}{z^2 K_2(z)}\,, \tag{2.70}$$

$$S_j^{(\text{gauge})} = 0.218 \frac{\kappa_j}{z^2 K_2(z)}\,. \tag{2.71}$$

where the parameter $\kappa_j$ is as in Eq. (2.37), namely

$$\kappa_j = \frac{\tilde{m}_j}{m_*}, \tag{2.72}$$

where $\tilde{m}_j \equiv (Y^\dagger Y)_{jj} v^2/(2M_j)$.

Using the generic relations for the wash-out terms (see, e.g., Eq. (2.39)),

$$W_j^D = \frac{2}{3} D_j N_{N_j}^{\text{eq}}, \tag{2.73}$$

$$W_j^{s,t} = \frac{2}{3} S_j^{s,t} N_{N_j}^{\text{eq}}, \tag{2.74}$$

we get:

$$W_j^D = 0.058\ \kappa_j, \tag{2.75}$$

$$W_j^{(\text{quarks})} = 0.0255\ \kappa_j, \tag{2.76}$$

$$W_j^{(\text{gauge})} = 0.0545\ \kappa_j. \tag{2.77}$$

The sum of the three terms is compatible with the result obtained in Ref. [197].

We emphasise that Eqs. (2.69) - (2.71) and (2.75) - (2.77) are valid only for $z < 1$. Moreover, as $z^2 K_2(z) \simeq 2$ for $z \ll 1$, all the terms given in Eqs. (2.69) - (2.71) and (2.75) - (2.77) are basically constant at $z \ll 1$. The behaviour at $z > 1$ is not relevant to baryogenesis via LG when $M \leq 100$ GeV, because the sphaleron conversion of the lepton asymmetry into the baryon asymmetry stops at $z_{\text{sph}} < 1$.

### The CP-asymmetry and thermal effects

The CP-asymmetry, with the inclusion of thermal effects as in Ref. [189], and taking into account the flavour effects, is given by [192, 193, 198]

$$\epsilon_{\ell\ell}^{(j)} = \sum_{j \neq k} \text{sgn}(M_k - M_j)\, I_{jk,\ell\ell}\, \frac{2x^{(0)}\gamma(z)}{4\frac{\Gamma_{22}}{\Gamma_{kk}}(x^{(0)} + x_T(z))^2 + \frac{\Gamma_{kk}}{\Gamma_{22}}\gamma^2(z)}\,, \tag{2.78}$$

where

$$I_{jk,\ell\ell} = \frac{\Im\left[Y_{\ell j}^* Y_{\ell k} \left(Y^\dagger Y\right)_{jk}\right] + (M_j/M_k)\Im\left[Y_{\ell j}^* Y_{\ell k} \left(Y^\dagger Y\right)_{kj}\right]}{\left(Y^\dagger Y\right)_{jj} \left(Y^\dagger Y\right)_{kk}}\,. \tag{2.79}$$

In Eq. (2.78) the quantity $x^{(0)} \equiv \Delta M^{(0)}/\Gamma_{22}$, $\Delta M^{(0)}$ being the $N_2 - N_1$ mass splitting at zero temperature [16]. The term that multiplies $\mathrm{sgn}(M_k - M_j)\, I_{jk,\ell\ell}$ in Eq. (2.78) is due to heavy-neutrino mixing effects. Thermal corrections to the $N_2 - N_1$ mass splitting, $\Delta M_T$, with the total mass splitting given by $\Delta M = \Delta M^{(0)} + \Delta M_T$, are relevant in the denominator of the expression for $\epsilon^{(j)}_{\ell\ell}$ only and are accounted for by the term $x_T(z)$ [189]:

$$x_T(z) \equiv \frac{\Delta M_T(z)}{\Gamma_{22}} \simeq \frac{\pi}{4z^2}\sqrt{\left(1 - \frac{\Gamma_{11}}{\Gamma_{22}}\right)^2 + 4\frac{|\Gamma_{12}|^2}{\Gamma_{22}^2}}\,, \tag{2.80}$$

where $\Gamma_{jk} \equiv (Y^\dagger Y)_{jk}\sqrt{M_j M_k}/8\pi$. The function $\gamma(z)$ in Eq. (2.78) quantifies the thermal effects to the $N_{1,2}$ self-energy cut [189] and is determined by $\gamma(z) \equiv \langle p_\mu L^\mu/(p_\nu q^\nu)\rangle$, where $p$ and $q$ are the charged lepton and heavy Majorana neutrino four-momenta respectively, $L$ is defined in Ref. [199] and the angular brackets indicate a thermal average.

The function $\gamma(z)$ depends on the masses of the Higgs boson $m_H(T)$, charged leptons $m_\ell(T)$ and heavy Majorana neutrinos $M_1 \simeq M_2 = M$ (it does not depend on the mass splitting $\Delta M$). At $T > T_{\rm EW} \simeq 160$ GeV, $T_{\rm EW}$ being the temperature at which the EWPT sets in [62], the Universe is in the symmetric phase and the Higgs VEV is zero. The Higgs boson and the charged leptons possess only thermal masses [17]. For the charged lepton thermal masses we use the expression given in Ref. [200]:

$$m_\ell(T) \simeq \frac{T}{4}\sqrt{3\,g^2 + (g')^2}\,, \tag{2.81}$$

where $g = 0.65$ and $g' = 0.35$ (we can safely neglect the effects of the running). At $T < T_{\rm EW}$, the Higgs VEV $v(T)$ grows approximately as (see, e.g., [62,189]): $v^2(T) = (1 - T^2/T^2_{\rm EW})\, v^2\Theta(T_{\rm EW} - T)$, where $v \equiv v(T=0) \simeq 246$ GeV is the VEV value at zero temperature. Correspondingly, the charged lepton mass $m_\ell$ receives a non-zero contribution $m_\ell(v(T))$ in the interval $T_{\rm sph} \leq T < T_{\rm EW}$ due to $v(T) \neq 0$: $m^2_\ell = m^2_\ell(v(T)) + m^2_\ell(T)$, $\ell = e,\, \mu,\, \tau$. The EWPT contribution under discussion $m_\ell(v(T))$ is proportional to the zero temperature experimentally determined mass $m_\ell$ of the charged lepton $\ell$: $m_\ell(v(T)) = m_\ell\, v(T)/v$. It is not difficult to convince oneself that for $T$ in the interval $T_{\rm sph} \leq T < T_{\rm EW}$ one has $m^2_\ell(v(T)) \ll m^2_\ell(T)$. Thus, for $T \geq T_{\rm sph}$ of interest, the charged lepton masses are given by their thermal contributions specified in Eq. (2.81).

For the Higgs mass $m_H(T)$ we consider the results obtained from the thermal effective potential given, e.g., in Refs. [201, 202], which takes into account the effects of the EWPT in the interval of temperatures $T_{\rm sph} \lesssim T \lesssim T_{\rm EW}$. The discussion of the behaviour of $m_H(T)$ in the interval of temperatures of interest is outside the scope of the present Thesis; it can be inferred from the aforementioned EWPT effective potential. We give here only the expression for the thermal contribution to the Higgs mass:

$$m_H^{\rm therm}(T) \simeq \frac{T}{4}\sqrt{3\,g^2 + (g')^2 + 4\,h_t^2 + 8\,\lambda}\,. \tag{2.82}$$

[16] The first term in the numerator of the expression in Eq. (2.79), as can be shown, is lepton number violating (LNV), while the second term is lepton number conserving (LNC). Our numerical analyses in Pub. [II] showed that, in the LG scenarios of interest, the dominant contribution in the generation of the baryon asymmetry compatible with the observations is given by the LNV term, with the LNC term giving typically a subdominant contribution; in certain specific cases the LNC contribution is of the order of, but never exceeds, the LNV one.

[17] The thermal corrections to the masses of the heavy Majorana neutrinos $N_{1,2}$ are negligibly small [164, 200].

Here, $h_t$ and $\lambda$ are the top Yukawa coupling and the Higgs quartic coupling, respectively. In the numerical analysis of Pub. [II] we have used $h_t = 0.993$ and $\lambda = 0.129$, which correspond to the top and zero temperature Higgs masses of 172.76 GeV and 125 GeV, respectively, and Higgs VEV of 246 GeV.

With the chosen values of the couplings we have

$$m_\ell(T) \simeq 0.296\, T\,, \qquad m_H(T) \simeq 0.632\, T\,. \tag{2.83}$$

It is easy to check using $m_\ell(T)$ and $m_H(T)$ given in the preceding equation that for the values of $z$ lying approximately in the interval $0.34 \lesssim z \lesssim 0.93$ the Higgs and heavy Majorana decay processes are kinematically forbidden [189, 200]. For $z \lesssim 0.34$ the only allowed processes are Higgs decays to heavy Majorana neutrinos and charged leptons, whereas at larger $z \gtrsim 0.93$ only the heavy Majorana neutrino decays are allowed. This is reflected in the behaviour of the function $\gamma(z)$: for $0.34 \lesssim z \lesssim 0.93$ one has $\gamma(z) = 0$. We find also that for $z \ll 1$, $\gamma(z) \simeq 23.5$ and for $z \gg 1$, $\gamma(z) \simeq 1$ [II].

For $T > T_{\rm sph}$ of interest, the charged lepton masses satisfy $m_\ell(T) > 0.296\, T_{\rm sph} \simeq 39$ GeV. This implies that in order for the decays of the heavy Majorana neutrinos $N_{1,2}$ to be in principle kinematically possible at $T > T_{\rm sph}$, the masses of $N_{1,2}$ must satisfy $M_{1,2} > m_\ell(T_{\rm sph}) \simeq 39$ GeV. Taking into account also the Higgs mass leads obviously to a larger lower bound on $M_{1,2}$ (see, e.g., Ref. [189]).

We note further that in the interval of temperatures $T_{\rm sph} \leq T < T_{\rm EW}$, the thermal contribution to the masses of the SM top quark, Higgs, $W^\pm$ and $Z^0$ bosons are all of the order of $\tilde{g}T$, $\tilde{g}$ being one of the SM couplings $g$, $g'$, $h_t$ and $\lambda$, and that the contribution to these masses of the non-zero temperature dependent Higgs vacuum expectation value $v(T)$, determined earlier, is of the same order. At the same time, the momenta of the particles in the thermal bath are of the order of $\pi T$ and are much larger than the masses, so all the particles relevant for our discussion are ultrarelativistic at the temperatures on interest [203]. This implies also, in particular, that the expressions for the decay and scattering terms introduced in the preceding subsection are valid actually for $T \geq T_{\rm sph} \simeq 131.7$ GeV.

When collinear emissions of soft gauge bosons, present in the thermal bath of the Universe at the epoch of interest, are also included in the decay processes, the disallowed region discussed earlier becomes accessible to the Higgs decays due to the increased range of kinematic possibilities [200]. In Pub. [II] we have estimated the effects of these emissions by adding an interpolation of $\gamma(z)$ across the "gap" interval $0.34 \lesssim z \lesssim 0.93$ [18]. For a given value of $M$, the behaviour of $\gamma(z)$ at $z \geq z_{sph}$ (or at $T \leq T_{\rm sph}$) is not relevant and should be ignored since the sphalerons decouple at $T_{\rm sph}$. We note that, at high temperatures, $\gamma(z)$ is sensitive to precise values of Higgs and charged lepton thermal masses. As we have indicated, the Higgs and charged lepton thermal masses we have considered are in agreement with that of Ref. [200].

We finally stress that, in the absence of thermal effects, namely setting $\gamma(z) = 1$ and $x_T(z) = 0$, the second term in Eq. (2.78) is maximised for $x^{(0)} \simeq 0.5$. This is the "resonant" behaviour typical to the conventional RLG scenario without thermal corrections. However, when thermal corrections are taken into account, it is not possible to choose one value of $x^{(0)}$ for which we have resonance at all temperatures.

In the analysis presented in Pub. [II], performed after having implemented all the thermal effects in the `ULYSSES` code, we have solved the relevant equations and scanned the parameter

[18] The effects of collinear emissions of soft gauge bosons are included also in the decay terms $D_j$ and $W_j^D$ given in Eqs. (2.69), (2.74) and (2.75), as discussed in the preceding section.

space of viable RLG. We are going to discuss about the results of Pub. [II], namely the most interesting features of such scenario and the possibilities to test it at low energy experiments, in Chapter 4 and proceed further with a brief description of the unification of the discussed RLG scenario with the framework of LG via oscillations.

### 2.3.3 Low-Scale Leptogenesis Including Oscillations

In Refs. [101, 102], the so-called "freeze-in" LG mechanism by which the lepton asymmetry (translated into the present BAU via usual sphaleron processes) is generated through heavy neutrino oscillations during the epoch when the heavy Majorana neutrinos $N_j$ are being produced out-of-equilibrium by processes involving particles in the SM bath, was put forward. The heavy neutrinos produced in this way, being interaction states, do not necessarily coincide with the mass eigenstates and therefore can oscillate violating CP. This mechanism, referred to as LG via (neutrino) oscillations, was extensively studied (see, e.g., Refs. [204–213] and references quoted therein) and shown to be viable at scales even lower than that of successful RLG.

Usually, RLG and LG via neutrino oscillations were generically treated as separate in baryogenesis mechanisms. Only recently, the parameter space of the two scenarios was studied within a unified framework in Ref. [161] (see also Ref. [162]) based on density matrix-like equations (see, e.g., Refs. [214, 215] for a review of the formal treatments for RLG). The DMEs relevant to this scenario are a sets of integro-differential equations for the phase-space density matrix distributions of the heavy neutrinos. In principle, one should solve the equations for any given momentum and then integrate the solution, but the equations can be solved numerically by averaging over the momenta first, leading only to $\mathcal{O}(1)$ differences [162, 205, 212, 216]. The resulting system of momentum-averaged DMEs corresponds to a set of semi-classical BEs describing the evolution of diagonal and off-diagonal elements of the density matrix of the heavy neutrino states [19]. It lies beyond the scope of this Thesis to introduce the cumbersome DMEs in this context (see, e.g., Ref. [162] where the equations are given and discussed in great details). It is sufficient to mention that these equations include the thermal effects (thermal masses and soft processes), flavour effects, as well as contributions from $1 \leftrightarrow 2$ decays and inverse decays, $2 \leftrightarrow 2$ scattering processes, and heavy neutrino oscillations [20]. The regime introduced in the previous section within the BE formalism can be understood effectively as the united scenario discussed in Ref. [161] in the limit of fast oscillations and strong wash-out effects [162], so that the contributions from heavy neutrino oscillations to the generation of the BAU is efficiently washed-out.

The unified treatment of low-scale LG was extended in Ref. [160] to the case of three quasi-degenerate heavy Majorana neutrinos $N_{1,2,3}$, with $M_{1,2,3} \simeq M$. In view of the results of Ref. [160] for which LG is viable for masses in the range $10^{-1} \lesssim M/\text{GeV} \lesssim 7\times10^{4}$ and relatively large $(RV)_{\ell j}$ couplings, reaching, e.g., $\sum_{\ell j}|(RV)_{\ell j}|^2 \sim 5\times10^{-2}$ for $M \simeq 100\,\text{GeV}$, we have shown in Pub. [III] the potentiality of currently running and/or future low-energy experiments on charged lepton flavour violating (cLFV) processes, such as $\mu \to e\gamma$ and $\mu \to eee$ decays, and $\mu \to e$ conversion in nuclei, to test this intriguing LG scenario. We will discuss in details our findings in Chapter 4.

[19] The equations are analogous to those introduced in Sec. 2.3.1 in Eqs. (2.52) and (2.53) but the density matrix is for the heavy neutrino states, not for the charged lepton flavour states, with the off-diagonal elements describing the oscillations between the heavy neutrino states. The flavour asymmetries can be treated independently in this scenario since the flavour decoherence effects are not effective for $M \lesssim 100\,\text{TeV}$.

[20] The authors of Refs. [161, 162] also split the contributions form different heavy neutrino helicities.

# CHAPTER 3

# High-Scale Leptogenesis with Low-Energy Leptonic CP-Violation

The simplest scenario of high-scale thermal LG typically necessitates relatively large heavy Majorana neutrino masses and remains difficult to test directly at laboratories. Nevertheless, there is the intriguing possibility to relate high-scale LG to low-energy observables when the required CP-violation is provided only by the Dirac and/or Majorana phases of the PMNS neutrino mixing matrix. This possibility has been explored in the literature already (see, e.g., Ref. [143]). However, in the extensive study we presented in Pub. [I], we have analysed in greater detail such scenario in the case of a strong hierarchy in the heavy neutrino mass spectrum, covering a wide range of mass scales (from $10^8$ to $10^{14}$ GeV) and making use of the efficient and fast `ULYSSES` Python package [IV] to solve the relevant sets of equations (see Appendix A for details on the code).

As already emphasised in Sec. 2.3.1, the classical BEs do not include the quantum flavour decoherence effects and can be regarded as limiting cases of the DMEs, which instead do account for these quantum contributions. Consequently, the BEs can be valid only in ranges of temperatures for which either none, one or all the lepton flavours are fully decoherent, while the DMEs can correctly describe the 1-to-2 and 2-to-3 flavour transitional regimes. In our work of Pub. [I] we have compared the results obtained with both DMEs and BEs and highlighted the main differences between the solutions to the different sets of equations. This comparison, together with the detailed analysis of the behaviour of the baryon asymmetry in the transitional regimes, led us to discover peculiar features of the LG scenarios of interest and to establish the ranges of mass scales and values of the PMNS phases for having successful LG in the cases of normal and inverted hierarchical light neutrino mass spectrum. In the subsequent sections, we are going to illustrate in details the results of our work in Pub. [I].

Specifically, the present chapter is organised as follows. In Sec. 3.1 we discuss about the peculiar baryon asymmetry sign change in the 1-to-2 and 2-to-3 flavour transitional regimes in the case of three heavy Majorana neutrinos $N_{1,2,3}$ with hierarchical masses, $M_1 \ll M_2 \ll M_3$, $M_1 \gtrsim 10^8$ GeV, as well as the general conditions under which the sign change takes place. Next, we present a detailed analysis of the transitions between the different flavour regimes. We dedicate Sec. 3.2 to the description of the results in the case of decoupled $N_3$, in which the number of parameters is significantly smaller than in the general case with three heavy Majorana neutrinos. This analysis was mainly performed with the CP-violation necessary for the generation of the baryon asymmetry provided solely by the low-energy Dirac or/and Majorana phases present in the PMNS neutrino mixing matrix. We conclude in Sec. 3.3 with a summary of our results. We remind that the sets of relevant equations used in our analysis

were introduced in Sec. 2.3.1 of this Thesis, where we have also described in details the flavour decoherence effects and different flavour regimes.

## 3.1 The Baryon Asymmetry Sign Change

We first consider two-flavoured LG in the case of three heavy Majorana neutrinos $N_{1,2,3}$ with hierarchical masses, $M_1 \ll M_2 \ll M_3$, $M_1 \gtrsim 10^8$ GeV. In this case, generically, only the CPV decays of the lighter Majorana neutrino $N_1$ contribute to the generation of a lepton asymmetry, which is converted into a baryon asymmetry by the sphaleron effects. In the two-flavoured regime, the DMEs introduced in Sec. 2.3.1 describing the evolution of the number of $N_1$ in a comoving volume, $N_{N_1}$, and of the CPV asymmetries in the lepton charges $L_\tau$ and $L_{\tau^\perp} = L_{e+\mu} = L_e + L_\mu$ have the following form:

$$\frac{dN_{N_1}}{dz} = -D_1(N_{N_1} - N_{N_1}^{\rm eq})\,, \tag{3.1}$$

$$\frac{dN_{\tau\tau}}{dz} = \epsilon^{(1)}_{\tau\tau} D_1(N_{N_1} - N_{N_1}^{\rm eq}) - W_1\left(p_{1\tau} N_{\tau\tau} + \Re\left[C_{1\tau^\perp} C^*_{1\tau} N_{\tau\tau^\perp}\right]\right)\,, \tag{3.2}$$

$$\frac{dN_{\tau^\perp\tau^\perp}}{dz} = \epsilon^{(1)}_{\tau^\perp\tau^\perp} D_1(N_{N_1} - N_{N_1}^{\rm eq}) - W_1\left(p_{1\tau^\perp} N_{\tau^\perp\tau^\perp} + \Re\left[C_{1\tau^\perp} C^*_{1\tau} N_{\tau\tau^\perp}\right]\right)\,, \tag{3.3}$$

$$\frac{dN_{\tau\tau^\perp}}{dz} = \epsilon^{(1)}_{\tau\tau^\perp} D_1(N_{N_1} - N_{N_1}^{\rm eq}) - \frac{1}{2} W_1\left(N_{\tau\tau^\perp} + C_{1\tau} C^*_{1\tau^\perp} N_{B-L}\right) - \frac{\Gamma_\tau}{Hz} N_{\tau\tau^\perp}\,. \tag{3.4}$$

The $B-L$ asymmetry is given by $N_{B-L} = N_{\tau\tau} + N_{\tau^\perp\tau^\perp}$. We find that (see Appendix B):

$$N_{B-L}(z_f) = N^{\rm 1BE1F}_{B-L}(z_f) + N^{\rm decoh}_{B-L}(z_f) \tag{3.5}$$

where

$$N^{\rm 1BE1F}_{B-L}(z) \equiv \int_{z_0}^{z} e^{-\int_{z'}^{z_f} W_1(z'')dz''} \epsilon^{(1)} D_1(z')(N_{N_1}(z') - N^{\rm eq}_{N_1}(z'))\, dz'\,, \tag{3.6}$$

$$N^{\rm decoh}_{B-L}(z) \equiv \int_{z_0}^{z} e^{-\int_{z'}^{z_f} W_1(z'')dz''} W_1(z')\lambda(z')\, dz'\,, \tag{3.7}$$

with $z_0$ corresponding to the beginning of LG, which we have set to $z_0 = 10^{-3}$ in all our numerical calculations, and

$$\lambda(z) \equiv 2\int_{z_0}^{z} \Re\left[C^*_{1\tau} C_{1\tau^\perp} N_{\tau\tau^\perp}(z') \frac{\Gamma_\tau}{Hz'}\right] dz'\,. \tag{3.8}$$

The term $N^{\rm 1BE1F}_{B-L}$ is the solution to the 1BE1F set of equations and vanishes if the CP-violation in LG is due only to the physical Dirac and/or Majorana CPV phases in the PMNS matrix, since in that case [141] $\epsilon^{(1)} = \epsilon^{(1)}_{\tau\tau} + \epsilon^{(1)}_{\tau^\perp\tau^\perp} = \epsilon^{(1)}_{\tau\tau} + \epsilon^{(1)}_{ee} + \epsilon^{(1)}_{\mu\mu} = 0$. The term $N^{\rm decoh}_{B-L}$ incorporates the decoherence effects and one can have $N^{\rm decoh}_{B-L} > (\gg)\ N^{\rm 1BE1F}_{B-L}$. As was shown in Ref. [143], $N^{\rm decoh}_{B-L}$ can be the only source of lepton asymmetry if the CP-violation in LG is provided exclusively by the physical CPV phases in the PMNS matrix. In the discussion that follows we focus on this case.

The factor $\Lambda_\tau \equiv \Gamma_\tau/(Hz) = \text{const.}/M_1$ and can be taken out of the integration in (3.8). In the high-scale regime ($M \gtrsim 10^{12}$ GeV) we can work in the limit of $\Lambda_\tau \to 0$ and neglect all the

terms of order $\mathcal{O}(\Lambda_\tau^2)$ in the lepton asymmetry. Since in our case $N_{B-L}^{\rm decoh}$ is the only source of lepton asymmetry, at $M_1 \gtrsim 10^{12}$ GeV we have $N_{B-L} = N_{B-L}^{\rm decoh} = \mathcal{O}(\Lambda_\tau)$. Solving Eq. (3.4) at zero order in $\Lambda_\tau$ [1] with the integrating factor method we find:

$$N_{\tau\tau^\perp}(z) = \int_{z_0}^{z} e^{-\frac{1}{2}\int_{z'}^{z} W_1(z'')\,dz''} \epsilon^{(1)}_{\tau\tau^\perp} D_1 (N_{N_1} - N_{N_1}^{\rm eq})\,dz' + \mathcal{O}(\Lambda_\tau)\,. \tag{3.9}$$

Inserting this result in Eq. (3.8) we get:

$$\lambda(z) = \Lambda_\tau \mathcal{I}_1(\kappa_1; z)(p_{1\tau^\perp}\epsilon^{(1)}_{\tau\tau} + p_{1\tau}\epsilon^{(1)}_{\tau^\perp\tau^\perp}) + \mathcal{O}(\Lambda_\tau^2), \tag{3.10}$$

where

$$\mathcal{I}_1(\kappa_1; z) \equiv \int_{z_0}^{z} dz' \int_{z_0}^{z'} dz'' e^{-\frac{1}{2}\int_{z_0}^{z'} W_1(\tilde{z})\,d\tilde{z}} D_1(z'')(N_{N_1}(z'') - N_{N_1}^{\rm eq}(z''))\,, \tag{3.11}$$

and we have used the relation $2\Re[C^*_{1\tau}C_{1\tau^\perp}\epsilon_{\tau\tau^\perp}] = p_{1\tau^\perp}\epsilon^{(1)}_{\tau\tau} + p_{1\tau}\epsilon^{(1)}_{\tau^\perp\tau^\perp}$ (see Appendix B for a derivation of this relation). To leading order in $\Lambda_\tau$ the final asymmetry reads:

$$N_{B-L}(z_f) = \Lambda_\tau \mathcal{I}_2(\kappa_1; z_f)(p_{1\tau^\perp}\epsilon^{(1)}_{\tau\tau} + p_{1\tau}\epsilon^{(1)}_{\tau^\perp\tau^\perp}) + \mathcal{O}(\Lambda_\tau^2), \tag{3.12}$$

where $p_{1\tau^\perp}\epsilon^{(1)}_{\tau\tau} + p_{1\tau}\epsilon^{(1)}_{\tau^\perp\tau^\perp} = (1-2p_{1\tau})\epsilon^{(1)}_{\tau\tau}$ and

$$\mathcal{I}_2(\kappa_1; z) \equiv \int_{z_0}^{z} e^{-\int_{z_0}^{z} W_1(\tilde{z})\,d\tilde{z}} W_1(z')\mathcal{I}_1(\kappa_1; z')\,dz'\,. \tag{3.13}$$

Since $\epsilon^{(1)} \propto M_1$ and $\Lambda_\tau \propto 1/M_1$, the asymmetry given by Eq. (3.12) is constant with the mass scale $M_1$. Thus, when the CP-violation is provided by the CPV phases of the PMNS matrix, at $M_1 > 10^{12}$ GeV there should exist an interval of values of $M_1$ in which the baryon asymmetry $\eta_B$ is constant, i.e., does not change with $M_1$. Indeed, the numerical solutions of the DMEs show the existence of a plateau at values of $M_1 > 10^{12}$ GeV [143], as is illustrated in Fig. 3.1, right panels.

We note that if the CP-violation in LG is due to the Casas-Ibarra matrix $O$, and thus $\epsilon^{(1)} \neq 0$, $N_{B-L}^{\rm 1BE1F} \propto M_1$ eventually starts to dominate over $N_{B-L}^{\rm decoh}$ as $M_1$ increases, recovering the single-flavour approximation as is clearly seen in Fig. 3.1, left panels.

As $M_1$ decreases from $M_1 \sim 10^{12}$ GeV, $\Lambda_\tau$ increases and the solution of DMEs approaches the solution of the 1BE2F sets of equations in Eqs. (2.42) to (2.44), which we denote by $N_{B-L}^{\rm 1BE2F}$. In the mass range of $10^9 \lesssim M_1/{\rm GeV} \lesssim 10^{12}$, the asymmetry is approximately given by $N_{B-L}^{\rm 1BE2F}$. However, the transition at $M \sim 10^{12}$ GeV may take place with a sudden sign change of the baryon asymmetry, as Fig. 3.1 shows. The sign change can happen if the solution given in Eq. (3.12) has a different sign with respect to the solution $N_{B-L}^{\rm 1BE2F}$ [2]. As Fig. 1 also indicates, we can have $\eta_B > 0$ either at $M_1 \gtrsim 10^{12}$ GeV or at $M_1 \lesssim 10^{12}$ GeV. More generally, if we denote by $M_{10}$ the value of $M_1$ at which $\eta_B = 0$, we can have $\eta_B > 0$ and viable LG for certain values of $M_1$ lying either in the interval $M_1 > M_{10}$ or in the interval $M_1 < M_{10}$. Because of the change

[1] The term $\propto N_{B-L}$ in Eq. (3.4) can be neglected since for $\epsilon^{(1)} = 0$ it leads to correction $\mathcal{O}(\Lambda_\tau^2)$ in the asymmetry.

[2] A sign change of $\eta_B$ can occur also at $M_1 \sim 10^9$ GeV, where the transition between the two-flavour and three-flavour regimes takes place. If $\epsilon^{(1)} \neq 0$, another sign change can occur at a mass scale $M_1 \gtrsim 10^{12}$ GeV when $N_{B-L}^{\rm 1BE1F}$ starts dominating over $N_{B-L}^{\rm decoh}$. However, investigating the conditions under which these sign changes of $\eta_B$ take place is beyond the scope of our work.

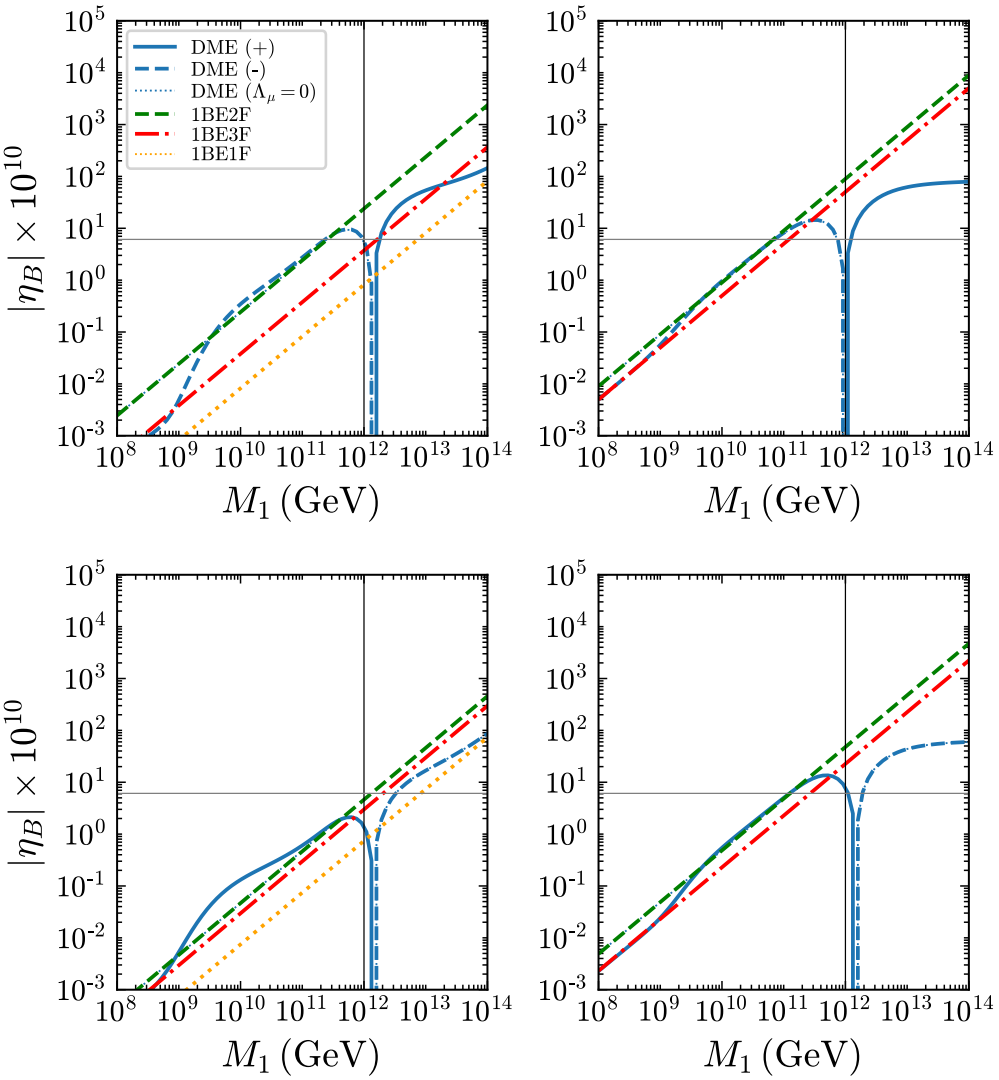


**Figure 3.1.** The baryon asymmetry $|\eta_B|$ as a function of the mass scale $M_1$ calculated with DMEs (blue curve), and single-, two- and three-flavoured Boltzmann equations 1BE1F (orange dotted line), 1BE2F (green dashed line) and 1BE3F (red dash-dotted line). The solid (dashed) blue curve corresponds to $\eta_B > 0$ ($\eta_B < 0$), while the dotted blue curve is obtained for $\Lambda_\mu = 0$. The lightest neutrino and the heavy Majorana neutrino masses, the Dirac and Majorana CPV phases and Casas-Ibarra parameters are set to: $m_1 = 0.0159$ eV, $M_3 = 5M_2 = 50M_1$, $\delta = 228°$, $\alpha_{21} = 200°$, $\alpha_{31} = 175°$, $x_1 = -/+10°$, $x_2 = -/+20°$, $x_3 = -/+10°$ in the top/bottom panels and $y_1 = y_2 = 0$ and $y_3 = 30°/0$ in the left/right panels, respectively. In the top-right and bottom-right panels the CP-violation is due only to the CPV phases in the PMNS matrix ($y_{1,2,3} = 0$), i.e. $\epsilon^{(1)} = 0$, and the corresponding 1BE1F solution vanishes at any mass scale. The horizontal (vertical) grey (black) line corresponds to the observed value of $\eta_B$ (to $M_1 = 10^{12}$ GeV).

of the sign of $\eta_B$, there is the possibility of finding the predicted $|\eta_B|$ equal to the observed value of the baryon asymmetry but $\eta_B$ having the wrong (negative) sign and so no successful LG (Fig.3.1, bottom-left panel). In view of this, it is of crucial importance to understand the conditions under which $\eta_B$ changes sign as well as what determines the value(s) of $M_1$ at which $\eta_B = 0$.

We discuss in the next subsections the circumstances under which the sign change of $\eta_B$ can take place in the cases of *strong* and *weak* wash-out regimes, for which $\kappa_1 \gg 1$ and $\kappa_1 \ll 1$, respectively. We concentrate on the physically interesting possibility of the requisite CP-violation provided only by the Dirac and/or Majorana CPV phases of the PMNS matrix, which leads also to the existence of a the plateau at $M_1 > 10^{12}$ GeV where to a good approximation $\eta_B$ does not depend on $M_1$.

### 3.1.1 Strong Wash-Out Regime

In the strong wash-out regime the solution to the 1BE2F does not depend on the initial conditions since any initially generated asymmetry is erased by the strong wash-out processes. A sufficiently accurate analytic expression of the solution to the 1BE2F, valid in the strong wash-out regime, is given by (see Appendix C.1):

$$N^{\rm 1BE2F}_{B-L}(z_f) \simeq \frac{2N^{\rm eq}_{N_1}(0)}{\kappa_1 z_d(\kappa_1)}\,\frac{p_{1\tau^\perp}\epsilon^{(1)}_{\tau\tau} + p_{1\tau}\epsilon^{(1)}_{\tau^\perp\tau^\perp}}{p_{1\tau}p_{1\tau^\perp}} = \frac{2N^{\rm eq}_{N_1}(0)}{\kappa_1 z_d(\kappa_1)}\,\frac{(1-2p_{1\tau})\epsilon^{(1)}_{\tau\tau}}{p_{1\tau}(1-p_{1\tau})}\,. \tag{3.14}$$

Since $p_{1\tau}(1-p_{1\tau}) > 0$, a difference in sign between the solution $N^{\rm 1BE2F}_{B-L}(z_f)$ given above and the solution of Eq. (3.12) occurs when $\mathcal{I}_2(\kappa_1; z_f)$ is negative. We show in Fig. 3.2 the behaviour of $\mathcal{I}_2(\kappa_1; z_f)$ for $z_f = 1000$ computed numerically with the `ULYSSES` Python package [IV] from Eq. (3.13) [3] in the cases of vanishing initial abundance (VIA) of $N_1$, $N_{N_1}(z_0) = 0$, and thermal initial abundance (TIA) of $N_1$, $N_{N_1}(z_0) = N^{\rm eq}_{N_1}(z_0)$. As follows from the behaviour of $\mathcal{I}_2(\kappa_1; z_f)$ shown in Fig. 3.2, a sign change of $\eta_B$ at $M_1 \sim 10^{12}$ GeV in the strong wash-out regime always happens for VIA, but never for TIA.

### 3.1.2 Weak Wash-Out Regime

In the weak wash-out regime we need to consider separately the cases of the two different initial conditions – VIA ($N_{N_1}(z_0) = 0$) and TIA ($N_{N_1}(z_0) = N^{\rm eq}_{N_1}(z_0)$).

#### Vanishing Initial Abundance

In the VIA case the asymmetry of interest in the two-flavoured LG reads (see Appendix C.2):

$$\begin{aligned} N^{\rm 1BE2F}_{B-L}(z_f) &= \frac{81\pi^2}{1024 N^{\rm eq}_\ell}\kappa_1^2(\epsilon^{(1)}_{\tau\tau}p_{1\tau} + \epsilon^{(1)}_{\tau^\perp\tau^\perp}p_{1\tau^\perp}) \\ &= -\frac{81\pi^2}{1024 N^{\rm eq}_\ell}\,\kappa_1^2\epsilon^{(1)}_{\tau\tau}(p_{1\tau^\perp} - p_{1\tau}). \end{aligned} \tag{3.15}$$

[3] We recall that $N_{B-L}(z)$, and therefore also $\mathcal{I}_2(\kappa_1; z)$, is frozen and kept constant after the wash-out processes become ineffective at $z_d(\kappa_1) \ll z_f$.

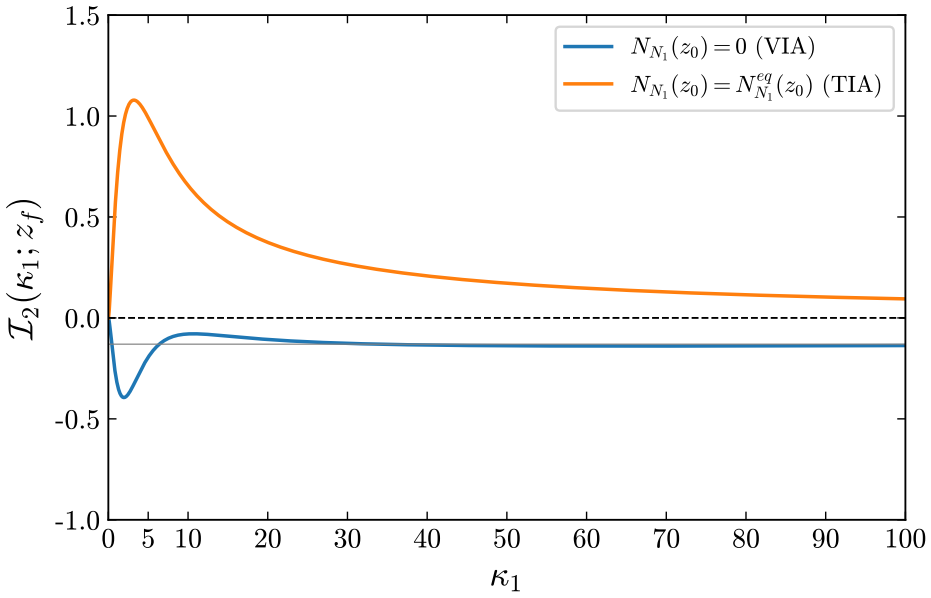


**Figure 3.2.** The dependence of the function $\mathcal{I}_2(\kappa_1; z_f)$ (defined in Eq. (3.13)) on $\kappa_1$, computed numerically at $z_f = 1000$ in the cases of VIA (blue) and TIA (orange) initial abundances of $N_1$. Note that in the strong wash-out regime in the VIA case for $k \gtrsim 10$ we have to a good approximation $\mathcal{I}_2 \approx -0.13$ – the value marked by the horizontal grey line. See the text for further details.

where to get the last equation we have used the fact that $\epsilon^{(1)} = \epsilon^{(1)}_{\tau\tau} + \epsilon^{(1)}_{\tau^\perp\tau^\perp} = 0$. Using this condition also in Eq. (3.12) we find:

$$N_{B-L}(z_f) = \Lambda_\tau \mathcal{I}_2(\kappa_1; z_f)\epsilon^{(1)}_{\tau\tau}(p_{1\tau^\perp} - p_{1\tau}) + \mathcal{O}(\Lambda^2_\tau). \tag{3.16}$$

It is then clear from the comparison of the last two equations that $\mathcal{I}_2(\kappa_1; z_f)$ needs to be positive in order for a sign change of $\eta_B$ to occur at $M_1 \sim 10^{12}$ GeV. Since, as shown in Fig. 3.2, $\mathcal{I}_2(\kappa_1; z_f)$ is always negative if $N_{N_1}(z_0) = 0$, the transition at $M \sim 10^{12}$ GeV in the weak wash-out regime in the VIA case always takes place without a sign change.

### Thermal Initial Abundance

In the case of TIA, for which $N_{N_1}(z_0) = N^{\rm eq}_{N_1}(z_0)$, and CP-violation due only to the CPV phases in the PMNS matrix, the asymmetry of interest in the two-flavoured LG is described by the following analytic expression (see Appendix C.2):

$$N^{\rm 1BE2F}_{B-L}(z_f) = \epsilon^{(1)}_{\tau\tau}\,(p_{1\tau^\perp} - p_{1\tau})\mathcal{A}(\kappa_1; z_f), \tag{3.17}$$

where

$$\mathcal{A}(\kappa_1; z) \equiv \int_{z_D}^{z} dz' D_1(z') N_{N_1}(z') \int_{z'}^{z} dz'' W_1(z'')\, dz' > 0. \tag{3.18}$$

The comparison of (3.17) with Eq. (3.16) tells us that no sign change of $\eta_B$ should occur at the 1-to-2 flavour transition also in this case, given the fact that $\mathcal{I}_2(\kappa_1; z_f)$ is always positive for TIA.

### 3.1.3 Transitions Between Different Flavour Regimes: Detailed Analysis

The discussion and the results obtained in the preceding subsections led to the important conclusion that we should expect a sign change of the baryon asymmetry at the transition between the single- and two-flavoured LG in the case of VIA and strong wash-out regime of baryon asymmetry generation. However, certain important points could not be addressed within the approach used in the discussion leading to this conclusion. For example, the intermediate cases in which the asymmetries in different flavours $N_{\tau\tau}$ and $N_{\tau^\perp\tau^\perp}$ are generated in different wash-out regimes – strong and weak – could not and have not been considered. The analysis performed by us also does not allow to determine the mass scale $M_{10}$ at which $\eta_B = 0$ and the transition between the two different flavour regimes considered takes place. Clearly, having different wash-out regimes for the different flavour asymmetries and having a value of $M_{10}$ which differs significantly from $\sim 10^{12}$ GeV, might be possible, in principle, for choices of the parameters, namely the $O$-matrix angles $x_1 + iy_1$, $x_2 + iy_2$, $x_3 + iy_3$, the PMNS phases $\delta$, $\alpha_{21}$, $\alpha_{31}$ and the mass of the lightest neutrino $m_1$, which differ from the choices considered by us. To address, in particular, the aforementioned points, we consider an alternative approach to the problem of interest.

We start from the following equation for $N_{B-L}$ in the case of $\epsilon^{(1)} = 0$ (a detailed derivation of this equation is provided in Appendix B), which is valid as long as $M_1 \gtrsim 10^9$ GeV where $\Lambda_\mu$ can be safely neglected:

$$\frac{dN_{B-L}}{dz} = -W_1(z)\,(N_{B-L}(z) - \lambda(z))\,. \tag{3.19}$$

The functions $W_1(z)$ and $\lambda(z)$ are given in Eqs. (2.39) and (3.8), respectively. Within this apparently simple equation for $N_{B-L}$, we have encoded all the complications due to the decoherence effects on the system in the term $W_1\,\lambda$, which, in particular, contains both a source and a wash-out term, as will be clarified later on. The term $W_1 N_{B-L}$ is the usual wash-out term which tends to cancel any initially generated asymmetry.

Taking into account the expression for $N_{\tau\tau^\perp}$ given in Eq. (B.10) of Appendix B, the function $\lambda(z)$ can be cast in the form:

$$\begin{aligned}\lambda(z) =& \Lambda_\tau\,\epsilon^{(1)}_{\tau\tau}(p_{1\tau^\perp} - p_{1\tau}) \int_{z_0}^{z} dz' \int_{z_0}^{z'} dz''\, D_1(z'')(N_{N_1}(z'') - N^{\rm eq}_{N_1}(z''))e^{-\Lambda_\tau(z'-z'')}e^{-\frac{1}{2}\int_{z''}^{z'} d\widetilde{z}\, W_1(\widetilde{z})} \\ &- \Lambda_\tau p_{1\tau}p_{1\tau^\perp} \int_{z_0}^{z} dz' \int_{z_0}^{z'} dz''\, W_1(z'')N_{B-L}(z'')e^{-\Lambda_\tau(z'-z'')}e^{-\frac{1}{2}\int_{z''}^{z'} d\widetilde{z}\, W_1(\widetilde{z})}.\end{aligned} \tag{3.20}$$

The first term in this expression for $\lambda(z)$ is the only source of $B - L$ asymmetry, while the second is an *integrated* wash-out term. In the limit of $\Lambda_\tau \to 0$, i.e., for $M \gg 10^{12}$ GeV, the first term scales as $\Lambda_\tau$, while the second term scales as $\Lambda_\tau^2$ and can be neglected. We note also that the integrated wash-out term can be suppressed by a small value of $p_{1\tau}p_{1\tau^\perp}$ as well. Given that the source term is proportional to $\Lambda_\tau\epsilon^{(1)}_{\tau\tau}(p_{1\tau^\perp} - p_{1\tau})$, also the $B - L$ asymmetry will be proportional to it at any $z$:

$$N_{B-L}(z) \equiv \Lambda_\tau\epsilon^{(1)}_{\tau\tau}(p_{1\tau^\perp} - p_{1\tau})\widetilde{N}_{B-L}(z), \tag{3.21}$$

where $\widetilde{N}_{B-L}$ can only depend, apart from $z$, on $\kappa_1$, $\Lambda_\tau$ and $p_{1\tau}$ (through the product $p_{1\tau}p_{1\tau^\perp}$). This means that the function $\lambda(z)$ can be written as:

$$\lambda(z) = \Lambda_\tau \, \epsilon^{(1)}_{\tau\tau}(p_{1\tau^\perp} - p_{1\tau})\mathcal{S}(p_{1\tau}, \kappa_1, \Lambda_\tau; z)\,, \tag{3.22}$$

with

$$\begin{aligned}\mathcal{S}(p_{1\tau}, \kappa_1, \Lambda_\tau; z) \equiv & \int_{z_0}^{z} dz' \int_{z_0}^{z'} dz''\, D_1(z'')(N_{N_1}(z'') - N^{\rm eq}_{N_1}(z''))e^{-\Lambda_\tau(z'-z'')}e^{-\frac{1}{2}\int_{z''}^{z'} d\widetilde{z} W_1(\widetilde{z})} \\ & - \Lambda_\tau p_{1\tau}(1-p_{1\tau}) \int_{z_0}^{z} dz' \int_{z_0}^{z'} dz''\, W_1(z'')\widetilde{N}_{B-L}(z'')e^{-\Lambda_\tau(z'-z'')}e^{-\frac{1}{2}\int_{z''}^{z'} d\widetilde{z} W_1(\widetilde{z})}.\end{aligned} \tag{3.23}$$

It follows from Eqs. (3.19) – (3.23) that in the VIA case of interest we have:

$$\widetilde{N}_{B-L}(z_f) = \int_{z_0}^{z_f} W_1(z)\mathcal{S}(p_{1\tau}, \kappa_1, \Lambda_\tau; z)\, e^{-\int_z^{z_f} W_1(z')\, dz'}\, dz. \tag{3.24}$$

The last equation, combined with Eq. (3.21), cannot be used to compute the final asymmetry because inside $\mathcal{S}$ a dependence on $\widetilde{N}_{B-L}$ is "hidden". However, it is clear from the last expression and Eqs. (3.21) and (3.22) that, given the signs of $\epsilon^{(1)}_{\tau\tau}$ and of $(p_{1\tau^\perp} - p_{1\tau}) = (1 - 2\, p_{1\tau})$, the sign of the asymmetry $N_{B-L}$ depends on the sign evolution of $\mathcal{S}$. We therefore analyse the behaviour of the function $\mathcal{S}$ to better understand the sign change at the 1-to-2 flavour transition. We construct the function $\mathcal{S}$ by first solving numerically the full set of DMEs with the `ULYSSES` Python package [IV] and then we compute explicitly $\mathcal{S}$ using the definition of $\lambda(z)$ in Eq. (3.8) together with Eqs. (3.22) and (B.9) [4].

We consider the case of heavy Majorana neutrinos having a vanishing initial abundance (VIA), i.e., $N_{N_1}(z_0) = 0$. At the beginning of LG at $z > z_0$, but $z$ relatively close to $z_0$, both the term involving $N_{N_1}(z'')$ and the integrated wash-out term in Eq. (3.23) are much smaller than the term involving $N^{\rm eq}_{N_1}(z'')$ [5], so that $\mathcal{S}$ starts its evolution with a negative sign. As $z$ increases, $\mathcal{S}$ receives contributions from both terms in Eq. (3.23). At values of $z > z_{eq}$, where $z_{eq}$ corresponds to the time of evolution at which $N_{N_1} = N^{\rm eq}_{N_1}$, we have, as our numerical analysis shows, $N_{N_1}(z) - N^{\rm eq}_{N_1}(z) > 0$. As $z$ increases, the source term in Eq. (3.23) goes through zero and becomes positive. Let us call $\widetilde{z}_\Lambda$ the value of $z$ at which $\mathcal{S} = 0$, so that at $z < \widetilde{z}_\Lambda$ ($z > \widetilde{z}_\Lambda$) we have $\mathcal{S} < 0$ ($\mathcal{S} > 0$).

It should be clear from Eq. (3.24) that for $z < \widetilde{z}_\Lambda$, $\widetilde{N}_{B-L} < 0$ and therefore also the second (integrated wash-out) term in Eq. (3.23) is positive. However, it is significantly smaller than the absolute value of the negative source term involving $N^{\rm eq}_{N_1}$. At $z = \widetilde{z}_\Lambda$, this negative term is compensated by the sum of the source term involving $N^{\rm eq}_{N_1}(z'')$ and the integrated wash-out term. At $z > \widetilde{z}_\Lambda$, $\mathcal{S}$ is positive and remains so as $z$ increases.

In the TIA case, as our numerical analysis shows, $\widetilde{z}_\Lambda$ does not exist since, in particular, $N_{N_1}(z) > N^{\rm eq}_{N_1}(z)$ for $z > z_0$ and correspondingly the function $\mathcal{S}$ has a positive sign for the entire period of LG. This explains why no sign change can be present in the TIA case, as proven in the previous section. In what follows we focus our discussion on the VIA case only.

[4] More specifically, the `ULYSSES` Python code allows to calculate numerically $N_{B-L}$, $N_{\tau\tau^\perp}$ and $\lambda(z)$, which then can be used to obtain $\mathcal{S}$.

[5] The integrated wash-out term is negligible because both $W_1(z'')$ and $\widetilde{N}_{B-L}(z'')$ are strongly suppressed.

If, in the VIA case, the $B-L$ asymmetry is frozen at $z_f < \widetilde{z}_\Lambda$, then, as we have discussed, $\mathcal{S} < 0$ and therefore $\widetilde{N}_{B-L}(z_f) < 0$ (see Eq. (3.24)). Thus, we can have $\widetilde{N}_{B-L}(z_f) > 0$ only if $z_f > \widetilde{z}_\Lambda$.

To highlight this behaviour we focus on the strong wash-out regime. Suppose that $\kappa_1 \gg 1$, so that there exist two moments $z_{\rm in}$ and $z_{\rm out}$ for which $W_1(z_{\rm in} < z < z_{\rm out}) \gtrsim 1$. Then, for $z_{\rm in} < z < z_{\rm out}$ to a good approximation we have $dN_{B-L}/dz \cong 0$ [6] (see, e.g., Ref. [217]), and following the same steps as in Appendix C, from Eq. (3.19) we get:

$$N_{B-L}(z) \simeq \lambda(z). \tag{3.25}$$

After $z_{\rm out}$ the asymmetry gets frozen so that:

$$N_{B-L}(\infty) \simeq \lambda(z_{\rm out}). \tag{3.26}$$

Hence, as follows from Eq. (3.22), the sign of the final asymmetry reads:

$$\mathrm{sgn}(N_{B-L}(\infty)) = \begin{cases} -\mathrm{sgn}(\epsilon^{(1)}_{\tau\tau})\mathrm{sgn}(p_{1\tau^\perp} - p_{1\tau})\,, & \text{if } z_{\rm out} < \widetilde{z}_\Lambda \quad (\mathcal{S} < 0)\,; \\ \mathrm{sgn}(\epsilon^{(1)}_{\tau\tau})\mathrm{sgn}(p_{1\tau^\perp} - p_{1\tau})\,, & \text{if } z_{\rm out} > \widetilde{z}_\Lambda \quad (\mathcal{S} > 0)\,. \end{cases} \tag{3.27}$$

At $z_{\rm out} = \widetilde{z}_\Lambda$ we have $\mathcal{S} = 0$ and therefore $N_{B-L}(\infty) = 0$. Analytic expression for both $z_{\rm in}$ and $z_{\rm out}$ are given in Ref. [97]:

$$z_{\rm in}(\kappa_1) \simeq \frac{2}{\sqrt{\kappa_1}}\,, \qquad z_{\rm out} \simeq 1.25\log(25\kappa_1)\,. \tag{3.28}$$

In the weak wash-out regime the analysis is more complicated as the asymmetry may freeze at $z_f \neq z_{\rm out}$ and we do not have any analytic expression for this case. However, on the basis of the numerical analysis we did, we expect LG to end at $z_f$ smaller than a few tens.

We note that $\widetilde{z}_\Lambda$ depends only on $p_{1\tau}$, $\kappa_1$ and $\Lambda_\tau$, i.e. $\widetilde{z}_\Lambda = \widetilde{z}_\Lambda\,(p_{1\tau}, \kappa_1, \Lambda_\tau)$. If we neglect the weak dependence on the mass scale $M_1$ of $\kappa_1$, which comes from the loop contribution to the light neutrino masses [151], the only dependence of $\widetilde{z}_\Lambda$ on $M_1$ is inside $\Lambda_\tau \propto 1/M_1$. Therefore we have $\widetilde{z}_\Lambda \simeq \widetilde{z}_\Lambda\,(p_{1\tau}, \kappa_1, M_1)$. In addition, in the limit of $\Lambda_\tau \to 0$, i.e., at $M_1 \gg 10^{12}$ GeV, the integrated wash-out term – the second term in Eq. (3.23) – can be neglected so that the dependence of $\mathcal{S}$, and therefore of $\widetilde{z}_\Lambda$, on $p_{1\tau}$ drops off, i.e., $\widetilde{z}_\Lambda \simeq \widetilde{z}_\Lambda(\kappa_1, M_1)$. In terms of the Casas-Ibarra parametrisation this means that $\widetilde{z}_\Lambda$ does not depend on the PMNS phases. As the mass scale $M_1$ decreases, the integrated wash-out term becomes non-negligible activating a dependence on the PMNS phases through the product $p_{1\tau}p_{1\tau^\perp}$.

In the general case of three heavy Majorana neutrinos having non-degenerate but also non-hierarchical masses (e.g., $M_3 = 3M_2$, $M_2 = 3M_1$), the discussion is rather complicated due to the large number of parameters present in the Casas-Ibarra parametrisation. To make the discussion the most transparent as possible, we have considered the case of decoupled $N_3$, in which the number of parameters is significantly smaller than in the general case. We discuss the results in this case in the next section.

[6] We have checked numerically that $dN_{B-L}/dz \cong 0$ is indeed a sufficiently good approximation within the analysis performed by us.

## 3.2 The Case of Decoupled $N_3$

In the case of decoupled heavy Majorana neutrino $N_3$ ($M_1 \ll M_2 \ll M_3$), the lightest neutrino, as is well known, is massless at tree and one loop level, i.e., $m_1 \cong 0$ ($m_3 \cong 0$), and the light neutrino mass spectrum is normal (inverted) hierarchical, denoted as NH (IH). The set of parameters relevant for our discussion includes: the masses of the two heavy Majorana neutrinos $M_1$ and $M_2$; the three CPV phases $\delta$, $\alpha_{21}$, $\alpha_{31}$ of the PMNS matrix; the real and imaginary parts $x$ and $y$ of the complex angle of the Casas-Ibarra orthogonal $O$-matrix. The $O$-matrix for the NH and IH light neutrino mass spectra of interest has the form given in Eqs. (2.26) and (2.27). In what follows we will illustrate the results in the case of hierarchical mass spectrum of the two heavy Majorana neutrinos, $M_1 \ll M_2$. In particular, for numerical purposes, we fix $M_2 = 10M_1$.

### 3.2.1 Low-Energy CP-Violation

We are interested in the scenario of LG in which the CP-violation is due exclusively to the low-energy CPV phases present in the PMNS matrix. Correspondingly, we should avoid contributions to CP-violation in LG associated with the $O$-matrix. To satisfy this requirement we can [141] either set i) $y = 0$ and $x \neq 0$, which corresponds to a real $O$-matrix; or 2) $x = k\pi$, $k = 0, 1, 2$, and $y \neq 0$, so that in the case of NH (IH) spectrum the product $O_{12}O_{13}$ ($O_{11}O_{12}$) of the $O$-matrix elements (see Eqs. (2.26) and (2.27)), which enters into the expression for the CP-asymmetry $\epsilon^{(1)}_{\tau\tau}$, is purely imaginary.

We first report the expressions for $\kappa_1$, $p_{1\tau}$ and $\epsilon^{(1)}_{\tau\tau}$ in the NH case for $y = 0$ (real $O_{12}O_{13}$), relevant for our further analysis:

$$k_1 = \frac{1}{m_*}\frac{f^{-1}(M_1)}{M_1}\left(m_2\cos^2 x + m_3 \sin^2 x\right), \tag{3.29}$$

$$p_{1\tau} = \frac{m_2|U_{\tau 2}|^2\cos^2 x + m_3|U_{\tau 3}|^2\sin^2 x + \sqrt{m_2 m_3}\Re\left(U^*_{\tau 2}U_{\tau 3}\right)\sin 2x}{m_2\cos^2 x + m_3\sin^2 x}, \tag{3.30}$$

$$\epsilon^{(1)}_{\tau\tau} = \frac{3M_1}{16\pi v^2}\frac{f^{-1}(M_2)}{M_2}\frac{\sqrt{m_2 m_3}(m_3 - m_2)\sin 2x}{m_2\cos^2 x + m_3\sin^2 x}\Im\left(U^*_{\tau 2}U_{\tau 3}\right) + \mathcal{O}\left(\frac{M_1}{M_2}\right), \tag{3.31}$$

where $m_*$ and $f(M_{1,2})$ are defined in Eqs. (2.38) and (2.16). The corresponding expressions for the IH spectrum can formally be obtained from those given above by changing $m_{2(3)} \to m_{1(2)}$ and $U_{\tau 2(\tau 3)} \to U_{\tau 1(\tau 2)}$.

For the $M_1$ and $M_2$ mass ranges we are going to consider, namely $M_1 = (10^9 - 10^{13})$ GeV, $M_2 = 10M_1$, the factors $f^{-1}(M_1)/M_1$ and $f^{-1}(M_2)/M_2$ in the expressions for $k_1$ and $\epsilon^{(1)}_{\tau\tau}$ vary slowly in the intervals $1.16 - 1.27$ and $1.19 - 1.30$, respectively, increasing from the minimal values as $M_1$ and $M_2$ increase.

The combinations of the PMNS entries that appear in equations (3.29) - (3.31) are given

by:

$$|U_{\tau 1}|^2 = s^2_{12}s^2_{23} + c^2_{12}c^2_{23}s^2_{13} - 2s_{12}c_{12}s_{23}c_{23}s_{13}\cos\delta\,, \tag{3.32}$$

$$|U_{\tau 2}|^2 = c^2_{12}s^2_{23} + s^2_{12}c^2_{23}s^2_{13} + 2s_{12}c_{12}s_{23}c_{23}s_{13}\cos\delta\,, \tag{3.33}$$

$$|U_{\tau 3}|^2 = c^2_{23}c^2_{13}\,, \tag{3.34}$$

$$\Im\left(U^*_{\tau 2}U_{\tau 3}\right) = c_{23}c_{13}\left[c_{12}s_{23}\sin\left(\frac{\alpha_{21}-\alpha_{31}}{2}\right) + s_{12}c_{23}s_{13}\sin\left(\frac{\alpha_{21}-\alpha_{31}}{2}+\delta\right)\right]\,, \tag{3.35}$$

$$\Re\left(U^*_{\tau 2}U_{\tau 3}\right) = -c_{23}c_{13}\left[c_{12}s_{23}\cos\left(\frac{\alpha_{21}-\alpha_{31}}{2}\right) + s_{12}c_{23}s_{13}\cos\left(\frac{\alpha_{21}-\alpha_{31}}{2}+\delta\right)\right]\,, \tag{3.36}$$

$$\begin{aligned}\Im\left(U^*_{\tau 1}U_{\tau 2}\right) = &-s_{12}c_{12}\left(s^2_{23}-c^2_{23}s^2_{13}\right)\sin\left(\frac{\alpha_{21}}{2}\right) + \\ &-s_{23}c_{23}s_{13}\left[c^2_{12}\sin\left(\delta-\frac{\alpha_{21}}{2}\right) + s^2_{12}\sin\left(\frac{\alpha_{21}}{2}+\delta\right)\right]\,,\end{aligned} \tag{3.37}$$

$$\begin{aligned}\Re\left(U^*_{\tau 1}U_{\tau 2}\right) = &-s_{12}c_{12}\left(s^2_{23}-c^2_{23}s^2_{13}\right)\cos\left(\frac{\alpha_{21}}{2}\right) \\ &+s_{23}c_{23}s_{13}\left[c^2_{12}\cos\left(\delta-\frac{\alpha_{21}}{2}\right) - s^2_{12}\cos\left(\frac{\alpha_{21}}{2}+\delta\right)\right]\,.\end{aligned} \tag{3.38}$$

In the NH (IH) case, only the Majorana CPV phase difference (phase) $\alpha_{21}-\alpha_{31}$ ($\alpha_{21}$) is physically relevant [7]. We note also that the dependence on $\delta$ is always suppressed by $\sin\theta_{13}$. Thus, for the NH (IH) neutrino mass spectrum $\widetilde{z}_\Lambda$ is predominantly a function of the Majorana phase $\alpha_{23}$ ($\alpha_{21}$), of the real part of the $O$-matrix angle $x$ and of the mass scale $M_1$, exhibiting also subleading dependence on $\delta$.

For the CP-conserving values of the Dirac and Majorana phases, $\delta = 0, \pi$, $\alpha_{21} = k_{21}\pi$ and $\alpha_{31} = k_{31}\pi$, $k_{21} = 0, 1, 2, ...$, $k_{31} = 0, 1, 2, ...$, with $\alpha_{23} \neq \pm 2n\pi$ ($\alpha_{21} \neq 2n\pi$), $n = 0$, 1, 2, in the NH (IH) case, and real values of the elements of the $O$-matrix, $x \neq 0$, $y = 0$, the CP-symmetry is nevertheless violated in LG due to the interplay of the CP-conserving PMNS and real $O$ matrices [141] and $\epsilon^{(1)}_{\tau\tau} \neq 0$, as also follows from Eqs. (3.31), (3.35) and (3.37).

We present graphically in Fig. 3.3 the dependence of the decay parameter $\kappa_1$ on $x$ for NH and IH neutrino mass spectra when $y = 0$. As Fig. 3.3 shows, in both the NH and IH cases LG occurs in the strong wash-out regime, i.e., $\kappa_1 \gg 1$ for any choice of $x$. We can therefore rely on Eq. (3.27) to study the change of sign of $\eta_B$ in the 1-to-2 flavour transition when $y = 0$ and $x \neq 0$.

For $y = 0$ and $x \neq 0$, i.e., for real elements of the $O$-matrix, the final baryon asymmetry $\eta_B$ is always suppressed in the IH case with respect to that in the NH case [141]. This is a consequence of the fact that the CP-asymmetry $\epsilon^{(1)}_{\tau\tau}$ in the NH and IH cases, $\epsilon^{(\rm NH)}$ and $\epsilon^{(\rm IH)}$, are proportional respectively to $m_3 - m_2$ and $m_2 - m_1$ (see Eq. (3.31) and the subsequent discussion), $m_{3,2} \equiv m_{3,2}(\rm NH)$ and $m_{2,1} \equiv m_{2,1}(\rm IH)$ being the corresponding light neutrino masses of the two spectra (see Sec. 2.1), so that

$$\frac{\left|\epsilon^{(\rm IH)}\right|}{\left|\epsilon^{(\rm NH)}\right|} \propto \frac{1}{2}\left(\frac{\Delta m^2_{21}}{\Delta m^2_{\rm atm}}\right)^{3/4} \approx \frac{1}{30}. \tag{3.39}$$

As a consequence, it is impossible to have viable LG for IH neutrino mass spectrum with CP-violation provided only by the CPV phases in the PMNS matrix and real $O$-matrix for

[7] We will call the Majorana phase difference $\alpha_{23}$ simply "Majorana phase" and will denote it as $\alpha_{23}$ in what follows.

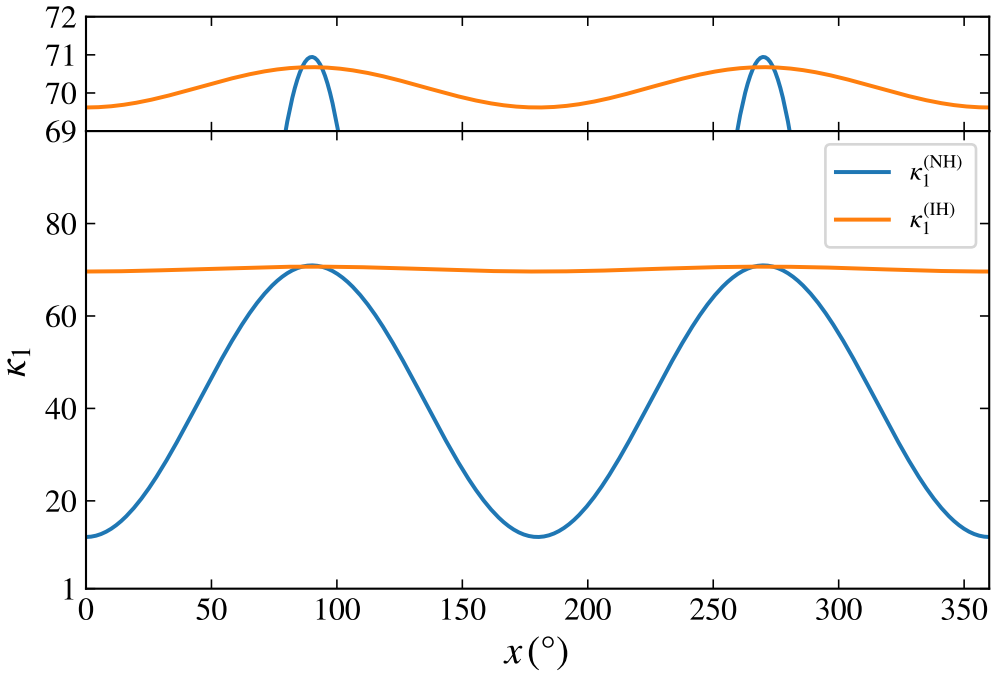


**Figure 3.3.** The decay parameter $\kappa_1$ versus $x$ for NH (blue) and IH (orange) light neutrino mass spectra with real $O$-matrix, i.e., $y = 0$. As the figure shows, $\kappa_1 \gg 1$, meaning that LG occurs always in the strong wash-out regime. The figure illustrates also the periodicity of $\pi$ in the $\kappa_1$ dependence on $x$. The top panel illustrates the small oscillations of the IH curve.

$M_1 \lesssim 10^{13}$ GeV. The suppression can be avoided in the considered scenario if the product $O_{11}O_{12}$ of the $O$-matrix elements is purely imaginary [141], i.e., if $x = k\pi$, $k = 0, 1, 2$, and $y \neq 0$. Under the conditions $x = k\pi$ and $y \neq 0$, the expressions for $\kappa_1$, $p_{1\tau}$ and $\epsilon^{(1)}_{\tau\tau}$ in the IH case take the form:

$$k_1 = \frac{1}{m_*}\frac{f^{-1}(M_1)}{M_1}\left(m_1\cosh^2 y + m_2\sinh^2 y\right), \tag{3.40}$$

$$p_{1\tau} = \frac{m_1|U_{\tau 1}|^2\cosh^2 y + m_2|U_{\tau 2}|^2\sinh^2 y - \sqrt{m_1 m_2}\Im\left(U^*_{\tau 1}U_{\tau 2}\right)\sinh 2y}{m_1\cosh^2 y + m_2\sinh^2 y}, \tag{3.41}$$

$$\epsilon^{(1)}_{\tau\tau} = -\frac{3M_1}{16\pi v^2}\frac{f^{-1}(M_2)}{M_2}\frac{\sqrt{m_1 m_2}(m_2+m_1)\sinh 2y}{m_1\cosh^2 y + m_2\sinh^2 y}\Re\left(U^*_{\tau 1}U_{\tau 2}\right) + \mathcal{O}\left(\frac{M_1}{M_2}\right). \tag{3.42}$$

The corresponding expressions for the NH spectrum can formally be obtained from those given above by changing $m_{1(2)} \to m_{2(3)}$ and $U_{\tau 1(\tau 2)} \to U_{\tau 2(\tau 3)}$.

The suppression of $\eta_B$ in the IH case is now avoided due to the presence of the factor $(m_1 + m_2)$ in the CPV-asymmetry $\epsilon^{(1)}_{\tau\tau}$.

For $x = k\pi$, $k = 0, 1, 2$, and $y \neq 0$, the strong wash-out condition $\kappa_1 \gg 1$ is always satisfied, as is shown in Fig. 3.4. Thus, also in this case we can rely on Eq. (3.27) to discuss the the sign change of $\eta_B$ at the 1-to-2 flavour transition.

For the $O$-matrix corresponding to the NH (IH) spectrum with elements $O_{12}$ and $O_{13}$ ($O_{11}$ and $O_{12}$) whose product is purely imaginary, i.e., $x = k\pi$ and $y \neq 0$, CP can also be violated in LG due to the interplay between the $O$-matrix and the CP-conserving PMNS matrix [141].

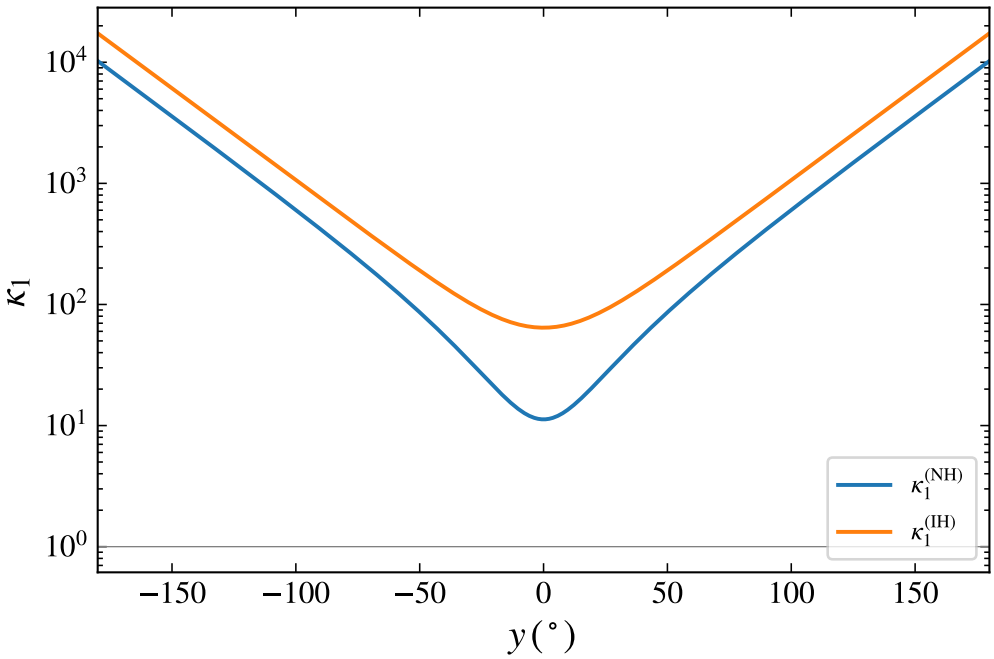


**Figure 3.4.** The decay parameter $\kappa_1$ as a function of $y$ for NH (blue) and IH (orange) light neutrino mass spectra in the case of purely imaginary product $O_{12}O_{13}$ ($O_{11}O_{12}$), i.e., $x = 0,\ \pi,\ ...$ . As the figure shows, $\kappa_1 \gg 1$, meaning that LG always takes place in the strong wash-out regime.

This possibility is realised for the CP-conserving values of the Dirac and Majorana phases, $\delta = 0, \pi$, $\alpha_{21} = k_{21}\pi$ and $\alpha_{31} = k_{31}\pi$, $k_{21} = 0, 1, 2, ...$, $k_{31} = 0, 1, 2, ...$, with $\alpha_{23} \neq \pm(2n+1)\pi$ ($\alpha_{21} \neq (2n+1)\pi$), $n = 0,\ 1$, in the NH (IH) case. Under these conditions we have $\epsilon^{(1)}_{\tau\tau} \neq 0$, as also follows from Eqs. (3.42), (3.36) and (3.38).

Given that the asymmetry $\eta_B$ is approximately constant in the plateau region at $M_1 \gtrsim 3 \times 10^{12}$ GeV and decreases with the mass scale (see, e.g., Fig. 3.1 and the discussion in Sec. 3.1), the condition ensuring that $\eta_B$ is greater than or equal to the present BAU corresponds to the region of the parameter space for which we can have successful LG at $M_1 \gtrsim 3 \times 10^{12}$ GeV. Using Eqs. (1.6), (2.57) and (3.12), together with the fact that $\mathcal{I}_2(k_1; z_f) \approx -0.13$ in the strong wash-out regime in the VIA case (see Fig. 3.2), we get for the condition of interest:

$$\eta_B = -\,0.13\ \frac{c_s}{27}\Lambda_\tau \epsilon^{(1)}_{\tau\tau}(1 - 2p_{1\tau}) \gtrsim 6.1 \times 10^{-10}. \tag{3.43}$$

### 3.2.2 CP-Violation due to the Dirac Phase

We consider in this subsection the scenario of LG with decoupled $N_3$ and CP-violation due only to the Dirac phase $\delta$. To this end. the Majorana phase $\alpha_{23}$ ($\alpha_{21}$) is set in the NH (IH) case to the following CP-conserving values: i) $\pm 2n\pi$ ($2n\pi$), $n = 0,\ 1,\ 2$, when $x \neq 0$ and $y = 0$; ii) $\pm(2n+1)\pi$ ($(2n+1)\pi$), $n = 0,\ 1$, when $x = k\pi$, $k = 0, 1, 2$, and $y \neq 0$. With the choices of the values of $\alpha_{23}$ ($\alpha_{21}$) made we avoid the situation in which one of the sources of CP-violation in LG is the interplay between CP-conserving Majorana phases and $O$-matrix elements [141] that could be generated by the first term in the right hand side of Eq. (3.35) (Eq. (3.37)).

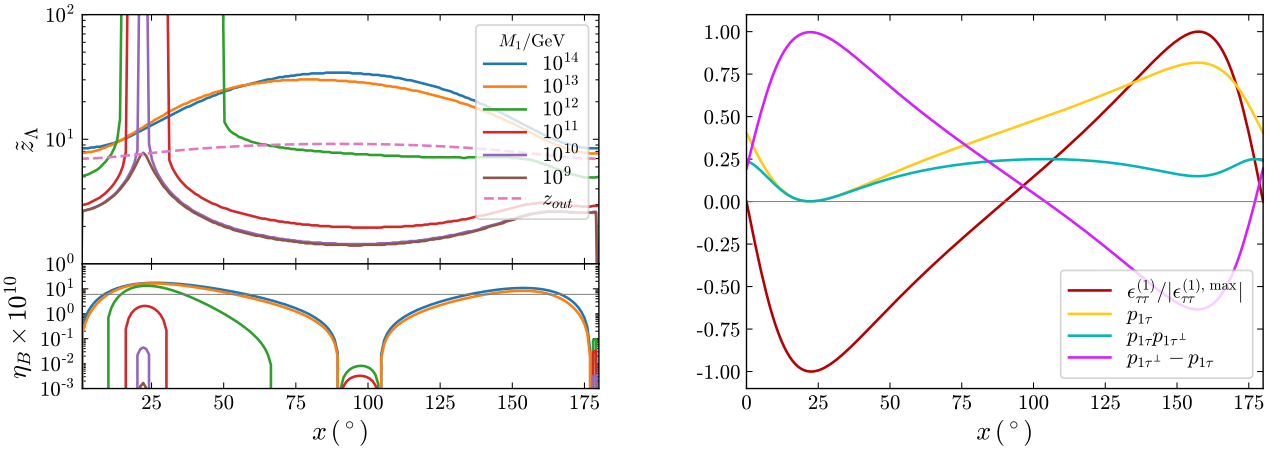


**Figure 3.5.** Top-left panel: $\widetilde{z}_\Lambda$ versus $x$ for different mass scales $M_1 = 10^{14}$ (blue), $10^{13}$ (orange), $10^{12}$ (green), $10^{11}$ (red), $10^{10}$ (purple), $10^9$ (brown) GeV. The dashed pink line corresponds to $z_{\rm out}$, when the generated $\eta_B$ gets frozen. Bottom-left panel: the final baryon asymmetry (with the correct positive sign) $\eta_B$ versus $x$ for the set of values of $M_1$ used to obtain the top panel. The horizontal grey line marks the present BAU at $6.1 \times 10^{-10}$. The right panel shows $\epsilon^{(1)}_{\tau\tau}$ normalised to its maximal value (dark blue), $p_{1\tau}$ (yellow), $p_{1\tau}p_{1\tau^\perp}$ (magenta) and $p_{1\tau^\perp} - p_{1\tau}$ (cyan). The sign of $\epsilon^{(1)}_{\tau\tau}(p_{1\tau^\perp} - p_{1\tau})$ is related to the sign of $\eta_B$ via Eq. (3.27). The plots are obtained for $M_2 = 10M_1$, $\delta = 3\pi/2$, $\alpha_{21} = \alpha_{31} = 0$ and NH spectrum. See the text for further details.

### The Case of Real $O$-Matrix ($x \neq 0$ and $y = 0$)

We show in the top-left panel of Fig. 3.5 the curves of $\widetilde{z}_\Lambda$ versus the angle $x$ for different mass scales $M_1$ assuming NH mass spectrum. The other parameters are set to: $\delta = 3\pi/2$, $\alpha_{23} = 0$ and $y = 0$. The interpretation of the figure in this panel on the basis of Eq. (3.27) should be the following. The values of $M_1$ and $x$ for which the $\widetilde{z}_\Lambda$ curve lies above the $z_{\rm out}$ curve correspond to $\mathrm{sgn}(N_{B-L}(\infty)) = -\mathrm{sgn}(\epsilon^{(1)}_{\tau\tau})\mathrm{sgn}(p_{1\tau^\perp} - p_{1\tau})$. Alternatively, if the $\widetilde{z}_\Lambda$ curve lies below the $z_{\rm out}$ one, then $\mathrm{sgn}(N_{B-L}(\infty)) = \mathrm{sgn}(\epsilon^{(1)}_{\tau\tau})\mathrm{sgn}(p_{1\tau^\perp} - p_{1\tau})$. The intersection points correspond to a vanishing $\eta_B$ and mark the 1-to-2 flavour transition. In the bottom-left panel the generated baryon asymmetry $\eta_B$ (with the correct sign) at different mass scales $M_1$ is also depicted. In the right panel we show the behaviour with $x$ of the relevant quantities: $\epsilon^{(1)}_{\tau\tau}$ (normalised to its absolute maximal value), $p_{1\tau}$, $p_{1\tau}p_{1\tau^\perp}$ and $p_{1\tau^\perp} - p_{1\tau}$. For the considered choice of the parameters, depending on $x$ we can have different scenarios. At $x \lesssim 10^\circ$ and $x \gtrsim 60^\circ$, the $10^{13,\,14}$ GeV curves lie above the $z_{\rm out}$ line while the $10^{12,\,11,\,10,\,9}$ GeV curves lie below (with the $10^{12}$ GeV curve lying near the $z_{\rm out}$ line). We can conclude that, for $x \lesssim 10^\circ$ and $x \gtrsim 60^\circ$, the 1-to-2 flavour transition occurs at values of $M_1$ slightly larger than $10^{12}$ GeV and with a sign change. According to the bottom-left panel, in the indicated ranges of $x$ we can have successful LG for values of $x \approx 150^\circ$ at $M \gtrsim 10^{13}$ GeV. At $x^{\rm min} \simeq 22.2^\circ$ the magenta curve in the right panel of Fig. 3.5, corresponding to $p_{1\tau}p_{1\tau^\perp}$, reaches an absolute minimum for the chosen value of $\alpha_{23} = 0$. We then note that in the range $10^\circ \lesssim x \lesssim 60^\circ$, the transition occurs at $M \lesssim 10^{12}$ GeV, and the more the range of $x$ is squeezed around $x^{\rm min}$, the lower is the mass scale of the transition. At $x^{\rm min}$ no sign change occurs at the transition, given that all the $\widetilde{z}_\Lambda$ curves obtained for $M_1 > 10^9$ GeV lie above the $z_{\rm out}$ line. As is shown in the bottom-left panel of Fig. 3.5,

at $x^{\rm min}$ the final baryon asymmetry $\eta_B$ is positive at any mass scale and reaches the observed value at $10^{11} \lesssim M_1/{\rm GeV} \lesssim 10^{12}$.

In Fig. 3.6 we plot $\eta_B$ as a function of $M_1$, calculated using the density matrix equations (DMEs), two-flavoured (1BEF2) and three-flavoured (1BEF3) Boltzmann equations, for different values of $x$, namely $x = 150°$ (top-left panel), $40°$ (top-right panel), $30°$ (bottom-left panel) and $22.2°$ (bottom-right panel).

The PMNS phases and $M_2$ are the same as in Fig. 3.5. The solid (dashed) blue curve corresponds to $\eta_B > 0$ ($\eta_B < 0$) and is obtained including the contributions from the $\mu$-Yukawa interactions, thus allowing to account for the 2-to-3 flavour transition when using the DMEs. The sign change of $\eta_B$ at the 1-to-2 (2-to-3) flavour transition is present in both the top and the bottom-left (in the top-right and bottom-left) panels. The mass scale $M_1$ of the 1-to-2 (2-to-3) flavour transition decreases with $x$ as it approaches the value $x^{\rm min} = 22.2°$ (stays essentially constant at $M_1 \simeq 10^9$ GeV). In the bottom-right panel the two transitions overlap so that the solution to the DMEs never approaches the 1BE2F solution.

For $x = 150°$ corresponding to the top-left panel in Fig. 3.6, successful LG takes place at $M_1 \simeq 4.0 \times 10^{12}$ GeV and the 1-to-2 flavour transition happens around $M_1 \simeq 10^{12}$ GeV, as one would have expected from the considerations made after Eq. (2.32). This panel shows an example of what we will call "standard" scenario of a 1-to-2 flavour transition at $\sim 10^{12}$ GeV under the assumption made about the source of CP-violation as well as the strong wash-out regime of $\eta_B$ generation. We note also that the 2-to-3 flavour transition happens at $M_1 \sim 10^9$ GeV with no sign change, as the DME solution (solid blue line) interpolates smoothly between the 1BE2F (green) line and the 1BE3F (red) one.

The remaining three panels of Fig. 3.6 represent examples of "non-standard" scenarios of the transition of interest, as the 1-to-2 flavour transition happens at a mass scale which decreases from $10^{12}$ GeV as $x$ decreases approaching $x^{\rm min}$, the value of $x$ at which the sign change does not occur and, as we will discuss, $\epsilon^{(1)}_{\tau\tau}$ has an absolute maximum (bottom-right panel). The scenarios in these panels are "non-standard" for the following reasons. Firstly, the product $p_{1\tau}p_{1\tau^\perp} \simeq p_{1\tau} \simeq 2.5 \times 10^{-2}$, $(1.5 \times 10^{-3})$ for $x = 30°$, $(22.2°)$ is so small that the integrated wash-out term in $\lambda$ is additionally strongly suppressed, allowing the plateau due the $\tau\tau^\perp$-decoherence contribution to extend below $10^{12}$ GeV. Secondly, since for $x = 30°\,(22.2°)$ we have

$$p_{1\tau}\kappa_1 \simeq 0.63,\ (2.8 \times 10^{-2}), \quad p_{1\tau^\perp}\kappa_1 \simeq \kappa_1 \simeq 24,\ (19), \tag{3.44}$$

the asymmetry in the $\tau^\perp$-flavour is generated in the strong wash-out regime, while the asymmetry in the $\tau$-flavour is produced in the weak wash-out regime. This scenario could not and was not considered in Sec. 3.1 [8]. Finally, Fig. 3.6 shows that the two-flavour approximation in the range $10^9 \lesssim M_1/{\rm GeV} \lesssim 10^{12}$ based on 1BE2F is not always accurate. For the case considered in the bottom-right panel of the figure, the DME solution for the asymmetry $\eta_B$ is enhanced by a factor of $\sim 10$ with respect to the asymmetry obtained by solving the Boltzmann equations in the two-flavour approximation. This leads, in particular, to successful LG at $M_1 \gtrsim 2.5 \times 10^{11}$ GeV. Most remarkably, in the case shown in the bottom-left panel, the asymmetry $\eta_B$ predicted by the DMEs (blue solid curve) at $M_1 \gtrsim 4.8 \times 10^{11}$ GeV has the correct sign allowing for successful LG, while the 1BE2F solution (green curve) gives $\eta_B < 0$ in the indicated range of $M_1$ and thus non-viable LG.

[8] Moreover, since $p_{1\tau}\kappa_1 \gtrsim 10^{-2}$, the analytic approximation used in Sec. 3.1 in the weak wash-out regime is not sufficiently accurate [97].

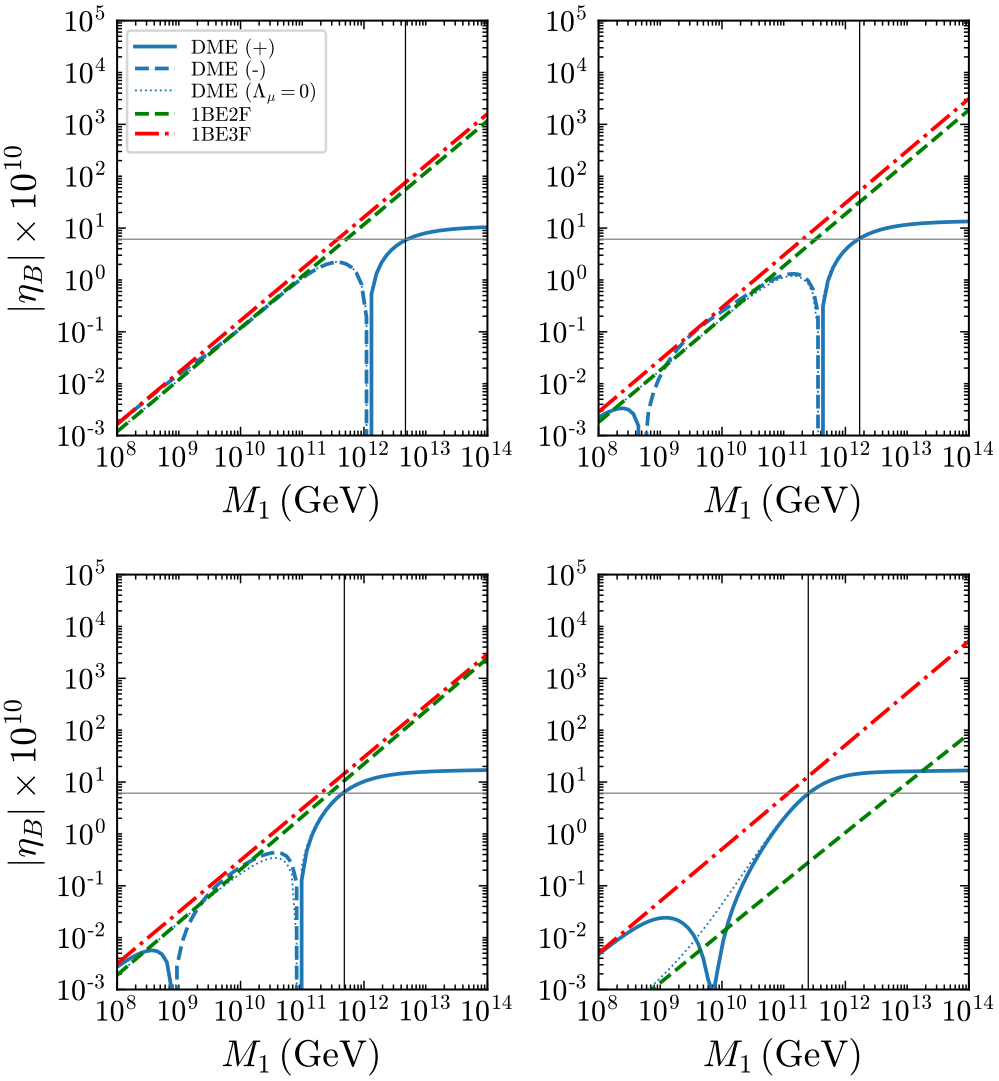


**Figure 3.6.** The four plots show the absolute value of the baryon asymmetry $\eta_B$ versus $M_1$ for NH spectrum, obtained with different sets of equations: DME (blue), 1BE2F (green), 1BE3F (red). The PMNS phases are chosen as in Fig. 3.5, $\delta = 3\pi/2$, $\alpha_{23} = 0$. The top-left, top-right, bottom-left and bottom-right panels are obtained for $x = 150°$, $40°$, $30°$ and $22.2°$, respectively. The solid (dashed) blue line corresponds to $\eta_B > 0$ ($\eta_B < 0$); the dotted blue line is obtained for $\Lambda_\mu = 0$. The horizontal grey line marks the present BAU at $6.1 \times 10^{-10}$ and is reproduced with the solution of DMEs at the minimal mass scales marked by the vertical black line, namely at $M_1 \simeq 4.7\,(1.7) \times 10^{12}$ GeV top-left (top-right) panel and $4.8\,(2.5) \times 10^{11}$ GeV bottom-left (bottom-right) panel. See the text for further details.

We note also that, as the top-right and bottom-left panels in Fig. 3.6 show, at the 2-to-3 flavour transitions at $M_1 \cong 10^9$ GeV, the baryon asymmetry $\eta_B$ changes sign going through zero, in contrast to the behaviour of $\eta_B$ shown in the top-left and bottom-right panels. For the chosen values of the CPV phases of the PMNS matrix the presence of this zero in $\eta_B$, as Fig. 3.6 indicates, depends on the value of $x$. For $x = 22.2^\circ$ (bottom-right panel), the 2-to-3 flavour transition takes place with $\eta_B$ not going through zero but only through a relatively shallow minimum at $M_1 \cong 10^{10}$ GeV.

**Ranges of $M_1$ and $\delta$ for Viable LG**

The case illustrated in the bottom-right panel of Fig. 3.6 is interesting for the following additional reasons. As our scan of the relevant parameter space shows, it is the case in which successful LG with two hierarchical in mass heavy Majorana neutrinos and CP-violation provided by the Dirac phases $\delta$ takes place for the minimal for the considered scenario value of $M_{1\min} \cong 2.5 \times 10^{11}$ GeV. The value of $x = x^{\min} = 22.2^\circ$ maximises the CP-asymmetry $\epsilon^{(1)}_{\tau\tau}$. Indeed, $\epsilon^{(1)}_{\tau\tau}$ depends on $x$ through the factor

$$f_\epsilon(x) = \frac{\sqrt{a}\,\sin 2x}{a\,\cos^2 x + \sin^2 x}\,, \quad a \equiv m_2/m_3\,, \tag{3.45}$$

which has an absolute maximum at [9] $x^{\min} = 22.2^\circ$: $f_\epsilon(x^{\min}) \cong 1.00$. The chosen value of $\delta$ also maximises $|\epsilon^{(1)}_{\tau\tau}|$. As $M_1$ increases from the value $M_1 \cong 2.5 \times 10^{11}$ GeV, $\eta_B$ also increases from $\eta_B = 6.1 \times 10^{-10}$ and, as Fig. 3.6 bottom-right panel shows, for $x = x^{\min}$ and $\delta = 3\pi/2$ reaches a plateau at $M_1 = 2.7 \times 10^{12}$ GeV, where $\eta_B = 1.60 \times 10^{-9}$ and [10] is larger than the observed value of $\eta_B$ by the factor $C_{P1} \cong 2.62$. For the value of $M_1 \gtrsim 2.7 \times 10^{12}$ GeV of the plateau, we have $\eta_B \propto (-\epsilon^{(1)}_{\tau\tau})$ (see Eq. (3.43)). Thus, $\eta_B$ will be compatible with the observed value of BAU for smaller value of $(-\epsilon^{(1)}_{\tau\tau}) > 0$, i.e., for smaller $(-f_\epsilon(x)\sin\delta) > 0$. The plateau value of $\eta_B$ corresponds to $x = x^{\min}$ and $\delta = 3\pi/2$ for which $(-f_\epsilon(x^{\min}\sin(3\pi/2)) = 1$. Thus, fixing $x = x^{\min}$ we get the minimal value of $(-\sin\delta) > 0$ for which we can have successful LG at $M_1 \gtrsim 2.7 \times 10^{12}$ GeV:

$$(-\sin\delta) \gtrsim C^{-1}_{P1} \cong 0.38\,, \quad \text{or} \quad 202.4^\circ \lesssim \delta \lesssim 337.6^\circ \tag{3.46}$$

The derived condition on $\delta$ is a necessary condition for successful LG within the considered scenario [11].

As $M_1$ decreases from $2.7 \times 10^{12}$ GeV to $2.5 \times 10^{11}$ GeV, $\eta_B$ decreases from the value at the plateau to the observed value and correspondingly, the interval of values of $\delta$ for which one can

[9] To be more precise, $f_\epsilon(x)$ has an absolute maximum at $x^{\max} = 0.5\arccos((m_3 - m_2)/(m_3 + m_2)) = 22.5^\circ$, where we have made use of $m_3 = \sqrt{\Delta m^2_{31}}$, $m_2 = \sqrt{\Delta m^2_{21}}$ and the best-fit values of $\Delta m^2_{31}$ and $\Delta m^2_{21}$ given in Table 2.1. However, as can be easily checked, $f_\epsilon(x^{\max}) - f_\epsilon(x^{\min}) \cong 10^{-4}$.

[10] As $M_1$ increases beyond $2.7 \times 10^{12}$ GeV, $\eta_B$ continues to grow very slowly due to the dependence of $\epsilon^{(1)}_{\tau\tau}$ on $f^{-1}(M_2)/M_2$, and at $M_1 = 10^{14}$ GeV ($M_2 = 10M_1$) we have $\eta_B \cong 1.67 \times 10^{-9}$.

[11] In Ref. [141], in the same scenario, the following condition for successful LG was obtained using the 1BE2F and assuming that the two-flavoured LG regime does not extend beyond $M_1 = 5 \times 10^{11}$ GeV: $|\sin\theta_{13}\sin\delta| \gtrsim 0.090$. In the same article the minimal scale of viable LG was found to be $M_{1\min} \cong 2.2 \times 10^{11}$ GeV, to be compared with $M_{1\min} \cong 2.5 \times 10^{11}$ GeV found by us. The lower limit on $(-\sin\delta)$ we have obtained in Eq. (3.46) implies $|\sin\theta_{13}\sin\delta| \gtrsim 0.057$, where we have used the best fit value of $\theta_{13}$ from Table 2.1. It is clear that our results based on the DME, in particular, extend the ranges of $\delta$ and $M_1$, for which we can have successful LG, derived in Ref. [141].

have viable LG also decreases shrinking to the point $\delta = 3\pi/2$ at $M_1 = 2.5\times10^{11}$. Clearly, there exists a correlation between the value of $\delta$ and the scale $M_1$ of viable LG. It follows from the preceding discussion also that in the considered scenario of CP-violation provided by the Dirac CPV phase $\delta$ of the PMNS matrix, it is possible to reproduce the observed value of BAU for values of $M_1$ spanning at least three orders of magnitude, i.e., for $2.5\times10^{11} \lesssim M_1/\text{GeV} \lesssim 10^{14}$.

In the case we have considered with $\alpha_{23} = 0$ and $x = x^{\min} = 22.2^\circ$, we can have successful LG, as Eq. (3.46) shows, for $\delta$ lying in the interval $\pi < \delta < 2\pi$, where $\sin\delta < 0$. So, the sign of $\sin\delta$ is anticorrelated with the sign of the observed $\eta_B$. This result holds also for the alternative possible values of $\alpha_{23} = \pm2\pi$ and all possible value of $x$, for which we can have viable LG. In other words, in the case under study there are no values of $\delta$ from the interval $0 < \delta < \pi$ where $\sin\delta > 0$, for which it is possible to reproduce the observed value of BAU.

Indeed, we note first that there is a periodicity of $\pi$ in the dependence on $x$, and of $4\pi$ in the dependence on $\alpha_{23}$, of all relevant quantities on which the predicted sign of $\eta_B$ depends: $\epsilon^{(1)}_{\tau\tau}$, $k_1$ and $p_{1\tau}$ (see Eqs. (3.29) - (3.38)). Therefore one gets the same results for $x$ and $x - \pi$. In the example with $\alpha_{23} = 0$ and $x = 22.2^\circ$ we have considered, we get the same result for $x = -157.8^\circ$ (or equivalently $x = 202.2^\circ$). If we set $\alpha_{23} = 2\pi$, the results will be the same for $\alpha_{23} = -2\pi$. Therefore the only possibility to have viable LG with $\sin\delta > 0$ is when $\alpha_{23} = 2\pi$. The quantities $\Re(U^*_{\tau2}U_{\tau3})\sin2x \propto -\beta_\alpha \sin2x$ and $\Im(U^*_{\tau2}U_{\tau3})\sin2x \propto \beta_\alpha \sin\delta\sin2x$, on which respectively $p_{1\tau}$ and $\epsilon^{(1)}_{\tau\tau}$ depend, change sign when $\alpha_{23}$ is changed from 0 to $2\pi$: $\beta_\alpha = 1$ $(-1)$ for $\alpha_{23} = 0$ $(2\pi)$. In addition $\Re(U^*_{\tau2}U_{\tau3})$ and $p_{1\tau}$ exhibit a sub-leading dependence on $\delta$ via terms proportional to $\sin\theta_{13}\cos\delta$. Thus, in what concerns the present discussion, changing the sign of $\sin\delta$ has negligible effect on $p_{1\tau}$. We recall that for $\alpha_{23} = 0$, $p_{1\tau}$ has a minimum at $x^{\min} = 22.2^\circ$ where $p_{1\tau} \ll 1$, so that we have $(1 - 2p_{1\tau}) > 0$ for the quantity on which, in particular, the sign of $\eta_B$ depends. The change of the sign of $\Re(U^*_{\tau2}U_{\tau3})\sin2x$ leads to a significant change of the value of $p_{1\tau}$, leading for $x^{\min} = 22.2^\circ$ to $(1 - 2p_{1\tau}) < 0$ and thus to non-viable LG for $\sin\delta > 0$.

It follows from the preceding considerations that the change of the signs of both $\Re(U^*_{\tau2}U_{\tau3})$ and $\Im(U^*_{\tau2}U_{\tau3})$ in the expressions for $p_{1\tau}$ and $\epsilon^{(1)}_{\tau\tau}$ can only be compensated simultaneously by changing $x$ to $\pi - x$, i.e., by a change of the sign of $\sin2x$. This implies that in addition to the solutions we have found for $\alpha_{23} = 0$ for certain ranges of $x$ (e.g., for $0 < x < \pi/2$) and of $\delta$ in the interval $\pi < \delta < 2\pi$, for $\alpha_{23} = 2\pi$ we will have successful LG in the range of $\pi - x$ (e.g., for $\pi/2 < x < \pi$) and for $\delta$ in the same interval. Thus, in the case of $\alpha_{23} = 2\pi$, a value of $\delta$ from the interval $0 < \delta < \pi$ with $\sin2x < 0$ $(\sin2x > 0)$ leads either to a wrong sign of $\eta_B$ due to the interplay of the signs of $p_{1\tau}$ and $\epsilon^{(1)}_{\tau\tau}$, or else to a value of $\eta_B$ which is smaller than the observed one.

The conclusions of the preceding discussions are confirmed by the numerical scan of the parameters $\delta$ and $x$ in the case of $\alpha_{23} = 0$ and $2\pi$ and several fixed values of $M_1$, the results of which are shown in Fig. 3.7. Thus, in the considered scenario there is a direct and unique relation between the sign of $\sin\delta$ and the sign of the baryon asymmetry of the Universe. If the measurement of $\delta$ in the low-energy neutrino oscillation experiments will show that $\delta$ lies in the interval $[0, \pi]$, the considered LG scenario will be ruled out. If, however, $\delta$ will be found to lie in the lower half-plane, $\pi < \delta < 2\pi$, this will not only lend support for the discussed scenario, but also will allow to obtain constraints on the LG scale.

Given that for $x \neq 0$, $y = 0$ and CP-violation due only to the Dirac phase $\delta$ LG is unsuccessful at any mass scale in the IH case (see Eq. (3.39) and the discussion related to it) we have not considered this case.

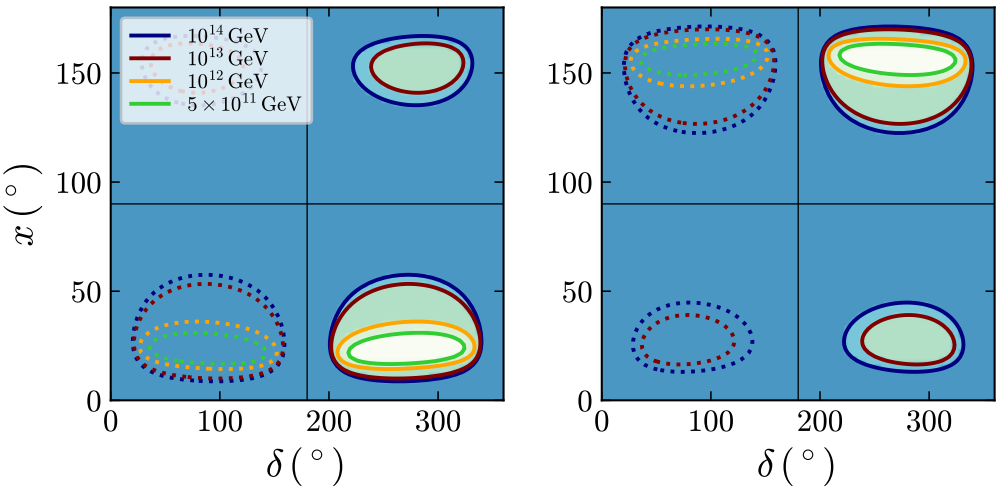


**Figure 3.7.** Regions of viable LG in the $\delta - x$ half plane, $0 \leq x \leq \pi$, for NH spectrum, real $O$-matrix, CP-violation due to the Dirac phase $\delta$, $\alpha_{23} = 0$ (left panel) and $2\pi$ (right panel) and different values of $M_1$. The solid contours corresponding to fixed values of $M_1$ surround the regions in which there is a combination of values of $\delta$ and $x$ for which $\eta_B = 6.1 \times 10^{-10}$. The dotted contours surround regions where one can have $|\eta_B| = 6.1 \times 10^{-10}$ but $\eta_B < 0$. The predicted $\eta_B$ outside the contours is always smaller in magnitude than the observed BAU. The regions of viable LG in the half-plane $-\pi \leq x \leq 0$ (or $\pi \leq x \leq 2\pi$), which are not shown, can be obtained from those in the figure by substituting $x$ with $x - \pi$. See the text for further details.

### Purely imaginary $O_{11}O_{12}$ $(O_{12}O_{13})$ $(x = k\pi,\ k = 0, 1, 2,\ y \neq 0)$

We discuss next the LG scenario in which CP-violation is still provided by the Dirac phase only, but now $x = k\,\pi$, $k = 0, 1, 2$, and $y \neq 0$ so that the product $O_{12}O_{13}$ $(O_{11}O_{12})$ is purely imaginary in the NH (IH) case and the suppression of the CP-asymmetry shown in Eq. (3.39) is avoided.

### NH Spectrum

The analysis is similar to that performed in the preceding subsection. We report below the results on the ranges of $\delta$ and $M_1$ for which one can have successful LG. For the minimal value of $M_1$ we get $M_1 = 1.7 \times 10^{11}$ GeV, which is obtained for $\delta = \pi/2$, $y = 26^\circ$ $(y = -26^\circ)$ and $\alpha_{23} = \pi$ or $-3\pi$ $(3\pi$ or $-\pi)$. This case is illustrated by Fig. 3.8. The value of $y$ maximises the factor

$$g_\epsilon(x) = \frac{\sqrt{a}\,\sinh 2y}{a\,\cosh^2 y + \sinh^2 y}\,, \quad a \equiv m_2/m_3\,, \tag{3.47}$$

in the expression for $\epsilon^{(1)}_{\tau\tau}$, and thus maximises $\epsilon^{(1)}_{\tau\tau}$ with respect to $y$. For $\alpha_{23} = \pi$ or $(-3\pi)$ the value of $\delta = \pi/2$ maximises $\epsilon^{(1)}_{\tau\tau}$ which is proportional to $\sin\delta$. At the plateau which begins at $M_1 \cong 2.1 \times 10^{12}$ GeV we have $\eta_B \cong C_{P2}\,6.1 \times 10^{-10}$ with $C_{P2} \cong 3.9$. Correspondingly, at $M_1 \gtrsim 2.1 \times 10^{12}$ GeV we can have successful LG for

$$\sin\delta \gtrsim C^{-1}_{P2} \cong 0.25\,, \quad \text{or} \quad 14.6^\circ \lesssim \delta \lesssim 165.4^\circ\,, \tag{3.48}$$

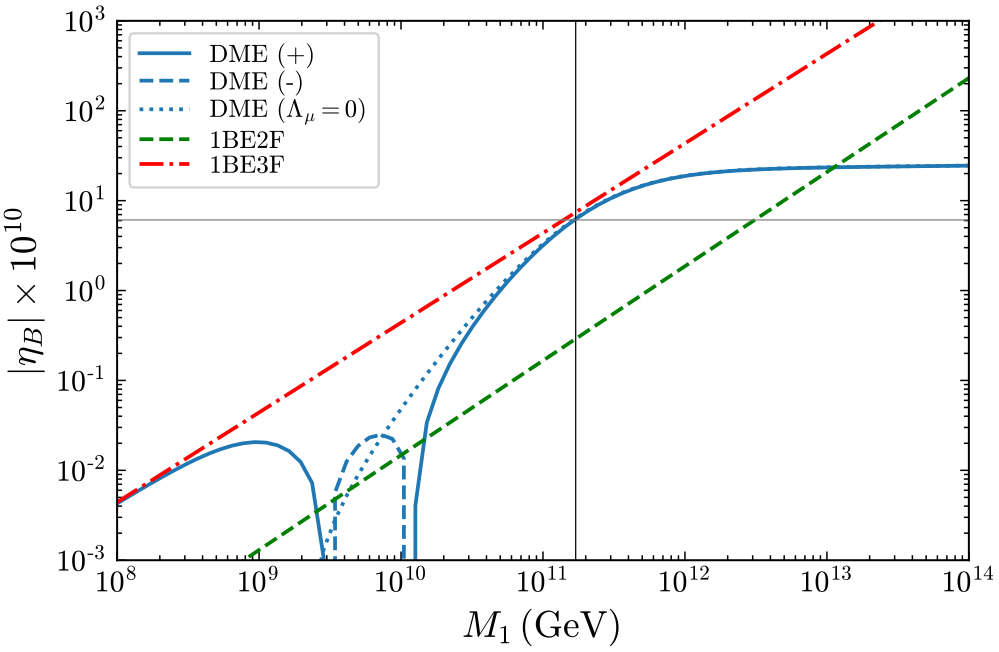


**Figure 3.8.** The baryon asymmetry $\eta_B$ versus $M_1$ for NH spectrum, $x = 0$, $y = 26°$ $(-26°)$, $\delta = \pi/2$ and $\alpha_{23} = \pi$ $(3\pi)$, for which successful LG takes place for the minimal value of $M_1 \cong 1.7 \times 10^{11}$ GeV (vertical black line). The requisite CP-violation is provided by the Dirac phase $\delta$. The horizontal black line corresponds to the observed $\eta_B = 6.1 \times 10^{-10}$. See the text for further details.

As $M_1$ decreases from $2.1 \times 10^{12}$ GeV to $1.7 \times 10^{11}$ GeV, $\eta_B$ decreases from the value at the plateau to the observed value and the width of the intervals of values of $\delta$ in Eq. (3.48) decreases. At $M_1 = 1.7 \times 10^{11}$ GeV it shrinks to the point $\delta = \pi/2$. In what concerns $M_1$, successful LG is possible for values of $M_1 \gtrsim 1.7 \times 10^{11}$ GeV, which span at least three orders of magnitude.

It follows from the preceding discussion that for $\alpha_{23} = \pi$ or $(-3\pi)$, one can have successful LG for value of $\delta$ from the interval $0 < \delta < \pi$ where $\sin\delta > 0$. Performing an analysis similar to that in the preceding subsection, we find that also in this case there is a direct relation between the sign of $\sin\delta$ and the sign of the observed BAU in the sense that for the values of the parameters in the considered case, no region with viable LG exists for $\delta$ from the interval $\pi < \delta < 2\pi$, where $\sin\delta < 0$. Changing the value of $\alpha_{23}$ from $\pi$ to $3\pi$, for example, one finds that the viable regions of values of $y$ and $\delta$ from the interval $0 < \delta < \pi$, for which it is possible to reproduce the observed value of BAU, shift to the regions corresponding to $(-y)$ with $\delta$ remaining in the same interval $0 < \delta < \pi$. This is confirmed by the numerical scan of the $y - \delta$ parameter space for $\alpha_{23} = \pi$ and $3\pi$, the results of which are shown in Fig. 3.9.

Obviously, the discussed LG scenario will be ruled out if $\delta$ determined in neutrino oscillation experiments is found definitely to lie in the interval $[\pi, 2\pi]$; if $\delta$ is found to be in the upper half-plane, $0 < \delta < \pi$, the scenario will be proven viable and it will be possible to obtain also constraints on the LG scale of the scenario.

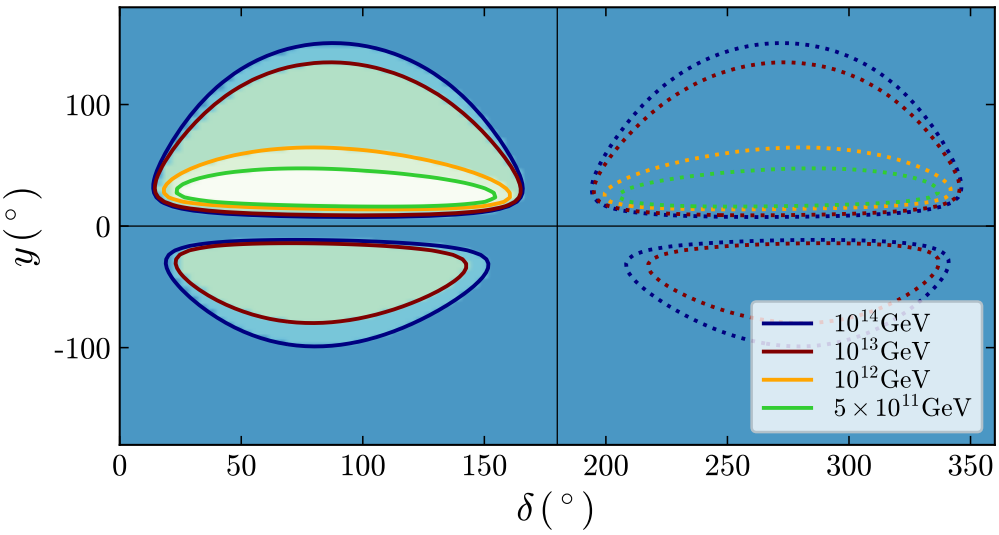


**Figure 3.9.** Regions of viable LG in the $\delta - y$ plane for NH spectrum, $x = k\pi$, $k = 0, 1, 2$, $\alpha_{23} = \pi$ and different $M_1$. The solid contours corresponding to fixed values of $M_1$ surround the regions in which there is a combination of values of $\delta$ and $y$ for which $\eta_B = 6.1 \times 10^{-10}$. The dotted contours surround regions where one can have $|\eta_B| = 6.1 \times 10^{-10}$ but $\eta_B < 0$. The predicted $\eta_B$ outside the contours is smaller in magnitude than the present BAU. Setting $\alpha_{23} = 3\pi$ leads to a figure which can be obtained from the present by changing $y$ to $-y$. See the text for further details.

### IH Spectrum

We analyse in somewhat greater detail the case of IH spectrum. We show in Fig. 3.10 the modulus of the baryon asymmetry $\eta_B$ versus $M_1$ for the IH spectrum with $\delta = 3\pi/2$, $\alpha_{21} = \pi$, $y = -100°$ (left panel) and $y = -46.5°$ (right panel). The dependence of $\eta_B$ on $M_1$ exhibits a number of interesting features. The 1-to-2 flavour transition described by DME takes place with a sign change of $\eta_B$. At values of $M_1 < M_{10}$ ($M_1 > M_{10}$), $M_{10}$ being the value of $M_1$ at which $\eta_B = 0$, we have $\eta_B < 0$ ($\eta_B > 0$). In the case illustrated in Fig. 3.10, we have $M_{10} \ll 10^{12}$ GeV. When $y$ changes from $(-100°)$ to $(-46.5°)$, $M_{10}$ decreases from $6.0 \times 10^{10}$ GeV to $2.4 \times 10^{10}$ GeV. Most importantly, the minimal value of $M_1$ at which one can have successful LG also decreases from $M_1 = 1.6 \times 10^{11}$ GeV to $M_1 = 6.2 \times 10^{10}$, with both values being $\ll 10^{12}$ GeV.

Further, the DME solution for $\eta_B$ shown in the left (right) panel of Fig. 3.10 is at $M_1 \leq 10^{12}$ GeV larger than (similar in magnitude to) $|\eta_B|$ found with 1BE2F, except in a narrow region around $M_{10}$. Still, $\eta_B$ obtained from the 1BE2F equations shown in both panels, in contrast to that derived from DME ones, has a wrong sign, i.e., predicts $\eta_B < 0$ and thus non-viable LG. The value of $|\eta_B|$ obtained with 1BE3F is in both cases, as the panels show, significantly smaller than those found with DME and 1BE2F. Moreover, the 2-to-3 flavour transition described by the DME solution takes place at $M_1 \lesssim 10^8$ GeV, with the $\mu$-Yukawa interaction having the effect of enhancing the DME solution for $|\eta_B|$ in the interval $10^8 \lesssim M_1/\text{GeV} \lesssim 10^{10}$. Both these features are in the region of values of $M_1$ for which the calculated $|\eta_B|$ is significantly smaller that the observed $\eta_B$. However, they might be relevant in a LG scenario with three heavy Majorana neutrinos with non-hierarchical masses, e.g., with $M_3 \cong 3M_2 \cong 9M_1$.

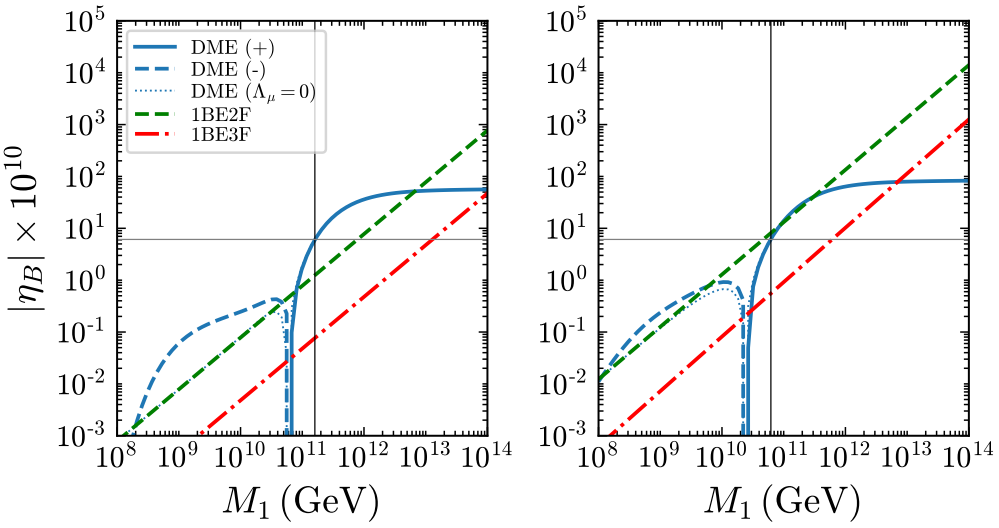


**Figure 3.10.** The same as in Fig. 3.6 but for $x = 0$ and $y \neq 0$ and in the IH case. The two panels correspond to CP-violation from the Dirac phase only with $\delta = 3\pi/2$, $\alpha_{21} = \pi$, $y = -100°$ (left panel) and $y = -46.5°$ (right panel). The vertical black lines correspond to $M_1 \simeq 1.6 \times 10^{11}$ GeV (left panel) and $M_1 \simeq 6.2 \times 10^{10}$ GeV (right panel). See the text for further details.

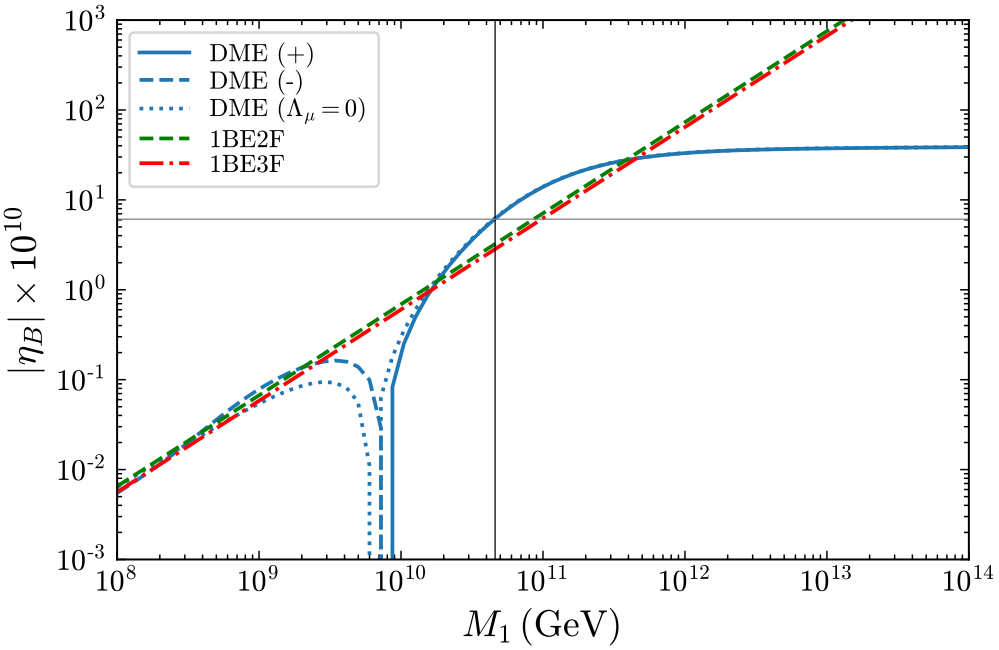


**Figure 3.11.** The baryon asymmetry $\eta_B$ versus $M_1$ for IH spectrum, $x = 0, \pi$, $y = -73°$ ($y = 73°$), $\alpha_{21} = \pi$ ($3\pi$) and $\delta = 211°$, for which successful LG takes place for the minimal value of $M_1 \cong 4.6 \times 10^{10}$ GeV (vertical black line). The requisite CP-violation is provided by the Dirac phase $\delta$. The horizontal black line corresponds to the observed $\eta_B = 6.1 \times 10^{-10}$. See the text for further details.

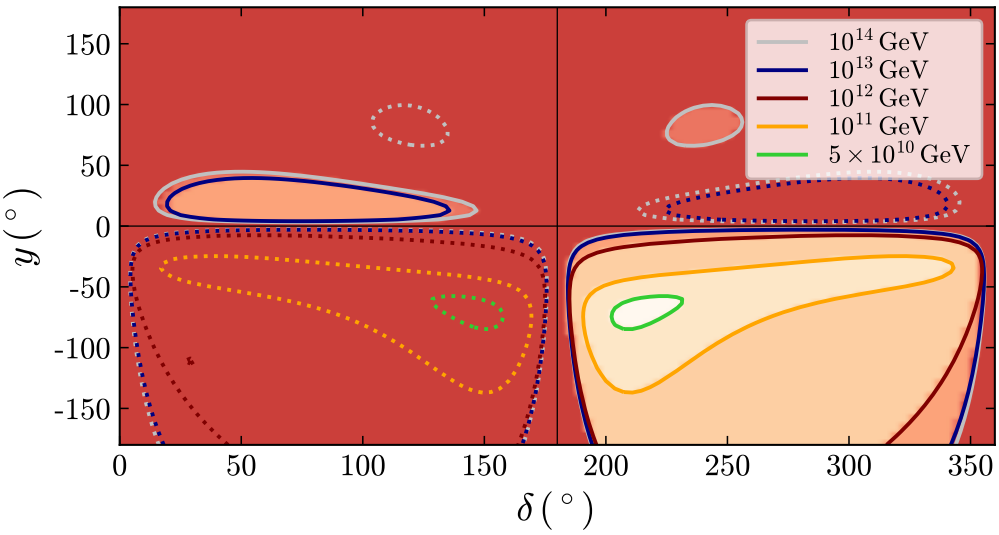


**Figure 3.12.** Regions of viable LG in the $\delta - y$ plane for IH spectrum, $x = k\pi$, $k = 0, 1, 2$, $\alpha_{21} = \pi$, corresponding to CP-violation due to the Dirac phase $\delta$, and different $M_1$. The solid contours corresponding to fixed values of $M_1$ surround the regions in which there exists a combination of values of $\delta$ and $y$ for which $\eta_B = 6.1 \times 10^{-10}$. The dotted contours surround regions where one can have $|\eta_B| = 6.1 \times 10^{-10}$ but $\eta_B < 0$. The predicted $\eta_B$ outside the contours is smaller in magnitude than the present BAU. Setting $\alpha_{21} = 3\pi$ leads to a figure which can be obtained from the present by changing $y$ to $-y$. See the text for further details.

In what concerns the range of $\delta$ and $M_1$ for which we have successful LG, we find that (see Fig. 3.11): i) the minimal value of $M_1$ is $M_1 \cong 4.6 \times 10^{10}$ GeV and corresponds to the values of $\alpha_{21} = \pi$ ($3\pi$), $y = -73^\circ$ ($y = +73^\circ$) and $\delta = 211^\circ$; ii) the plateau of values of $\eta_B$ is present at $M_1 \gtrsim 1.2 \times 10^{12}$ GeV; iii) at the plateau $\eta_B \cong C_{P3}\, 6.1 \times 10^{-10}$ with $C_{P3} \cong 6.1$. Correspondingly, at $M_1 \gtrsim 1.2 \times 10^{12}$ GeV successful LG is possible for

$$|\sin\delta| \gtrsim C_{P3}^{-1}\, |\sin(\delta = 211^\circ)| \cong 0.084\,, \quad \text{or } 185^\circ \lesssim \delta \lesssim 355^\circ\,, \tag{3.49}$$

where we have used the fact that the plateau value of $\eta_B$ corresponds to $\delta = 211^\circ$. We note that for the chosen values of $\alpha_{21} = \pi$, $y = -73^\circ$, $\epsilon_{\tau\tau}^{(1)}$ is proportional to $\sin\delta$ and thus at $\delta = 211^\circ$ $|\epsilon_{\tau\tau}^{(1)}|$ is smaller by the factor 0.515 than for $\delta = 3\pi/2$. However, due to the fact that, as can be shown, the value of $p_{1\tau}$ at $\delta = 211^\circ$ is smaller approximately by a factor of 6 than that at $\delta = 3\pi/2$, the minimal $M_1$ at which we can have successful LG is also smaller than the one for $3\pi/2$ which reads $M_1 \cong 10^{11}$ GeV. At the same time, $\eta_B$ at the plateau for $\delta = 3\pi/2$ is by a factor of approximately 1.9 times larger than the plateau value of $\eta_B$ for $\delta = 211^\circ$ and reads: $\eta_B = 7.3 \times 10^{-9}$.

As we have seen, in the discussed case of Dirac CP-violation and IH neutrino mass spectrum, successful LG is possible for values of $\delta$ from the interval $\pi < \delta < 2\pi$ where $\sin\delta < 0$. Performing a scan over $y$ and $\delta$ for the possible values of $\alpha_{21} = \pi$ and $3\pi$ with $x = k\pi$, $k = 0, 1, 2$, we find that for $M_1 \gtrsim 10^{13}$ GeV one can have a successful LG also for values of $\delta$ from the interval $0 < \delta < \pi$, and a small range of values of $y$ from the interval $0 < y < 50^\circ$. The appearance of this second region is related to the slow increase of $\epsilon_{\tau\tau}^{(1)}$ and thus of $\eta_B$ with $M_1$ due to the factor $f^{-1}(M_2)/M_2$. The results of the scan are presented graphically in Fig. 3.12. Thus, in this case

we have a direct relation between the sign of $\sin\delta$ and the sign of the baryon asymmetry of the Universe only for $M_1 < 10^{13}$ GeV.

### 3.2.3 CP-Violation due to the Majorana Phases

We illustrate next the results for the considered LG scenario with two heavy Majorana neutrinos with hierarchical masses in which the CP-violation is provided only by the Majorana phases of the PMNS matrix. Thus, the Dirac phase and the $O$-matrix elements are chosen not to contribute to the CP-violation necessary for the generation of BAU. We note that in the case of CP-violation due to the Majorana phases, the additional CP-violation due to the Dirac phase has sub-leading effects in LG as a consequence of the suppression by the factor $\sin\theta_{13}$. However, in certain cases these effects are non-negligible.

#### NH Spectrum

For real $O$-matrix it is impossible to have successful LG for IH light neutrino mass spectrum and CP-violation originating from CPV phases of the PMNS matrix, as we have already discussed, so we consider only the case of NH spectrum. We show in Fig. 3.13, top-left (top-right) panel, example of the behaviour of $\eta_B$ as a function of $M_1$ for $y = 0$ (real $O$-matrix), $x = 30^\circ\,(20.4^\circ)$, $\delta = \pi$, and $\alpha_{23} = 3\pi/2\,(700^\circ)$. The vertical black lines are at $M_1 \simeq 2.7 \times 10^{12}$ GeV (left panel) and $M_1 \simeq 1.7 \times 10^{11}$ GeV (right panel) and intersect the horizontal grey line of the observed BAU at the points of successful LG. The scenarios illustrated in the top-left and top-right panels of Fig. 3.13 correspond respectively to what we dubbed "standard" and "non-standard" behaviour of the baryon asymmetry $\eta_B$. The salient features of the behaviour of $\eta_B$ in the two cases are analogous to those discussed in detail in the two preceding subsections and we are not going to comment on them further.

We show in the bottom-left (right) panel of Fig. 3.13 the dependence of $\eta_B$ on $M_1$ for real (purely imaginary) $O_{12}O_{13}$ and $\delta = \pi$ in the case in which it is possible to have successful LG with CP-violation provided by the Majorana phase $\alpha_{23}$ for the minimal in the considered scenario value of $M_1$. The other relevant parameters have the following values in the left (right) panels: $x = 20^\circ$, $y = 0$ ($x = k\pi$, $k = 0, 1, 2$, $y = 19^\circ$) and $\alpha_{23} = 102^\circ$ ($80^\circ$). We will discuss in some detail in what follows first the case of $x = 20^\circ$, $y = 0$ and $\alpha_{23} = 102^\circ$, extending the discussion after that to the whole plane $0 < x < 180^\circ$.

The bottom-left panel of Fig. 3.13 illustrates one example of ranges of values of the Majorana phase $\alpha_{23}$ and $M_1$, for which one can have successful LG in the case of $0 < x < 90^\circ$, $y = 0$, $\delta = \pi$ and CP-violation provided by $\alpha_{23}$. As we have already remarked, this example corresponds to minimal $M_1$ for having viable LG in the case under study and is by far not exhaustive. We identify next qualitatively all the regions of $\alpha_{23}$ in the interval $0 < \alpha_{23} < 720^\circ$ and of $M_1$ where it is possible to have viable LG with $0 < x < 90^\circ$, $y = 0$ and $\delta = \pi$.

We note first that in the case under discussion $\eta_B$ goes through zero and changes sign in the 1-to-2 flavour regime transition in any of the regions of the parameter space of interest and there is always a plateau of values of $|\eta_B|$ at $M_1 > M_{10}$, $M_{10}$ being the value of $M_1$ at which $\eta_B = 0$. We recall that $\mathrm{sgn}(\eta_B)$ at the plateau is determined by $\mathrm{sgn}(-(1-2p_{1\tau})\epsilon^{(1)}_{\tau\tau})$ (see Eq. (3.43)), where $\mathrm{sgn}(\epsilon^{(1)}_{\tau\tau}) = \mathrm{sgn}(\Im(U^*_{\tau 2}U_{\tau 3})\sin 2x)$. It is not difficult to check that for the best-fit values of the neutrino oscillation parameters $\theta_{12}$, $\theta_{13}$, $\theta_{23}$, $\Delta m^2_{21}$ and $\Delta m^2_{31}$ given in Table 2.1, we have:

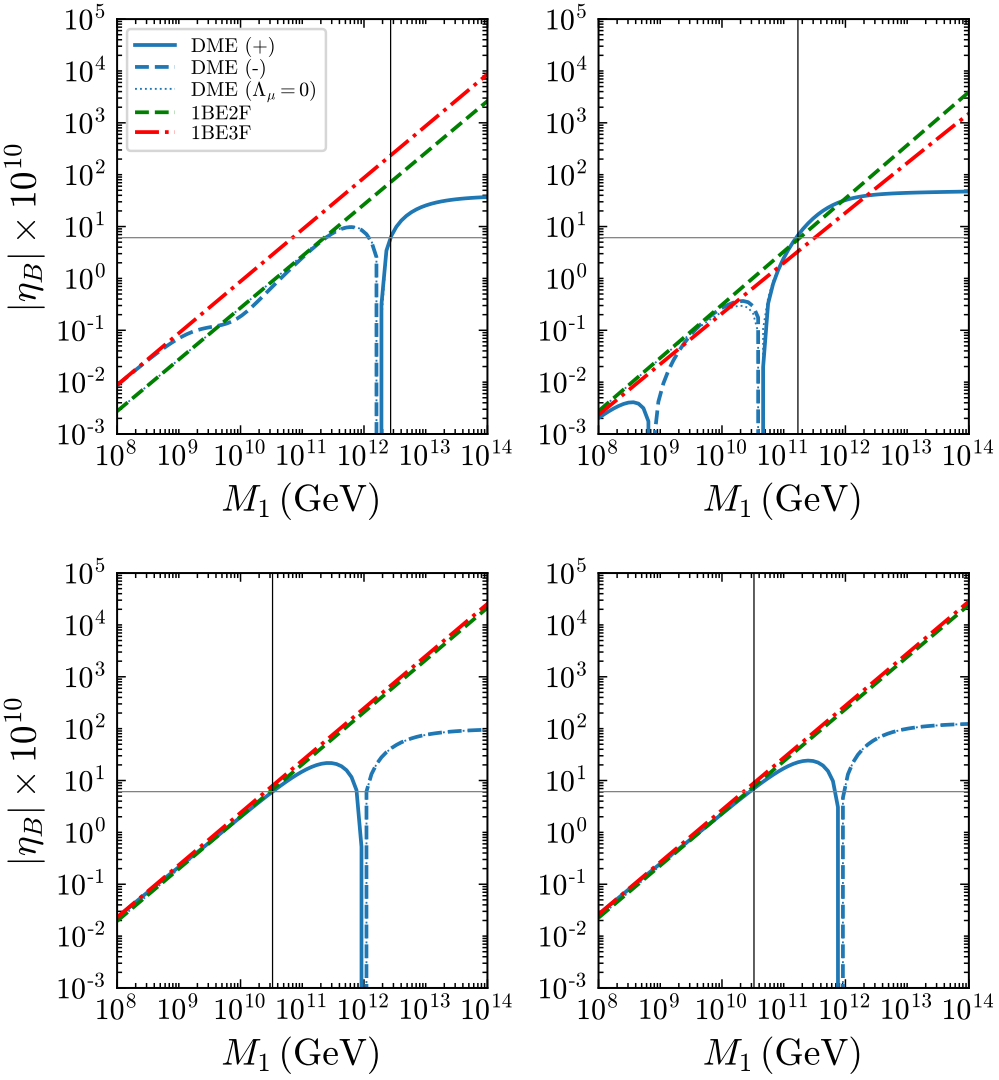


**Figure 3.13.** LG with CP-violation due to the Majorana phases of the PMNS matrix in the case of NH spectrum. Top panels: Two examples of "standard" (left) and "non-standard" (right) behaviour of $\eta_B$ as a function of $M_1$. The results shown are obtained as those in Fig. 3.6. The parameters in the left (right) panel are set to $\delta = \pi$, $y = 0$, $x = 30^\circ$ ($20.4^\circ$) and $\alpha_{23} = 3\pi/2$ ($700^\circ$). The vertical black lines are at $M_1 \simeq 2.7\times10^{12}$ GeV (left) and $M_1 \simeq 1.7\times10^{11}$ GeV (right) and intersect the horizontal grey line of the observed BAU at the points of successful LG. Bottom panels: The left (right) panel show the dependence of $\eta_B$ on $M_1$ for real (purely imaginary) $O_{12}O_{13}$ and $\delta = \pi$ in the case of minimal $M_1$ for which it is possible to have successful LG with CP-violation provided by the Majorana phase $\alpha_{23}$: the left (right) panel are obtained for $x = 20^\circ$, $y = 0$ ($x = k\pi$, $k = 0, 1, 2$, $y = 19^\circ$) and $\alpha_{23} = 102^\circ$ ($80^\circ$). See the text for further details.

i) for $5^\circ < x < 90^\circ$, $(1 - 2p_{1\tau}) > 0$ for $0 \leq \alpha_{23} < 220^\circ$ and $500^\circ < \alpha_{23} \leq 720^\circ$, with $(1 - 2p_{1\tau}) = 0$ at $\alpha_{23} \cong 220^\circ$ and $500^\circ$, where the precise values at which $(1 - 2p_{1\tau}) = 0$ depend somewhat on $x$: those corresponding to $x = 10^\circ$ are given approximately by $\alpha_{23} \cong 250^\circ$ and $470^\circ$; for $0 < x \lesssim 5^\circ$ we have $(1 - 2p_{1\tau}) > 0$ for any $\alpha_{23}$ from the interval $[0, 720^\circ]$;

ii) $\mathrm{sgn}(\Im(U^*_{\tau 2}U_{\tau 3})\sin 2x) > 0$ $(< 0)$ for $0 < \alpha_{23} < 360^\circ$ $(360^\circ < \alpha_{23} < 720^\circ)$.

We can conclude on the basis if these observations that, except for $0 < x \lesssim 5^\circ$, the plateau values of $\eta_B$

a) are negative approximately for $0 < \alpha_{23} < 220^\circ$ and $360^\circ < \alpha_{23} < 500^\circ$;

b) are positive for $220^\circ < \alpha_{23} < 360^\circ$ and $500^\circ < \alpha_{23} < 720^\circ$.

In the case of $x$ in the interval $0 < x \lesssim 5^\circ$, the plateau values of $\eta_B$ are negative (positive) for $0 < \alpha_{23} < 360^\circ$ $(360^\circ < \alpha_{23} < 720^\circ)$. However, as our numerical study shows, in this case it is possible to reproduce the observed value of $\eta_B$ only in a very a narrow interval of values of $x$, namely, for $2.5^\circ$ $(1.6^\circ) \lesssim x \lesssim 5^\circ$ with $\alpha_{23}$ in the range $0 < \alpha_{23} < 250^\circ$ $(450^\circ < \alpha_{23} < 720^\circ)$. As a consequence, this makes only a relatively small addition to regions in the space of parameters of the considered scenario for which one can have successful LG. Therefore we concentrate further on the case of $5^\circ < x < 90^\circ$.

It follows from the preceding discussion that if we denote by $M_{10}^{(1,2,3,4)}$ the values of $M_1$ at which $\eta_B = 0$ at the 1-to-2 flavour regime transitions taking place when $\alpha_{23}$ lies respectively in the intervals $(0, 220^\circ)$, $(360^\circ, 500^\circ)$, $(220^\circ, 360^\circ)$ and $(500^\circ, 720^\circ)$, we can expect successful LG to occur for certain ranges of values of $M_1 < M_{10}^{(1)}$ $(M_1 < M_{10}^{(2)})$ if $0 < \alpha_{23} < 220^\circ$ $(360^\circ < \alpha_{23} < 500^\circ)$, and of $M_1 > M_{10}^{(3)}$ $(M_1 > M_{10}^{(4)})$ extending into $\eta_B$ plateau region when $220^\circ < \alpha_{23} < 360^\circ$ $(500^\circ < \alpha_{23} < 720^\circ)$. Moreover, the results for $90^\circ < x < 180^\circ$ can be obtained from those derived for $0 < x < 90^\circ$ by making the simultaneous change $x \to \pi - x$ and $\alpha_{23} \to \alpha_{23} \pm 2\pi$ and taking into account that the results are invariant with respect to the change $\alpha_{23} \to \alpha_{23} \pm 4\pi$.

These qualitative conclusions are essentially confirmed by a thorough numerical analysis, the results of which are shown graphically in Fig. 3.14. We next summarise briefly these results giving the ranges of $\alpha_{23}$ and $M_1$ of viable LG in the four intervals of values of $\alpha_{23}$ identified earlier for $5^\circ < x < 90^\circ$. We will do it for the representative value of $x = 20.5^\circ$ at which some of the ranges of interest are maximal, commenting first the results for the specific values of $\alpha_{23}$ at which viable LG occurs for the minimal for the case value of $M_1$.

**Region I:** $0 < \alpha_{23} < 220^\circ$
The minimal mass scale $M_{1\mathrm{min}}$ for successful LG is found at $\alpha_{23} = 102^\circ$: $M_{1\mathrm{min}} = 3.3 \times 10^{10}$ GeV. For $\alpha_{23} = 102^\circ$:

i) viable LG is possible for $3.3 \times 10^{10}$ GeV $\lesssim M_1 \lesssim 7.7 \times 10^{11}$ GeV;

ii) the maximal value of the baryon asymmetry $\eta_B$ is reached at $M_1 \simeq 2.55 \times 10^{11}$ GeV and reads $\eta_B^{\mathrm{max}} \simeq 2.2 \times 10^{-9}$.

The range of $M_1$ and the maximal value of $\eta_B$ change when $\alpha_{23}$ increases (decreases) from $102^\circ$ to $208^\circ$ $(64.5^\circ)$, $208^\circ$ $(64.5^\circ)$ being the maximal (minimal) value of $\alpha_{23}$ at which it is possible to have

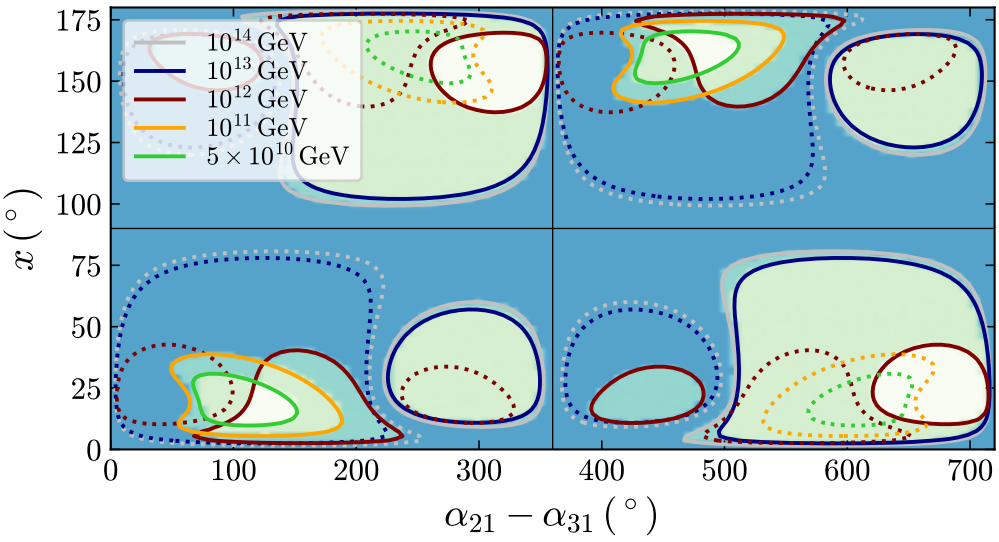


**Figure 3.14.** Regions of viable LG in the $\alpha_{23} - x$ plane for NH spectrum, $y = 0$, $\delta = \pi$, corresponding to CP-violation due to the Majorana phase $\alpha_{23}$, and different $M_1$. The solid contours corresponding to fixed values of $M_1$ surround the regions in which there is a combination of values of $\alpha_{23}$ and $x$ for which $\eta_B = 6.1 \times 10^{-10}$. The dotted contours surround regions where one can have $|\eta_B| = 6.1 \times 10^{-10}$ but $\eta_B < 0$. The predicted $\eta_B$ outside the contours is smaller in magnitude than the present BAU. See the text for further details.

successful LG (for $x = 20.5°$). As $\alpha_{23}$ increases to $\alpha_{23} = 170°$, the range of $M_1$ corresponding to $\alpha_{23}$ essentially shifts to larger values, with $\eta_B^{\max}$ remaining practically unchanged. More specifically, at $\alpha_{23} = 120°$, for example, the range of $M_1$ changes to $(3.3 \times 10^{10} - 1.1 \times 10^{12})$ GeV; at 170° it reads $(8.2 \times 10^{10} - 1.9 \times 10^{12})$ GeV. At $\alpha_{23} = 120°$ (170°), we have $\eta_B^{\max} \simeq 2.75\ (2.32) \times 10^{-9}$, which occurs at $M_1 \simeq 3.6\ (6.3) \times 10^{11}$ GeV.

As $\alpha_{23}$ increases further, $\eta_B^{\max}$ and the range of $M_1$ begin to decrease. At $\alpha_{23} = 195°$ we find $\eta_B^{\max} \simeq 1.2 \times 10^{-9}$ and $1.7 \times 10^{11} \lesssim M_1/\text{GeV} \lesssim 1.7 \times 10^{12}$, with $\eta_B^{\max}$ taking place at $M_1 \simeq 6.3 \times 10^{11}$ GeV. Finally, at $\alpha_{23} \simeq 208°$, $\eta_B^{\max}$ coincides with the observed value of BAU and the related range of $M_1$ reduced to the point $M_1 \simeq 6.3 \times 10^{11}$.

We find a similar pattern when $\alpha_{23}$ decreases from 102° to 64.5°. At $\alpha_{23} = 90°$ (75°), for example, we find for the range of interest of $M_1$: $3.4\,(4.4) \times 10^{10} \lesssim M_1/\text{GeV} \lesssim 5.2\,(2.7) \times 10^{11}$. The maximal asymmetry is $\eta_B^{\max} \simeq 1.7\ (1.0) \times 10^{-9}$ and occurs at $M_1 \simeq 2.1\,(1.4) \times 10^{11}$ GeV. When $\alpha_{23}$ decreases further, the range of $M_1$ and $\eta_B^{\max}$ also decrease further and, e.g., at $\alpha_{23} = 65°$ we have: $7.8 \times 10^{10} \lesssim M_1/\text{GeV} \lesssim 1.2 \times 10^{11}$, $\eta_B^{\max} \simeq 6.3 \times 10^{-10}$ which occurs at $M_1 \simeq 9.8 \times 10^{10}$ GeV. At 64.5° $\eta_B^{\max}$ coincides with observed value of $\eta_B$ and the range of $M_1$ reduces to the point $M_1 \simeq 9.0 \times 10^{10}$ GeV.

The interval of values of $\alpha_{23}$ and the related interval of values of $M_1$, where we can have successful LG, depend also on $x$, although this dependence is relatively weak. We find that at $x = 7.5°$ we get the largest maximal (smallest minimal) value $\alpha_{23}$ at which we still have successful LG in the considered range of $x$. These values read: $\alpha_{23}^{\min} = 37°$, $\alpha_{23}^{\max} = 233°$. The ranges of $M_1$ corresponding to $\alpha_{23}^{\min}$ and $\alpha_{23}^{\max}$ are just the points $M_1 \simeq 2.98 \times 10^{11}$ GeV and $M_1 \simeq 6.3 \times 10^{11}$ GeV, respectively. For $\alpha_{23} = 102°$, for example, we have at $x = 7.5°$: i) the range of $M_1$ of successful LG is $6.8 \times 10^{10} \lesssim M_1/\text{GeV} \lesssim 1.4 \times 10^{12}$, ii) $\eta_B^{\max} \simeq 1.69 \times 10^{-9}$, takes

place at $M_1 \simeq 4.33 \times 10^{11}$ GeV and is bigger than the observed $\eta_B$ by the factor $C_{M1} = 2.77$. These values should be compared with those given above for $x = 20.5°$. When $\alpha_{23}$ increases (decreases) to 233° (37°), we find quite similar behaviour of the correlation between the values of $\alpha_{23}$ and $M_1$ to that described for $x = 20.5°$, so we are not going to comment on it further.

**Region II:** $220° < \alpha_{23} < 360°$
The minimal mass scale $M_{1\min}$ for successful LG is found at $\alpha_{23} = 301°$: $M_{1\min} = 3.1 \times 10^{12}$ GeV. For $\alpha_{23} = 301°$:

i) the plateau of $\eta_B$ begins at $M_{1P} \simeq 8.9 \times 10^{13}$ GeV;

ii) the asymmetry at the plateau $\eta_B \simeq 3.38 \times 10^{-9}$.

The asymmetry at the plateau is larger than the observed value of $\eta_B$ by the factor $C_{M2} \simeq 5.54$. Knowing this factor allows us to determine the minimal and maximal values of $\alpha_{23}$ for having successful LG. The total range of values of $\alpha_{23}$ of interest reads:

$$227° \lesssim \alpha_{23} \lesssim 352°. \tag{3.50}$$

For the corresponding range of $M_1$ we get: $3.11 \times 10^{12} \lesssim M_1/\text{GeV} \lesssim 10^{14}$. with the minimal value obtained for $\alpha_{23} \simeq 301°$.

**Region III:** $360° < \alpha_{23} < 500°$
The minimal mass scale of LG is obtained for $\alpha_{23} = 433°$. For this choice of $\alpha_{23}$:

i) LG is successful for $1.54\times10^{11} \lesssim M_1/\text{GeV} \lesssim 1.59\times10^{12}$, where the maximal $M_1$ corresponds also to $\alpha_{23} = 433°$;

ii) the maximal value of $\eta_B$ is reached at $M_1 \simeq 6.28\times10^{11}$ GeV and reads $\eta_B^{\max} \simeq 1.37\times10^{-9}$.

The asymmetry $\eta_B$ at its maximum is greater than the observed value by a factor $C_{M3} \simeq 2.25$. The range of $\alpha_{23}$ of viable LG is

$$382° \lesssim \alpha_{23} \lesssim 482°\,. \tag{3.51}$$

**Region IV:** $500° < \alpha_{23} < 720°$
The minimal $M_1$ for having successful LG is found at $\alpha_{23} = 691°$ and reads $M_1 \simeq 1.53 \times 10^{11}$ GeV. At this value of $\alpha_{23}$,

i) the plateau of $\eta_B$ begins at $M_1 \simeq 4.98 \times 10^{12}$ GeV;

ii) the asymmetry at the plateau $\eta_B \simeq 4.11 \times 10^{-9}$.

This value is larger than the observed value of $\eta_B$ by the factor $C_{M4} \simeq 6.73$. Successful LG is possible for the following range of values of $\alpha_{23}$:

$$506° \lesssim \alpha_{23} \lesssim 716°. \tag{3.52}$$

For the quoted range of $\alpha_{23}$ we have viable LG for $1.54\times10^{11} \lesssim M_1/\text{GeV} \lesssim 10^{14}$. If $x \lesssim 5°$, the lower bound in the interval (3.52) is somewhat smaller at $\approx 470°$, but successful LG is possible only for $M_1 \gtrsim 10^{13}$ GeV.

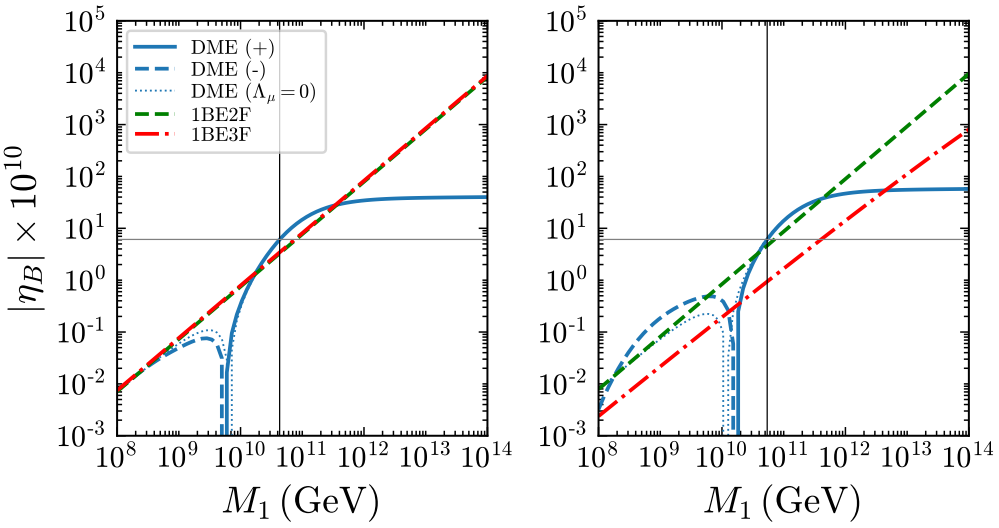


**Figure 3.15.** The asymmetry $\eta_B$ versus $M_1$ in the case of IH spectrum with CP-violation due to the Majorana phase $\alpha_{21}$ (Majorana and Dirac phases $\alpha_{21}$ and $\delta$) of the PMNS matrix. The results shown in the left (right) panel are obtained for $x = k\pi$, $k = 0, 1, 2$, $y \neq 0$ (purely imaginary $O_{11}O_{12}$) and $\alpha_{21} = 164^\circ$ ($190^\circ$) $\delta = \pi$ ($3\pi/2$) and $y = -76^\circ$ ($-50^\circ$). See the text for further details.

In all four cases we have discussed there exists a correlation between the value of the CPV phase $\alpha_{23}$ and the scale of LG $M_1$. Thus, obtaining constraints on $\alpha_{23}$ in low-energy experiments, in principle, can constrain the LG scale of the considered scenario, or even rule out this scenario.

### IH Spectrum

Viable LG in the scenario of interest is possible only for purely imaginary product $O_{11}O_{12}$ of elements of the $O$-matrix ($x = k\pi$, $k = 0, 1, 2$, $y \neq 0$). In Fig. 3.15 we show the modulus of $\eta_B$ versus $M_1$ for $\delta = \pi$ ($3\pi/2$) and values of the other parameters for which successful LG takes place for the minimal for the considered scenario value of $M_1$: $\alpha_{21} = 164^\circ$ ($190^\circ$), $y = -76^\circ$ ($-50^\circ$), for the left (right) panel. The right panel is obtained for $\delta = 3\pi/2$, so it illustrates the case of viable LG with CP-violation generated by both the Majorana and Dirac CPV phases of the PMNS matrix. It also illustrates the non-negligible effects the CP-violating Dirac phase $\delta$ can have in LG when the CP-violation is provided by the Majorana phase(s).

In both cases illustrated in Fig. 3.15, $\eta_B$ exhibits a "non-standard" behaviour as a function of $M_1$ going through zero in the 1-to-2 flavour transition at $M_1 \sim 10^{10}$ GeV $\ll 10^{12}$ GeV. In the left (right) panel the minimal value of $M_1$ at which the calculated $\eta_B$ matches the observed value of $\eta_B$ is $M_1 = 4.3 \times 10^{10}$ ($5.4 \times 10^{10}$) GeV. The plateau value of $\eta_B \cong 3.9 \times 10^{-9}$ ($5.6 \times 10^{-9}$) and is reached at $M_1 \cong 1.1 \times 10^{12}$ ($1.8 \times 10^{12}$) GeV. Performing a detailed numerical analysis we have determined the regions of viable LG in the space of parameters in the considered scenario with IH spectrum, CP-violation provided by $\alpha_{21}$, $x = k\pi$, $k = 0, 1, 2$, $y \neq 0$ (purely imaginary $O_{11}O_{12}$) and $\delta = \pi$. The values of $y$ were varied in the interval $[-180^\circ, +180^\circ]$. For $y = 0$ we have, obviously, $\eta_B = 0$. Due to symmetries of the quantities involved in the generation of $\eta_B$, the results for $0 \leq y \leq 180^\circ$ can formally be obtained from those derived for $-180^\circ \leq y \leq 0$

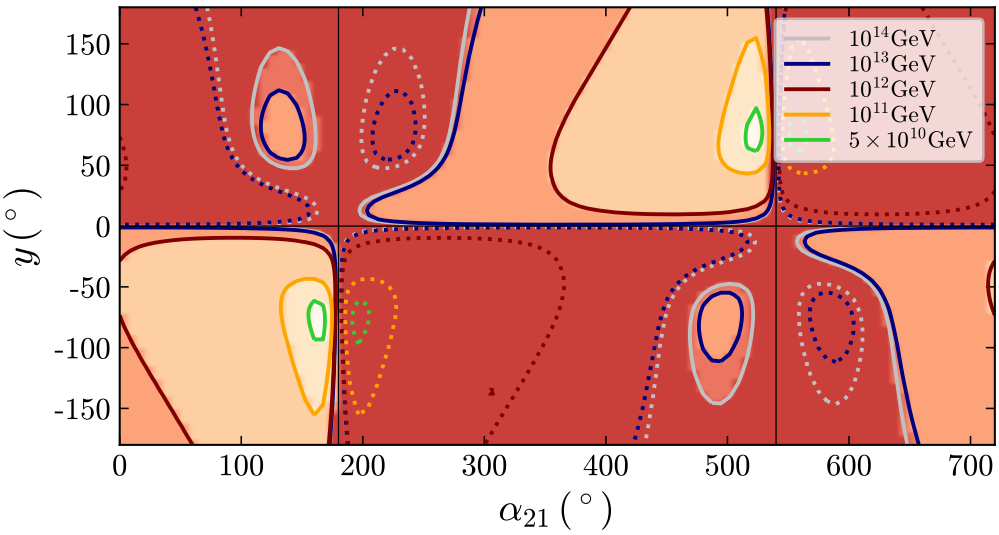


**Figure 3.16.** The regions of successful LG in the $\alpha_{21} - y$ plane in the case of IH spectrum and for $\delta = \pi$, purely imaginary $O_{11}O_{12}$ (i.e. $x = k\pi$, $k = 0, 1, 2$, $y \neq$) and different $M_1$. The solid contours corresponding to fixed values of $M_1$ surround the regions where there exists a combination of values of $\alpha_{21}$ and $y$ for which $\eta_B = 6.1 \times 10^{-10}$. The dotted contours surround regions where one can have $|\eta_B| = 6.1 \times 10^{-10}$ but $\eta_B < 0$. The predicted $\eta_B$ outside the contours is smaller in magnitude than the present BAU. The results for $0 \leq y \leq 180^\circ$ can be obtained from those derived for $-180^\circ \leq y \leq 0$ by making the simultaneous change $y \to -y$ and $\alpha_{21} \to \alpha_{21} \pm 2\pi$. See the text for further details.

by making the change $y \to -y$ and $\alpha_{21} \to \alpha_{21} \pm 2\pi$ and using the invariance with respect to $\alpha_{21} \to \alpha_{21} \pm 4\pi$. The results of this analysis are shown graphically in Fig. 3.16. A few comments are in order.

As we have already pointed out, the minimal value of $M_1$ for successful LG is found to take place at $y = -76^\circ$ and $\alpha_{21} = 164^\circ$. For $y = -76^\circ$ and $\alpha_{21} = 164^\circ$, the plateau value of $\eta_B$ given earlier is larger than the observed value of $\eta_B$ by the factor $C_{M5} \simeq 6.39$. We can determine then the range of $\alpha_{21}$ for viable LG the case of $y = -76^\circ$ and $\delta = \pi$ from the condition:

$$\cos(\alpha_{21}/2)\,(1 - 2p_{1\tau}(\alpha_{21})) \simeq C_{M5}^{-1}\cos(82^\circ)(1 - 2p_{1\tau}(164^\circ)) \tag{3.53}$$

For the range of interest we get:

$$0 \leq \alpha_{21} \lesssim 177.5^\circ \quad \text{and} \quad 632^\circ \lesssim \alpha_{21} \leq 720^\circ \tag{3.54}$$

When $y$ increases from $(-76^\circ)$ to near zero, the lower bound of the right interval decreases to $\simeq 560^\circ$. The corresponding range of values of $M_1$ extends from $M_1 \simeq 4.3 \times 10^{10}$ GeV to the beginning of the plateau at $M_1 \cong 1.1 \times 10^{12}$ and further on the plateau at least to $M_1 \simeq 10^{14}$ GeV. When $M_1$ decreases starting from $M_1 \simeq 1.1 \times 10^{12}$ at the plateau to $M_1 \simeq 4.3 \times 10^{10}$ GeV, the intervals of values of $\alpha_{21}$ of successful LG also decrease and at $M_1 \simeq 4.3 \times 10^{10}$ GeV shrink to the point $\alpha_{21} \simeq 164^\circ$.

There is an additional relatively small region of values of $\alpha_{21}$ and $M_1$ around $\alpha_{21} \sim 500^\circ$, for which it is possible to reproduce the observed value of BAU. It is clearly seen in Fig. 3.16. In this case the minimal mass scale takes place at $\alpha_{21} \simeq 493^\circ$, $y \simeq -76^\circ$ and reads $M_1 \simeq 5.9 \times 10^{12}$

GeV. At the plateau we have $\eta_B \simeq C_{M6}\, 6.1 \times 10^{-10}$, with $C_{M6} \simeq 1.83$. The range of $\alpha_{21}$ of viable LG can be determined using the equation:

$$\cos(\alpha_{21}/2)\ (1 - 2p_{1\tau}(\alpha_{21})) \simeq C_{M6}^{-1}\ \cos(246.5^\circ)\,(1 - 2p_{1\tau}(493^\circ))\,. \tag{3.55}$$

Solving the preceding equation we get for the range of $\alpha_{21}$:

$$468^\circ \lesssim \alpha_{21} \lesssim 522^\circ\,. \tag{3.56}$$

The corresponding range of the LG scale is $5.9 \times 10^{12} \lesssim M_1/\text{GeV} \lesssim 10^{14}$.

As in the previous scenarios discussed by us, also in the scenario considered in the present subsection there is a correlation between the low-energy phase – in this case $\alpha_{21}$ – responsible for the CP-violation in LG and the scale of LG $M_1$. Clearly, obtaining constraints on $\alpha_{21}$ in low-energy experiments can rule out the considered scenario or constrain the LG scale of the scenario.

## 3.3 Summary of the Results

In the work of Pub. [I], the results of which were illustrated in this chapter, we have considered the generation of the baryon asymmetry of the Universe $\eta_B$ in the (GUT) high-scale LG scenario based on the type-I seesaw mechanism of neutrino mass generation. Using the DMEs for high-scale LG in which the CP-violation is provided exclusively by the low-energy Dirac or/and Majorana phases of the neutrino mixing (PMNS) matrix, we have investigated the 1-to-2 and the 2-to-3 flavour regime transitions, and compared the results with those obtained with the BEs in the single-, two- and three-flavour regimes. Concentrating on the 1-to-2 flavour transitions in LG with three heavy Majorana neutrinos $N_{1,2,3}$ with hierarchical mass spectrum, $M_1 \ll M_2 \ll M_3$, we have determined the general conditions under which the baryon asymmetry $\eta_B$ goes through zero and changes sign in the transition. We have shown, in particular, that the asymmetry $\eta_B$ goes through zero changing its sign when LG proceeds in the strong wash-out regime with zero initial abundance of the heavy Majorana neutrinos.

In order to make the discussion of all the salient features of the transitions between the different flavour regimes of interest as transparent as possible, we have investigated further the case of decoupled heaviest Majorana neutrinos $N_3$, in which the number of parameters in LG is significantly smaller than in the general case of three heavy Majorana neutrinos. In particular, the complex orthogonal matrix $O$, which takes part in the Casas-Ibarra parametrisation of the neutrino Yukawa couplings we have employed in the analysis, depends only on one complex angle $\theta = x + iy$, where $x$ and $y$ are real parameters. With only two heavy Majorana neutrinos ($N_{1,2}$) active in the seesaw mechanism, the light neutrino mass spectrum can only be either NH with $m_1 \cong 0$, or IH, with $m_3 \cong 0$. Furthermore, in the case of interest of CP-violation in LG provided only by the low-energy CPV phases of the PMNS matrix, one can avoid the contributions to the CP-violation associated with the $O$-matrix only if the angle $\theta$ is such that for NH (IH) spectrum $\sin 2\theta \neq 0$ is real (purely imaginary) [141], $\sin 2\theta = \sin 2x$ ($\sin 2\theta = \pm i \sinh 2y$).

Analysing in detail the behaviour of $\eta_B$ in the transition in the case of two heavy Majorana neutrinos $N_{1,2}$ with hierarchical masses, $M_1 \ll M_2$, allowed us not only to gain a better understanding of the transitions, but also to discover new unexpected features of the transitions. We have found, in particular, that:

i) the BEs in many cases fail to describe correctly the generation of the baryon asymmetry $\eta_B$ in the single-, two- and three-flavour regimes, in particular, underestimating $\eta_B$ by a factor $\sim 10$ in certain cases;

ii) depending on the values of the relevant parameters, the transitions between the different flavour regimes can be "non-standard" as, e.g., the 1-to-2 and the 2-to-3 flavour transitions can take place at the same mass scale $M_1$, with $\eta_B$ going through a relatively shallow minimum at the transition value of $M_1$;

iii) the two-flavour regime can persist above $5 \times 10^{11} - 10^{12}$ GeV (below $\sim 10^9$ GeV), and

iv) the flavour decoherence effects in LG persist beyond what is usually thought to be the maximum LG scale for these effects of $\sim 10^{12}$ GeV, with the requisite CP-violation provided by the Dirac or/and Majorana phases present in the low-energy PMNS neutrino mixing matrix.

At $M_1 \sim 10^{12}$ GeV, $|\eta_B|$ reaches a "plateau" where it remains practically constant as $M_1$ increases and flavour effects are fully operative. We further have determined the minimal scale $M_{1\min}$ at which we can have successful LG when the CP-violation is provided only by the Dirac ($\delta$) or Majorana ($\alpha_{23} \equiv \alpha_{21} - \alpha_{31}$ or $\alpha_{21}$) phases of the PMNS matrix as well as the ranges of the scales and the values of the phases for having successful LG. In the case of Dirac phase CP-violation we found that $M_{1\min} \cong 2.5\ (1.7) \times 10^{11}$ GeV for NH light neutrino mass spectrum and $\delta$ lying in the interval $\pi < \delta < 2\pi$ ($0 < \delta < \pi$) for real (purely imaginary) Casas-Ibarra parameter $\sin 2\theta$ (Figs. (3.7) and (3.9)). As $M_1$ increases from $M_{1\min}$ to $M_1 \cong 2.7\ (2.1) \times 10^{12}$ GeV, at which $\eta_B$ reaches the plateau value, the range of interest of $\delta$ increases from the point $\delta = 3\pi/2$ ($\pi/2$) to $202.4^\circ \lesssim \delta \lesssim 337.6^\circ$ ($14.6^\circ \lesssim \delta \lesssim 166.4^\circ$) and remains practically the same up to $M_1 \sim 10^{14}$ GeV. We get similar results for $M_{1\min}$ and the ranges of $\delta$ and $M_1$ in the case of IH light neutrino mass spectrum and purely imaginary Casas-Ibarra parameter $\sin 2\theta$, with $M_{1\min} \cong 4.6 \times 10^{10}$ GeV for $\delta = 3\pi/2$ and $185^\circ \lesssim \delta \lesssim 355^\circ$ for $1.2 \times 10^{12}$ GeV $\lesssim M_1 \lesssim 10^{14}$ GeV (Fig. (3.12)). We found also that in the case of NH spectrum there is a direct relation between the sign of $\sin\delta$ and the sign of the baryon asymmetry of the Universe in the regions of viable LG; for IH spectrum such a relation holds for $M_{1\min} \cong 4.6 \times 10^{10}$ GeV $\lesssim M_1 \lesssim 10^{13}$ GeV.

We have investigated also the generation of $\eta_B$ when the CP-violation is provided solely by the Majorana phases $\alpha_{21}$ and $\alpha_{31}$ of the PMNS matrix. In the considered scenario with two heavy Majorana neutrinos only the phase $\alpha_{23} \equiv \alpha_{21} - \alpha_{31}$ ($\alpha_{21}$) is physically relevant for NH (IH) light neutrino mass spectrum. We have performed a thorough analysis and have determined the ranges of values of the Majorana phase $\alpha_{23}$ ($\alpha_{21}$) and the related ranges of the scale $M_1$, for which we can have successful LG with CP-violation provided exclusively by $\alpha_{23}$ ($\alpha_{21}$) in the case of NH (IH) spectrum, real (purely imaginary) Casas-Ibarra factor $\sin 2\theta = \sin 2x \neq 0$ ($\sin 2\theta = \pm i \sinh 2y \neq 0$) and CP-conserving value of $\delta = \pi$ (the results of these analyses are presented graphically in Figs. (3.13), (3.14), (3.15) and (3.16)). Our results show, in particular, that there exist relatively large regions of the relevant spaces of parameters where it is possible to reproduce the observed value of BAU and that in these regions the values of the respective Majorana phases providing the requisite LG CP-violation are strongly correlated with the value of LG scale $M_1$.

It is worth noting that the authors of Ref. [218] performed a study of high-scale LG in which the corrections due to the running group equations (RGE) for the neutrino Yukawa

matrices were included in the calculations of the lepton asymmetry through a modified Casas-Ibarra parametrisation. Without these corrections, within the formalism employed in Ref. [218], which is based on the BEs, all lepton flavour dependencies (contained in the PMNS matrix) cancel at LG scales $\gtrsim 10^{12}$ GeV from the total CP-asymmetries. Once the RGE-corrections are included, this cancellation no longer occurs and a corrective term approximately proportional to the square of the $\tau$-Yukawa coupling is added to the total CP-asymmetry. The authors of Ref. [218] then show that this correction is sufficient in some regions of the parameter space at scales $\gtrsim 10^{12}$ GeV for successful LG from purely low-energy CP-violation due to the PMNS phases in the absence of the usual flavour effects. However, this correction is subdominant to the flavour effects discussed in our work, typically being smaller by a factor of $\sim 10$ to $\sim 100$ in the regions of the parameter space of the scenarios we have considered, where LG successfully generates the observed BAU. Thus, the mechanism of generation of BAU considered in Ref. [218] is subdominant to the mechanism discussed in this chapter.

To conclude, as it follows from the results obtained in the our paper in Pub. [I] and presented in this chapter, viable LG based on the type-I seesaw mechanism with two hierarchical in mass heavy Majorana neutrinos and CP-violation provided only by the physical low-energy Dirac or/and Majorana phases present in the PMNS neutrino mixing matrix is possible for rather wide ranges of values of the CPV phases and of the scale of LG. The scenarios of LG investigated by us are falsifiable in low-energy experiments on the nature – Dirac or Majorana – of massive neutrinos. As far as the nature of massive neutrinos is not known or if the massive neutrinos are proven to be Majorana particles, the cases of LG we have considered are still testable and falsifiable in low-energy experiments on CP-violation in neutrino oscillations, on the determination of the type of spectrum the neutrino masses obey and on the absolute neutrino mass scale. The data from these experiments can severely constrain the corresponding LG parameter spaces and even rule out some of, if not all, the cases presented in detail in this chapter.

# CHAPTER 4

# Low-Scale Leptogenesis and its Testability at Low-Energy Experiments

The scenario of RLG in which two heavy neutrinos ($N_{1,2}$) are separated in mass ($M \simeq M_{1,2}$) by a tiny mass splitting ($\Delta M \ll M$) is viable at scales that are smaller than the electroweak scale, thus at energies that are in principle accessible at laboratories. In this low-energy regime, processes involving the heavy neutrinos ($N_{1,2}$ and Higgs direct and inverse decays) can still provide the right amount of CP-violation to produce the present BAU through LG. In Pub. [II] we have investigated such compelling framework of RLG within the type-I seesaw extension of the SM with two heavy neutrinos forming a pseudo-Dirac pair and masses $M \lesssim 100$ GeV. The set-up for this scenario, as was already illustrated in Sec. 2.3.2, is based on the three-flavoured BEs with two heavy neutrinos and the inclusion of flavour and thermal effects (2BE3F in Eqs. (2.59) and (2.60)). As we are going to describe in details in this chapter, we have performed the study in Pub. [II] by distinguishing between thermal and vanishing initial conditions (TIA and VIA) and shown that it is possible to reproduce the present BAU for masses of the heavy neutrinos in the range $0.3 - 100$ GeV by relying only on the heavy Majorana neutrino and Higgs decay mechanism (and scatterings), without taking into account the $N_1 - N_2$ oscillations, and with the flavour effects playing a crucial role. Moreover, the parameter space of viable RLG in this scenario is compatible with couplings of the heavy Majorana neutrinos in the CC and NC SM weak interaction that could be probed in large part in the frontier SHiP [219, 220] experiment and in future experiments at the discussed FCC-ee collider [221, 222].

While we were working on Pub. [II], a similar paper [161] came out in which the scenario of RLG was treated together with the "freeze-in" mechanism of LG via oscillations in a unifying framework (with a follow-up explanatory article published later [162]). Considering also the case of two heavy Majorana neutrinos $N_{1,2}$ forming a pseudo-Dirac pair, in Ref. [161] it was shown that i) the observed baryon asymmetry can be generated for all experimentally allowed values of the heavy Majorana neutrino masses $M_{1,2} \simeq M \gtrsim 100$ MeV and up to the TeV scale, and that ii) LG is effective in a broad range of the relevant parameters, including mass splitting between the two Majorana neutrinos as large as $\Delta M/M \sim 0.1$, as well as couplings of $N_{1,2}$ in the weak charged lepton current which depend on the value of $M$: for, e.g., $M = 1$ and 50 GeV, they are in the range of $(10^{-5} - 10^{-3})$ and $(10^{-6} - 3 \times 10^{-5})$, respectively. The results derived in Ref. [161] and in our work of Pub. [II] are largely compatible in the LG parameter space regions where they can be compared, such as, e.g., in the regions corresponding to the case of TIA, for which the oscillation mechanism should not be relevant, and light neutrino mass spectrum with NO. In the VIA case, where the oscillation mechanism becomes important, the parameter space of viable LG considered in Ref. [161] is larger than that found by us in Pub. [II]. As we

have already emphasised, we have concentrated in our work on the decay mechanism of baryon asymmetry generation. We wanted to identify the parameter space in which the observed value of the BAU could be generated via the decay mechanism only. Thus, effectively, we exploited a part of the parameter space explored in Ref. [161].

Afterwards, the authors of Ref. [160] extended the unified picture of low-scale LG to the case of three quasi-degenerate heavy Majorana neutrinos $N_{1,2,3}$, with masses $M_{1,2,3} \simeq M$ (see also Ref. [223] for an earlier study of low-scale leptogenesis with three heavy Majorana neutrinos). They presented the results for $M$ between 50 MeV and 70 TeV, focusing on the case of light neutrino mass spectrum with NO, either NH or QD, and considered both VIA and TIA initial conditions. The major finding in Ref. [160] is that the range of heavy Majorana neutrino CC and NC couplings for which one can have successful LG is by several orders of magnitude larger than the range in the scenario with two heavy Majorana neutrinos [1], reaching at, e.g., $M = 100$ GeV values $\sim 5 \times 10^{-2}$ in the case of TIA and even somewhat larger values in the case of VIA. For heavy Majorana neutrinos with masses below the TeV scale, a large range of couplings can already be probed in direct searches at the LHC [224–228], as well as in fixed target experiments [227, 228] and future colliders [221, 228–230]. In our work in Pub. [III], we have investigated the potential to test the unified low-scale LG scenarios discussed in Ref. [160] in upcoming high precision experiments on cLFV processes, in particular searching for $\mu^\pm \to e^\pm + \gamma$ and $\mu^\pm \to e^\pm + e^+ + e^-$ decays and for $\mu - e$ conversion in nuclei. We next present in details the main results of our works in Pubs. [II] and [III] in the following Secs. 4.1 and 4.2, respectively.

## 4.1 Flavoured Resonant Leptogenesis at Sub-TeV Scales

We present in this section the main results of the analysis performed in our work of Pub. [II]. We remind that the equations and related quantities, as well as the effects that were taken into account in our analysis, were introduced in Sec. 2.3.2. We further subdivide the section as follows. We first discuss in Subsecs. 4.1.1 and 4.1.2 the cases of thermal and vanishing initial conditions, respectively, concentrating on the NH light neutrino mass spectrum. We will then show and discuss the parameter space of viable RLG in the $\sum_{\ell,j} |(RV)_{\ell j}|^2 - M$ plane in Subsec. 4.1.3, showing the results also in the IH case [2].

Before presenting the results, it is necessary to notice that in the expression of the CP-asymmetry in Eq. (2.78), for $e^{|\xi|} \gg e^{-|\xi|}$, the term involving the Yukawa couplings given in Eq. (2.79) is proportional to $\sin(2\omega)e^{-2|\xi|}$. Hence, large values of $|\xi|$ suppress the CP-asymmetry, while $\omega = (2n+1)\pi/4$, $|n| = 0, 1, 2, ...$, maximises it (in absolute value). For $|\xi| \lesssim 1$, a slightly different dependence on $\omega$ appears in both the Yukawa coupling term (in the denominator) and in the mixing term of Eq. (2.78), so that the maximal value of the CP-asymmetry is actually reached for different values of $\omega$ (depending on $\xi$). We have found, however, that a more precise choice of $\omega$ would not lead to significant differences in the BAU. Therefore, in obtaining our results of Pub. [II] we have set $\omega = \pi/4$ or $3\pi/4$ (to match the sign of the BAU) in order to

[1] It was first noticed in Ref. [223] that in this case of three quasi-degenerate in mass $N_j$, their CC and NC couplings can be a few orders of magnitude larger than in the case of two heavy Majorana neutrinos.

[2] The final results in Pub. [II] were presented in the $\xi - M$ plane and only for the NH case. To allow for a better comparison with current limits and other works, in this Thesis we translate the region of successful RLG from the $\xi - M$ plane presented in Pub. [II] to the $\sum_{\ell,j} |(RV)_{\ell j}|^2 - M$ plane and perform for completeness the analysis also in the IH case. Moreover, we include in the final plots the most up-to-date expected sensitivities of FCC-ee on $\sum_{j=1,2,3} |(RV)_{j\mu}|^2$ and on $\sum_{j=1,2,3} |(RV)_{j\mu}|^2$ for the SHiP experiment.

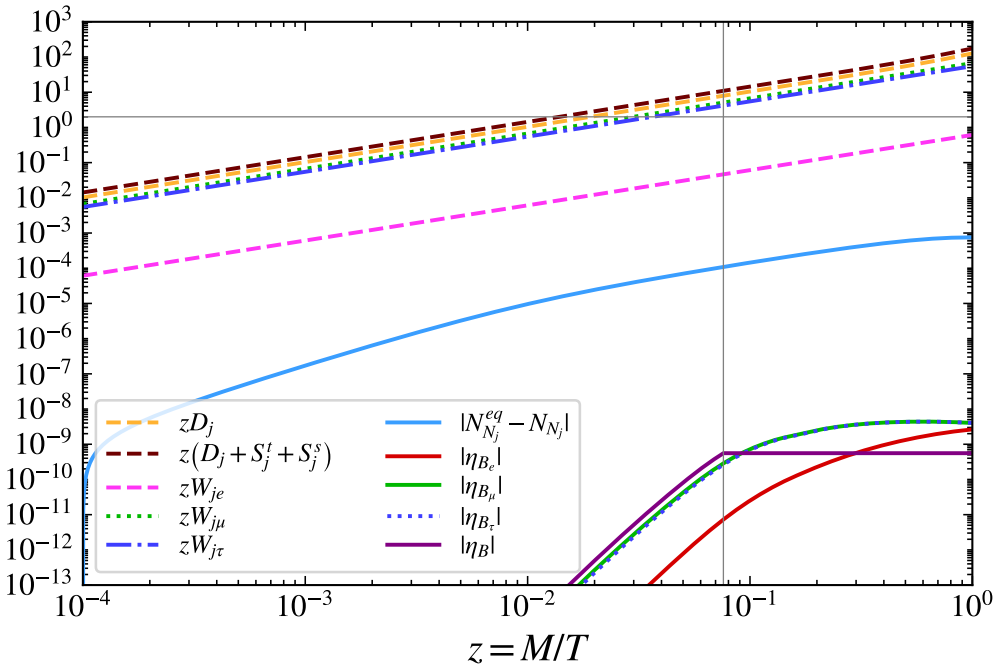


**Figure 4.1.** The evolution of the lepton flavour and baryon asymmetries, of $|N_{N_j}^{\rm eq} - N_{N_j}|$ and of the corresponding decay, scattering and wash-out rates that govern the evolution of the asymmetries in Eqs. (2.59) and (2.60) in the case of TIA of $N_{1,2}$. The figure is obtained for $\delta = 3\pi/2$, $M = 10$ GeV, $x^{(0)} = 100$ and $\xi = 2.05$. The vertical grey line is at $z_{\rm sph} = 0.076$ and is the endpoint of evolution of the baryon asymmetry $\eta_B$. The horizontal grey line at 2 is roughly indicating where the different processes get into equilibrium. See the text for further details.

maximise the CPV asymmetry at large values of $|\xi|$ . We also adopt the same choice for $\omega$ throughout this chapter, unless specified otherwise. Also, in the discussion which follows, we consider only values of $\xi \geq 0$, noting that the results are symmetric for the corresponding $\xi < 0$.

### 4.1.1 Thermal Initial Abundance

Consider the case of TIA for the heavy Majorana neutrinos, $N_{N_j}(z_0) = N_{N_j}^{\rm eq}(z_0)$, $j = 1, 2$. We can set the ratio $N_{N_j}/N_{N_j}^{\rm eq} = 1$ in the right hand side of Eq. (2.60) since, under the indicated initial condition, the deviations of $N_{N_j}$ from $N_{N_j}^{\rm eq}$ for any $z > z_0$ of interest for our analysis are sufficiently small and can be neglected. For the sum of three wash-out factors, $W_j$, in this case we get:

$$W_j^{\rm TIA} \equiv W_j^D + W_j^t + W_j^s \tag{4.1}$$

$$= W_j^D + W_j^{(\rm quarks)} + W_j^{(\rm gauge)} \simeq 0.138\, \kappa_j\,. \tag{4.2}$$

The flavoured wash-out terms in Eq. (2.60) are given by $W_{j\ell} \equiv p_{j\ell} W_j^{\rm TIA}$. Due to the projection probability $p_{j\ell}$ the wash-out terms exhibit strong flavour dependence. We depict in Fig. 4.1 the evolution of the lepton and baryon asymmetries, the difference $|N_{N_j}^{\rm eq} - N_{N_j}|$, the decay, scattering and wash-out rates for $\delta = 3\pi/2$, $M = 10$ GeV, $x^{(0)} = 100$ and $\xi = 2.05$, the maximal value of $\xi$

for which we can have successful LG for $M = 10$ GeV, and $x^{(0)} = 100$. The baryon asymmetry $\eta_{B\ell}$ originates from the CP-asymmetry in the lepton charge (flavour) $L_\ell$ ($\ell$), $\ell = e$, $\mu$, $\tau$. Thus, the total baryon asymmetry is $\eta_B = \eta_{Be} + \eta_{B\mu} + \eta_{B\tau}$. The figure illustrates the typical scenario of "freeze-out" LG, namely, the case when the departure from equilibrium of $N_{N_j}(z)$ is what drives the generation of the lepton (and baryon) asymmetry. The total baryon asymmetry, to which all flavour CPV asymmetries contribute, freezes at $z_{\rm sph} = M/T_{\rm sph} \simeq 0.076$, $T_{\rm sph} = 131.7$ GeV being the sphaleron decoupling temperature, which is marked by the vertical grey line in the figure.

For the choice of parameters in the figure, the asymmetries $|\eta_{B\mu}|$ and $|\eta_{B\tau}|$ exhibit almost identical evolution for $z \leq z_{\rm sph}$ and are by a factor $\sim 100$ larger than $|\eta_{Be}|$. This difference reflects the difference between $\epsilon^{(j)}_{\mu\mu}$ ($\epsilon^{(j)}_{\tau\tau}$) and $\epsilon^{(j)}_{ee}$. Thus, in this case, $\eta_B \simeq \eta_{B\mu} + \eta_{B\tau}$. The fact that $|\eta_{B\mu}| \simeq |\eta_{B\tau}| \gg |\eta_{Be}|$ can have important implications in what concerns the possibility of wash-out of the baryon asymmetry by lepton number non-conserving effective operators of dimension higher than four that might be "active" at the energy scales of interest [231, 232]. For $z > z_{\rm sph}$, and therefore after sphaleron freeze-out, the asymmetry $|\eta_{Be}|$ converges to the asymmetries $|\eta_{B\mu}|$ and $|\eta_{B\tau}|$. Qualitatively similar behaviour is seen for a range of $x^{(0)}$ and $M$ values, with the main difference being the overall scale of the asymmetry evolution.

To understand the impact of flavour effects, we compare the obtained results with the results in the unflavoured case. The unflavoured approximation is equivalent to taking in Eq. (2.60) $p_{j\ell} = 1$ for every $\ell$ and then sum over all the flavours. It roughly corresponds to taking the total asymmetry to be the asymmetry in the dominant flavour (either muon or tauon in in the considered case). As it is then clear from Fig. 4.1, this approximation would only lead to a $\mathcal{O}(2)$ difference in the value of $\eta_B$. A more detailed analysis shows that flavour effects in the TIA case lead, in general, to a moderate enhancement by a factor of $\sim (2-3)$ of the baryon asymmetry.

### 4.1.2 Vanishing Initial Abundance

We analyse next the case of VIA for the heavy neutrinos, namely $N_{1,2}$, i.e. $N_{1,2}(z_0) = 0$. For the wash-out terms, we assume on the basis of the results reported in Ref. [164] that

$$W^{(\rm gauge)}_{A_t j} \simeq W^{(\rm gauge)}_{A_s j}\,, \tag{4.3}$$

$$W^{(\rm quark)}_{H_t j} \simeq W^{(\rm quark)}_{H_s j}\,. \tag{4.4}$$

Under these conditions [3] the wash-out term in Eq. (2.60) in the case of interest has the form:

$$\begin{aligned} W^{\rm VIA}_j &\equiv W^D_j + W^t_j + \frac{N_{N_j}}{N^{\rm eq}_{N_j}} W^s_j \\ &\simeq \left(0.1113 + 0.0267\,\frac{N_{N_j}}{N^{\rm eq}_{N_j}}\right)\kappa_j\,, \end{aligned} \tag{4.5}$$

The flavoured wash-out terms in Eq. (2.60) are given by $W_{j\ell} \equiv p_{j\ell} W^{\rm VIA}_j$.

In Figs. 4.2, 4.3 and 4.4 we show the evolution of the leptonic asymmetries $N_{\ell\ell}$ respectively for i) $\delta = 0$, $M = 15$ GeV ($z_{\rm sph} = 0.114$), $x^{(0)} = 10^6$ and maximal $\xi = 1.53$, ii) $\delta = 300°$,

[3] We have checked that choosing different relations between $W^{(\rm gauge)}_{A_t j}$ and $W^{(\rm gauge)}_{A_s j}$, and between $W^{(\rm quark)}_{H_t j}$ and $W^{(\rm quark)}_{H_s j}$, does not lead to significant change of the results obtained using Eqs. (4.3) and (4.4).

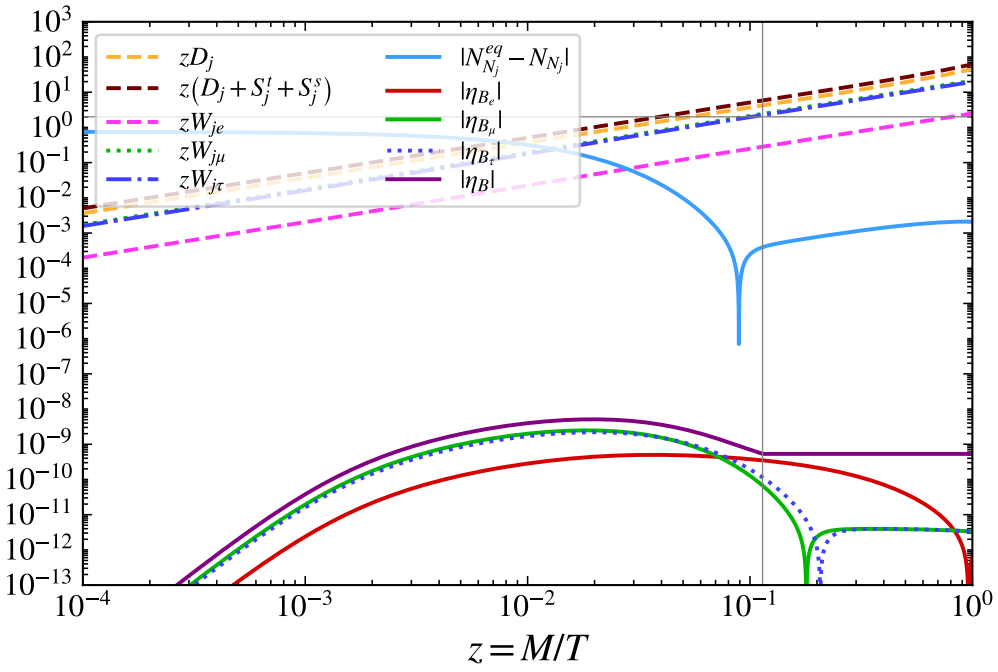


**Figure 4.2.** The evolution of the lepton-flavour and baryon asymmetries, of $|N_{N_j}^{\rm eq} - N_{N_j}|$ and of the corresponding decay, scattering and wash-out rates that govern the evolution of the asymmetries in Eqs. (2.59) and (2.60) in the case of vanishing initial abundance (VIA) of $N_{1,2}$. The figure is obtained for $\delta = 0$, $M = 15$ GeV, $x^{(0)} = 10^6$ and $\xi = 1.53$. The vertical grey line at $z_{\rm sph} = 0.114$ is the endpoint of the evolution of the baryon asymmetry $\eta_B$. The horizontal grey line at 2 is roughly indicating where the different processes get into equilibrium. At $z \ll z_{\rm sph}$, the asymmetry $|\eta_{Be}|$ (solid red curve) is smaller in magnitude than the asymmetries $|\eta_{B\mu}|$ and $|\eta_{B\tau}|$. However, the weaker wash-out of $\eta_{Be}$ results in it dominating $\eta_{B\mu}$ and $\eta_{B\tau}$ by the time of sphaleron decoupling and in $\eta_B \simeq \eta_{Be}$. See the text for further details.

$M = 20$ GeV ($z_{\rm sph} = 0.15$), $x^{(0)} = 10^6$ and $\xi = 1.33$, and iii) $\delta = 3\pi/2$, $M = 16$ GeV ($z_{\rm sph} = 0.121$), $x^{(0)} = 10^3$ and maximal $\xi = 2.18$, respectively. Also shown is the growth of $N_{N_j}$ ($N_{N_1} \simeq N_{N_2}$) towards the evolving equilibrium distribution $N_{N_j}^{\rm eq}(z)$, governed by the combination $D_j + S_j^t + S_j^s$. The sphaleron transition occurs at $z_{\rm sph}$ marked by the vertical grey line after which the baryon asymmetry $\eta_B$ is "frozen" and remains constant at the value at $z_{\rm sph}$. Sharp dips in the asymmetries correspond to sign changes as we always plot absolute values.

As is seen in Fig. 4.2, the asymmetries $\eta_{B\mu}$ and $\eta_{B\tau}$, which are generated by the $\mu$- and $\tau$-flavour CP-asymmetries, are strongly suppressed in the interval $0.07 \lesssim z \leq z_{\rm sph}$ due to the relatively large wash-out factors. This is reflected in the sudden dips of the corresponding curves as they are driven through zero by the wash-out effects. As a consequence, by the time of sphaleron decoupling most of the baryon asymmetry is due to the lepton CP-asymmetry residing in the electron flavour, $\eta_B \simeq \eta_{Be}$. Since $\eta_{Be}$ was mostly generated during the production of heavy Majorana neutrinos, i.e., before $N_{N_j}(z)$ reached $N_{N_j}^{\rm eq}(z)$, this case formally corresponds to a "freeze-in" scenario of generation of baryon asymmetry.

We highlight the fact that, in contrast to the TIA case, in the VIA scenario illustrated in Fig. 4.2 flavour effects are crucial. Here, the "dominant flavours" are the muon and tauon, in the sense that both respective CP-asymmetries $\epsilon_{\mu\mu}^{(j)}$ and $\epsilon_{\tau\tau}^{(j)}$ and projection probabilities $p_{j\mu}$ and

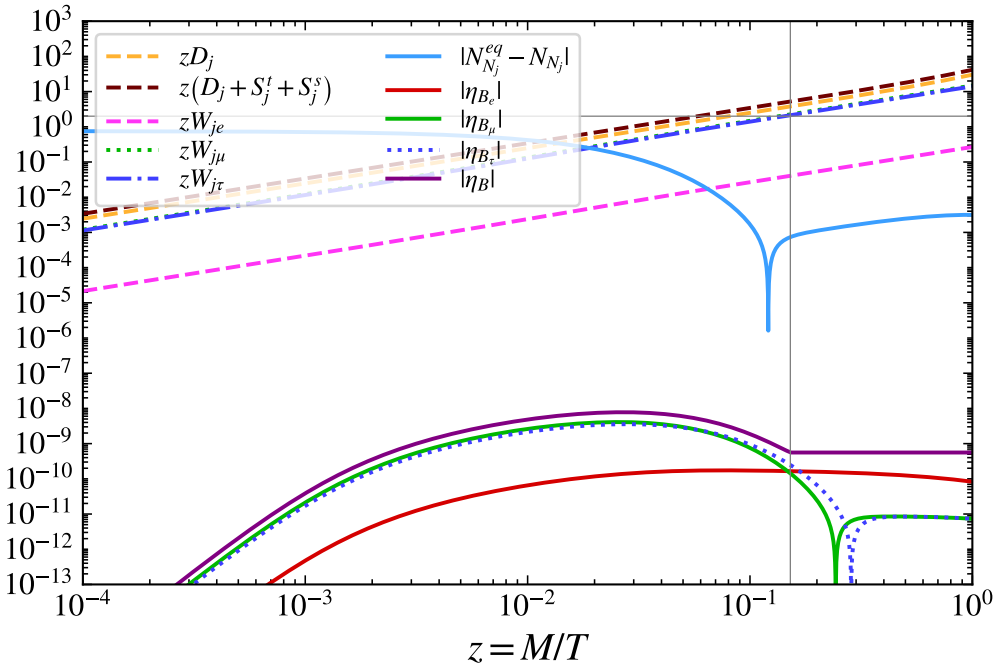


**Figure 4.3.** The same as in Fig. 4.2 but for $\delta = 300°$, $M = 20$ GeV, $x^{(0)} = 10^6$ and $\xi = 1.33$. The vertical grey line at $z_{\rm sph} = 0.15$ is the endpoint of the evolution of the baryon asymmetry $\eta_B$. The horizontal grey line at 2 is roughly indicating where the different processes get into equilibrium. In this case $\eta_B = \eta_{Be} + \eta_{B\mu} + \eta_{B\tau}$. See the text for further details.

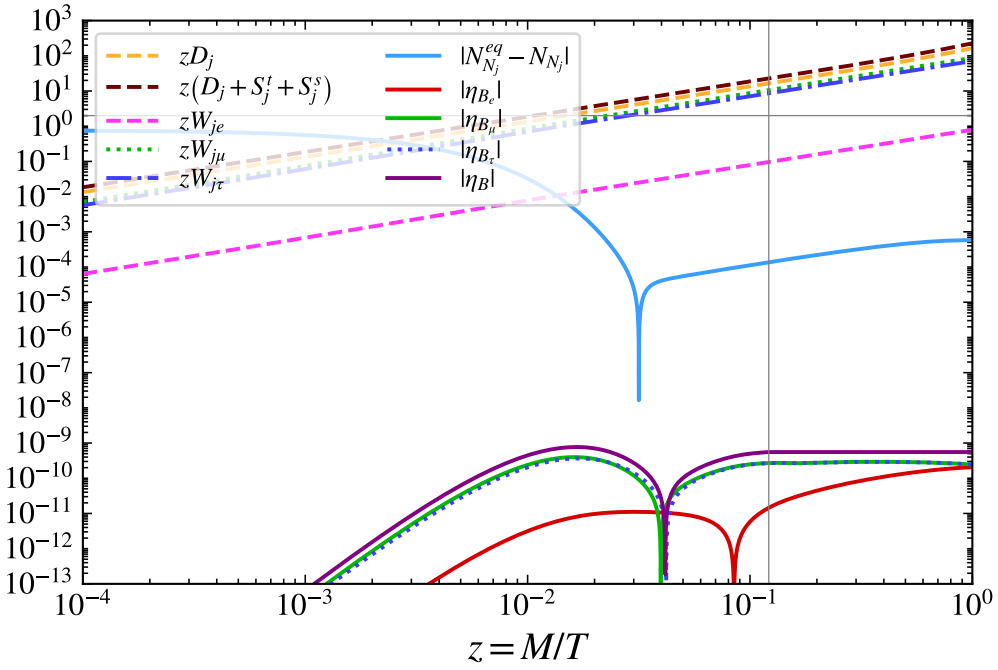


**Figure 4.4.** The same as in Fig. 4.2 but for $\delta = 3\pi/2$, $M = 16$ GeV, $x^{(0)} = 10^3$ and $\xi = 2.18$. The vertical grey line at $z_{\rm sph} = 0.12$ is the endpoint of the evolution of the baryon asymmetry $\eta_B$. The horizontal grey line at 2 is roughly indicating where the different processes get into equilibrium. The figure illustrates a case of $\eta_B \simeq \eta_{B\mu} + \eta_{B\tau}$. See the text for further details.

$p_{j\tau}$ are greater than the electron flavour ones, $\epsilon^{(j)}_{ee}$ and $p_{je}$: $|\epsilon^{(j)}_{\mu\mu}|, |\epsilon^{(j)}_{\tau\tau}| > |\epsilon^{(j)}_{ee}|$, $p_{j\mu}, p_{j\tau} > p_{je}$. The unflavoured approximation would then neglect the electron CP-asymmetry and consequently $\eta_{Be}$, which actually contributes most in the flavoured scenario. In this particular case, flavour effects lead to a $\mathcal{O}(300)$ enhancement with respect to the unflavoured case [4].

We find that the enhancement of the baryon asymmetry due to flavour effects depends strongly on the CPV phase $\delta$. This is illustrated in Fig. 4.3, which shows a "freeze-in" scenario of LG for $\delta = 300°$, in which, in contrast to case with $\delta = 0$ reported in Fig. 4.2, the flavour enhancement of the baryon asymmetry is approximately by a factor of 60. The results presented in Fig. 4.3 show also that, depending on the values of LG parameters, all three lepton CPV asymmetries residing in the electron, muon and tauon flavours can give significant contributions to the baryon asymmetry so that $\eta_B = \eta_{Be} + \eta_{B\mu} + \eta_{B\tau}$.

The features reported in the preceding discussion can be obtained for other choices of the parameters and we find, in general, that in the mass range of interest, varying $x^{(0)}$ and $\delta$ accordingly, flavour effects can lead to enhancement of the generated baryon asymmetry by a factor ranging from a few to a few hundred.

In Fig. 4.4 instead, the final baryon asymmetry is generated after all the three lepton flavour asymmetries, initially generated during the production of RH neutrinos, are fully erased by the wash-out processes. Therefore this corresponds to the "freeze-out" RLG case. Since the dominant lepton flavour related asymmetries are $\eta_{B\mu}$ and $\eta_{B\tau}$ and $\eta_B \simeq \eta_{B\mu} + \eta_{B\tau}$, the flavour effects are not significant in this scenario. However, it is quite remarkable that in the case of the same initial condition – zero initial abundance of $N_j$ – the "freeze-in" mechanism of baryon asymmetry generation can transform into the "freeze-out" mechanism for different choices of the parameters.

### 4.1.3 Parameter Space for Viable Resonant Leptogenesis

We next present the scan of the parameter space for viable RLG at sub-TeV scales. The results are summarised in the two plots of Fig. 4.5. Note that we have plotted curves for different choices of $\omega$. The contours, for different values of $\omega$, are obtained for $\alpha_{23} \equiv \alpha_{21} - \alpha_{31} = 2\pi$ ($\alpha_{31} = 0$) and $\delta = 3\pi/2$ [5] and connect the points for which there exists a choice of $x^{(0)}$ that makes the predicted BAU equal to the one observed today. More specifically, at each point of the contours $x^{(0)}$ is chosen so to maximise the mixing factor appearing in Eq. (2.78) for $j = 1$ at $z = z_{\rm sph}$, namely

$$f^{(1)}_{\rm mix}(z_{\rm sph}) \equiv \frac{2x^{(0)}\gamma(z_{\rm sph})}{4\left[x^{(0)} + x_T(z_{\rm sph})\right]^2 + \gamma^2(z_{\rm sph})}\,, \tag{4.6}$$

[4] The enhancement can also come with a peculiar difference in sign, which reflects the fact that in this intermediate regime the unflavoured scenario may correspond to the "freeze-out" type LG, while the flavoured one – to the "freeze-in" type. The correct sign can always be recovered by switching $\omega$ from $\pi/4$ to $3\pi/4$, or vice versa.

[5] This set of PMNS phases maximises the contours (as also described in details in our paper), though an alternative choice that would also maximise the asymmetry would only slightly affect the results. In particular, our detailed analysis in Pub. [II] showed that, in the maximal case, the wash-out factor for the asymmetry in the $e$-lepton charge and the related baryon asymmetry $\eta_{Be}$ exhibit weak dependence on the Majorana phases, while the wash-out factors for the asymmetries in the $\mu$- and $\tau$- lepton charges and, correspondingly, the flavour baryon asymmetries $\eta_{B\mu}$ and $\eta_{B\tau}$, change significantly with $\alpha_{23}$. However these changes are "'anti-correlated" in the sense that the sum $\eta_{B\mu} + \eta_{B\tau}$ remains practically constant when $\alpha_{23}$ is varied. As a consequence, also the total baryon asymmetry $\eta_B = \eta_{Be} + \eta_{B\mu} + \eta_{B\tau}$ does not show any noticeable dependence on the Majorana phases.

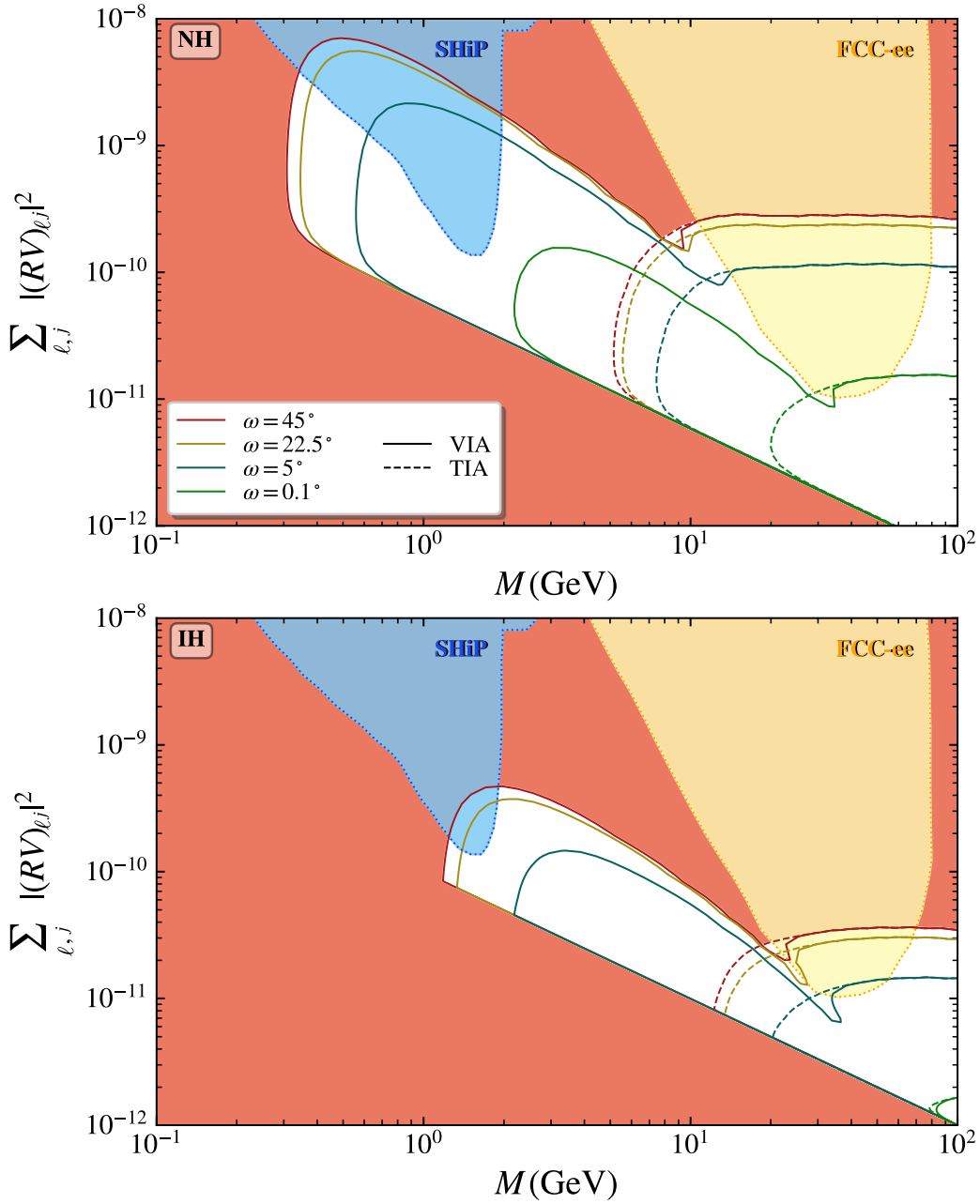


**Figure 4.5.** We show the region (in red) in the $\sum_{\ell j} |(RV)_{\ell j}|^2 - M$ plane excluded by the request of predicting the BAU within the RLG mechanism. The top (bottom) panel is for NH (IH). At the contours and in the white region, there always exists a choice of the parameters $\omega$ and $x^{(0)}$ for which the predicted BAU equals the observed value $\eta_B \simeq 6.1 \times 10^{-10}$. In particular, the different curves are obtained for (from left to right) $\omega = 45°$ (red), $22.5°$ (yellow), $5°$ (blue) and $0.1°$ (green) and maximised over $x^{(0)}$, with the solid and dashed styles corresponding to the VIA and TIA cases, respectively. The yellow (blue) area is the expected sensitivity region of the FCC-ee (SHiP) experiment on $\sum_{lj} |(RV)_{\ell j}|^2$ ($\sum_j |(RV)_{\mu j}|^2$), extrapolated from Ref. [233].

with the maximum at

$$x^{(0)}_{\mathrm{MAX},\,1} = \frac{1}{2}\sqrt{4x_T(z_{\mathrm{sph}}) + \gamma^2(z_{\mathrm{sph}})}\,. \tag{4.7}$$

Note that the above choice of $x^{(0)}_{\mathrm{MAX},\,1}$ maximises also the regulator factor of the CP-asymmetry when $j = 2$, i.e. $f^{(2)}_{\mathrm{mix}}$, only if $\omega = (2n+1)\pi/4$ for any $\xi$ or for $|\xi| \gg 1$ and any $\omega$. In general, the CP-asymmetry $f^{(2)}_{\mathrm{mix}}$ is maximal at (see Eq. (2.78))

$$x^{(0)}_{\mathrm{MAX},\,2} = \frac{1}{2}\sqrt{4x_T(z_{\mathrm{sph}}) + \left[\frac{\Gamma_{11}}{\Gamma_{22}}\gamma(z_{\mathrm{sph}})\right]^2}\,. \tag{4.8}$$

The presence of the factor $\Gamma_{11}/\Gamma_{22}$ makes the two CP-asymmetries slightly different when $\omega \neq (2n+1)\pi/4$ and for $|\xi| \lesssim 1$. However, choosing $x^{(0)}$ as in Eq. (4.7) for any $\xi$ and $\omega$ does not lead to any significant difference.

In the figure, we have separated between the cases of VIA and TIA with solid and dashed lines, respectively, with the top (bottom) panel corresponding to the NH (IH) case. In the red region, the predicted BAU is always smaller than the observed value, while in the white region is bigger. However, in the white region, we can always choose a different sets of parameters (i.e. $x^{(0)}$ and/or $\omega$) and get the observed value for the BAU (see, e.g., the various curves corresponding to different choices of $\omega$). The yellow (blue) area represents the expected sensitivity region of the FCC-ee (SHiP) experiment on $\sum_{\ell j}|(RV)_{\ell j}|^2$ ($\sum_j |(RV)_{\mu j}|^2$), extrapolated from Ref. [233], revealing the potential to probe a large part of the RLG parameter space in the future.

Some comments on the picture are in order. In the TIA scenario, for a given $x^{(0)}$, the lower the mass, the less is the time for the system to depart from equilibrium before $z_{\mathrm{sph}}$, and so greater the CP-asymmetry must be, and slower the processes keeping $N_j$ in equilibrium, so that the baryon asymmetry freezes at the observed value. Correspondingly, by lowering the mass, the maximal value of $\xi$, and thus of $\sum_{\ell j}|(RV)_{\ell j}|^2$ (see Eq. (2.28)), for which we can have successful RLG decreases. This leads to a lower bound on the mass $M$ for which RLG can be successful, with the minimal value obtained for $\omega = \pi/4$ at $M_1 \simeq 5$ GeV (10 GeV) for the NH (IH) case. In the region of smallest $\sum_{\ell j}|(RV)_{\ell j}|^2$ corresponding to $\xi \lesssim 1$, the dependence on $\xi$ of the CP-asymmetry and wash-out terms is less trivial and strongly dependent on the leptonic CPV phases. In the VIA case, compared to the TIA case, the region of successful RLG extends to lower masses. In particular, we find that the minimal lower bound on the mass is reached for $\omega = \pi/4$ and reads $M \approx 0.3\,\mathrm{GeV}$ (1 GeV) in the NH (IH) case. The values of the observable $\max(\sum_{\ell,j}|(RV)_{\ell j}|^2)$ and $\min(\sum_{\ell,j}|(RV)_{\ell j}|^2)$ for $M \gtrsim 10\,\mathrm{GeV}$ we find in the VIA case are the same as those reported for the TIA case. This is in agreement with the fact that in the "freeze-out" LG scenario we are analysing, in which the observed BAU is generated in the strong wash-out regime, there is no dependence on the initial conditions. At $M \lesssim 10\,\mathrm{GeV}$ the VIA case differs from the TIA one because of the "freeze-in" mechanism that comes into play. For both the TIA and VIA conditions, the minimal lower curves on $\sum_{\ell,j}|(RV)_{\ell j}|^2$ correspond to the case of $\xi = 0$.

We now briefly comment on the reason why, even for small values of $\omega$ such as $0.1°$, the BAU can still be reproduced in the NH case for a large region of the parameter space. For $|\xi| \gg 1$, the CP-asymmetry is proportional to $\sin(2\omega)\mathrm{e}^{-2|\xi|}$ while the parameter $\kappa_j \propto (\mathrm{e}^{2\xi})$ (see Eq. (2.72)). Therefore, the smaller $\omega$ is, the smaller the CP-asymmetry will be, while the wash-outs remains unaffected. In order to predict the observed BAU we then need smaller values of $\xi$ to both

enlarge the CP-asymmetry and weaken the wash-out effects. Indeed, considering the analytical approximation valid in the "freeze-out" regime for which $\eta_B \propto \sum_j \epsilon^{(j)}/\kappa_j \propto \sin(2\omega)\mathrm{e}^{-4|\xi|}$, for $M = 100$ GeV, $\omega = \{22.5°, 5°, 0.1°, 0.05°\}$ and $\xi = \{3.21, 2.87, 1.89, 1.70\}$ (corresponding to the maximal values in the figure), we get $\sin(2\omega)\mathrm{e}^{-4|\xi|} = \{1.87, 1.82, 1.79, 1.94\} \times 10^{-6}$.

To summarise, the figure shows that RLG with the decay mechanism can be successful across the whole of the experimentally accessible region of $M_{1,2} \simeq (0.3(1) - 100)$ GeV in the case of NH (IH) light neutrino mass spectrum. Furthermore, we have found that RLG at the considered sub 100 GeV scales is compatible with values of the CC and NC couplings of $N_{1,2}$ in the weak interaction Lagrangian, whose squares are in the range of $10^{-12} - 10^{-8}$ (see Fig. 4.5). A large part of the viable parameter space can be probed in the frontier SHiP experiment and at the discussed future FCC-ee facility.

## 4.2 Low-Scale Leptogenesis with Three Quasi-Degenerate Heavy Neutrinos

We illustrate in this section the results of our work in Pub. [III], unveiling how current and future experiments searching for cLFV processes can probe the parameter space of low-scale LG with three heavy Majorana neutrinos $N_{1,2,3}$ quasi-degenerate in mass, $M \simeq M_{1,2,3}$, and the baryon asymmetry being generated by both the decay mechanism, typical of RLG scenarios, and the $N_j$ oscillations [160]. We start by elucidating what the current and prospective sensitivities of cLFV experiments are in Sec. 4.2.1 and then show the scan of the parameter space for viable LG in Sec. 4.2.2.

### 4.2.1 Current and Prospective Sensitivities of cLFV Experiments

The low-energy phenomenology of the considered type-I seesaw scenario has been investigated, e.g., in Refs. [150, 234–236]. The CC and NC couplings in Eqs. (2.20) and (2.21) can induce (via one-loop diagrams with exchange of virtual $N_{1,2,3}$) cLFV processes $\mu^\pm \to e^\pm + \gamma$, $\mu^\pm \to e^\pm + e^+ + e^-$, $\mu - e$ conversion in nuclei, and so on. [237, 238].

The most stringent upper limits on the rates of these processes have been obtained in experiments with muons. The best experimental limits on $\mu \to e\gamma$ and $\mu \to eee$ decay branching ratios, $\mathrm{BR}(\mu \to e\gamma)$ and $\mathrm{BR}(\mu \to eee)$, and on the relative $\mu - e$ conversion cross section in a nucleus ${}^A_Z\mathcal{N}$, $\mathrm{CR}(\mu\, {}^A_Z\mathcal{N} \to e\, {}^A_Z\mathcal{N})$ ($Z$ and $A$ are the atomic and mass numbers, respectively), have been reported by the MEG [239], SINDRUM [240] and SINDRUM II [241, 242] Collaborations:

$$\mathrm{BR}(\mu \to e\gamma) < 4.2 \times 10^{-13} \ (90\%\ \mathrm{C.L.})\,, \tag{4.9}$$

$$\mathrm{BR}(\mu \to eee) < 1.0 \times 10^{-12} \ (90\%\ \mathrm{C.L.})\,, \tag{4.10}$$

$$\mathrm{CR}(\mu\, {}^{48}_{22}\mathrm{Ti} \to e\, {}^{48}_{22}\mathrm{Ti}) < 4.3 \times 10^{-12} \ (90\%\ \mathrm{C.L.})\,, \tag{4.11}$$

$$\mathrm{CR}(\mu\, {}^{197}_{79}\mathrm{Au} \to e\, {}^{197}_{79}\mathrm{Au}) < 7.0 \times 10^{-13} \ (90\%\ \mathrm{C.L.})\,. \tag{4.12}$$

The planned MEG II update of the MEG experiment [243] aims at reaching sensitivity to $\mathrm{BR}(\mu \to e\gamma) \simeq 6 \times 10^{-14}$. The sensitivity to $\mathrm{BR}(\mu \to eee)$ is planned to be increased by up to three (four) orders of magnitude to $\mathrm{BR}(\mu \to eee) \sim 10^{-15}$ ($10^{-16}$) with the realisation of Phase I (Phase II) of the Mu3e Project [244]. The Mu2e [245] and COMET [246] collaborations studying $\mu - e$ conversion in aluminium plan to reach sensitivity to $\mathrm{CR}(\mu\, {}^{27}_{13}\mathrm{Al} \to e\, {}^{27}_{13}\mathrm{Al}) \sim 6 \times 10^{-17}$. The

planned PRISM/PRIME experiment [247] aims at a dramatic increase of sensitivity to the $\mu-e$ conversion rate in titanium, allowing to probe values as small as $\mathrm{CR}(\mu\,^{48}_{22}\mathrm{Ti} \to e\,^{48}_{22}\mathrm{Ti}) \sim 10^{-18}$, an improvement by six orders of magnitude of the current bound given in Eq. (4.11).

The predictions of the seesaw model under discussion, e.g., for the rates of the $\mu \to e\gamma$ and $\mu \to eee$ decays and $\mu - e$ conversion in nuclei, as can be shown, depend on the quantity $|\sum_{j=1,2,3}(RV)^*_{\mu j}(RV)_{ej}|^2$, and, for $|M_j - M_k| \ll M_n$, $j \neq k = 1,2,3$, $n = 1,2,3$, on the mass $M_{1,2,3} \simeq M$ of the heavy Majorana neutrinos $N_{1,2,3}$. The expressions for $\mathrm{BR}(\mu \to e\gamma)$, $\mathrm{BR}(\mu \to eee)$ and $\mathrm{CR}(\mu\,^A_Z\mathcal{N} \to e\,^A_Z\mathcal{N})$ in the case of interest can be easily obtained from those given in Refs. [234, 235, 248, 249] and we present them in Appendix D. Let us add that the rates of the cLFV decays of the $\tau$ lepton are proportional to the product of couplings $|\sum_{j=1,2,3}(RV)^*_{\tau j}(RV)_{\ell' j}|^2$, $\ell' = e, \mu$. However, the current constraints and the prospective improvements of the sensitivity of the experiments on cLFV decays of $\tau^\pm$ are respectively less stringent and not so significant as in the case of experiments on cLFV processes with $\mu^\pm$ and we are not going to consider them here.

In the region of viable LG, the quantity of interest $|\sum_{j=1,2,3}(RV)^*_{\mu j}(RV)_{ej}|$ can be as large as $10^{-1}$ (see Fig. 4.6), which opens up the possibility to test the low-scale LG scenario with three quasi-degenerate heavy Majorana neutrinos in experiments on cLFV with $\mu^\pm$. Indeed, consider as an example the experiments on $\mu \to e\gamma$ decay. The $\mu \to e\gamma$ decay branching ratio is given by [234] (see also Refs. [237, 238, 250] and Appendix D):

$$\mathrm{BR}(\mu \to e\gamma) = \frac{\Gamma(\mu \to e + \gamma)}{\Gamma(\mu \to e + \nu_\mu + \overline{\nu}_e)} \;=\; \frac{3\alpha_{\mathrm{em}}}{32\pi}\,|T|^2\,, \tag{4.13}$$

where $\alpha_{\mathrm{em}} \simeq 1/137$ is the electromagnetic fine structure constant and

$$T \;\cong\; [G(X) - G(0)] \sum_{j=1,2,3} (RV)^*_{\mu j}\,(RV)_{ej}\,. \tag{4.14}$$

Here, $G(X)$ is a loop integration function, $X \equiv (M/M_W)^2$ and we have taken into account that the differences between $M_1$, $M_2$ and $M_3$ are negligibly small, with $M_{1,2,3} \cong M$. The function $G(X)$ is monotonic [6] and takes values in the interval $[4/3, 10/3]$, with $G(X) \cong 10/3 - X$ for $X \ll 1$. At, e.g., $M = M_W$ ($M = 1000$ GeV) we have $G(X) - G(0) = -0.5\,(\simeq -1.9)$. It is not difficult to show, using these values of $G(X) - G(0)$ and Eqs. (4.13) and (4.14), that the MEG II experiment aiming to probe $\mathrm{BR}(\mu \to e\gamma)$ down to $6\times10^{-14}$, will be sensitive for $M = M_W$ ($M = 1000$ GeV) to values of $|\sum_{j=1,2,3}(RV)^*_{\mu j}\,(RV)_{ej}| \gtrsim 3.3\times10^{-5}$ ($8.9\times10^{-6}$). This is approximately by 1 to 3 orders of magnitude smaller than the maximal value of $|\sum_{j=1,2,3}(RV)^*_{\mu j}\,(RV)_{ej}|$ at $M = M_W$ ($M = 1000$ GeV) for which we can have successful low-scale LG in the scenario with three quasi-degenerate in mass heavy Majorana neutrinos in the TIA and VIA cases.

Even smaller values of $|\sum_{j=1,2,3}(RV)^*_{\mu j}\,(RV)_{ej}|$ can be probed in the Mu3e experiment [244], planning to reach sensitivity to $\mathrm{BR}(\mu \to eee) \sim 10^{-15}$ ($10^{-16}$) and especially in the upcoming Mu2e [245], and COMET [246] experiments on $\mu - e$ conversion in aluminium, aiming ultimately to be sensitive to $\mathrm{CR}(\mu\,^{27}_{13}\mathrm{Al} \to e\,^{27}_{13}\mathrm{Al}) \sim 6 \times 10^{-17}$. Values as small as $|\sum_{j=1,2,3}(RV)^*_{\mu j}\,(RV)_{ej}| \sim 10^{-7}$ at $M \sim 100$ GeV can be probed in planned PRISM/PRIME experiment [247], aiming at an impressive increase of sensitivity to the $\mu - e$ conversion rate in titanium to $\mathrm{CR}(\mu\,^{48}_{22}\mathrm{Ti} \to e\,^{48}_{22}\mathrm{Ti}) \sim 10^{-18}$.

[6] The explicit analytic expression for the function $G(X)$ can be found in Eq. (D.2) Appendix D of this Thesis (see also, e.g., Ref. [234]).

### 4.2.2 Projecting cLFV Sensitivities in the Parameter Space of Leptogenesis

In order to obtain the region of viable LG in terms of the cLFV observable quantities, we have solved the DMEs from Refs. [160,161], and scanned the parameter space for the largest allowed values of $|\sum_{j=1,2,3}(RV)^*_{\mu j}\,(RV)_{ej}|$. [7] In Fig. 4.6 we show the regions of viable low-scale LG in the considered scenario in the $|\sum_{j=1,2,3}(RV)^*_{\mu j}\,(RV)_{ej}|-M$ plane for $|\sum_{j=1,2,3}(RV)^*_{\mu j}\,(RV)_{ej}| \geq 10^{-11}$ and $M$ in the interval $M = (0.1 - 7\times 10^4)$ GeV in the TIA and VIA cases (regions below the dotted and solid black lines, respectively). The light neutrino mass spectrum is assumed to be with NO. The lightest neutrino mass is set to $m_1 = 0$ (top panel) and $m_1 = 0.03$ eV (bottom panel). The subregion which is excluded by the current low-energy data [251], including the current upper limitations on BR($\mu \to e\gamma$) and on CR($\mu\,{}^{197}_{79}\mathrm{Au} \to e\,{}^{197}_{79}\mathrm{Au}$) given in Eqs. (4.9) and (4.12), is shown in grey. The green, blue, yellow and red lines represent, from top to bottom, the prospective sensitivities of the planned experiments on $\mu \to e\gamma$ and $\mu \to eee$ decays, as well as on $\mu - e$ conversion in aluminium and titanium [8]. As the two figures clearly indicate, the planned experiments on cLFV with $\mu^\pm$ can probe significant region of the LG parameter space, which cannot be explored by any other experiments. If any of these cLFV experiments finds a positive result, that will serve also as an indication in favour of the considered low-scale LG scenario with three heavy Majorana neutrinos.

It deserves to be mentioned that a study along the same lines was presented in Ref. [163]. The authors of Ref. [163] also demonstrated the potentiality of cLFV experiments to test the parameter space of LG with three quasi-degenerate heavy neutrinos. A difference of our work with respect to Ref. [163] is that the region of viable LG in the $|\sum_{j=1,2,3}(RV)^*_{\mu j}(RV)_{ej}| - M$ plane, considered in our analysis, was derived directly from the solution to the corresponding DMEs without relying on any assumption regarding the magnitude of the couplings $\sum_j |(RV)_{ej}|^2$, $\sum_j |(RV)_{\mu,j}|^2$ and $\sum_j |(RV)_{\tau j}|^2$. The authors of Ref. [163] had to use some assumptions on the ratios $\sum_j |(RV)_{ej}|^2 : \sum_j |(RV)_{\mu,j}|^2 : \sum_j |(RV)_{\tau j}|^2$ in order to relate $|\sum_{j=1,2,3}(RV)^*_{\mu j}(RV)_{ej}|$ with $\sum_{\ell j} |(RV)_{\ell j}|^2$ and project the sensitivities of cLFV experiments and LG bounds in the $\sum_{\ell j} |(RV)_{\ell j}|^2 - M$ plane. Our results are thus more general as we have directly shown the cLFV and LG bounds in the $|\sum_{j=1,2,3}(RV)^*_{\mu j}(RV)_{ej}| - M$ plane, without assuming any ad hoc relation between $\sum_j |(RV)_{ej}|^2$, $\sum_j |(RV)_{\mu,j}|^2$ and $\sum_j |(RV)_{\tau j}|^2$. Nevertheless, the cLFV constraints obtained in Ref. [163] in the region of viable LG for $M \leq 70$ TeV are compatible with our results in Pub. [III] outlined in this section.

Summing up, we have shown that the upcoming and planned experiments on charged lepton flavour violation with $\mu^\pm$, MEG II on the $\mu \to e\gamma$ decay, Mu3e on $\mu \to eee$ decay, Mu2e and COMET on $\mu - e$ conversion in aluminium and PRISM/PRIME on $\mu - e$ conversion in titanium, can probe significant region of the viable parameter space of low-scale LG based on the type-I seesaw mechanism with three quasi-degenerate in mass heavy Majorana neutrinos $N_{1,2,3}$, and thus can test this very attractive LG scenario, with a potential for a discovery.

[7] To make the numerical analysis more straightforward, we have adopted the parametrisation for the matrix $O$ as in Eq. (2.25).

[8] The spikes in the curves related to $\mu - e$ conversions, appearing for different heavy neutrino masses in relation to the considered nucleus, are present because the relative rates of the processes, calculated at leading (one-loop) order and neglecting the differences between the masses of $N_{1,2,3}$, go through zero [235].

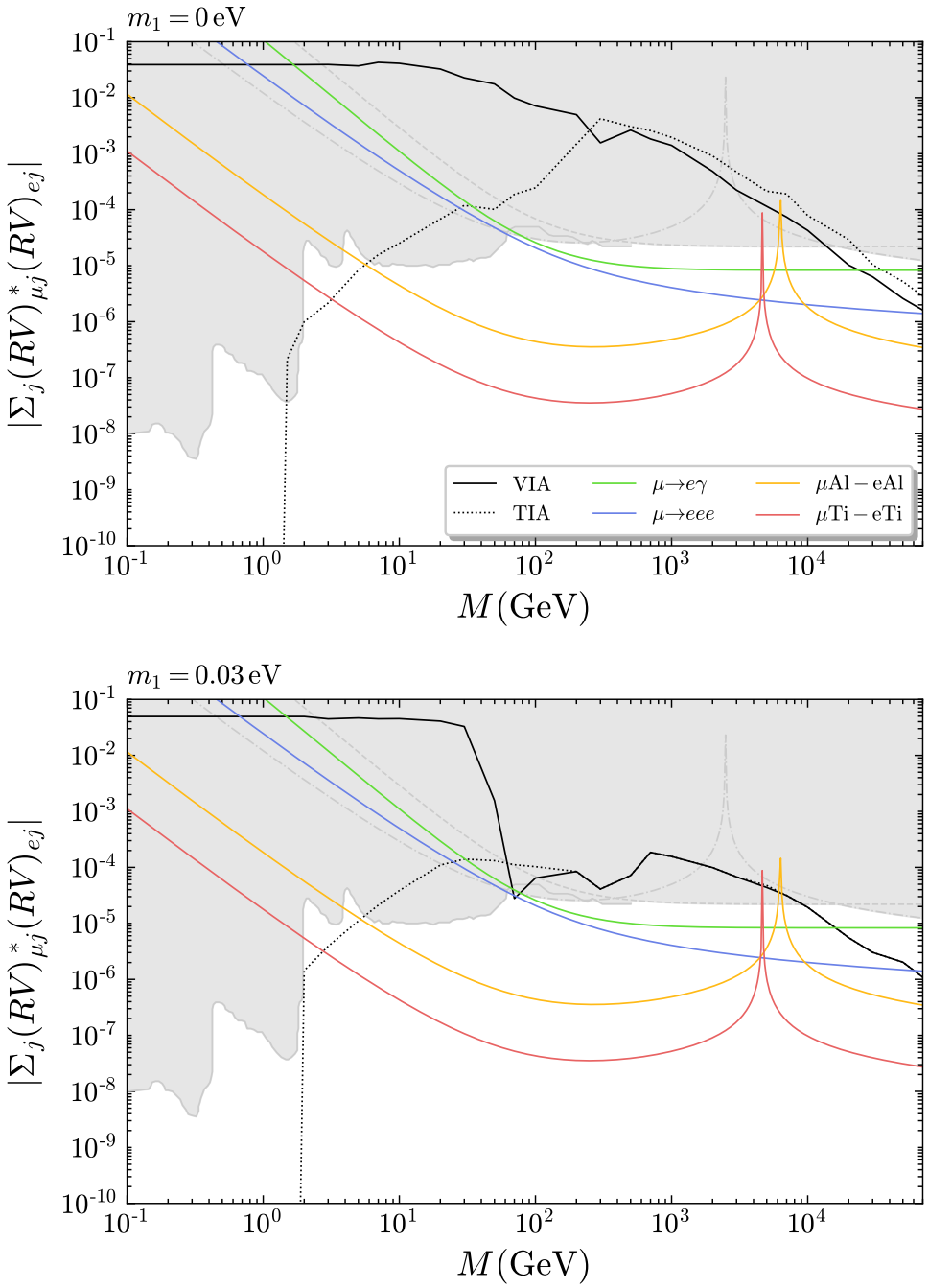


**Figure 4.6.** The region in the $|\sum_{j=1,2,3}(RV)^*_{\mu j}(RV)_{ej}| - M$ plane of successful low-scale LG in the case of NH light neutrino mass spectrum with $m_1 = 0$ (top panel) and for NO spectrum with $m_1 = 0.03$ eV (bottom panel). The solid and dotted black curves are the constraints from successful LG in the VIA and TIA cases, respectively. The grey region with solid contour that extends to $M \sim 500$ GeV is excluded by low-energy experiments as shown in [251], that with dashed and dot-dashed contours are excluded by the current upper limits $\mathrm{BR}(\mu \to e\gamma) < 4.2 \times 10^{-13}$ [239] and $\mathrm{CR}(\mu\,{}^{27}_{13}\mathrm{Au} \to e\,{}^{27}_{13}\mathrm{Au}) < 7 \times 10^{-13}$ [242], respectively. The green, blue, yellow and red lines correspond, from top to bottom, to the sensitivities of the upcoming experiments on $\mu^\pm \to e^\pm + \gamma$, $\mu^\pm \to e^\pm + e^+ + e^-$ decays and on $\mu - e$ conversion in aluminium and titanium. See the text for further details.

# CHAPTER 5

## Summary and Concluding Remarks

In Chapter 1 we have introduced the fact that the present Universe has a net imbalance between matter and antimatter, the former dominating over the latter. The Standard Model of particle physics fails in the attempt of explaining a dynamical generation of the cosmic matter-antimatter asymmetry – the baryon asymmetry of the Universe (BAU) $\eta_B$ – with an initial condition being essentially ruled out by the inflation paradigm. It follows that, to explain why the Universe is made of matter, by the way making our own existence possible, one has to assume new physics beyond the Standard Model. Within the Standard Model it is also impossible to explain the existence of neutrino masses and mixing – which also requires new physics beyond the Standard Model.

To this end, the type-I seesaw extension of the Standard Model, which we have reviewed in Chapter 2, is an elegant attempt to explain both the generation of neutrino masses and mixing and the matter-antimatter asymmetry of the Universe via leptogenesis. Despite being a rather simple extension in mathematical terms requiring only few ($\geq 2$) additional right-handed neutrino fields having a Majorana mass term, the amount of phenomenological aspects that flows from the type-I seesaw scenario is quite impressive – from the observed neutrino oscillation pattern, to the generation of the present baryon asymmetry of the Universe, as well as charged lepton flavour violating processes in the "low-scale" versions of the scenario.

We have briefly reviewed in Chapter 2 how the leptogenesis mechanism within the type-I seesaw mechanism works. In brief, the processes involving the right-handed neutrinos, or, equivalently, the associated heavy Majorana neutrinos $N_j$, that violate C, CP and the lepton number (total and of individual flavour), when happening out-of-equilibrium in the early Universe, lead to a cosmic lepton asymmetry, which is then translated into the present baryon asymmetry of the Universe by the Standard Model sphaleron processes. Since the mass and spectrum of heavy Majorana neutrinos within the type-I seesaw extension are not constrained by the observed light neutrino masses and mixing pattern, a variety of scenarios for the generation of the matter-antimatter asymmetry of the Universe via leptogenesis is possible. In the various scenarios, depending on the scale and mass hierarchy of the heavy Majorana neutrinos, many effects with different timescales can be crucial, such as thermal, flavour and quantum decoherence effects, decay, scattering, soft and oscillation processes, resonant enhancements, that we have considered in our multiple analyses. The inclusion of all the specific effects makes the formulation of a full theory of leptogenesis challenging, with the relevant equations becoming rather complicated and the solutions numerically demanding. Given the complexity and variety of scenarios, it should not be surprising that the leptogenesis idea has been, and continues to be, actively studied since it was proposed more than three decades ago. In turns,

the efficiency and power of the numerical codes we have at present (see, for instance, the work we have done in Pub. [IV]) enables one to compute the baryon asymmetry very precisely and relatively fast. Besides, the effort that the experimental community is continuously investing on neutrino physics stimulates comprehensive examinations of the leptogenesis scenarios in connection to low-energy observables. These are the broad directions that our studies published in Pubs. [I, II, III, IV] and discussed in the present Thesis were following.

In our work of Pub. [I] that we have reviewed in Chapter 3, we have studied the scenario of high-scale leptogenesis based on the type-I seesaw mechanism with two and three (right-handed) heavy Majorana neutrinos $N_j$, $j = 1, 2$ or $j = 1, 2, 3$, possessing hierarchical spectrum, with the lightest heavy Majorana neutrino $N_1$ having a mass in the range $M_1 \sim (10^8 - 10^{14})$ GeV, and in which the CP-violation is provided solely by the low-energy Dirac or/and Majorana phases of the neutrino mixing (PMNS) matrix. We have considered the quantum density matrix equations and classical Boltzmann equations and compared their different predictions in the various flavour regimes of generation of the BAU. The rather detailed numerical analysis we have performed was entirely based on the `ULYSSES` Python package we have developed and presented in Pub. [IV] (see Appendix A) which allowed us to compute the baryon asymmetry fast and efficiently for each of the considered set of equations. We have found that the quantum flavour decoherence effects accounted for in the formalism of density matrix equations can play a dominant role in the generation of the BAU in the whole considered mass range, while the Boltzmann equations may fail to describe the generation of the BAU generation in certain cases. More precisely, when the CP-violation is provided solely by the PMNS phases, the Boltzmann equations do not predict any baryon asymmetry in the regime when the three lepton flavours are indistinguishable during the period of leptogenesis, i.e. for masses above $10^{12}$ GeV. In contrast, the density matrix equations can successfully reproduce the present baryon asymmetry of the Universe in this regime, predicting a novel and unexpected constant behaviour of $\eta_B$ against the mass scale ($M_1$). The results we have found revealed that the density matrix equations predictions can strongly differ from the Boltzmann equations ones even in the regime where one lepton flavour decoheres from the other two. Moreover, the sign of the solution to the density matrix equations depends on the mass scale of leptogenesis in the sense that, for a given set of parameters, the predicted BAU can have different signs in the different flavour regimes. This led us to discover important consequences in terms of ranges of mass scales and values of the PMNS phases for having successful leptogenesis in the cases of normal and inverted hierarchical light neutrino mass spectrum. The most remarkable one is that, when the CP-violation is only due to the Dirac phase $\delta$, there is a one-to-one correspondence between the sign of $\sin\delta$ and the sign of the BAU in the regions of viable leptogenesis. This result could not have been found in the classical Boltzmann equations formalism. The situation is somewhat more complicated when the CP-violation is provided solely by the Majorana phases $\alpha_{21}$ and/or $\alpha_{31}$, but still an eventual measurement of the Dirac and/or Majorana phases could fix or constrain the allowed range of mass scales for having successful leptogenesis. We have thus demonstrated that future low-energy neutrino experimental data on PMNS phases can support or significantly constrain the corresponding leptogenesis parameter spaces of the cases studied in our work.

Another example of leptogenesis scenario that can be connected to low-energy observables is that of resonant leptogenesis in which two heavy Majorana neutrinos $N_{1,2}$ are separated in mass by a tiny mass splitting and can have masses even smaller than the electroweak scale. Their decays into Higgs bosons and leptons, as well as the corresponding Higgs bosons decays into heavy Majorana neutrinos and leptons that can be allowed kinematically due to thermal masses,

may still provide the right amount of CP-violation to produce the present baryon asymmetry of the Universe through leptogenesis. We have investigated this scenario within the type-I seesaw model below the electroweak scale in Pub. [II] and discussed the results in Chapter 4. We have performed the study using the formalism of Boltzmann equations, including flavour and thermal effects and excluding the processes of heavy neutrino oscillations. We have found that reproducing the present baryon asymmetry of the Universe is feasible for heavy Majorana neutrino masses in the range $0.3 - 100$ GeV by relying exclusively on the heavy Majorana neutrino and Higgs decay mechanism. Moreover, the results obtained in Pub. [II] revealed that, depending on the values of the leptogenesis parameters, the dominant of the three flavour components of the total baryon asymmetry $\eta_B$, namely, $\eta_{B_e}$, $\eta_{B_\mu}$ and $\eta_{B_\tau}$, generated by the corresponding CP-asymmetries in the $e$-, $\mu$- and $\tau$-flavour (lepton charge), could be $\eta_{B_e}$ or the sum $\eta_{B_\mu}+\eta_{B_\tau}$, or else the contribution from all three components can be significant, i.e., one can have $\eta_B \simeq \eta_{B_e}$, or $\eta_B \simeq \eta_{B_\mu} + \eta_{B_\tau}$, or else $\eta_B = \eta_{B_e} + \eta_{B_\mu} + \eta_{B_\tau}$. Quite remarkably, the results of our work in Pub. [II] revealed also that, in the case of vanishing initial abundance of heavy Majorana neutrinos and for the masses of $N_{1,2}$ of interest, the baryon asymmetry of the Universe surviving after sphalerons decouple can be produced solely by the $1 \leftrightarrow 2$ and $2 \leftrightarrow 2$ processes either during the production ("freeze-in") or departure from equilibrium ("freeze-out") of the heavy Majorana neutrinos – clearly, since there is no initial production of heavy neutrinos, the case of thermal initial abundance can only correspond to the "freeze-out" scenario. Finally and more importantly, we have demonstrated that such scenario is compatible with values of the charged and neutral current couplings of the heavy Majorana neutrinos in the weak interaction Lagrangian that can be tested in, e.g., the frontier SHiP experiment and future experiments at the FCC-ee collider, opening up the exciting possibility of probing the considered leptogenesis scenarios in future low-energy experiments.

When the effects of heavy neutrino oscillations are considered together with the resonant decay mechanism within the formalism of density matrix equations, the parameter space of viable leptogenesis enlarges considerably. In particular, if one additionally considers three quasi-degenerate heavy Majorana neutrinos with masses in the range $\sim (0.05 - 7 \times 10^4)$ GeV, viable leptogenesis is compatible with charged current and neutral current weak interaction couplings of the heavy neutrinos as large as $\mathcal{O}(10^{-2})$, entering in the sensitivity regions of currently running and future planned experiments on charged lepton flavour violating processes. We have presented in Chapter 4 the constraints we derived in Pub. [III] on the parameter space of this low-scale leptogenesis scenario from the existing data from low-energy experiments, including the current limits from the experiments on $\mu \to e\gamma$ decay and on the rate of $\mu - e$ conversion in gold. We have shown also that the planned and upcoming experiments on charged lepton flavour violation with $\mu^\pm$, MEG II on the $\mu \to e\gamma$ decay, Mu3e on $\mu \to eee$ decay, Mu2e and COMET on $\mu - e$ conversion in aluminium and PRISM/PRIME in titanium, can probe significant region of the viable leptogenesis parameter space. These tests will be performed within the next ten years.

In summary, our results showed many novel interesting features of leptogenesis within the type-I seesaw extension of the Standard Model from grand unification to sub-TeV scales and confirmed possible connections to low-energy observables. We demonstrated that there is the thrilling possibility to test the considered scenarios at currently running and future experimental facilities, which actually have a potential for a discovery. We are looking forward to seeing the results of these very important experiments on beyond the Standard Model physics.

As a next step, further improvements on the numerical code for solving the leptogenesis

equations would definitely allow us to extend and refine the analysis, perhaps elucidating other interesting features of leptogenesis. The type-I seesaw model is the minimal extension one can think of to explain the observed light neutrino masses and mixing scheme, but many theoretical questions, such as the emergence of three flavours and/or the light neutrino mass and mixing patterns and/or the right-handed neutrino masses (e.g. the latter can arise from a dynamical breaking of a high-scale U(1) lepton number symmetry) remain unanswered. Extending further the model to a larger theory could, at the same time, solve some of these open problems and reveal other interesting features of leptogenesis, eventually in further connections to low-energy observables.

# APPENDIX A

## ULYSSES: the Universal LeptogeneSiS Equation Solver

The *Universal LeptogeneSiS Equation Solver* (ULYSSES) introduced in our work of Pub. [IV] is a Python package that solves numerically the sets of semi-classical differential Boltzmann equations relevant to LG scenarios within the type-I seesaw extension of the SM with up to three heavy Majorana neutrinos. To our knowledge, ULYSSES is the first publicly available code for this task.

The package is based on an extensive library of functions where all the quantities entering the equations, such as the decay parameters, the wash-out terms, the heavy neutrino number densities at equilibrium, the projection probabilities and the CP-asymmetry parameters (see Secs. 2.3.1 and 2.3.2 for definitions), are defined and expressed in terms of the Casas-Ibarra parametrisation (arbitrary parameterisations can also be adopted depending on the User's purposes). The parameters of the model, namely the heavy neutrinos masses, the Casas-Ibarra angles, the PMNS angles and phases, as well as the light neutrino masses, can be fixed externally.

The systems of differential equations are defined in separate modules so that, depending on the necessity of the User, the equations that are more appropriate to the regime of interest can be selected and solved numerically for a given set of parameters. The equations implemented in the first available version of the code include the ones defined in Secs. 2.3.1 and 2.3.2, namely 1BE1F, 1BE2F, 1BE3F, 2BE3F, DMEs [1].

The code can be used in two manners. One relatively fast method is dedicated to Users with limited Python programming skills, or limited amount of time, or for rather simple necessities, which can directly utilise ULYSSES from the terminal by providing a text file with the chosen parameters and typing few command lines (the details of this procedure are described in the manual in Pub. [IV]). For the given point in the model parameter space, ULYSSES calculates the BAU (either in terms of the baryon-to-photon ratio $\eta_B$, the baryon-to-entropy density ratio $Y_B$ or the baryonic density parameter $\Omega_B h^2$) and plots the lepton asymmetry number density as a function of the evolution parameter. Otherwise, the package can be imported inside the User's own code and adapted for more advanced purposes. In particular, the package can be adjusted to return a table containing the number densities of the heavy neutrinos $N_{N_{1,2,3}}(z)$ and lepton asymmetries $N_{ee,\,\mu\mu,\,\tau\tau}(z)$, also $\eta_{B_{e,\mu,\tau}}(z)$, for chosen values of $z = M_1/T$, with $M_1$ being the mass of the lightest heavy Majorana neutrino (the User can select the starting and final $z$ values, as well as the number of points). Besides, all the function in the main library can be called and computed at a given $z$ point. This makes the code largely adaptable to the User's purpose.

[1] The equations in the cases for which up to three heavy Majorana neutrinos contribute to the generation of the BAU are also included.

Entering more specifically in the programming details and core dependencies, the code is written in Python3 and heavily uses the widely available modules `NumPy` [252, 253], and `SciPy` [254]. The computation is drastically accelerated with the *just-in-time* compiler provided by `Numba` [255] where meaningful. To undertake the central task of solving sets of coupled differential equations, the package `ODEINTW` [256] is adopted, which provides a wrapper of `scipy.integrate.odeint` that allows it to handle complex and matrix differential equations. The latter is redistributed with `ULYSSES` and does not need to be downloaded separately. These dependencies for `ULYSSES` are automatically resolved during the installation process with `pip`. The aforementioned packages provide the minimal functionality for solving BEs at a given point in the model parameter space.

We summarise in the following list the most important characteristics of the code.

- **Exhaustive.** It can calculate the evolution of all the LG ingredients (e.g., the heavy neutrino number densities, the decay and wash-out factors, the lepton and CP-asymmetries in different flavours).
- **Universal.** It can solve many different sets of equations like, e.g., 1BE1F, 1BE2F, 1BE3F, 2BE3F, DMEs, also with arbitrary numbers of heavy neutrinos [2], that are appropriate to LG scenarios covering more than 14 orders of magnitude, from 0.1 GeV to $10^{14}$ GeV scales. In this sense `ULYSSES` performs an "Odissey" across a vast set of LG frameworks and "travels" towards universality.
- **Precise.** The calculations of the BAU can be made more accurate by including the contributions from, e.g., loop corrections, scattering and spectator processes, flavour effects.
- **Flexible.** The code is easily modify-able and implement-able with new models and sets of equations. Hence, it is widely adaptable to the User's purpose.
- **Slim.** The computation of the BAU performed by `ULYSSES` is tremendously fast due to the multi-core computation provided by the package `NUMBA`, with the code being also small in size ($\sim$ 400 kB).
- **Public.** The code is freely available in the Github folder at this link [IV]. The User can easily download the code from the source or install it directly via `pip`.

Some drawbacks of the code are, e.g., the lack of a module for solving the equations in the scenario of LG via oscillations and the phase-space integro-differential equations at a given momentum, the inclusion of accurate estimates of thermal production rates at finite temperature, next-to-leading-order corrections for the source term and partially equilibrated spectator processes. Some of these features and other improvements are being implemented in an updated and upcoming version of the code [3].

[2] The existing modules work up to three heavy neutrinos, but they can be simply extended to larger number of $N_j$.

[3] Also, the version of the code with the inclusion of thermal effects as we have implemented for the study in Pub. [II] have not been released publicly yet.

# APPENDIX B

## Density Matrix Equations in Different Flavour Bases

We consider here the scenario of two-flavoured leptogenesis within the formalism of DMEs. This is equivalent to set $\Gamma_\mu/(Hz) = 0$ in the DMEs defined in Eqs. (2.52)-(2.53). We describe here in detail how to arrive from the DMEs in the three-flavour basis in Eqs. (2.52)-(2.53) to the ones in the two-flavour basis given in Eqs. (3.1)-(3.4). We also discuss how the formal solution to those is obtained and how, under the single-flavour approximation, they recover the single-flavoured Boltzmann equations in Eqs. (2.34)-(2.35).

In the calculations that follow, it will prove convenient to use the CP-asymmetry in Eqs. (2.56) also for the $\tau^\perp$-flavour and for the $j^{\text{th}}$ heavy Majorana neutrino $N_j$, which, in terms of the $C_{j\alpha}$ coefficients defined in Eq. (2.31), is given by

$$\begin{aligned}\epsilon^{(j)}_{\alpha\beta} = \frac{3}{32\pi}\sum_{k\neq j}\left(Y^\dagger Y\right)_{kk}\Bigg\{ & i\left[C_{j\alpha}C^*_{k\beta}(C^\dagger C)_{kj} - C^*_{j\beta}C_{k\alpha}(C^\dagger C)_{jk}\right] f_1\left(\frac{x_k}{x_j}\right) \\ & + i\left[C_{j\alpha}C^*_{k\beta}(C^\dagger C)_{jk} - C^*_{j\beta}C_{k\alpha}(C^\dagger C)_{kj}\right] f_2\left(\frac{x_k}{x_j}\right)\Bigg\},\end{aligned} \tag{B.1}$$

with $j$, $k = 1$, 2, 3 and $\alpha$, $\beta = e$, $\mu$, $\tau$, $\tau^\perp$. Explicitly, the diagonal terms are

$$\epsilon^{(j)}_{\alpha\alpha} = \frac{3}{16\pi}\sum_{k\neq j}\left(Y^\dagger Y\right)_{kk}\left\{\Im\left[C^*_{j\alpha}C_{k\beta}(C^\dagger C)_{jk}\right] f_1\left(\frac{x_k}{x_j}\right) + \Im\left[C^*_{j\alpha}C_{k\beta}(C^\dagger C)_{kj}\right] f_2\left(\frac{x_k}{x_j}\right)\right\}. \tag{B.2}$$

We remind also that $\left(Y^\dagger Y\right)_{jj} = \sum_\gamma |Y_{\gamma j}|^2$, $\left(C^\dagger C\right)_{jk} = \sum_\gamma C^*_{j\gamma}C_{k\gamma}$ and $p_{j\gamma} \equiv |C_{j\gamma}|^2$ with $\gamma = e$, $\mu$, $\tau$, while $p_{j\tau^\perp} \equiv p_{je} + p_{j\mu}$ and $p_{j\tau} + p_{j\tau^\perp} = p_{j\tau} + p_{je} + p_{j\mu} = 1$. To use Eqs. (B.1) and (B.2) we should define the coefficients $C_{j\tau^\perp}$ and $C^*_{j\tau^\perp}$. However, the relation $\epsilon^{(j)}_{\tau^\perp\tau^\perp} \equiv \epsilon^{(j)}_{ee} + \epsilon^{(j)}_{\mu\mu}$ imposes that

$$C_{j\tau^\perp}C^*_{k\tau^\perp} = C_{je}C^*_{ke} + C_{j\mu}C^*_{k\mu}, \tag{B.3}$$

which for $j = k$ means $|C_{j\tau^\perp}|^2 = |C_{je}|^2 + |C_{j\mu}|^2 = p_{j\tau^\perp}$. Since the physical quantities (e.g., $N_{B-L}$) depend on $|C_{j\tau^\perp}|^2$ (in our case of interest $j = 1$), there is actually no need to define the coefficients $C_{j\tau^\perp}$ and $C^*_{j\tau^\perp}$, apart from imposing the constraint in Eq. (B.3), so we are going to let them free in our calculations.

An important relation that derives from Eqs. (B.1) and (B.2) and that is going to be used further is

$$2\Re\left[C_{j\beta}C^*_{j\alpha}\epsilon^{(k)}_{\alpha\beta}\right] = p_{j\beta}\epsilon^{(k)}_{\alpha\alpha} + p_{j\alpha}\epsilon^{(k)}_{\beta\beta}\,, \tag{B.4}$$

with $\alpha$, $\beta = e$, $\mu$, $\tau$, $\tau^\perp$.

We now concentrate again on the hierarchical case for which only the decay of the heavy neutrino $N_1$ is relevant for leptogenesis (i.e. $j = 1$). Firstly, we sum the equations for $N_{ee}$ and $N_{\mu\mu}$, which result from taking $\alpha = \beta = e, \mu$ in Eqs. (2.53) respectively, and get an equation for $N_{\tau^\perp\tau^\perp} = N_{ee} + N_{\mu\mu}$:

$$\begin{aligned}\frac{dN_{\tau^\perp\tau^\perp}}{dz} =& \epsilon^{(1)}_{\tau^\perp\tau^\perp} D_1 (N_{N_1} - N^{\rm eq}_{N_1}) + \\ & - W_1 \Big\{ p_{1e} N_{ee} + p_{1\mu} N_{\mu\mu} + 2\Re \left[ C_{1e} C^*_{1\mu} N_{\mu e} \right] + \\ & + \Re \left[ C_{1e} C^*_{1\tau} N_{\tau e} \right] + \Re \left[ C_{1\mu} C^*_{1\tau} N_{\tau\mu} \right] \Big\}.\end{aligned} \tag{B.5}$$

The second line of the above equation is actually $p_{1\tau^\perp} N_{\tau^\perp\tau^\perp}$. This can be shown by considering the equations for $p_{1\mu} N_{ee}$, $p_{1e} N_{\mu\mu}$ and $2\Re \left[ C_{1e} C^*_{1\mu} N_{ee} \right]$, from which we can write:

$$\begin{aligned}2\Re \left[ C_{1e} C^*_{1\mu} \frac{dN_{\mu e}}{dz} \right] =& \, 2\Re \left[ C_{1e} C^*_{1\mu} \epsilon^{(1)}_{\mu e} \right] D_1 (N_{N_1} - N^{\rm eq}_{N_1}) + \\ & - W_1 \Re \left[ C_{1e} C^*_{1\mu} \left\{ P^{0(1)}, N \right\}_{\mu e} \right] \\ =& \, (p_{1\mu} \epsilon^{(1)}_{ee} + p_{1e} \epsilon^{(1)}_{\mu\mu}) D_1 (N_{N_1} - N^{\rm eq}_{N_1}) + \\ & - W_1 \Big\{ p_{1e} p_{1\mu} (N_{ee} + N_{\mu\mu}) + \\ & + (p_{1e} + p_{1\mu}) \Re \left[ C_{1e} C^*_{1\mu} N_{\mu e} \right] + p_{1\mu} \Re \left[ C_{1e} C^*_{1\tau} N_{\tau e} \right] + p_{1e} \Re \left[ C_{1\mu} C^*_{1\tau} N_{\tau\mu} \right] \Big\} \\ =& \, p_{1\mu} \frac{dN_{ee}}{dz} + p_{1e} \frac{dN_{\mu\mu}}{dz} \, .\end{aligned} \tag{B.6}$$

By assuming that at the beginning of leptogenesis ($z_0$) all the asymmetries are zero, the following condition must hold at any $z \geq 0$: [1]

$$2\Re \left[ C_{1e} C^*_{1\mu} N_{\mu e} \right] = p_{1\mu} N_{ee} + p_{1e} N_{\mu\mu} \, , \tag{B.7}$$

which leads to

$$p_{1e} N_{ee} + p_{1\mu} N_{\mu\mu} + 2\Re \left[ C_{1e} C^*_{1\mu} N_{\mu e} \right] = p_{1\tau^\perp} N_{\tau^\perp\tau^\perp} \, . \tag{B.8}$$

We then define

$$N_{\tau\tau^\perp} \equiv \left( \frac{C_{1e}}{C_{1\tau^\perp}} N_{\tau e} + \frac{C_{1\mu}}{C_{1\tau^\perp}} N_{\tau\mu} \right) \tag{B.9}$$

and $N_{\tau^\perp\tau} = N^*_{\tau\tau^\perp}$, so that the equations for $N_{\tau\tau}$ and $N_{\tau^\perp\tau^\perp}$ can be recast in the forms given in Eqs. (3.2) and (3.3). By using the relation $C_{j\tau^\perp} \epsilon^{(k)}_{\tau\tau^\perp} = C_{je} \epsilon^{(k)}_{\tau e} + C_{j\mu} \epsilon^{(k)}_{\tau\mu}$ (with $j = 1$ in our case), which follows from Eqs. (B.1) and (B.3), combined with all the previous relations, we get the equation for $N_{\tau\tau^\perp}$ as in Eq. (3.4) and the DMEs in the two-flavour basis are recovered.

The formal expression of $N_{\tau\tau^\perp}$ can be obtained by solving Eq. (3.4) with the integrating factor method, which leads to

$$\begin{aligned}N_{\tau\tau^\perp}(z) = & \, \epsilon^{(1)}_{\tau\tau^\perp} \int_{z_0}^{z} D_1(z') (N_{N_1}(z') - N^{\rm eq}_{N_1}(z')) e^{-\Lambda_\tau (z - z')} e^{-\frac{1}{2} \int_{z'}^{z} W_1 \, dz''} \, dz' + \\ & - \frac{1}{2} C_{1\tau} C^*_{1\tau^\perp} \int_{z_0}^{z} W_1(z') N_{B-L}(z') e^{-\Lambda_\tau (z - z')} e^{-\frac{1}{2} \int_{z'}^{z} W_1(z'') \, dz''} \, dz',\end{aligned} \tag{B.10}$$

[1] We stress that this is only valid if $\Gamma_\mu / (Hz) = 0$, as in our case.

where the initial asymmetry was assumed to be zero, namely $N_{\tau\tau^\perp}(z_0) = 0$. Notice that the above expression contains a term with $N_{B-L}$ which cannot be ignored in general, if not, e.g., in the limit of $\Gamma_\tau/(Hz) \to 0$ (see Sec. 3.1).

To get the resulting equation for $N_{B-L} = N_{\tau\tau} + N_{\tau^\perp\tau^\perp}$ we first notice that:

$$\begin{aligned} 2\Re\left[C_{1\tau^\perp}C^*_{1\tau}\frac{dN_{\tau\tau^\perp}}{dz}\right] &= 2\Re\left[C_{1\tau^\perp}C^*_{1\tau}\epsilon^{(1)}_{\tau\tau^\perp}\right] D_1(N_{N_1} - N^{\rm eq}_{N_1}) + \\ &\quad - W_1\left\{\Re\left[C_{1\tau^\perp}C^*_{1\tau}N_{\tau\tau^\perp}\right] + p_{1\tau}p_{1\tau^\perp}N_{B-L}\right\} - 2\Re\left[C_{1\tau^\perp}C^*_{1\tau}N_{\tau\tau^\perp}\frac{\Gamma_\tau}{Hz}\right] \\ &= (p_{1\tau^\perp}\epsilon^{(1)}_{\tau\tau} + p_{1\tau}\epsilon^{(1)}_{\tau^\perp\tau^\perp})D_1(N_{N_1} - N^{\rm eq}_{N_1}) + \\ &\quad - W_1\left\{\Re\left[C_{1\tau^\perp}C^*_{1\tau}N_{\tau\tau^\perp}\right] + p_{1\tau}p_{1\tau^\perp}N_{B-L}\right\} - 2\Re\left[C_{1\tau^\perp}C^*_{1\tau}N_{\tau\tau^\perp}\frac{\Gamma_\tau}{Hz}\right] \end{aligned} \tag{B.11}$$

Then we write the equation for $p_{1\tau^\perp}N_{\tau\tau} + p_{1\tau}N_{\tau^\perp\tau^\perp}$, that is:

$$\begin{aligned} \frac{d}{dz}(p_{1\tau^\perp}N_{\tau\tau} + p_{1\tau}N_{\tau^\perp\tau^\perp}) &= (p_{1\tau^\perp}\epsilon^{(1)}_{\tau\tau} + p_{1\tau}\epsilon^{(1)}_{\tau^\perp\tau^\perp})D_1(N_{N_1} - N^{\rm eq}_{N_1}) + \\ &\quad - W_1\left\{\Re\left[C_{1\tau^\perp}C^*_{1\tau}N_{\tau\tau^\perp}\right] + p_{1\tau}p_{1\tau^\perp}N_{B-L}\right\} \\ &= 2\Re\left[C_{1\tau^\perp}C^*_{1\tau}\frac{dN_{\tau\tau^\perp}}{dz}\right] + 2\Re\left[C_{1\tau^\perp}C^*_{1\tau}N_{\tau\tau^\perp}\frac{\Gamma_\tau}{Hz}\right] \end{aligned} \tag{B.12}$$

Then, given that

$$p_{1\tau^\perp}N_{\tau\tau} + p_{1\tau}N_{\tau^\perp\tau^\perp} = N_{B-L} - (p_{1\tau}N_{\tau\tau} + p_{1\tau^\perp}N_{\tau^\perp\tau^\perp}) \tag{B.13}$$

we get

$$p_{1\tau}\frac{dN_{\tau\tau}}{dz} + p_{1\tau^\perp}\frac{dN_{\tau^\perp\tau^\perp}}{dz} + 2\Re\left[C_{1\tau^\perp}C^*_{1\tau}\frac{dN_{\tau\tau^\perp}}{dz}\right] = \frac{dN_{B-L}}{dz} - 2\Re\left[C_{1\tau^\perp}C^*_{1\tau}N_{\tau\tau^\perp}\frac{\Gamma_\tau}{Hz}\right]. \tag{B.14}$$

Since all the asymmetries are assumed to be zero at $z_0$, the above relation converts to

$$p_{1\tau}N_{\tau\tau}(z) + p_{1\tau^\perp}N_{\tau^\perp\tau^\perp}(z) + 2\Re\left[C_{1\tau^\perp}C^*_{1\tau}N_{\tau\tau^\perp}(z)\right] = N_{B-L}(z) - \lambda(z)\,, \tag{B.15}$$

with $\lambda(z)$ defined as in Eq. (3.8). We note that $\lambda(z) = 0$ in the single-flavour approximation, namely for $\Gamma_\tau/(Hz) = 0$.

Finally, by summing Eqs. (3.2) and (3.3) and using the previous relations we get an equation for $N_{B-L}$ that reads:

$$\frac{dN_{B-L}}{dz} = \epsilon^{(1)}D_1(z)(N_{N_1}(z) - N^{\rm eq}_{N_1}(z)) - W_1(z)N_{B-L}(z) + W_1(z)\lambda(z). \tag{B.16}$$

In the case of $\lambda(z) = 0$, the above equation corresponds to the Boltzmann equation for the $B - L$ asymmetry in the single-flavour approximation given in Eq. (2.35). Moreover, when $\epsilon^{(1)} = 0$, as in the case of CP violation solely provided by the PMNS phases, Eq. (B.16) reduces to Eq. (3.19).

The formal solution to Eq. (B.16) reads:

$$N_{B-L}(z) = \int_{z_0}^{z} e^{-\int_{z'}^{z_f} W_1(z'')dz''} \epsilon^{(1)} D_1(z')(N_{N_1}(z') - N_{N_1}^{\rm eq}(z'))\, dz' + \int_{z_0}^{z} W_1(z')\lambda(z') e^{-\int_{z'}^{z} W_1\, dz''}\, dz', \tag{B.17}$$

where, as usual, we have assumed vanishing initial asymmetry $N_{B-L}(z_0) = 0$.

# APPENDIX C

# Analytical Approximations for the Solutions to the Boltzmann Equations

In this appendix we illustrate the passages that lead to the analytical approximations to the Boltzmann Equations (BEs) in various regimes. Useful references with similar calculations are Refs. [97, 257]. The BEs are:

$$\frac{dN_{N_1}}{dz} = -D_1(N_{N_1} - N_{N_1}^{\rm eq}), \tag{C.1}$$

$$\frac{dN_{\ell\ell}}{dz} = \epsilon_{\ell\ell}^{(1)} D_1(N_{N_1} - N_{N_1}^{\rm eq}) - W_1 p_{1\ell} N_{\ell\ell}, \tag{C.2}$$

where $\ell = \tau$, $\tau^\perp$ or $e$, $\mu$, $\tau$ in the two- or three-flavour basis, respectively. The single-flavour BEs can be recovered by formally substituting $N_{\ell\ell}$ with $N_{B-L}$ and setting $p_{1\ell} = 1$ in (C.2). The strength of the decays and inverse decays is quantified by $\kappa_1 p_{1\ell}$. When $\kappa_1 p_{1\ell} \gg 1$, the flavour $\ell$ is said to be in the *strong* wash-out regime. Conversely, if $\kappa_1 p_{1\ell} \ll 1$, the flavour $\ell$ is in the *weak* wash-out regime. The formal solution to the BEs can be found by means of the integrating factor method:

$$N_{N_1}(z) = N_{N_1}(z_0) e^{-\int_{z_0}^{z} D_1(z')\, dz'} + \int_{z_0}^{z} D_1(z') N_{N_1}^{\rm eq}(z') e^{-\int_{z'}^{z} D_1(z'')\, dz''}\, dz', \tag{C.3}$$

$$N_{\ell\ell}(z) = N_{\ell\ell}(z_0) e^{-\int_{z_0}^{z} W_1(z') p_{1\ell}\, dz'} + \tag{C.4}$$
$$+ \epsilon_{\ell\ell}^{(1)} \int_{z_0}^{z} D_1(z') \left(N_{N_1}(z') - N_{N_1}^{\rm eq}(z')\right) e^{-\int_{z'}^{z} W_1(z'') p_{1\ell}\, dz''}\, dz'.$$

Assuming zero asymmetry at $z_0$, the first term in Eq. (C.4) vanishes.

## C.1 Strong Wash-Out Regime

In the strong wash-out regime for a certain lepton flavour $\ell$, there is a period $z_\ell^{\rm in} \leq z \leq z_\ell^{\rm out}$ for which $W_1(z) p_{1\ell} \geq 1$. Assuming that the wash-outs are effective enough, any asymmetry in the flavour $\ell$ generated before $z_\ell^{\rm in}$ is fully erased by wash-outs. Therefore, there is no dependence on the initial condition in this case. An analytical approximation for the asymmetry for $z_\ell^{\rm in} \leq$

$z \leq z_\ell^{\rm out}$ can then be found by setting the right-hand side of Eq. (C.2) to zero (this corresponds to the so-called *strong wash-out balance approximation* [217, 257]):

$$N_{\ell\ell}(z) \simeq -\frac{\epsilon^{(1)}_{\ell\ell}}{W_1 p_{1\ell}}\frac{dN_{N_1}}{dz} \simeq -\frac{\epsilon^{(1)}_{\ell\ell}}{W_1 p_{1\ell}}\frac{dN^{\rm eq}_{N_1}}{dz} = \frac{2N^{\rm eq}_\ell}{z\kappa_1 p_{1\ell}}\epsilon^{(1)}_{\ell\ell}\,, \tag{C.5}$$

where we have used the approximation $N_{N_1}(z) \simeq N^{\rm eq}_{N_1}(z) = \frac{1}{2}z^2 K_2(z) N^{\rm eq}_N(0)$ valid in this regime and $d(z^2K_2(z))/dz = -z^2K_1(z)$. After $z_\ell^{\rm out}$, the asymmetry in the flavour $\ell$ gets frozen so that:

$$N_{\ell\ell}(\infty) \simeq \frac{2N^{\rm eq}_\ell}{\kappa_1}\frac{\epsilon^{(1)}_{\ell\ell}}{z^{\rm out}_\ell p_{1\ell}}, \tag{C.6}$$

with $z^{\rm out}_\ell \simeq 1.25\ln(25\kappa_1 p_{1\ell})$.

In the two-flavour approximation, since usually $z_d \equiv z^{\rm out}_\tau \simeq z^{\rm out}_{\tau^\perp}$, the final $B-L$ asymmetry is given by

$$N^{\rm 1BE2F}_{B-L}(\infty) \simeq \frac{2N^{\rm eq}_\ell}{z_d\kappa_1}\frac{\epsilon^{(1)}_{\tau\tau}p_{1\tau^\perp} + \epsilon^{(1)}_{\tau^\perp\tau^\perp}p_{1\tau}}{p_{1\tau}p_{1\tau^\perp}}. \tag{C.7}$$

## C.2 Weak Wash-Out Regime

In the weak wash-out regime we need to distinguish between two different initial conditions, namely thermal initial abundance (TIA) and vanishing initial abundance (VIA) for which $N_{N_1}(z_0) = N^{\rm eq}_{N_1}(z_0)$ and $N_{N_1}(z_0) = 0$ respectively.

### Vanishing Initial Abundance

The number of heavy neutrinos evolving with $z$ in the VIA case, for which $N_{N_1}(z_0) = 0$, follows from Eq. (C.3):

$$\begin{aligned} N_{N_1}(z) &\simeq \int_{z_0}^{z} D_1(z')N^{\rm eq}_{N_1}(z')e^{-\int_{z'}^{z} D_1(z'')\,dz''}\,dz' \\ &= 2N^{\rm eq}_\ell \int_{z_0}^{z} W_1(z')e^{-\int_{z'}^{z} D_1(z'')\,dz''}\,dz' \end{aligned} \tag{C.8}$$

We define $z_{eq}$ as the time at which $N_{N_1}(z_{eq}) = N^{\rm eq}_{N_1}(z_{eq})$, that corresponds to a maximum for $N_{N_1}(z)$. Indeed, from Eq. (C.1) it follows that, at $z_{eq}$, $dN_{N_1}/dz = 0$ and $d^2N_{N_1}/dz^2 = D_1 dN^{\rm eq}_{N_1}/dz < 0$. The number of RH neutrinos at $z_{eq}$ can be computed using some analytical approximations such as in Ref. [97], of which we employ the same result:

$$N(\kappa_1) \equiv N_{N_1}(z_{eq}) \simeq \frac{9\pi}{16}\kappa_1. \tag{C.9}$$

For $z < z_{eq}$, we can assume $N^{\rm eq}_{N_1} \gg N_{N_1}$. Then, from Eq. (C.4) and using Eq. (2.39), we find that the asymmetry up to $z_{eq}$ reads:

$$\begin{aligned} N_{\ell\ell}(z_{eq}) &\simeq \epsilon^{(1)}_{\ell\ell}\int_{z_0}^{z_{eq}} D_1(z')N^{\rm eq}_{N_1}(z')e^{-\int_{z'}^{z_{eq}} W_1(z'')p_{1\ell}\,dz''}\,dz' \\ &= 2N^{\rm eq}_\ell\frac{\epsilon^{(1)}_{\ell\ell}}{p_{1\ell}}\left(1 - e^{-p_{1\ell}\frac{N(\kappa_1)}{2N^{\rm eq}_\ell}}\right) \simeq -N(\kappa_1)\epsilon^{(1)}_{\ell\ell} + \frac{N(\kappa_1)^2}{4N^{\rm eq}_\ell}\epsilon^{(1)}_{\ell\ell}p_{1\ell}. \end{aligned} \tag{C.10}$$

For $z > z_{eq}$, we can instead write the asymmetry as:

$$\begin{aligned} N_{\ell\ell}(z) - N_{\ell\ell}(z_{eq}) &= -\epsilon^{(1)}_{\ell\ell} \int_{z_{eq}}^{z} \frac{dN_{N1}}{dz'} e^{-\int_{z'}^{z} W_1(z'') p_{1\ell}\, dz''}\, dz' \\ &\simeq -\epsilon^{(1)}_{\ell\ell} \int_{z_{eq}}^{z} \frac{dN_{N1}}{dz'} \left(1 - p_{1\ell} \int_{z'}^{z} W_1(z'')\, dz''\right) dz' \\ &\simeq \epsilon^{(1)}_{\ell\ell} \left(N(\kappa_i) - N_{N_1}(z)\right) - p_{1\ell}\epsilon^{(1)}_{\ell\ell} \int_{z_{eq}}^{z} dz'\, D_1(z') N_{N_1}(z') \int_{z'}^{z} dz''\, W_1(z'') \\ &\simeq \epsilon^{(1)}_{\ell\ell} \left(N(\kappa_i) - N_{N_1}(z)\right), \end{aligned} \tag{C.11}$$

where in the last passage we have neglected the (negative) term proportional to $p_{1\ell}$. This last approximation may be a bit inaccurate if $10^{-2} < \kappa_1 p_{1\ell} < 1$ [97].

The final asymmetry then reads ($N_{N_1}(\infty) = 0$):

$$N_{\ell\ell}(\infty) \simeq \epsilon^{(1)}_{\ell\ell} p_{1\ell} \frac{N(\kappa_1)^2}{4N^{\rm eq}_{\ell}} \simeq \frac{81\pi^2}{1024 N^{\rm eq}_{\ell}} \kappa_1^2 \epsilon^{(1)}_{\ell\ell} p_{1\ell}, \tag{C.12}$$

which, in the two-flavour approximations results in

$$N^{\rm 1BE2F}_{B-L}(\infty) \simeq \frac{81\pi^2}{1024 N^{\rm eq}_{\ell}} \kappa_1^2 (\epsilon^{(1)}_{\tau\tau} p_{1\tau} + \epsilon^{(1)}_{\tau^\perp\tau^\perp} p_{1\tau^\perp}) \tag{C.13}$$

### Thermal Initial Abundance

In the TIA case, $N_{N_1}(z_0) = N^{\rm eq}_{N_1}(z_0)$. We define $z_D$ so that $z_D D_1(z_D) = 2$, i.e. as the time at which decays are in equilibrium against the expanding Universe. In the weak wash-out regime $z_D \gg 1$.

For $z \lesssim 1$ we can consider $N^{\rm eq}_{N_1}(z) \simeq N^{\rm eq}_{N_1}(z_0)$. Hence,

$$\begin{aligned} N_{N_1}(z) &\simeq N^{\rm eq}_{N_1}(z_0) \int_{z_0}^{z} D_1 e^{-\int_{z'}^{z} D_1(z'')\, dz''}\, dz' + N^{\rm eq}_{N_1}(z_0) e^{-\int_{z_0}^{z} D_1(z') dz'} \\ &= N^{\rm eq}_{N_1}(z_0) \left(1 - e^{-\int_{z_0}^{z} D_1(z') dz'}\right) + N^{\rm eq}_{N_1}(z_0) e^{-\int_{z_0}^{z} D_1(z') dz'} = N^{\rm eq}_{N_1}(z_0). \end{aligned} \tag{C.14}$$

For $1 < z \leq z_D$, the equilibrium number density is exponentially dropped so that $N^{\rm eq}_{N_1}(z) \ll N_{N_1}(z)$ and we have

$$N_{N_1}(z) \simeq N^{\rm eq}_{N_1}(z_0) e^{-\int_{1}^{z} D_1(z') dz'} \simeq N^{\rm eq}_{N_1}(z_0). \tag{C.15}$$

Then the asymmetry up to $z_D$ is roughly zero. At $z \simeq z_D$ the heavy neutrinos start to decay effectively and their abundance for $z \gtrsim z_D$ is exponentially damped:

$$N_{N_1}(z) \simeq N^{\rm eq}_{N_1}(z_0) e^{-\int_{z_D}^{z} D_1(z') dz'}. \tag{C.16}$$

The asymmetry at $z > z_D$ then reads:

$$\begin{aligned} N_{\ell\ell}(z) &\simeq -\epsilon^{(1)}_{\ell\ell} \int_{z_D}^{z} \frac{dN_{N_1}}{dz'} e^{-\int_{z'}^{z} W_1(z'') p_{1\ell}\, dz''}\, dz' \\ &\simeq -\epsilon^{(1)}_{\ell\ell} \int_{z_D}^{z} \frac{dN_{N_1}}{dz'} \left(1 - \int_{z'}^{z} W_1(z'') p_{1\ell}\, dz''\right) dz' \\ &\simeq \epsilon^{(1)}_{\ell\ell} \left(N^{\rm eq}_{N_1}(z_0) - N_{N_1}(z)\right) - p_{1\ell}\epsilon^{(1)}_{\ell\ell} \int_{z_D}^{z} dz' D_1(z') N_{N_1}(z') \int_{z'}^{z} dz'' W_1(z'')\,. \end{aligned} \tag{C.17}$$

The final asymmetry $B - L$ is then given by:

$$N_{\ell\ell}(\infty) = \epsilon^{(1)}_{\ell\ell} N^{\rm eq}_{N_1}(z_0) - \epsilon^{(1)}_{\ell\ell} p_{1\ell} \int_{z_D}^{+\infty} dz' D_1(z') N_{N_1}(z') \int_{z'}^{+\infty} dz'' W_1(z'') \,, \tag{C.18}$$

which in the two-flavour approximation becomes

$$N^{\rm 1BE2F}_{B-L}(\infty) = \epsilon^{(1)} N^{\rm eq}_{N_1}(z_0) - (\epsilon^{(1)}_{\tau\tau} p_{1\tau} + \epsilon^{(1)}_{\tau^\perp\tau^\perp} p_{1\tau^\perp}) \mathcal{A}(\kappa_1), \tag{C.19}$$

with

$$\mathcal{A}(\kappa_1) \equiv \int_{z_D}^{+\infty} dz' D_1(z') N_{N_1}(z') \int_{z'}^{+\infty} dz'' W_1(z'') \, dz'. \tag{C.20}$$

Note that, if not for the second term in (C.19), when $\epsilon^{(1)} = 0$ the final asymmetry would vanish.

# APPENDIX D

# Branching Ratios and Conversion Rates of cLFV Processes with Muons

We report here the relevant formulas for the branching ratios of the $\mu \to e\gamma$ and $\mu \to eee$ decays and rates of the $\mu - e$ conversion in the nuclei $^{48}_{22}$Ti, $^{27}_{13}$Al, $^{197}_{79}$Au and $^{208}_{82}$Pb in the context of the type-I seesaw extension of the SM with three quasi-degenerate in mass heavy Majorana neutrinos. In what follows, we neglect the differences in mass between the heavy neutrino masses $M_{1,2,3} \simeq M$. The formulas reported in this appendix were used in our analysis of Pub. [III] presented in Chapter 4, are in perfect agreement with those reported in Ref. [258] and, to leading order in the heavy Majorana neutrino mass splittings and couplings to the SM, with those used in Ref. [163].

## D.1 Branching Ratio of the $\mu \to e\gamma$ Decay

In the type-I seesaw scenario with three quasi-degenerate in mass heavy Majorana neutrinos, the $\mu \to e\gamma$ decay branching ratio is given by [235, 237, 238, 248, 250]:

$$\mathrm{BR}(\mu \to e\gamma) \simeq \frac{3\alpha_{\rm em}}{32\pi} \left| G(X) - G(0) \right|^2 \left| \sum_{j=1,2,3} (RV)^*_{\mu j} \, (RV)_{ej} \right|^2 , , \tag{D.1}$$

where $\alpha_{\rm em} \simeq 1/137$ is the electromagnetic fine structure constant and $X \equiv (M/M_W)^2$, with $M_W \simeq 80.4\,\mathrm{GeV}$ being the mass of the $W^\pm$ bosons. In the above equation, the loop integration function $G(x)$ reads [235]

$$G(x) = \frac{10 - 43x + 78x^2 - 49x^3 + 4x^4 + 18x^3 \log(x)}{3(x-1)^4} \, . \tag{D.2}$$

The above function $G(x)$ is monotonic and takes values in the interval $[4/3, 10/3]$, with $G(x \ll 1) \simeq 10/3 - x$.

## D.2 Rate of the $\mu - e$ Conversion in a Nucleus

In the type-I seesaw extension of the SM, the rate of the $\mu - e$ conversion in nuclei can be approximated by the following expression [235, 259]:

$$\mathrm{CR}(\mu\mathcal{N} \to e\mathcal{N}) \simeq \frac{\alpha^5_{\rm em}}{8\,\pi^4 \sin^4\theta_W} \frac{Z^4_{\rm eff}}{Z} \left| F(-m^2_\mu) \right|^2 \frac{G^2_F m^5_\mu}{\Gamma_{\rm capt}} \left| \mathcal{C}_{\mu e} \right|^2 \left| \sum_{j=1,2,3} (RV)^*_{\mu j} \, (RV)_{ej} \right|^2 . \tag{D.3}$$

In the above equation, $G_F \simeq 1.17 \times 10^{-5}\,\text{GeV}^{-2}$ is the Fermi coupling constant, $Z$ is the atomic number, i.e. the number of protons, of the nucleus $\mathcal{N}$, $\theta_w$ is the weak mixing angle, with $\sin^2\theta_w \simeq 0.23$, $F(-m_\mu^2)$ is the nuclear form factor at momentum transfer squared $q^2 = -m_\mu^2$, $m_\mu \simeq 105.7\,\text{MeV}$ being the muon mass, $Z_{\text{eff}}$ is the effective atomic charge and $\Gamma_{\text{capt}}$ is the experimentally known total muon capture rate. The loop integral factor $\mathcal{C}_{\mu e}$ reads [235]:

$$\mathcal{C}_{\mu e} \simeq Z\,[2F_u^{\mu e}(X) + F_d^{\mu e}(X)] + (A - Z)\,[F_u^{\mu e}(X) + 2F_d^{\mu e}(X)]\,, \tag{D.4}$$

where

$$F_q^{\mu e}(X) = Q_q \sin^2\theta_w\,[F_\gamma(X) - F_z^{\mu e}(X) + G_\gamma(X)] + \frac{1}{4}\,[2I_3 F_z^{\mu e}(X) + F_{\text{Box}}^{\mu eqq}(X)]\,. \tag{D.5}$$

Here, $A$ is the mass number, i.e. the number of nucleons, of the nucleus $\mathcal{N}$, and $q = u,\, d$ are the up and down quarks with electric charge (in unit of proton charge) $Q_{u(d)} = 2/3\,(-1/3)$ and third component of the weak isospin $I_3 = \pm 1/2$, with the positive (negative) sign associated to the up (down) quark. Also, the various functions appearing in Eq. (D.5) are given by [235]:

$$F_\gamma(x) = \frac{x(7x^2 - x - 12)}{12(1-x)^3} - \frac{x^2(12 - 10x + x^2)}{6(1-x)^4}\log x,\,, \tag{D.6}$$

$$G_\gamma(x) = -\frac{x(2x^2 + 5x - 1)}{4(1-x)^3} - \frac{3x^3}{2(1-x)^4}\log x\,, \tag{D.7}$$

$$F_z(x) = -\frac{5x}{2(1-x)} - \frac{5x^2}{2(1-x)^2}\log x\,, \tag{D.8}$$

$$G_z(x,y) = -\frac{1}{2(x-y)}\left[\frac{x^2(1-y)}{(1-x)}\log x - \frac{y^2(1-x)}{(1-y)}\log y\right]\,, \tag{D.9}$$

$$\begin{aligned} F_{\text{Box}}(x,y) = {} & \frac{1}{x-y}\left\{(4 + \frac{xy}{4})\left[\frac{1}{1-x} + \frac{x^2}{(1-x)^2}\log x - \frac{1}{1-y} - \frac{y^2}{(1-y)^2}\log y\right]\right. \\ & \left. -2xy\left[\frac{1}{1-x} + \frac{x}{(1-x)^2}\log x - \frac{1}{1-y} - \frac{y}{(1-y)^2}\log y\right]\right\}\,, \end{aligned} \tag{D.10}$$

$$\begin{aligned} F_{X\text{Box}}(x,y) = {} & -\frac{1}{x-y}\left\{(1 + \frac{xy}{4})\left[\frac{1}{1-x} + \frac{x^2}{(1-x)^2}\log x - \frac{1}{1-y} - \frac{y^2}{(1-y)^2}\log y\right]\right. \\ & \left. -2xy\left[\frac{1}{1-x} + \frac{x}{(1-x)^2}\log x - \frac{1}{1-y} - \frac{y}{(1-y)^2}\log y\right]\right\}\,, \end{aligned} \tag{D.11}$$

$$F_z^{\mu e}(x) = F_z(x) + 2G_z(0,x)\,, \tag{D.12}$$

$$F_{\text{Box}}^{\mu euu}(x) = F_{\text{Box}}(x,0) - F_{\text{Box}}(0,0)\,, \tag{D.13}$$

$$F_{\text{Box}}^{\mu edd}(x) = F_{X\text{Box}}(x,0) - F_{X\text{Box}}(0,0)\,. \tag{D.14}$$

We present in Table D.1 the numerical values of the nuclear form factor $F(-m_\mu^2)$, the effective atomic charge $Z_{\text{eff}}$ and the total muon capture rate $\Gamma_{\text{capt}}$ relative to the nuclei that are of interest for currently running and possible future $\mu - e$ conversion experiments, namely ${}^{48}_{22}\text{Ti}$, ${}^{27}_{13}\text{Al}$, ${}^{197}_{79}\text{Au}$ and ${}^{208}_{82}\text{Pb}$ [235, 251].

| Numerical Values of the Quantities Related to the $\mu - e$ Conversion Rate | | | |
|---|---|---|---|
| Nucleus | $Z_{\rm eff}$ | $F(-m_\mu^2)$ | $\Gamma_{\rm capt}$ $(10^6\,{\rm s}^{-1})$ |
| $^{48}_{22}$Ti | 17.6 | 0.54 | 2.59 |
| $^{27}_{13}$Al | 11.62 | 0.64 | 0.69 |
| $^{197}_{79}$Au | 33.64 | 0.20 | 13.07 |
| $^{208}_{82}$Pb | 34.0 | 0.15 | 13.45 |

**Table D.1.** We report in this table the numerical values of the nuclear form factor $F(-m_\mu^2)$, the effective atomic charge $Z_{\rm eff}$ and the total muon capture rate $\Gamma_{\rm capt}$ relative to the $\mu - e$ conversion rate in $^{48}_{22}$Ti, $^{27}_{13}$Al, $^{197}_{79}$Au and $^{208}_{82}$Pb (see, e.g., Refs. [235, 251]).

## D.3 Branching Ratio of the $\mu \to eee$ Decay

For the $\mu \to eee$ decay branching ratio, we consider the formula reported in Ref. [235] adapted to our scenario of interest, namely the type-I seesaw mechanism of neutrino mass generation with three quasi-degenerate in mass heavy Majorana neutrinos. The expression to leading order in the heavy Majorana neutrino coupling to the SM reads [235, 248]

$$\mathrm{BR}(\mu \to eee) = \frac{\alpha_{em}^2}{64\pi^2 \sin^4\theta_W}\, |C_{\mu 3e}(x)|^2 \left| \sum_{j=1,2,3} (RV)^*_{\mu j}\, (RV)_{ej} \right|^2 , \tag{D.15}$$

where

$$\begin{aligned} |C_{\mu 3e}(x)|^2 = {} & 2\left|0.5\, F_B^{\mu 3e} + F_z^{\mu 3e} - 2\sin^2\theta_W (F_z^{\mu 3e} - F_\gamma)\right|^2 + 4\sin^4\theta_W \left|F_z^{\mu 3e} - F_\gamma\right|^2 \\ & + 16\sin^2\theta_W \left[(F_z^{\mu 3e} + 0.5\, F_B^{\mu 3e}) G_\gamma\right] - 48\sin^4\theta_W \left[(F_z^{\mu 3e} - F_\gamma^{\mu 3e}) G_\gamma\right] \\ & + 32\sin^4\theta_W |G_\gamma|^2 \left[\log\left(m_\mu^2/m_e^2\right) - 11/4\right] , \end{aligned} \tag{D.16}$$

where $F_\gamma(x)$, $G_\gamma(x)$, $F_z(x)$, $G_z(x,y)$, $F_{X\rm Box}(x,y)$ are defined in Eqs. (D.6), (D.7), (D.8), (D.9) and (D.11), respectively, while

$$F_z^{\mu 3e}(x) = F_z(x) + 2G_z(0,x)\,, \tag{D.17}$$

$$F_B^{\mu 3e}(x) = -2[F_{X\rm Box}(0,x) - F_{X\rm Box}(0,0)]\,. \tag{D.18}$$

# Acknowledgements

I had been told that the journey of the Ph.D. student would have been stormy, with several difficulties and obstacles, and full of uncertainties regarding what comes after it. Nobody, however, could have ever told me in advance how the same path would have been during a global pandemic and remotely, for more than one year, in lockdown between the walls of a house. If it were not for the precious guidance of Serguey, The Prof., I would have certainly found myself shipwrecked in this turbulent sea. I am grateful to Serguey who, without losing the patience for my sometimes exaggerated insistence, provided me precious teachings at each step of my insidious path and for constantly motivating me with his infinite energy and passion for the scientific research.

I am also indebted with Piero for his valuable assistance during the last year of my Ph.D. adventure. The work with Piero allowed me to expand my horizon towards the fascinating mystery of dark matter. I have had the luck to share this "dark" deviation with Jin-Wei, who I thank for passing me a bit of his undeniable perseverance and experience. Thanks to Marc as well, who had to endure all our discussions in his office, while taking pictures of the sunset from the balcony.

All the people I have met in Trieste during my four year experience were absolutely relevant. I would like the fellas of my office and those at the opposite side of the corridor to know that the coffees, the lunches, the laughs, the chess matches, the discussions and the few evenings we passed together will always remain in my thoughts. I wish to see you all again somewhere while making the difference in this world. A special thank goes to Oleg, with whom I have established a tighter connection, and to whom I truly wish the best for the future. Thanks also to my roommates, especially Francesco and Riccardo, who brought me back to my University years and made me revive the unique feeling of sharing the same roofs with friends.

The experiences I have had during my adolescence and past ten years moulded me. I will never stop thanking my friends of a lifetime and of the Paduan era for making me what I am today and for the effort we keep investing to strengthen our friendship, so that not even the passing time and the increasing distance could ever erase it. A big thank goes also to my companions Thomas, Daniele and Davide for always being available in keeping the sparkle of Tacita Intesa burning, and to Filippo, the influence of whom will always be present in our music.

I wish to devote special thanks to the components of what I consider to be, without any doubt, my second family. That is, thanks to Giuliana, Stefano, Alberto and their adorable relatives for making me feel, at any minute I spend with them, as if I have always been one of their family. I sense all your affection, and I care about you as much.

I reserve infinite gratitude and love to my marvellous parents and brother. These have been hard times, from any point of view. We laughed and cried, travelled and fought, and realised how strong we actually are. Babbo, you once again proved to us that you really are

the strongest. We thought for the worst, but in the end, your toughness and resilience made through it. Mamma, despite the thousand difficulties you have encountered, you have always landed on your feet and held with nobility your head up, making it immune to the scratches they wanted to cause you. Andrea, I feel your spirit has changed, or, perhaps, it has always been like this and I have just never realised it before, but what makes you truly special for me is indeed the fact that your are dynamic, mutable and unstoppable. Thanks Babbo, Mamma and Andrea for being to me eternal sources of inspiration.

All my work and efforts are dedicated to Veronica, the person I care about the most. Our union is stronger than any bond and more significant than any other commitment. To me, staying with her is true living. Vero, I cannot thank you for being this special, it is your nature, but I can be grateful to the Universe for being so asymmetric and unbalanced in reserving for you most of the gentleness and beauty of the world. I love you.

# References


[1] P. A. M. Dirac, *The quantum theory of the electron*, *Proceedings of the Royal Society of London A* **117** (1928) 610.

[2] C. D. Anderson, *The Positive Electron*, *Physical Review* **43** (1933) 491.

[3] O. Chamberlain, E. Segrè, C. Wiegand and T. Ypsilantis, *Observation of Antiprotons*, *Physical Review* **100** (1955) 947.

[4] B. Cork, G. R. Lambertson, O. Piccioni and W. A. Wenzel, *Antineutrons Produced from Antiprotons in Charge-Exchange Collisions*, *Physical Review* **104** (1956) 1193.

[5] L. Di Lella and C. Rubbia, *The Discovery of the W and Z Particles*, in *60 Years of CERN Experiments and Discoveries*, pp. 137–163, World Scientific, (2015), DOI.

[6] G. Baur, G. Boero, A. Brauksiepe, A. Buzzo, W. Eyrich, R. Geyer et al., *Production of antihydrogen*, *Physics Letters B* **368** (1996) 251.

[7] S. Cherry and M. Dahlbom, *PET: Physics, Instrumentation, and Scanners*, *in Phelps, M.E. (eds) PET, Springer, New York, NY (2006)* (2006) .

[8] M. S. Briggs, V. Connaughton, C. Wilson-Hodge, R. D. Preece, G. J. Fishman, R. M. Kippen et al., *Electron-positron beams from terrestrial lightning observed with Fermi GBM*, *Geophysical Research Letters* **38** (2011) L02808.

[9] Particle Data Group Collaboration, *Review of Particle Physics*, *Progress of Theoretical and Experimental Physics* **2020** (2020) 083C01.

[10] A. Chaikin, *A man on the Moon: The voyages of the Apollo astronauts*. Penguin UK, 2019.

[11] National Aeronautics and Space Administration (NASA), *MARS 2020 Mission Perseverance Rover*, `https://mars.nasa.gov/mars2020/`, last access on September 7, 2022.

[12] European Space Agency (ESA), *The Rosetta Mission from ESA*, `https://www.esa.int/Science_Exploration/Space_Science/Rosetta`, last access on September 7, 2022.

[13] G. Steigman, *Observational Tests of Antimatter Cosmologies*, *Annual Review of Astronomy and Astrophysics* **14** (1976) 339.

[14] R. K. Leane and T. Linden, *First Analysis of Jupiter in Gamma Rays and a New Search for Dark Matter*, 2104.02068.

[15] D. Fargion and M. Khlopov, *Antimatter bounds from antiasteroid annihilation in collisions with planets and Sun*, *Astroparticle Physics* **19** (2003) 441, [hep-ph/0109133].

[16] V. L. Ginzburg and S. I. Syrovatskii, *The Origin of Cosmic Rays*. Elsevier, 2013.

[17] V. Berezinskii, S. Bulanov, V. Ginzburg, V. Dogel and V. Ptuskin, *Astrophysics of Cosmic Rays*. in Ginzburg V L. (ed), Amsterdam: North-Holland, 1990.

[18] T. K. Gaisser, R. Engel and E. Resconi, *Cosmic Rays and Particle Physics*. Cambridge University Press, 2016.

[19] P. Sreekumar, D. L. Bertsch, B. L. Dingus, C. E. Fichtel, R. C. Hartman, S. D. Hunter et al., *Constraints on the cosmic rays in the Small Magellanic Cloud*, *Physical Review Letters* **70** (1993) 127, [astro-ph/9302018].

[20] A. A. Abdo, M. Ackermann, M. Ajello, A. Allafort, W. B. Atwood, L. Baldini et al., *Fermi Large Area Telescope observations of Local Group galaxies: detection of M 31 and search for M 33*, *Astronomy & Astrophysics* **523** (2010) L2, [1012.1952].

[21] W. Baade and F. Zwicky, *Cosmic rays from super-novae*, *Proceedings of the National Academy of Sciences* **20** (1934) 259.

[22] D. Ter Haar, *Cosmogonical Problems and Stellar Energy*, *Reviews of Modern Physics* **22** (1950) 119.

[23] E. Parizot, *Cosmic Ray Origin: Lessons from Ultra-High-Energy Cosmic Rays and the Galactic/Extragalactic Transition*, *Nuclear Physics B - Proceedings Supplements* **256-257** (2014) 197, [1410.2655].

[24] S. Gabici, C. Evoli, D. Gaggero, P. Lipari, P. Mertsch, E. Orlando et al., *The origin of Galactic cosmic rays: Challenges to the standard paradigm*, *International Journal of Modern Physics D* **28** (2019) 1930022, [1903.11584].

[25] AMS Collaboration, *The Alpha Magnetic Spectrometer (AMS) on the international space station: Part II – Results from the first seven years*, *Physics Reports* **894** (2021) 1.

[26] F. Donato, N. Fornengo and P. Salati, *Anti-deuterons as a signature of supersymmetric dark matter*, *Physical Review D* **62** (2000) 043003, [hep-ph/9904481].

[27] R. Duperray, B. Baret, D. Maurin, G. Boudoul, A. Barrau, L. Derome et al., *Flux of light antimatter nuclei near Earth, induced by cosmic rays in the Galaxy and in the atmosphere*, *Physical Review D* **71** (2005) 083013, [astro-ph/0503544].

[28] AMS Collaboration, *Search for anti-helium in cosmic rays*, *Physics Letters B* **461** (1999) 387, [hep-ex/0002048].

[29] P. Chardonnet, J. Orloff and P. Salati, *The Production of antimatter in our galaxy*, *Physics Letters B* **409** (1997) 313, [astro-ph/9705110].

[30] V. Poulin, P. Salati, I. Cholis, M. Kamionkowski and J. Silk, *Where do the AMS-02 antihelium events come from?*, *Physical Review D* **99** (2019) 023016, [1808.08961].

[31] P. von Doetinchem, K. Perez, T. Aramaki, S. Baker, S. Barwick, R. Bird et al., *Cosmic-ray antinuclei as messengers of new physics: status and outlook for the new decade*, *Journal of Cosmology and Astroparticle Physics* **2020** (2020) 035, [2002.04163].

[32] G. Steigman, *When clusters collide: constraints on antimatter on the largest scales*, *Journal of Cosmology and Astroparticle Physics* **2008** (2008) 001, [0808.1122].

[33] L. Canetti, M. Drewes and M. Shaposhnikov, *Matter and Antimatter in the Universe*, *New Journal of Physics* **14** (2012) 095012, [1204.4186].

[34] M. Markevitch, A. H. Gonzalez, L. David, A. Vikhlinin, S. Murray, W. Forman et al., *A Textbook Example of a Bow Shock in the Merging Galaxy Cluster 1E 0657-56*, *The Astrophysical Journal* **567** (2002) L27, [astro-ph/0110468].

[35] A. G. Cohen, A. De Rujula and S. Glashow, *A Matter-Antimatter Universe?*, *The Astrophysical Journal* **495** (1998) 539.

[36] A. A. Penzias and R. W. Wilson, *A Measurement of Excess Antenna Temperature at 4080 Mc/s*, *The Astrophysical Journal* **142** (1965) 419.

[37] R. H. Dicke, P. J. E. Peebles, P. G. Roll and D. T. Wilkinson, *Cosmic Black-Body Radiation*, *The Astrophysical Journal* **142** (1965) 414.

[38] Particle Data Group Collaboration, *Review of Particle Physics, to be published in Progress of Theoretical and Experimental Physics* **2022** (2022) 083C01.

[39] N. Aghanim, Y. Akrami, M. Ashdown, J. Aumont, C. Baccigalupi, M. Ballardini et al., *Planck 2018 results*, *Astronomy & Astrophysics* **641** (2020) A6, [1807.06209].

[40] R. H. Cyburt, B. D. Fields, K. A. Olive and T.-H. Yeh, *Big bang nucleosynthesis: Present status*, *Reviews of Modern Physics* **88** (2016) 015004, [1505.01076].

[41] R. J. Cooke, M. Pettini and C. C. Steidel, *One Percent Determination of the Primordial Deuterium Abundance*, *The Astrophysical Journal* **855** (2018) 102, [1710.11129].

[42] E. W. Kolb and M. S. Turner, *The Early Universe*. CRC press, 2018.

[43] A. H. Guth, *The Inflationary Universe: A Possible Solution to the Horizon and Flatness Problems*, *Physical Review D* **23** (1981) 347.

[44] L. Senatore, *Lectures on Inflation*, in *Theoretical Advanced Study Institute in Elementary Particle Physics: New Frontiers in Fields and Strings*, pp. 447–543, 2017, 1609.00716, DOI.

[45] M. Dine and A. Kusenko, *The Origin of the matter - antimatter asymmetry*, *Reviews of Modern Physics* **76** (2003) 1, [hep-ph/0303065].

[46] D. Bödeker and W. Buchmüller, *Baryogenesis from the weak scale to the grand unification scale*, *Reviews of Modern Physics* **93** (2021) 035004, [2009.07294].

[47] S. Weinberg, *Cosmology*. Oxford University Press, 2008.

[48] C. Caprini and P. Ferreira, *Constraints on the electrical charge asymmetry of the universe*, *Journal of Cosmology and Astroparticle Physics* **2005** (2005) 006, [hep-ph/0310066].

[49] A. D. Dolgov, S. H. Hansen, S. Pastor, S. T. Petcov, G. G. Raffelt and D. V. Semikoz, *Cosmological bounds on neutrino degeneracy improved by flavor oscillations*, *Nucl. Phys. B* **632** (2002) 363, [hep-ph/0201287].

[50] G. Mangano, G. Miele, S. Pastor, O. Pisanti and S. Sarikas, *Updated BBN bounds on the cosmological lepton asymmetry for non-zero $\theta_1 3$*, *Physics Letters B* **708** (2012) 1, [1110.4335].

[51] I. M. Oldengott and D. J. Schwarz, *Improved constraints on lepton asymmetry from the cosmic microwave background*, *Europhysics Letters* **119** (2017) 29001, [1706.01705].

[52] A.-K. Burns, T. M. P. Tait and M. Valli, *Indications for a Nonzero Lepton Asymmetry in the Early Universe*, 2206.00693.

[53] A. J. Long, C. Lunardini and E. Sabancilar, *Detecting non-relativistic cosmic neutrinos by capture on tritium: phenomenology and physics potential*, *Journal of Cosmology and Astroparticle Physics* **08** (2014) 038, [1405.7654].

[54] A. D. Sakharov, *Violation of CP invariance, C asymmetry, and baryon asymmetry of the universe*, *Soviet Physics Uspekhi* **5** (1991) 34.

[55] L. Covi, E. Roulet and F. Vissani, *CP violating decays in leptogenesis scenarios*, *Physics Letters B* **384** (1996) 169, [hep-ph/9605319].

[56] G. Luders, *Proof of the TCP theorem*, *Annals of Physics* **2** (1957) 1.

[57] S. Davidson, E. Nardi and Y. Nir, *Leptogenesis*, *Physics Reports* **466** (2008) 105, [0802.2962].

[58] G. 't Hooft, *Symmetry Breaking Through Bell-Jackiw Anomalies*, *Physical Review Letters* **37** (1976) 8.

[59] S. R. Coleman, *The Uses of Instantons*, *Contribution to: 15th Erice School of Subnuclear Physics: The Why's of Subnuclear Physics* **15** (1979) 805.

[60] M. Trodden, *Electroweak baryogenesis*, *Reviews of Modern Physics* **71** (1999) 1463, [hep-ph/9803479].

[61] F. R. Klinkhamer and N. S. Manton, *A saddle-point solution in the Weinberg-Salam theory*, *Physical Review D* **30** (1984) 2212.

[62] M. D'Onofrio, K. Rummukainen and A. Tranberg, *Sphaleron Rate in the Minimal Standard Model*, *Physical Review Letters* **113** (2014) 141602, [1404.3565].

[63] D. Bödeker and D. Schröder, *Equilibration of right-handed electrons*, *Journal of Cosmology and Astroparticle Physics* **05** (2019) 010, [1902.07220].

[64] J. A. Harvey and M. S. Turner, *Cosmological baryon and lepton number in the presence of electroweak fermion number violation*, *Physical Review D* **42** (1990) 3344.

[65] S. Y. Khlebnikov and M. E. Shaposhnikov, *The Statistical Theory of Anomalous Fermion Number Nonconservation*, *Nuclear Physics B* **308** (1988) 885.

[66] M. Laine and M. E. Shaposhnikov, *A Remark on sphaleron erasure of baryon asymmetry*, *Physical Review D* **61** (2000) 117302, [hep-ph/9911473].

[67] V. A. Kuzmin, V. A. Rubakov and M. E. Shaposhnikov, *On the Anomalous Electroweak Baryon Number Nonconservation in the Early Universe*, *Physics Letters B* **155** (1985) 36.

[68] N. Cabibbo, *Unitary Symmetry and Leptonic Decays*, *Physical Review Letters* **10** (1963) 531.

[69] M. Kobayashi and T. Maskawa, *CP-Violation in the Renormalizable Theory of Weak Interaction*, *Progress of Theoretical Physics* **49** (1973) 652.

[70] C. Jarlskog, *Commutator of the Quark Mass Matrices in the Standard Electroweak Model and a Measure of Maximal CP Nonconservation*, *Physical Review Letters* **55** (1985) 1039.

[71] C. Jarlskog, *A Basis Independent Formulation of the Connection Between Quark Mass Matrices, CP Violation and Experiment*, *Zeitschrift für Physik C* **29** (1985) 491.

[72] M. E. Shaposhnikov, *Baryon Asymmetry of the Universe in Standard Electroweak Theory*, *Nuclear Physics B* **287** (1987) 757.

[73] M. B. Gavela, M. Lozano, J. Orloff and O. Pene, *Standard model CP violation and baryon asymmetry (I). Zero temperature*, *Nuclear Physics B* **430** (1994) 345, [hep-ph/9406288].

[74] M. B. Gavela, P. Hernandez, J. Orloff, O. Pene and C. Quimbay, *Standard model CP violation and baryon asymmetry (II). Finite temperature*, *Nuclear Physics B* **430** (1994) 382, [hep-ph/9406289].

[75] CMS Collaboration, *Measurements of properties of the Higgs boson decaying to a W boson pair in pp collisions at* $\sqrt{s} = 13$ *TeV*, *Physics Letters B* **791** (2019) 96, [1806.05246].

[76] ATLAS Collaboration, *Measurement of the Higgs boson mass in the* $H \to ZZ^* \to 4\ell$ *and* $H \to \gamma\gamma$ *channels with* $\sqrt{s} = 13$ *TeV pp collisions using the ATLAS detector*, *Physics Letters B* **784** (2018) 345, [1806.00242].

[77] K. Kajantie, M. Laine, K. Rummukainen and M. E. Shaposhnikov, *Is there a hot electroweak phase transition at* $m_H \gtrsim m_W$*?*, *Physical Review Letters* **77** (1996) 2887, [hep-ph/9605288].

[78] K. Rummukainen, M. Tsypin, K. Kajantie, M. Laine and M. E. Shaposhnikov, *The Universality class of the electroweak theory*, *Nuclear Physics B* **532** (1998) 283, [hep-lat/9805013].

[79] F. Csikor, Z. Fodor and J. Heitger, *Endpoint of the hot electroweak phase transition*, *Physical Review Letters* **82** (1999) 21, [hep-ph/9809291].

[80] R. N. Mohapatra et al., *Theory of neutrinos: A White paper*, *Reports on Progress in Physics* **70** (2007) 1757, [hep-ph/0510213].

[81] G. Bertone, D. Hooper and J. Silk, *Particle dark matter: Evidence, candidates and constraints*, *Physics Reports* **405** (2005) 279, [hep-ph/0404175].

[82] P. J. E. Peebles and B. Ratra, *The Cosmological Constant and Dark Energy*, *Reviews of Modern Physics* **75** (2003) 559, [astro-ph/0207347].

[83] S. Dimopoulos and L. Susskind, *Baryon Asymmetry in the Very Early Universe*, *Physics Letters B* **81** (1979) 416.

[84] M. Yoshimura, *Unified Gauge Theories and the Baryon Number of the Universe*, *Physical Review Letters* **41** (1978) 281.

[85] D. Toussaint, S. B. Treiman, F. Wilczek and A. Zee, *Matter - Antimatter Accounting, Thermodynamics, and Black Hole Radiation*, *Physical Review D* **19** (1979) 1036.

[86] S. Weinberg, *Cosmological Production of Baryons*, *Physical Review Letters* **42** (1979) 850.

[87] D. V. Nanopoulos and S. Weinberg, *Mechanisms for Cosmological Baryon Production*, *Physical Review D* **20** (1979) 2484.

[88] D. Croon, T. E. Gonzalo, L. Graf, N. Košnik and G. White, *GUT Physics in the era of the LHC*, *Frontiers in Physics* **7** (2019) 76, [1903.04977].

[89] P. Minkowski, $\mu \to e\gamma$ *at a Rate of One Out of* $10^9$ *Muon Decays?*, *Phys. Lett.* **B67** (1977) 421.

[90] T. Yanagida, *Horizontal Symmetry and Masses of Neutrinos*, *Progress of Theoretical Physics* **64** (1980) 1103.

[91] M. Gell-Mann, P. Ramond and R. Slansky, *Complex Spinors and Unified Theories*, *Conference Proceedings C* **790927** (1979) 315, [1306.4669].

[92] S. Glashow, *The Future of Elementary Particle Physics*, *NATO Advanced Study Institutes Series B* **61** (1980) 687.

[93] R. N. Mohapatra and G. Senjanovic, *Neutrino Mass and Spontaneous Parity Violation*, *Physical Review Letters* **44** (1980) 912.

[94] M. Fukugita and T. Yanagida, *Baryogenesis without grand unification*, *Physics Letters B* **174** (1986) 45.

[95] M. A. Luty, *Baryogenesis via leptogenesis*, *Physical Review D* **45** (1992) 455.

[96] W. Buchmüller, R. D. Peccei and T. Yanagida, *Leptogenesis as the Origin of Matter*, *Annual Review of Nuclear and Particle Science* **55** (2005) 311, [hep-ph/0502169].

[97] W. Buchmüller, P. Di Bari and M. Plümacher, *Leptogenesis for pedestrians*, *Annals of Physics* **315** (2005) 305, [hep-ph/0401240].

[98] A. Pilaftsis, *CP violation and baryogenesis due to heavy Majorana neutrinos*, *Physical Review D* **56** (1997) 5431, [hep-ph/9707235].

[99] A. Pilaftsis, *Heavy Majorana neutrinos and baryogenesis*, *International Journal of Modern Physics A* **14** (1999) 1811, [hep-ph/9812256].

[100] A. Pilaftsis and T. E. J. Underwood, *Resonant Leptogenesis*, *Nulcear Physics B* **692** (2004) 303, [hep-ph/0309342].

[101] E. K. Akhmedov, V. A. Rubakov and A. Yu. Smirnov, *Baryogenesis via Neutrino Oscillations*, *Physical Review Letters* **81** (1998) 1359, [hep-ph/9803255].

[102] T. Asaka and M. Shaposhnikov, *The $\nu$MSM, Dark Matter and Baryon Asymmetry of the Universe*, *Physics Letters B* **620** (2005) 17, [hep-ph/0505013].

[103] A. Davidson, *$B - L$ as the fourth color within an $\mathrm{SU}(2)_L \times \mathrm{U}(1)_R \times \mathrm{U}(1)$ model*, *Physical Review D* **20** (1979) 776.

[104] R. E. Marshak and R. N. Mohapatra, *Quark - Lepton Symmetry and B-L as the U(1) Generator of the Electroweak Symmetry Group*, *Physics Letters B* **91** (1980) 222.

[105] R. N. Mohapatra and R. E. Marshak, *Local B-L Symmetry of Electroweak Interactions, Majorana Neutrinos and Neutron Oscillations*, *Physical Review Letters* **44** (1980) 1316.

[106] W. Buchmüller, V. Domcke, K. Kamada and K. Schmitz, *The Gravitational Wave Spectrum from Cosmological $B - L$ Breaking*, *Journal of Cosmology and Astroparticle Physics* **10** (2013) 003, [1305.3392].

[107] W. Buchmüller, V. Domcke, H. Murayama and K. Schmitz, *Probing the scale of grand unification with gravitational waves*, *Physics Letters B* **809** (2020) 135764, [1912.03695].

[108] S. F. King, S. Pascoli, J. Turner and Y.-L. Zhou, *Confronting SO(10) GUTs with proton decay and gravitational waves*, *Journal of High Energy Physics* **10** (2021) 225, [2106.15634].

[109] J. A. Dror, T. Hiramatsu, K. Kohri, H. Murayama and G. White, *Testing the Seesaw Mechanism and Leptogenesis with Gravitational Waves*, *Physical Review Letters* **124** (2020) 041804, [1908.03227].

[110] S. Blasi, V. Brdar and K. Schmitz, *Fingerprint of low-scale leptogenesis in the primordial gravitational-wave spectrum*, *Physical Review Research* **2** (2020) 043321, [2004.02889].

[111] A. G. Cohen, D. B. Kaplan and A. E. Nelson, *Progress in electroweak baryogenesis*, *Annual Review of Nuclear and Particle Science* **43** (1993) 27, [hep-ph/9302210].

[112] D. E. Morrissey and M. J. Ramsey-Musolf, *Electroweak baryogenesis*, *New Journal of Physics* **14** (2012) 125003, [1206.2942].

[113] C. Caprini et al., *Detecting gravitational waves from cosmological phase transitions with LISA: an update*, *Journal of Cosmology and Astroparticle Physics* **03** (2020) 024, [1910.13125].

[114] J. M. Cline, *Is electroweak baryogenesis dead?*, *Philosophical Transactions of the Royal Society A* **376** (2018) 20170116, [1704.08911].

[115] ACME Collaboration, *Order of Magnitude Smaller Limit on the Electric Dipole Moment of the Electron*, *Science* **343**, (2014) 269, [1310.7534].

[116] ACME Collaboration, *Improved limit on the electric dipole moment of the electron*, *Nature* **562** (2018) 355.

[117] I. Affleck and M. Dine, *A New Mechanism for Baryogenesis*, *Nuclear Physics B* **249** (1985) 361.

[118] R. Allahverdi and A. Mazumdar, *A mini review on Affleck-Dine baryogenesis*, *New Journal of Physics* **14** (2012) 125013.

[119] K. Harigaya, *Nambu-Goldstone Affleck-Dine Baryogenesis*, *Journal of High Energy Physics* **08** (2019) 085, [1906.05286].

[120] R. T. Co and K. Harigaya, *Axiogenesis*, *Physical Review Letters* **124** (2020) 111602, [1910.02080].

[121] G. Lazarides and Q. Shafi, *Origin of matter in the inflationary cosmology*, *Physics Letters B* **258** (1991) 305.

[122] T. Asaka, K. Hamaguchi, M. Kawasaki and T. Yanagida, *Leptogenesis in inflaton decay*, *Physics Letters B* **464** (1999) 12, [hep-ph/9906366].

[123] K. Nakayama, S. Saito, Y. Suwa and J. Yokoyama, *Space laser interferometers can determine the thermal history of the early Universe*, *Physical Review D* **77** (2008) 124001, [0802.2452].

[124] K. Nakamura and S.T. Petcov, in M. Tanabashi et al. (Particle Data Group Collaboration), *Review of Particle Physics*, *Physical Review D* **98** (2018) 030001.

[125] B. Pontecorvo, *Neutrino Experiments and the Problem of Conservation of Leptonic Charge*, *Soviet Journal of Experimental and Theoretical Physics* **26** (1968) 984.

[126] B. Pontecorvo, *Mesonium and Antimesonium*, *Soviet Journal of Experimental and Theoretical Physics* **6** (1958) 429.

[127] B. Pontecorvo, *Inverse beta processes and nonconservation of lepton charge*, *Zh. Eksp. Teor. Fiz.* **34** (1957) 247.

[128] S. M. Bilenky, J. Hosek and S. T. Petcov, *On Oscillations of Neutrinos with Dirac and Majorana Masses*, *Physics Letters B* **94** (1980) 495.

[129] E. Molinaro and S. T. Petcov, *The Interplay Between the "Low" and "High" Energy CP-Violation in Leptogenesis*, *The European Physical Journal C* **61** (2009) 93, [0803.4120].

[130] F. Capozzi, E. Di Valentino, E. Lisi, A. Marrone, A. Melchiorri and A. Palazzo, *Addendum to "Global constraints on absolute neutrino masses and their ordering"*, *Physical Review D* **101** (2020) 116013.

[131] I. Esteban, M. Gonzalez-Garcia, M. Maltoni, T. Schwetz and A. Zhou, *The fate of hints: updated global analysis of three-flavor neutrino oscillations*, *Journal of High Energy Physics* **09** (2020) 178, [2007.14792].

[132] P. Langacker, S. T. Petcov, G. Steigman and S. Toshev, *On the Mikheev-Smirnov-Wolfenstein (MSW) Mechanism of Amplification of Neutrino Oscillations in Matter*, *Nuclear Physics B* **282** (1987) 589.

[133] T2K Collaboration, *Constraint on the matter–antimatter symmetry-violating phase in neutrino oscillations*, *Nature* **580** (2020) 339, [1910.03887].

[134] A. Himmel for the NO$\nu$A Collaboration, *New Oscillation Results from the NOvA Experiment*, *Talk given at the XXIX International Conference on Neutrino Physics and Astrophysics*.

[135] N. Cabibbo, *Time Reversal Violation in Neutrino Oscillation*, *Physics Letters B* **72** (1978) 333.

[136] V. D. Barger, K. Whisnant and R. J. N. Phillips, *CP Violation in Three Neutrino Oscillations*, *Physical Review Letters* **45** (1980) 2084.

[137] P. I. Krastev and S. T. Petcov, *Resonance Amplification and T-Violation Effects in Three Neutrino Oscillations in the Earth*, *Physics Letters B* **205** (1988) 84.

[138] S. M. Bilenky and S. T. Petcov, *Massive Neutrinos and Neutrino Oscillations*, *Reviews of Modern Physics* **59** (1987) 671.

[139] S. M. Bilenky, S. Pascoli and S. T. Petcov, *Majorana neutrinos, neutrino mass spectrum, CP violation and neutrinoless double beta decay. 1. The Three neutrino mixing case*, *Physical Review D* **64** (2001) 053010, [hep-ph/0102265].

[140] S.T. Petcov, *Neutrinoless double beta decay searches: theory and motivation*, *Talk given at the XXIX International Conference on Neutrino Physics and Astrophysics*.

[141] S. Pascoli, S. T. Petcov and A. Riotto, *Leptogenesis and low energy CP-violation in neutrino physics*, *Nuclear Physics B* **774** (2007) 1, [hep-ph/0611338].

[142] S. Pascoli, S. T. Petcov and A. Riotto, *Connecting low energy leptonic CP-violation to leptogenesis*, *Physical Review D* **75** (2007) 083511, [hep-ph/0609125].

[143] K. Moffat, S. Pascoli, S. T. Petcov and J. Turner, *Leptogenesis from Low Energy CP Violation*, *Journal of High Energy Physics* **03** (2019) 034, [1809.08251].

[144] KamLAND-Zen Collaboration, *Search for Majorana Neutrinos near the Inverted Mass Hierarchy Region with KamLAND-Zen*, *Physical Review Letters* **117** (2016) 082503, [1605.02889].

[145] GERDA Collaboration, *Final Results of GERDA on the Search for Neutrinoless Double-$\beta$ Decay*, *Physical Review Letters* **125** (2020) 252502, [2009.06079].

[146] J. T. Penedo and S. T. Petcov, *The $10^{-3}$ eV frontier in neutrinoless double beta decay*, *Physics Letters B* **786** (2018) 410, [1806.03203].

[147] KATRIN Collaboration, *Improved Upper Limit on the Neutrino Mass from a Direct Kinematic Method by KATRIN*, *Physical Review Letters* **123** (2019) 221802, [1909.06048].

[148] KATRIN Collaboration, *Direct neutrino-mass measurement with sub-electronvolt sensitivity*, Nature Physics, **18** (2022) 160–166, [2105.08533].

[149] J. Lesgourgues and L. Verde in P. A. Zyla et al. (Particle Data Group), *Neutrinos in Cosmology (Review of Particle Physics)*, *Progress of Theoretical and Experimental Physics* **2020** (2020) 083C01.

[150] A. Ibarra, E. Molinaro and S. T. Petcov, *TeV Scale See-Saw Mechanisms of Neutrino Mass Generation, the Majorana Nature of the Heavy Singlet Neutrinos and $(\beta\beta)_{0\nu}$-Decay*, *Journal of High Energy Physics* **09** (2010) 108, [1007.2378].

[151] K. Moffat, S. Pascoli, S. T. Petcov, H. Schulz and J. Turner, *Three-flavored nonresonant leptogenesis at intermediate scales*, *Physical Review D* **98** (2018) 015036, [1804.05066].

[152] J. Lopez-Pavon, E. Molinaro and S. T. Petcov, *Radiative Corrections to Light Neutrino Masses in Low Scale Type I Seesaw Scenarios and Neutrinoless Double Beta Decay*, *Journal of High Energy Physics* **11** (2015) 030, [1506.05296].

[153] A. Pilaftsis, *Radiatively induced neutrino masses and large Higgs-neutrino couplings in the Standard Model with Majorana fields*, *Zeitschrift für Physik C* **55** (1992) 275–282, [hep-ph/9901206].

[154] D. Aristizabal Sierra and C. E. Yaguna, *On the importance of the 1-loop finite corrections to seesaw neutrino masses*, *Journal of High Energy Physics* **2011** (2011) 13, [1106.3587].

[155] J. Lopez-Pavon, S. Pascoli and C.-F. Wong, *Can heavy neutrinos dominate neutrinoless double beta decay?*, *Physical Review D* **87** (2013) 093007, [1209.5342].

[156] W. Grimus and L. Lavoura, *One-loop corrections to the seesaw mechanism in the multi-Higgs-doublet Standard Model*, *Physics Letters B* **546** (2002) 86–95, [hep-ph/0207229].

[157] E. Fernandez-Martinez, J. Hernandez-Garcia, J. Lopez-Pavon and M. Lucente, *Loop level constraints on Seesaw neutrino mixing*, *Journal of High Energy Physics* **10** (2015) 130, [1508.03051].

[158] M. Blennow, P. Coloma, E. Fernandez-Martinez, J. Hernandez-Garcia and J. Lopez-Pavon, *Non-Unitarity, sterile neutrinos, and Non-Standard neutrino Interactions*, *Journal of High Energy Physics* **04** (2017) 153, [1609.08637].

[159] J. A. Casas and A. Ibarra, *Oscillating neutrinos and $\mu \to e, \gamma$*, *Nuclear Physics B* **618** (2001) 171, [hep-ph/0103065].

[160] M. Drewes, Y. Georis and J. Klarić, *Mapping the Viable Parameter Space for Testable Leptogenesis*, *Physical Review Letters* **128** (2022) 051801, [2106.16226].

[161] J. Klarić, M. Shaposhnikov and I. Timiryasov, *Uniting Low-Scale Leptogenesis Mechanisms*, *Physical Review Letters* **127** (2021) 111802, [2008.13771].

[162] J. Klarić, M. Shaposhnikov and I. Timiryasov, *Reconciling resonant leptogenesis and baryogenesis via neutrino oscillations*, *Physical Review D* **104** (2021) 055010, [2103.16545].

[163] K. A. U. Calderón, I. Timiryasov and O. Ruchayskiy, *Improved constraints and the prospects of detecting TeV to PeV scale Heavy Neutral Leptons*, 2206.04540.

[164] G. F. Giudice, A. Notari, M. Raidal, A. Riotto and A. Strumia, *Towards a complete theory of thermal leptogenesis in the SM and MSSM*, *Nuclear Physics B* **685** (2004) 89, [hep-ph/0310123].

[165] S. Davidson and A. Ibarra, *A Lower bound on the right-handed neutrino mass from leptogenesis*, *Physics Letters B* **535** (2002) 25, [hep-ph/0202239].

[166] E. Nardi, Y. Nir, E. Roulet and J. Racker, *The Importance of flavor in leptogenesis*, *Journal of High Energy Physics* **01** (2006) 164, [hep-ph/0601084].

[167] A. Abada, S. Davidson, F.-X. Josse-Michaux, M. Losada and A. Riotto, *Flavour issues in leptogenesis*, *Journal of Cosmology and Astroparticle Physics* **0604** (2006) 004, [hep-ph/0601083].

[168] A. Abada, S. Davidson, A. Ibarra, F. X. Josse-Michaux, M. Losada and A. Riotto, *Flavour Matters in Leptogenesis*, *Journal of High Energy Physics* **09** (2006) 010, [hep-ph/0605281].

[169] P. S. B. Dev, P. Di Bari, B. Garbrecht, S. Lavignac, P. Millington and D. Teresi, *Flavor effects in leptogenesis*, *International Journal of Modern Physics A* **33** (2018) 1842001, [1711.02861].

[170] R. Barbieri, P. Creminelli, A. Strumia and N. Tetradis, *Baryogenesis through leptogenesis*, *Nuclear Physics B* **575** (2000) 61, [hep-ph/9911315].

[171] H. B. Nielsen and Y. Takanishi, *Baryogenesis via lepton number violation and family replicated gauge group*, *Nuclear Physics B* **636** (2002) 305, [hep-ph/0204027].

[172] T. Endoh, T. Morozumi and Z.-h. Xiong, *Primordial lepton family asymmetries in seesaw model*, *Progress of Theoretical Physics* **111** (2004) 123, [hep-ph/0308276].

[173] S. Blanchet, P. D. Bari, D. A. Jones and L. Marzola, *Leptogenesis with heavy neutrino flavours: from density matrix to boltzmann equations*, *Journal of Cosmology and Astroparticle Physics* **2013** (2013) 041, [1112.4528].

[174] S. Blanchet, P. D. Bari and G. G. Raffelt, *Quantum Zeno effect and the impact of flavour in leptogenesis*, *Journal of Cosmology and Astroparticle Physics* **2007** (2007) 012, [hep-ph/0611337].

[175] I. Brivio, K. Moffat, S. Pascoli, S. Petcov and J. Turner, *Leptogenesis in the Neutrino Option*, *Journal of High Energy Physics* **10** (2019) 059, [1905.12642].

[176] L. Covi and E. Roulet, *Baryogenesis from mixed particle decays*, *Physics Letters B* **399** (1997) 113, [hep-ph/9611425].

[177] W. Buchmüller and M. Plümacher, *CP asymmetry in Majorana neutrino decays*, *Physics Letters B* **431** (1998) 354, [hep-ph/9710460].

[178] A. D. Simone and A. Riotto, *On the impact of flavour oscillations in leptogenesis*, *Journal of Cosmology and Astroparticle Physics* **2007** (2007) 005, [hep-ph/0611357].

[179] S. Biondini, D. Bödeker, N. Brambilla, M. Garny, J. Ghiglieri, A. Hohenegger et al., *Status of rates and rate equations for thermal leptogenesis*, *International Journal of Modern Physics A* **33** (2018) 1842004, [1711.02864].

[180] W. Buchmüller, P. Di Bari and M. Plümacher, *A bound on neutrino masses from baryogenesis*, *Physics Letters B* **547** (2002) 128, [hep-ph/0611357].

[181] W. Buchmüller, P. Di Bari, P. and M. Plümacher, *The Neutrino mass window for baryogenesis*, *Nuclear Physics B* **665** (2003) 445, [hep-ph/0302092].

[182] J. Liu and G. Segre, *Reexamination of generation of baryon and lepton number asymmetries by heavy particle decay*, *Physical Review D* **48** (1993) 4609, [hep-ph/9304241].

[183] M. Flanz, E. A. Paschos and U. Sarkar, *Baryogenesis from a lepton asymmetric universe*, *Physics Letters B* **345** (1995) 248, [hep-ph/9411366].

[184] M. Flanz, E. A. Paschos, U. Sarkar and J. Weiss, *Baryogenesis through mixing of heavy Majorana neutrinos*, *Physics Letters B* **389** (1996) 693, [hep-ph/9607310].

[185] L. Covi, E. Roulet and F. Vissani, *CP violating decays in leptogenesis scenarios*, *Physics Letters B* **384** (1996) 169, [hep-ph/9605319].

[186] J. Kersten and A. Yu. Smirnov, *Right-Handed Neutrinos at CERN LHC and the Mechanism of Neutrino Mass Generation*, *Physical Review D* **76** (2007) 073005, [0705.3221].

[187] L. Wolfenstein, *Different Varieties of Massive Dirac Neutrinos*, *Nulcear Physics B* **186** (1981) 147.

[188] S. T. Petcov, *On Pseudo-Dirac Neutrinos, Neutrino Oscillations and Neutrinoless Double $\beta$-Decay*, *Physics Letters B* **110** (1982) 245.

[189] T. Hambye and D. Teresi, *Higgs Doublet Decay as the Origin of the Baryon Asymmetry*, *Physical Review Letters* **117** (2016) 091801, [1606.00017].

[190] T. Hambye and D. Teresi, *Baryogenesis from L-violating Higgs-doublet decay in the density-matrix formalism*, *Physical Review D* **96** (2017) , [1705.00016].

[191] S. Blanchet, P. Di Bari, D. A. Jones and L. Marzola, *Leptogenesis with heavy neutrino flavours: from density matrix to Boltzmann equations*, *Journal of Cosmology and Astroparticle Physics* **1301** (2013) 041, [1112.4528].

[192] P. S. Bhupal Dev, P. Millington, A. Pilaftsis and D. Teresi, *Flavour Covariant Transport Equations: an Application to Resonant Leptogenesis*, *Nuclear Physics B* **886** (2014) 569, [1404.1003].

[193] P. S. Bhupal Dev, P. Millington, A. Pilaftsis and D. Teresi, *Kadanoff-Baym approach to flavour mixing and oscillations in resonant leptogenesis*, *Nuclear Physics B* **891** (2015) 128, [1410.6434].

[194] B. Garbrecht and M. Herranen, *Effective Theory of Resonant Leptogenesis in the Closed-Time-Path Approach*, *Nuclear Physics B* **861** (2012) 17, [1112.5954].

[195] P. Millington, private communication.

[196] D. Besak and D. Bödeker, *Thermal production of ultrarelativistic right-handed neutrinos: complete leading-order results*, *Journal of Cosmology and Astroparticle Physics* **2012** (2012) 029, [1202.1288].

[197] D. Bödeker and M. Laine, *Kubo relations and radiative corrections for lepton number washout*, *Journal of Cosmology and Astroparticle Physics* **2014** (2014) 041, [1403.2755].

[198] G. Bambhaniya, P. S. Bhupal Dev, S. Goswami, S. Khan and W. Rodejohann, *Naturalness, Vacuum Stability and Leptogenesis in the Minimal Seesaw Model*, *Physical Review* **D95** (2017) 095016, [1611.03827].

[199] T. Frossard, M. Garny, A. Hohenegger, A. Kartavtsev and D. Mitrouskas, *Systematic approach to thermal leptogenesis*, *Physical Review D* **87** (2013) 085009, [1211.2140].

[200] A. Anisimov, D. Besak and D. Bödeker, *Thermal production of relativistic Majorana neutrinos: strong enhancement by multiple soft scattering*, *Journal of Cosmology and Astroparticle Physics* **03** (2011) 042, [1012.3784].

[201] M. Quiros, *Finite temperature field theory and phase transitions*, in *ICTP Summer School in High-Energy Physics and Cosmology*, pp. 187–259, 1, 1999, hep-ph/9901312.

[202] E. Senaha, *Symmetry Restoration and Breaking at Finite Temperature: An Introductory Review*, *Symmetry* **12** (2020) 733.

[203] J. Ghiglieri and M. Laine, *Neutrino dynamics below the electroweak crossover*, *Journal of Cosmology and Astroparticle Physics* **07** (2016) 015, [1605.07720].

[204] M. Shaposhnikov, *A possible symmetry of the $\nu$MSM*, *Nuclear Physics B* **763** (2007) 49, [hep-ph/0605047].

[205] T. Asaka, S. Eijima and H. Ishida, *Kinetic equations for baryogenesis via sterile neutrino oscillation*, *Journal of Cosmology and Astroparticle Physics* **02** (2012) 021, [1112.5565].

[206] L. Canetti, M. Drewes, T. Frossard and M. Shaposhnikov, *Dark matter, baryogenesis and neutrino oscillations from right-handed neutrinos*, *Physical Review D* **87** (2013) 093006, [1208.4607].

[207] B. Shuve and I. Yavin, *Baryogenesis through Neutrino Oscillations: A Unified Perspective*, *Physical Review D* **89** (2014) 075014, [1401.2459].

[208] P. Hernández, M. Kekic, J. López-Pavón, J. Racker and N. Rius, *Leptogenesis in GeV scale seesaw models*, *Journal of High Energy Physics* **10** (2015) 067, [1508.03676].

[209] M. Drewes, B. Garbrecht, D. Gueter and J. Klarić, *Leptogenesis from Oscillations of Heavy Neutrinos with Large Mixing Angles*, *Journal of High Energy Physics* **12** (2016) 150, [1606.06690].

[210] P. Hernández, M. Kekic, J. López-Pavón, J. Racker and J. Salvado, *Testable Baryogenesis in Seesaw Models*, *Journal of High Energy Physics* **08** (2016) 157, [1606.06719].

[211] T. Asaka, S. Eijima, H. Ishida, K. Minogawa and T. Yoshii, *Initial condition for baryogenesis via neutrino oscillation*, *Physical Review D* **96** (2017) 083010, [1704.02692].

[212] J. Ghiglieri and M. Laine, *GeV-scale hot sterile neutrino oscillations: a derivation of evolution equations*, *Journal of High Energy Physics* **05** (2017) 132, [1703.06087].

[213] M. Drewes, B. Garbrecht, P. Hernández, M. Kekic, J. Lopez-Pavon, J. Racker et al., *ARS leptogenesis*, *International Journal of Modern Physics A* **33** (2018) 1842002, [1711.02862].

[214] B. Dev, M. Garny, J. Klaric, P. Millington and D. Teresi, *Resonant enhancement in leptogenesis*, *International Journal of Modern Physics A* **33** (2018) 1842003, [1711.02863].

[215] B. Garbrecht, *Why is there more matter than antimatter? Calculational methods for leptogenesis and electroweak baryogenesis*, *Progress in Particle and Nuclear Physics* **110** (2020) 103727, [1812.02651].

[216] J. Ghiglieri and M. Laine, *Precision study of GeV-scale resonant leptogenesis*, *Journal of High Energy Physics* **02** (2019) 014, [1811.01971].

[217] C. S. Fong and J. Racker, *On fast CP violating interactions in leptogenesis*, *Journal of Cosmology and Astroparticle Physics* **07** (2010) 001, [1004.2546].

[218] Z.-Z. Xing and D. Zhang, *A direct link between unflavored leptogenesis and low-energy CP violation via the one-loop quantum corrections*, *Journal of High Energy Physics* **04** (2020) 179, [2003.00480].

[219] S. Alekhin et al., *A facility to Search for Hidden Particles at the CERN SPS: the SHiP physics case*, *Reports on Progress in Physics* **79** (2016) 124201, [1504.04855].

[220] I. Boiarska, K. Bondarenko, A. Boyarsky, S. Eijima, M. Ovchynnikov, O. Ruchayskiy et al., *Probing baryon asymmetry of the Universe at LHC and SHiP*, 1902.04535.

[221] FCC Collaboration, *FCC-ee: The Lepton Collider: Future Circular Collider Conceptual Design Report Volume 2*, *The European Physical Journal Special Topics* **228** (2019) 261.

[222] FCC Collaboration, *FCC Physics Opportunities: Future Circular Collider Conceptual Design Report Volume 1*, *The European Physical Journal C* **79** (2019) 474.

[223] A. Abada, G. Arcadi, V. Domcke, M. Drewes, J. Klaric and M. Lucente, *Low-scale leptogenesis with three heavy neutrinos*, *JHEP* **01** (2019) 164, [1810.12463].

[224] A. Atre, T. Han, S. Pascoli and B. Zhang, *The Search for Heavy Majorana Neutrinos*, *Journal of High Energy Physics* **05** (2009) 030, [0901.3589].

[225] F. F. Deppisch, P. S. Bhupal Dev and A. Pilaftsis, *Neutrinos and Collider Physics*, *New Journal of Physics* **17** (2015) 075019, [1502.06541].

[226] Y. Cai, T. Han, T. Li and R. Ruiz, *Lepton Number Violation: Seesaw Models and Their Collider Tests*, *Frontiers in Physics* **6** (2018) 40, [1711.02180].

[227] P. Agrawal et al., *Feebly-interacting particles: FIPs 2020 workshop report*, *The European Physical Journal C* **81** (2021) 1015, [2102.12143].

[228] A. M. Abdullahi et al., *The Present and Future Status of Heavy Neutral Leptons*, in *2022 Snowmass Summer Study*, 3, 2022, 2203.08039.

[229] S. Antusch, E. Cazzato and O. Fischer, *Sterile neutrino searches at future $e^-e^+$, $pp$, and $e^-p$ colliders*, *International Journal of Modern Physics A* **32** (2017) 1750078, [1612.02728].

[230] CEPC Study Group Collaboration, *CEPC Conceptual Design Report: Volume 2 - Physics & Detector*, 1811.10545.

[231] F. F. Deppisch, J. Harz and M. Hirsch, *Falsifying High-Scale Leptogenesis at the LHC*, *Physical Review Letters* **112** (2014) 221601, [1312.4447].

[232] F. F. Deppisch, L. Graf, J. Harz and W.-C. Huang, *Neutrinoless Double Beta Decay and the Baryon Asymmetry of the Universe*, *Physical Review D* **98** (2018) 055029, [1711.10432].

[233] A. Blondel and P. Janot, *FCC-ee overview: new opportunities create new challenges*, *The European Physical Journal Plus* **137** (2022) 92, [2106.13885].

[234] A. Ibarra, E. Molinaro and S. T. Petcov, *Low Energy Signatures of the TeV Scale See-Saw Mechanism*, *Physical Review D* **84** (2011) 013005, [1103.6217].

[235] D. N. Dinh, A. Ibarra, E. Molinaro and S. T. Petcov, *The $\mu - e$ Conversion in Nuclei, $\mu \to e\gamma, \mu \to 3e$ Decays and TeV Scale See-Saw Scenarios of Neutrino Mass Generation*, *Journal of High Energy Physics* **08** (2012) 125, [1205.4671v4].

[236] J. T. Penedo, S. T. Petcov and T. Yanagida, *Low-Scale Seesaw and the CP Violation in Neutrino Oscillations*, *Nulcear Physics B* **929** (2018) 377, [1712.09922].

[237] S. T. Petcov, *The Processes $\mu \to e + \gamma, \mu \to e + \overline{e}, \nu' \to \nu + \gamma$ in the Weinberg-Salam Model with Neutrino Mixing*, *Soviet Journal of Nuclear Physics* **25** (1977) 340.

[238] S. M. Bilenky, S. T. Petcov and B. Pontecorvo, *Lepton Mixing, $\mu \to e + \gamma$ Decay and Neutrino Oscillations*, *Physics Letters B* **67** (1977) 309.

[239] MEG Collaboration, *Search for the lepton flavour violating decay $\mu^+ \to e^+\gamma$ with the full dataset of the MEG experiment*, *The European Physical Journal C* **76** (2016) 434, [1605.05081].

[240] SINDRUM Collaboration, *Search for the decay $\mu^+ \to e^+e^+e^-$*, *Nuclear Physics B* **299** (1988) 1.

[241] SINDRUM II Collaboration, *Test of lepton flavor conservation in $\mu \to e$ conversion on titanium*, *Physics Letters B* **317** (1993) 631.

[242] SINDRUM II Collaboration, *A Search for muon to electron conversion in muonic gold*, *The European Physical Journal C* **47** (2006) 337.

[243] MEG II Collaboration, *The design of the MEG II experiment*, *The European Physical Journal C* **78** (2018) 380, [1801.04688].

[244] Mu3e Collaboration, *Technical design of the phase I Mu3e experiment*, *Nuclear Instruments and Methods in Physics Research Section A* **1014** (2021) 165679, [2009.11690].

[245] Mu2e Collaboration, *Mu2e Technical Design Report*, 1501.05241.

[246] COMET Collaboration, *COMET Phase-I Technical Design Report*, *Progress of Theoretical and Experimental Physics* **2020** (2020) 033C01, [1812.09018].

[247] R. J. Barlow, *The PRISM/PRIME project*, *Nuclear Physics B - Proceedings Supplements* **218** (2011) 44.

[248] A. Ilakovac and A. Pilaftsis, *Flavor violating charged lepton decays in seesaw-type models*, *Nucl. Phys. B* **437** (1995) 491, [hep-ph/9403398].

[249] R. Alonso, M. Dhen, M. B. Gavela and T. Hambye, *Muon conversion to electron in nuclei in type-I seesaw models*, *Journal of High Energy Physics* **01** (2013) 118, [1209.2679].

[250] T. P. Cheng and L.-F. Li, *$\mu \to e\gamma$ in Theories With Dirac and Majorana Neutrino Mass Terms*, *Physical Review Letters* **45** (1980) 1908.

[251] M. Chrzaszcz, M. Drewes, T. E. Gonzalo, J. Harz, S. Krishnamurthy and C. Weniger, *A frequentist analysis of three right-handed neutrinos with GAMBIT*, *The European Physical Journal C* **80** (2020) 569, [1908.02302].

[252] T. E. Oliphant, *A guide to NumPy*, vol. 1. Trelgol Publishing USA, 2006.

[253] S. van der Walt, S. C. Colbert and G. Varoquaux, *The NumPy array: a structure for efficient numerical computation*, *Computing in Science & Engineering* **13** (2011) 22.

[254] P. Virtanen, R. Gommers, T. E. Oliphant, M. Haberland, T. Reddy, D. Cournapeau et al., *SciPy 1.0: fundamental algorithms for scientific computing in Python*, *Nature Methods* **17** (2020) 261.

[255] S. K. Lam, A. Pitrou and S. Seibert, *Numba: A llvm-based python jit compiler*, *Proceedings of the Second Workshop on the LLVM Compiler Infrastructure in HPC* (2015) 1.

[256] Warren Weckesser. *Odeintw: Complex and matrix differential equations*, https://github.com/WarrenWeckesser/odeintw,2014, last access on September 7, 2022.

[257] C. S. Fong, E. Nardi and A. Riotto, *Leptogenesis in the Universe*, *Advances in High Energy Physics* **2012** (2012) 1–59, [1301.3062].

[258] P. C. da Silva, D. Karamitros, T. McKelvey and A. Pilaftsis, *Tri-Resonant Leptogenesis in a Seesaw Extension of the Standard Model*, 2206.08352.

[259] J. Hisano, T. Moroi, K. Tobe and M. Yamaguchi, *Lepton-flavor violation via right-handed neutrino Yukawa couplings in the supersymmetric standard model*, *Physical Review D* **53** (1996) 2442, [hep-ph/9510309].